Kepler photometry of two open clusters NGC 6791 and NGC 6819

Author: Sachu Sanjayan

CENTRUM ASTRONOMICZNE IM. MIKOŁAJA KOPERNIKA
POLSKIEJ AKADEMII NAUK

Advisor: Dr. hab. Andrzej Baran

A thesis submitted in partial fulfillment of the requirements for the degree of
Doctor of Philosophy
in
Astronomy

January, 2024

"Lokah samastah sukhino bhavantu // May everyone, in the whole world, be happy"

Dedicated to
To my beloved Mother and Sister...

Abstract

This work focuses on the search and study of pulsating hot subdwarf stars in two open clusters observed during the *Kepler* mission, NGC 6791 and NGC 6819. Both clusters are relatively old with ages of around 9 Gyr and 2.5 Gyr, respectively. Hot subdwarf stars are hot, compact helium core burning stars with a very thin hydrogen envelope. Their temperature ranges from 20 000 to 80 000 K, with a typical mass of 0.47 M$\odot$ and surface gravity $\log(g/\mathrm{cm\,s^{-2}})$ of 5.0 to 5.8, resulting in radii of 0.1 to 0.3 R$\odot$. The formation of hot subdwarf stars can occur through various channels, including binary systems and white dwarf mergers.

Our work has confirmed three pulsating subdwarf B (sdB) stars, KIC 2569576 (B3), KIC 2438324 (B4), and KIC 2437937 (B5), in NGC 6791, while none in NGC 6819. As compared to previous reports, we extended the data coverage for the analysis of these stars, discovered additional pulsation frequencies and features in their amplitude spectra. Analysis of spectroscopic observations revealed that four stars (B3, B4, B5 and B6) have atmospheric parameters consistent with gravity mode dominated sdBs. Additionally, hints of radial velocity variability in B3, B5, and B6 suggest they may be part of binary systems. We present the outcomes of asteroseismic modeling, by means of MESA and GYRE models, of B3 and B4 along with two field pulsating sdB stars, KIC 2991403, and KIC 11159657. The modeling accounted for a pulsation mode assignment and spectroscopic parameters (T_{eff} and $\log g$). For B3 and B4, we tried using two cluster parameters (total age and metallicity) with limited success. In the case of B4, a spectroscopically constrained approach resulted in a unique solution. We derived unique solutions except for the hydrogen envelope mass and progenitor mass (B3 and KIC 2991403), and for convective core and progenitor masses (KIC 11179657). Our fits, assessed by relative pulsation period differences ($\Delta P/P$), were consistent within 1%, except for KIC 11179657. Our results should be encouraging for further asteroseismic modeling of sdB stars.

While searching for pulsating hot subdwarfs we identified variable stars in both clusters. In NGC 6791, we found 278 variable stars, including 119 previously unknown. We calculated cluster membership probabilities for the variable stars using *Gaia* astrometry and we found 129 to be cluster members, which also provided an insight into their evolutionary status. For eclipsing binary systems, we determined eclipse mid-times and identified three systems with significant orbital period variability. Spectroscopic analysis delivered stellar parameters for 111 objects and revealed inconsistencies in the metallicity among cluster members, suggesting the presence of multiple stellar populations. By fitting MIST isochrones, we estimated the metallicity range to be 0.26 – 0.28 and age of 8.91 Gyr, as well as its average distance of 4134 pc. The latter agrees with the estimate derived by means of *Gaia* EDR3 astrometry. In NGC 6819, we found 385 variable stars, including 270 previously unknown. We derived 128 variable stars to be cluster members. For eclipsing binary stars, we determined eclipse mid-times and we found five objects with significant orbital period variability. Using MIST isochrones, we estimated the age of 2.54 Gyr and metallicity of -0.03 – +0.01. The distance of 2300 pc agrees with the one derived by means of *Gaia* DR3 astrometry.

Streszczenie

Niniejsza praca koncentruje się na poszukiwaniach i badaniach pulsujących gorących podkarłów w dwóch gromadach otwartych obserwowanych w ramach misji *Kepler* NGC 6791 i NGC 6819. Obie gromady są stosunkowo stare i mają wiek odpowiednio około 9 i 2.5 lat. Gorące podkarły to zwarte obiekty z helowym jądrem i bardzo cienką wodorową otoczką. Ich temperatura zawiera się w przedziale 20 000 – 80 000 K, typowa masa wynosi 0.47 M⊙, a powierzchniowa grawitacja $\log(g/\mathrm{cm\,s^{-2}})$ od 5.0 do 5.8, co daje promień od 0.1 do 0.3 R⊙. Tworzenie się gwiazd sdB może zachodzić różnymi kanałami, w tym poprzez układy podwójne, a także łączenie się białych karłów.

Nasza praca potwierdziła obecność trzech pulsujących gwiazd sdB, KIC 2569576 (B3), KIC 2438324 (B4) i KIC 2437937 (B5) w NGC 6791, natomiast żadnej takiej gwiazdy w NGC 6819. W porównaniu z poprzednimi badaniami rozszerzyliśmy zakres czasowy analizowanych danych tych gwiazd, odkrywając dodatkowe częstotliwości pulsacji i cechy w ich widmach fourierowskich. Dzięki analizie spektroskopowej pokazaliśmy, że cztery gwiazdy (B3, B4, B5 i B6) mają parametry atmosferyczne zgodne z gwiazdami sdB pulsującymi głównie w modach grawitacyjnych. Dodatkowo, wskazówki dotyczące zmienności prędkości radialnej w B3, B5 i B6 sugerują, że mogą one być one układami podwójnymi. Przedstawiamy wyniki modelowania asterosejsmicznego, z użyciem modeli MESA i GYRE, dla gwiazd B3 i B4, a także dwóch pulsujących gwiazd sdB należących do pola galaktycznego, KIC 2991403 i KIC 11159657. W modelowaniu uwzględniliśmy identyfikację modów pulsacji i parametry spektroskopowe (T_{eff} i $\log g$). W przypadku B3 i B4 próbowaliśmy użyć dwóch parametrów gromady (całkowity wiek i metaliczność) z ograniczonym sukcesem. W przypadku B4, uwzględniając parametry spektroskopowe, otrzymaliśmy jednoznaczne rozwiązanie. Podobnie otrzymaliśmy jednoznaczne rozwiązania, za wyjątkiem masy wodorowej otoczki i masy gwiazdy progenitora, dla B3 i KIC 2991403, oraz za wyjątkiem masy konwekcyjnego jądra i masy progenitora, dla KIC 11179657. Za wyjątkiem KIC 11179657, nasze dopasowania, mierzone względnymi różnicami okresowych pulsacji ($\Delta P/P$), mieściły się w granicy 1%. Nasze wyniki powinny zachęcać do dalszego modelowania asterosejsmicznego gwiazd sdB.

Poszukując pulsujących gorących karłów, zidentyfikowaliśmy gwiazdy zmienne w obu gromadach. W NGC 6791 znaleźliśmy 278 gwiazd zmiennych, w tym 119 dotychczas nieznanych. Z użyciem astrometrii *Gaia*, obliczyliśmy prawdopodobieństwa przynależności gwiazd zmiennych do gromady i otrzymaliśmy, że 129 z nich należy do gromady, co również dało wgląd w ich status ewolucyjny. W przypadku układów podwójnych zaćmieniowych określiliśmy momenty minimów (zaćmień) i zidentyfikowaliśmy trzy układy o znacznej zmienności okresów orbitalnych. Analiza spektroskopowa dostarczyła parametry gwiazdowe dla 111 obiektów i ujawniła niespójności w metaliczności wśród członków gromady, co może sugerować obecność wielu populacji gwiazd. Dopasowując izochrony wyliczone w projekcie MIST, oszacowaliśmy zakres metaliczności na 0.26 – 0.28 i wiek na 8.91 Gyr, a także jego średnią odległość na 4134 pc. Odległość zgadza się z wynikiem uzyskanym z użyciem astrometrii *Gaia* EDR3. W NGC 6819 znaleźliśmy 385 gwiazd zmiennych, z czego 270 to nowo odkryte gwiazdy zmienne, a 128 zostało potwierdzonych jako gwiazdy przynależne do gromady. W przypadku zaćmieniowych układów podwójnych określiliśmy momenty minimów (zaćmień) i znaleźliśmy pięć obiektów o znacznej zmienności okresów orbitalnych. Korzystając z izochron MIST, oszacowaliśmy wiek na 2.54 Gyr i metaliczność na -0.01(2). Odległość 2300 pc jest zgodna z tą wyznaczoną z użyciem astrometrii *Gaia* DR3.

Acknowledgements

I am filled with deep gratitude for the extraordinary opportunity to pursue my PhD in astronomy, despite my initial limitations in both astronomy and coding. This journey would not have been possible without the unwavering guidance and support of my advisor, Prof. Andrzej Baran. His kindness, patience, and unwavering dedication have been an unending source of inspiration, guiding me through the challenges and keeping me focused until the very end. Under his mentorship, I have learned the immense dedication and effort required to transform a research idea into a successful endeavor. I express my heartfelt gratitude to him for his invaluable contributions to my growth.

Thank the scientific committee members and referees for their valuable comments and suggestion, which would help me keep the momentum moving forward. I extend my sincere appreciation to my collaborators, whose support has been instrumental in my research. Jakub Ostrowski, your continuous assistance in clarifying my layman doubts in modeling has been invaluable and deeply appreciated. Peter Nemeth, your expert guidance in the spectroscopy aspect of my research has been invaluable. I want to express my deep gratitude to Karen, Ingrid, Mike, Roy, John, and Josh for their invaluable contributions and collaboration. I would also like to thank Ruchi, Chandra, and Sumanta for being supportive colleagues throughout my research journey.

My deepest love and gratitude goes to my beloved family, who have been my unwavering support system. To my Mom, Bindu, Grandma Indira, and Sister Ammu, as well as all my cherished family members Sindu, Dileep, Drisya, and Rachana, thank you for standing by me and providing unwavering support throughout my career path. I am especially grateful to my cousin brothers and sisters, Sujith, Sumith, Aswathy, and Jiju, for inspiring me since my childhood. I am also thankful to my aunt Raji, guru Sanesh and my friends Praveen, and Athul, at Lyceum for their support.

I would like to express my heartfelt appreciation to my dear friends Unni and Arjun, who became my close family in Europe and supported me through all the ups and downs. Special thanks to my brother Syam for his endless support and guidance in improving my lifestyle. To Richard and Buddy, I extend my deepest gratitude for their unwavering support and inspiration whenever I needed it, as well as for introducing me to the joys of hiking and running, which helped me maintain an active lifestyle. Special thanks goes to Zaneta for inspiring me and helping me reconnect with nature through our weekend hikes, and I am grateful for my hiking family. Lastly, I express my immense gratitude to my Ukulele family: Joao, Edy, Ilona, Sylwia, and Bartek. Your friendship, camaraderie, and shared love for music have brought immense joy and balance to my life. Special thanks to Bestin and Adith for the inspiring conversations. Thanks to Darek for being a wonderful host and family during my stay in Poland. I am grateful to Wiw for the inspirations during the final stages of finishing my thesis.

To all those mentioned and those who have supported me silently, I offer my heartfelt thanks for being a part of my journey and for your invaluable contributions in shaping me both personally and professionally. I am forever grateful for your presence in my life.

Contents

Chapter 1

Introduction

1.1 Hot subdwarf B stars

Hot subdwarf B (sdB) stars are hot, luminous and compact objects that were discovered by Humason and Zwicky (1947) while searching for faint blue stars in the area of the North Galactic Pole. According to the results from the Palomar-Green (PG) Catalog of Ultraviolet-Excess Stellar Objects (R. F. Green et al., 1986), sdB stars are the dominant population of blue stars in our Galaxy. This makes them very important for understanding the Galactic content and evolution. Based on imaging and spectroscopic observations from Brown et al. (1998), O'Connell (1999) concluded that the ultraviolet excess upturn phenomenon observed in elliptical galaxies may be caused by ultraviolet flux from sdB stars. Subdwarf B stars may contribute to the evolution of our Galaxy through the production of chemical elements via radiation emission, which ionizes surrounding gas, and creates ionized regions, which are prone to collapse, facilitating the formation of new stars and clusters (Brown et al., 1997). Altmann et al. (2004) suggested that hot subdwarf stars would help us to understand the galactic structure and evolution. Wang and Han (2009) reported that short period subdwarf binary systems are excellent candidates for progenitor type Ia supernovae. Many studies were conducted in order to understand the formation channels of hot subdwarf stars, formations via a merger of hydrogen White Dwarfs (WD) (Webbink, 1984), enhanced stellar winds (D'Cruz et al., 1996), or late flashers (Sweigart, 1997). Substellar companions to subdwarf stars are of great interest to many studies, including the understanding of a hot subdwarf formation channel; methods and attempts to search for transiting planets around sdB stars have been done recently (Thuillier et al., 2022; Van Grootel et al., 2021).

Subdwarf B stars are characterized by a helium burning core, helium shell, and hydrogen envelope, where the latter represents less than 1% of their mass (Heber, 2009). The effective temperature ($T_{\rm eff}$) ranges from 20 000 to 32 000 K, the surface gravity $\log(g/{\rm cm\,s^{-2}})$ range is 5.0 – 5.8, and a typical mass is 0.47 $M_\odot$ (Fontaine et al., 2012). Assuming uniform density, these parameters translate into radii of 0.1 to 0.3 $R_\odot$. See the schematic cross section of an sdB star in Figure 1.1.

It is generally accepted that sdB stars are descendants of low mass Main Sequence (MS) stars. Heber (2016) reported a progenitor mass range of 0.7 – 1.9 $M_\odot$, in the case of a degenerate channel, which agrees with the result obtained by Ostrowski et al. (2021). A non-degenerate channel provides another way of producing sdB stars, with wider both the progenitor and sdB mass ranges. This channel allows for as low mass sdB stars as 0.3 $M_\odot$, while the upper level is not well constrained (Ostrowski et al., 2021). To become an sdB star, it is essential that a progenitor must lose most of its hydrogen envelope before the helium ignition.

Subdwarf B stars are one of a few types of the hot subdwarf population. Other types are sdOB, sdO, He-sdB, and He-sdO, where the upper-case letters denote spectral classification. The first three types are helium-poor, while the latter two are helium-rich subdwarfs. The spectra of sdB stars are dominated by strong `H` lines and weaker `HeI` lines. The spectra of sdO stars, which are hotter than sdB stars, with effective temperature between 45 000 and 80 000 K, show H lines along with `HeII` lines, however `HeI` lines, including 4471Å, are no longer present. An intermediate type, sdOB, is defined to be between 32 000 – 45 000 K and with the `HeII` 4686 line present.

The mechanism by which hot subdwarf stars efficiently strip their envelopes is not yet fully understood. According to a binary population synthesis (BPS) analysis (Han et al., 2002; Han, 2003), an interaction with a companion star, through a Roche lobe overflow (RLOF) or common envelope (CE) ejection, can be an essential process. BPS models suggest the formation of CE binaries containing sdBs typically exhibit short orbital periods ranging from 0.5 to 40 days, and stable RLOF results in long-period binaries with orbital periods extending up to 2000 days (Han et al., 2002). The efficiency of this envelope stripping depends on the mass of the companion star. As predicted by the BPS analysis, companions to hot subdwarfs can be WD or MS stars, and these cases were observed by *e.g.* Maxted et al. (2001), Napiwotzki et al. (2004), and Copperwheat et al. (2011). According to Charpinet et al. (2018), who presented results on stellar rotation analysis, substellar companions may also be responsible for mass-loss, while the objects are still observationally single. Kramer et al. (2020) suggested that sdBs can form with companions even down to the brown dwarf mass limit.

As mentioned in Baran et al. (2023a) sdO stars can form through two separate channels. He-poor ones are direct progenitors of sdB stars, while the majority, which are He-rich ones, are identified as direct post-RGB objects, created through late hot He-flash or as end products of merger events.

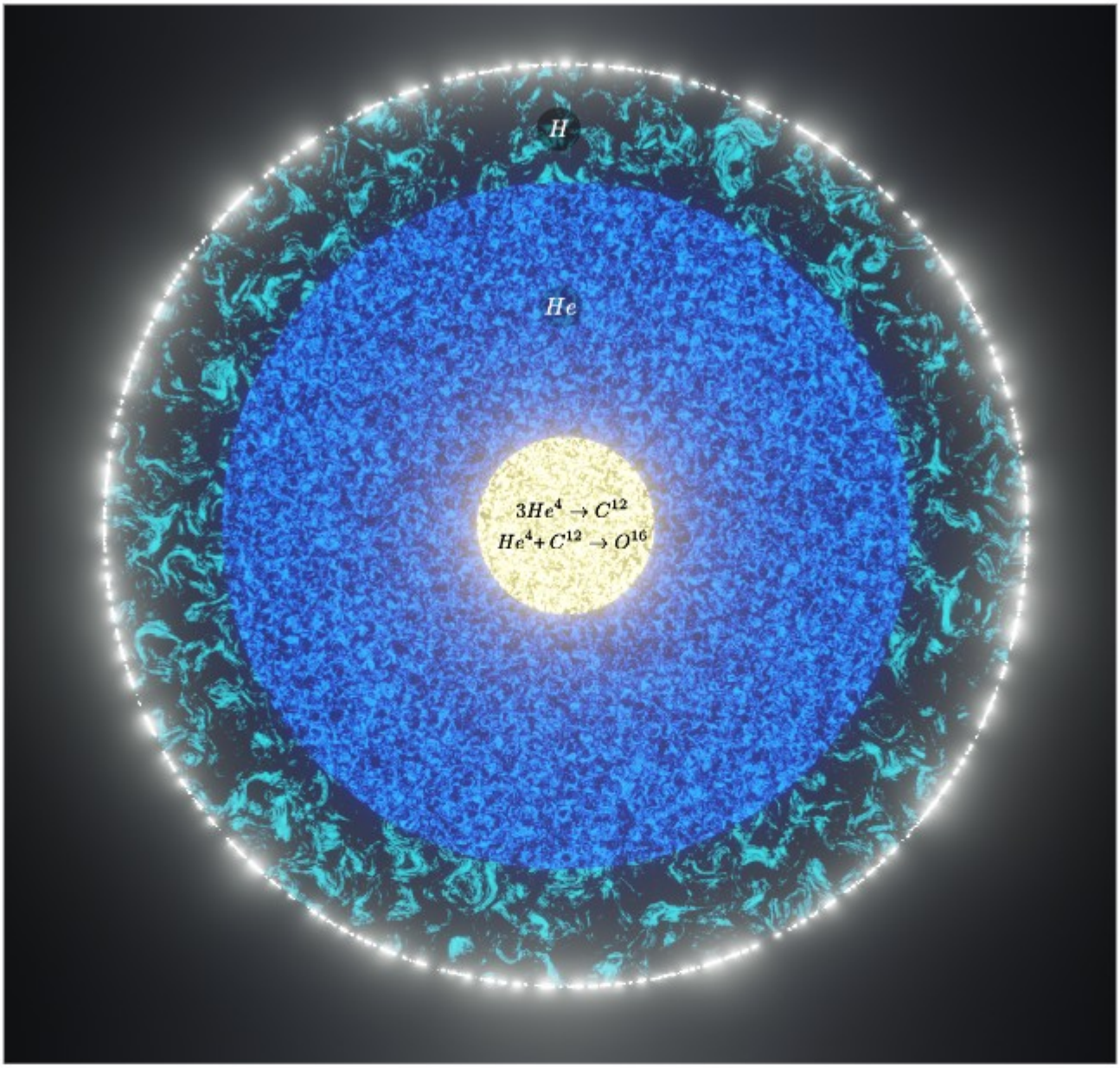

Figure 1.1: Schematic cross section of an sdB star.

1.2 Stellar pulsations in hot subdwarfs

Charpinet et al. (1996) predicted the existence of a light variability in sdB stars based on static theoretical models. Almost simultaneously, pulsations in sdB stars were observationally detected by Kilkenny et al. (1997) as rapid light variations in EC 14026-2647, giving a foundation for a new type of pulsating stars. These pulsating sdB stars are now referred to as V361 Hya stars and were identified with sdB stars pulsating in pressure (p) modes. Typical periods are of a few minutes and amplitudes up to tens of mmag. Later on, gravity (g) mode pulsations in sdB stars were first reported by E. M. Green et al. (2003). These stars show periods of hours with typical amplitudes below 10 mmag. Gravity mode sdB pulsators are often referred to as V1093 Her stars. There are also sdB stars that show both p-mode and g-mode pulsations, referred to as DW Lyn stars, such as the p-mode dominant pulsator with only one low amplitude g-mode, HS 0702+6043, observed by Schuh et al. (2006). A more convincing case of a hybrid hot subdwarf, Balloon 090100001 (V585 Peg), was published by Baran et al. (2005) and

Baran et al. (2009). Recently, Baran et al. (2023a) reported a list of sdB, sdOB, sdO and He-sdOB pulsators, including hybrid ones.

Pulsations in hot subdwarfs are driven by the so-called κ mechanism, which works on an opacity bump at $2{\cdot}10^5$ K as proposed by Charpinet et al. (1996). In hot subdwarfs the κ mechanism operates in the opacity of Fe and drives both p- and g-modes. The Fe bump opacity refers to the absorption of light by partial ionization of iron ions (Charpinet et al., 1997). According to Battich et al. (2018), the ε mechanism may also drive pulsations in hot subdwarfs, potentially leading to the creation of a new instability strip. No proved ε mechanism hot subdwarf pulsator has been detected so far.

By analyzing photometric data of pulsating stars, deriving pulsation periods and comparing them with those calculated from theoretical models, we can gain valuable insight into their interiors, *e.g* chemical profile, envelope mass, core mass. This technique is also known as asteroseismic modeling. In order to accurately match the observed pulsations to modeled ones, a range of parameters must be considered, including the age, chemical composition, initial mass, envelope mass, and central helium abundance of the star. The better we can constrain these parameters, the more reliable our asteroseismic modeling becomes.

1.3 Hot subdwarfs in star clusters

Usually, we do not have too much information, which would well constrain the asteroseismic modeling of Galactic field stars. However, in case of clusters, we can propagate information derived for a whole cluster onto individual member stars, *e.g.* age, chemical content. Open clusters (OC), groups of gravitationally bound stars and formed from the same molecular cloud, offer a unique opportunity for making the asteroseismic analysis easier. Of our particular interest are old open clusters, which have existed for billions of years, and provide a glimpse into the advanced stages of stellar evolution. Several studies examined the population of sdB stars in both field and cluster environments.

Moehler et al. (1997) observed 17 Horizontal Branch (HB) stars in NGC 6752, and interpreted them as hot subdwarf stars. The search for binary hot subdwarf stars by Moni Bidin et al. (2009) and Moni-Bidin (2006) has expanded the count of Extreme Horizontal Branch (EHB) stars, with 18 in NGC 6752, five in NGC 5986, and 11 in M80. Additionally, Salgado et al. (2013) reported observations of 71 HB stars in M22, and provided effective temperatures and surface gravities similar to those reported in the clusters mentioned earlier in this paragraph.

Spectroscopic observations of NGC 6752 conducted by Heber et al. (1986) have unveiled nine HB stars, with the bluest ones exhibiting atmospheric parameters comparable to field hot subdwarf stars. The authors reported NGC 6752 as high metallicity and, from the similarities of sdBs in the field and GCs, they provided observational evidence that the position of hot subdwarfs in the EHB does not depend on the metallicity. Moehler et al. (1995) conducted a detailed study of sdBs in GCs, examining NGC 6752, M15, and M22, using spectrophotometry to estimate physical parameters and determine masses using the distance to the cluster. They compared the physical parameters and evolutionary status of sdBs in GCs with field counterparts in the Milky Way. Moni-Bidin (2006) found that the proportion of sdB stars in binary systems is lower in GCs than in the Galactic field.

While GCs proved to be valuable objects for findings and studying the hot subdwarf population (Moehler, 2001), a high stellar density makes it difficult to observe most of the stars without being contaminated by neighboring stars in the area and the study is limited to the outskirts of GCs only. In contrast, OCs, which typically contain hundreds and up to thousands of stars, are not as crowded

with stars so, obtaining reasonable photometric data is less difficult. Majority of OCs are young, so less dense and not likely to have the HB developed yet. On the other hand old OCs are typically denser, and fewer, but it is more likely they will consist of stars in late evolutionary stages.

The oldest known OC, NGC 6791, which has a distinct EHB (Kaluzny & Shara, 1988), has an age of 8.9 Gyr (Sanjayan et al., 2022b) (Paper III). The age of 71 OCs were reported by Salaris et al. (2004) in their Table 1, of which 52 OCs are older than 1 Gyr and 18 OCs are older than 5 Gyrs.

Kaluzny and Udalski (1992) conducted a photometric study of NGC 6791, discovered eight blue objects, and named them B1, B2, ... B8. B4 was found to be a binary system (Kaluzny & Rucinski, 1993). Landsman et al. (1998) analyzed UV images of several OCs, including NGC 6791, M67, and NGC 188, and found that the fraction of hot HB stars in both NGC 6791 and NGC 188 is approximately 30%, implying that these OCs show a UV up turn phenomenon.

It is not only essential to use a cluster's parameters to study individual members, but also to use variable stars in clusters to provide valuable insights into the cluster. Using the light curves of variable stars, such as RR Lyrae, Cepheids or rotational variables, we can determine the distance to the cluster and/or its age and metallicity.

Our goal was to investigate the possibilities and limitations of seismic modeling for sdB stars in open clusters. As part of our search for hot subdwarf pulsators using *Kepler* observations, we conducted a comprehensive search for variable stars in two old OCs NGC 6791 and NGC 6819. We also performed further analysis of some of the cluster members. These OCs contain a vast population of variable stars, including only a handful of them documented in literature *e.g.* Kaluzny and Rucinski (1993) for NGC 6791 and Kaluzny and Shara (1988) for NGC 6819. Our modeling effort revolves around two pulsating sdB stars identified in NGC 6791, KIC 2569576 (B3) and KIC 2438324 (B4).

1.4 *Kepler* data processing

The *Kepler* mission, a milestone in a transit survey, was launched into an earth trailing heliocentric orbit in 2009 and lasted for almost 10 years. It featured a 0.95 m Schmidt telescope. The *Kepler* mission was completed in two phases. First, it was continuously observing 105 square degrees of the sky region between the Lyra and Cygnus constellations for the first four years. Then, as a result of failure of a second, out of four, reaction wheels, the mission was redesigned to observe along the ecliptic plane (K2). The K2 mission lasted almost five years and covered 19 campaigns. *Kepler* stored data in two modes: the short cadence mode (SC) lasting 58.85 sec, and the long cadence mode (LC), lasting 30 min.

The main goal of the mission was to detect planets by means of the transit method and since the onset of the mission, more than 2700 confirmed planets have been discovered. Over 500 000 stars and other objects, including star clusters, were observed. Among star clusters *Kepler* covered the area of two OCs NGC 6791 and NGC 6819 (Figure 1.2) in the "so-called" superstamps collected in the LC mode.

Kepler superstamps can be downloaded from the Mikulski Archive for Space Telescopes (MAST) database. They contain 200 x 200 pixels and cover 177.78 square arcmin in the sky. The superstamps are divided into two piles of ten 20 x 100 pixel boxes. One square pixel is 4 arcsec per side. The superstamps were collected during Quarters 1 – 17 (each Quarter lasts around three months and is abbreviated by Q if followed by a number), which corresponds to around 1460 days. *Kepler* superstamps of NGC 6791 and NGC 6819 cover hundreds of stars, however only for a handful of stars light curves

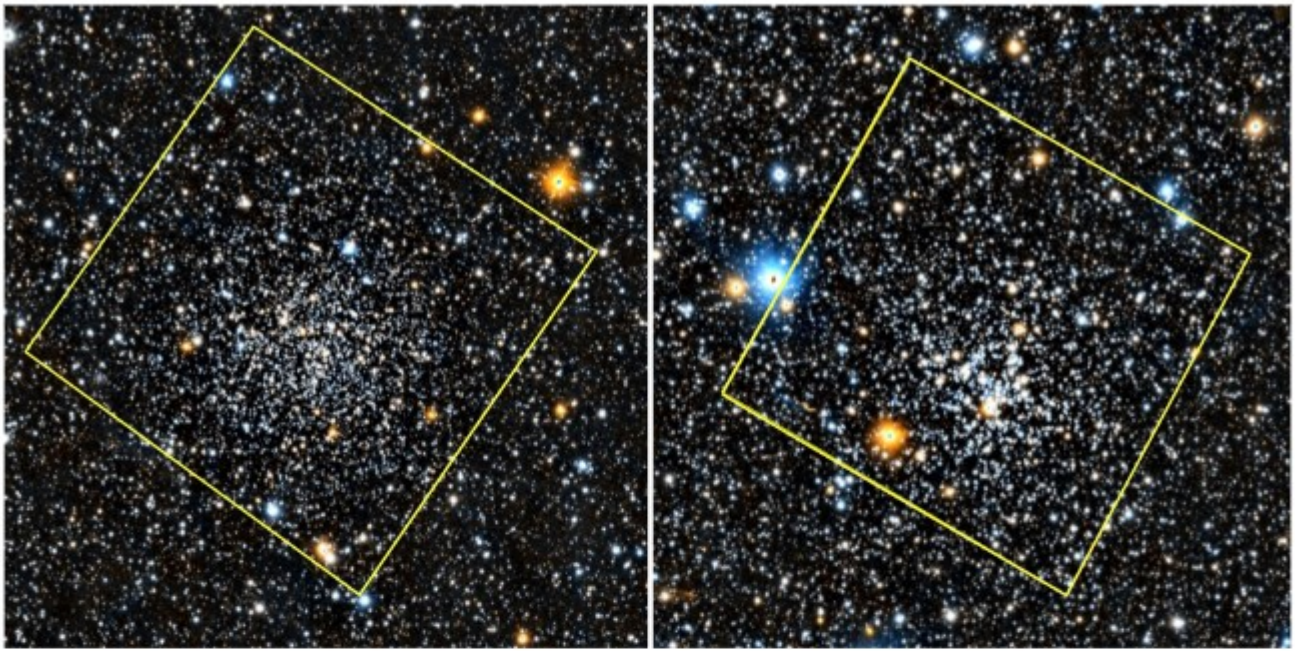

Figure 1.2: Two old open clusters analyzed in our work. The bright yellow line boxes indicate the fields covered by *Kepler*. Left panel: the field of the oldest OC NGC 6791. Right figure: the field of NGC 6819 (image credit: Pan-STARRs.)

were prepared and became available in the MAST database. Therefore, we had to analyze individual pixels and prepare time-series data of all remaining stars.

To work with such a large number of pixels we prepared a custom script with a Graphical User Interface that allowed us to interactively investigate individual pixels, mark those with a flux variability and define a contiguous aperture containing a variability signal. The *Kepler* spacecraft rotates by 90 deg every Quarter to keep its solar panels facing the Sun. This is why the location of stars on the CCD chips changes every Quarter (*e.g.* 2,3,4,5). However, the pointing repeats every four Quarters, hence the positions of the stars are the same in *e.g.* Q 2,6,10,14. We show a snapshot of one of the superstamp boxes, with numbers representing different variable stars we identified, in Figure 1.3.

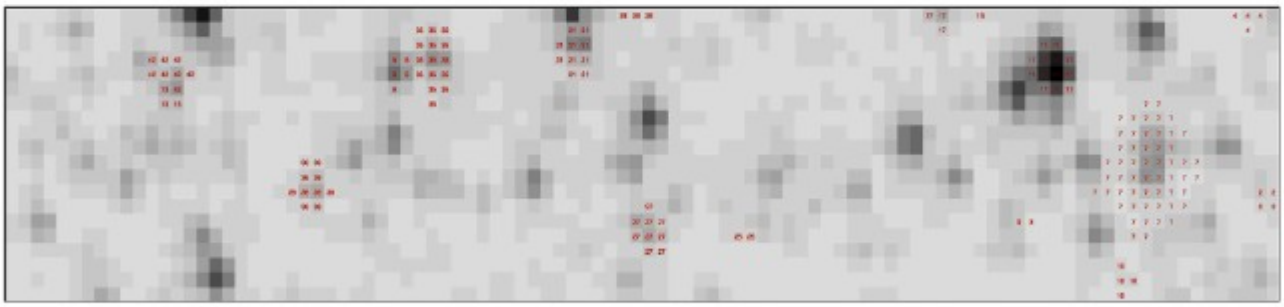

Figure 1.3: One of the superstamp boxes of the NGC 6819 obtained in Q2. In this figure, the numbers represent pixels with a flux variability of individual stars. These pixels define custom apertures used for a flux extraction.

To create time-series data, we used PyKE software (Kinemuchi et al., 2012) and other custom scripts. The final flux was obtained by adding up fluxes from all pixels within an aperture defined for a given star. We tried to avoid too much contamination from nearby stars, by not including pixels with decent signal of a star of our interest, but also significant contribution from contaminating stars. A

crowding parameter, like the one used for PDCSAP_FLUX delivered to the MAST, was not estimated. Sample custom target masks prepared for two pulsating sdB stars in different quarters are presented in Figure 1.4. Long term variability (if any) were removed and outliers clipped out. The detrending and clipping was based on individual cases. Fluxes in each time-series data set was divided by the average flux, subtracted one, and multiplied by 1000, which resulted in a *parts per thousand (ppt)* unit.

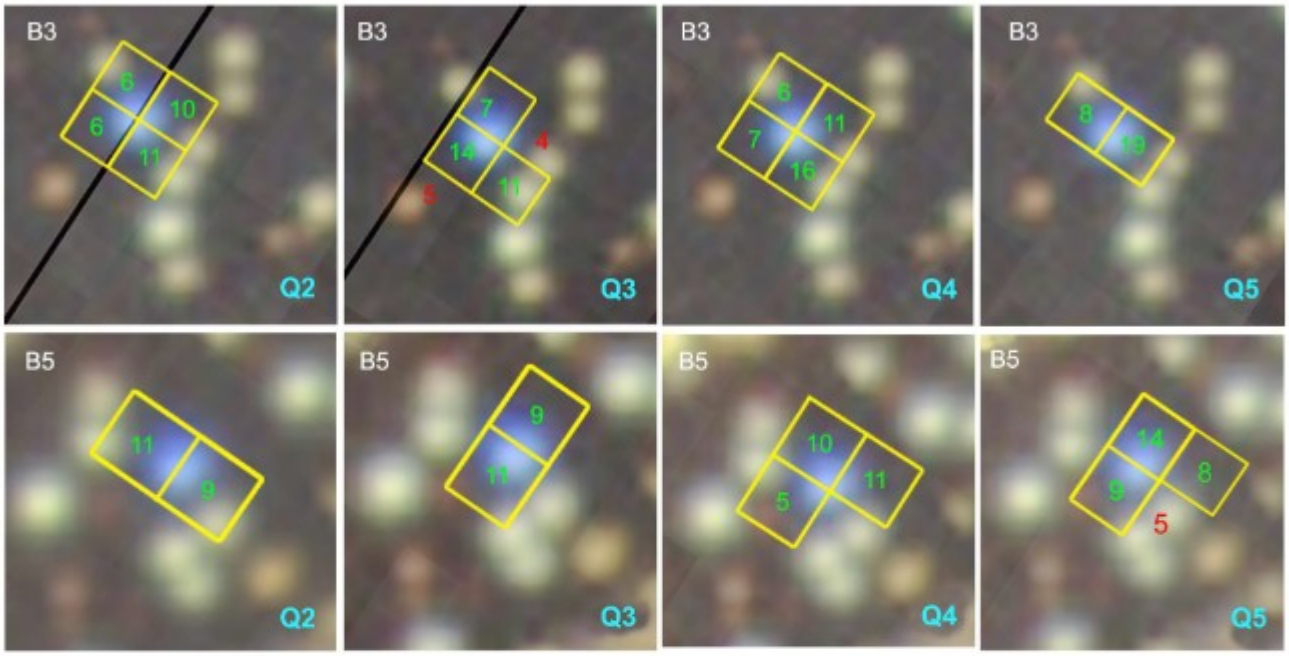

Figure 1.4: Optimal apertures defined for B3 and B5 in four different quarters (Q2, Q3, Q4, and Q5).

We classified variable stars, we found in our analysis, into three main types: binary, pulsating and rotational variables. Only a handful of stars were not assigned with any type since their variabilities are not too pronounced. Our type assignment was done based on both the time-series data and amplitude spectra. The amplitude spectra of the time series were calculated using the Fast Fourier Transform (FFT) algorithm (Cooley & Tukey, 1965). We show an exemplary light curve and an amplitude spectrum of a binary star *Gaia* EDR3 2051293186777509376, a member of NGC 6791, in Figure 1.5. We used the amplitude spectra of all variable stars to derive periods of dominant amplitude flux variabilities, and specifically in case of pulsating hot subdwarfs to list all detected pulsation periods. We utilized a commonly used method called prewhitening, which iteratively fits a sinusoidal curve to time-series data, and delivers amplitudes, periods and phases of a flux variability.

1.5 Asteroseismic modeling of sdBV stars in NGC 6791

Our work focused on a thorough exploration of pulsating hot subdwarfs in NGC 6791 and NGC 6819. The outcomes of our investigation were highly promising. We successfully identified three pulsating sdB stars in NGC 6791 and eight unidentified pulsators in NGC 6819. We utilized observing proposals at the Nordic Optical Telescope (NOT) and Apache Point Observatory (APO) 3.5m telescope to collect spectra of pulsators in NGC 6819, and verify their spectral status. Unfortunately, our analysis revealed that none of the eight pulsators observed in NGC 6819 turned out to be hot subdwarfs. A lack of pulsating hot subdwarfs in this open cluster may be surprising when considering the age of the cluster. Hot subdwarfs formed through a degenerate channel, depending on a progenitor mass,

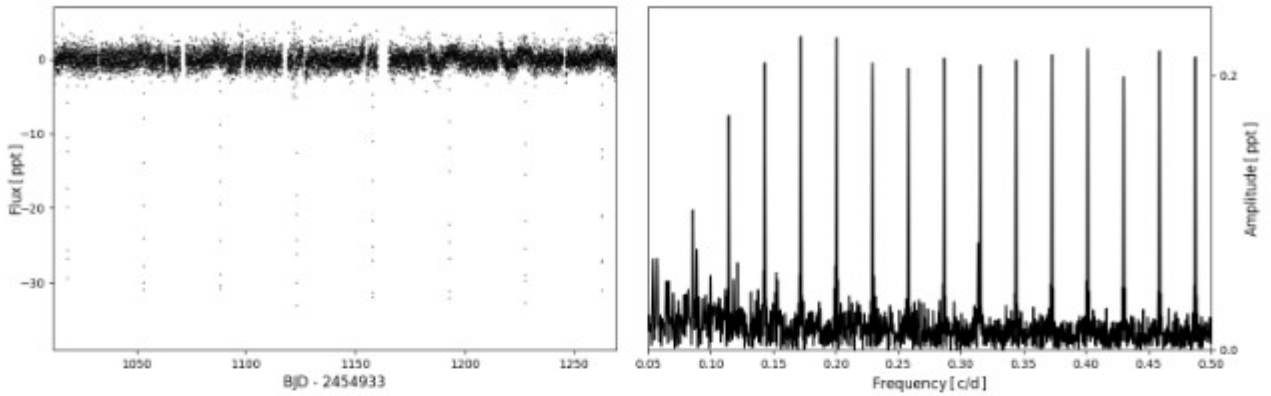

Figure 1.5: *Kepler* time-series data and an amplitude spectrum of a newly found eclipsing binary system, *Gaia* EDR3 2051293186777509376, in NGC 6791.

could (high mass end) or could not (low mass end) already arrive at the horizontal branch. The red clump area seems to be well populated in this cluster. Stars with 1.6 M⊙ had enough time to reach the EHB, if a required envelope striping occurred. Less massive progenitors of hot subdwarfs would still be at the MS or Red Giant Branch (RGB) evolutionary stage. The non-degenerate channel only works for progenitor masses beyond 2.2 M⊙, and stars forming through this formation channel would have already passed the hot subdwarf evolutionary stage.

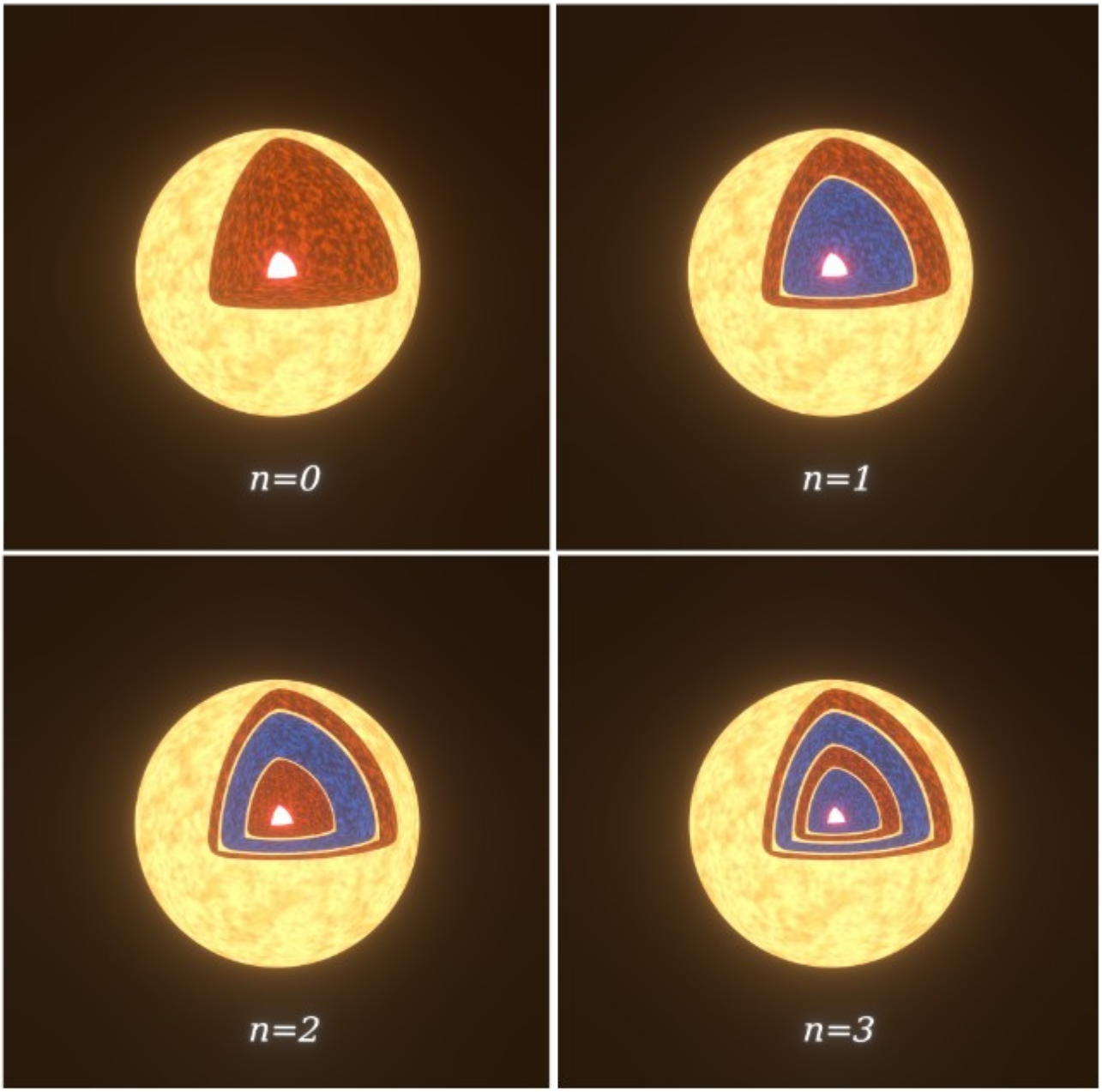

Figure 1.6: Radial orders n of 0,1,2 and 3. Red and blue colors represent lower and higher temperatures, respectively, which move in the opposite directions. Color of the surface is arbitrary.

Using astrometric data obtained from the *Gaia* EDR3 catalogue, we conducted an analysis to determine the membership probabilities of those three sdB stars in NGC 6791, and we ended up with over 95% probability that they are cluster members. The membership probabilities were determined using astrometric parameters (α, δ, μ_α, μ_δ, ϖ) (symbols are explained in Section 1.9) through an approach of clustering models known as Gaussian mixture models (GMM).

We analyzed spectra of B3, B5 and B6 collected with the GMOS at the Gemini North telescope and available from an archive[1]. We found that all analyzed stars show motions relative to the motion of the entire cluster, which can be interpreted as caused by the presence of companions in star systems. This shows that all three stars are likely residing in binary systems.

[1] https://archive.gemini.edu

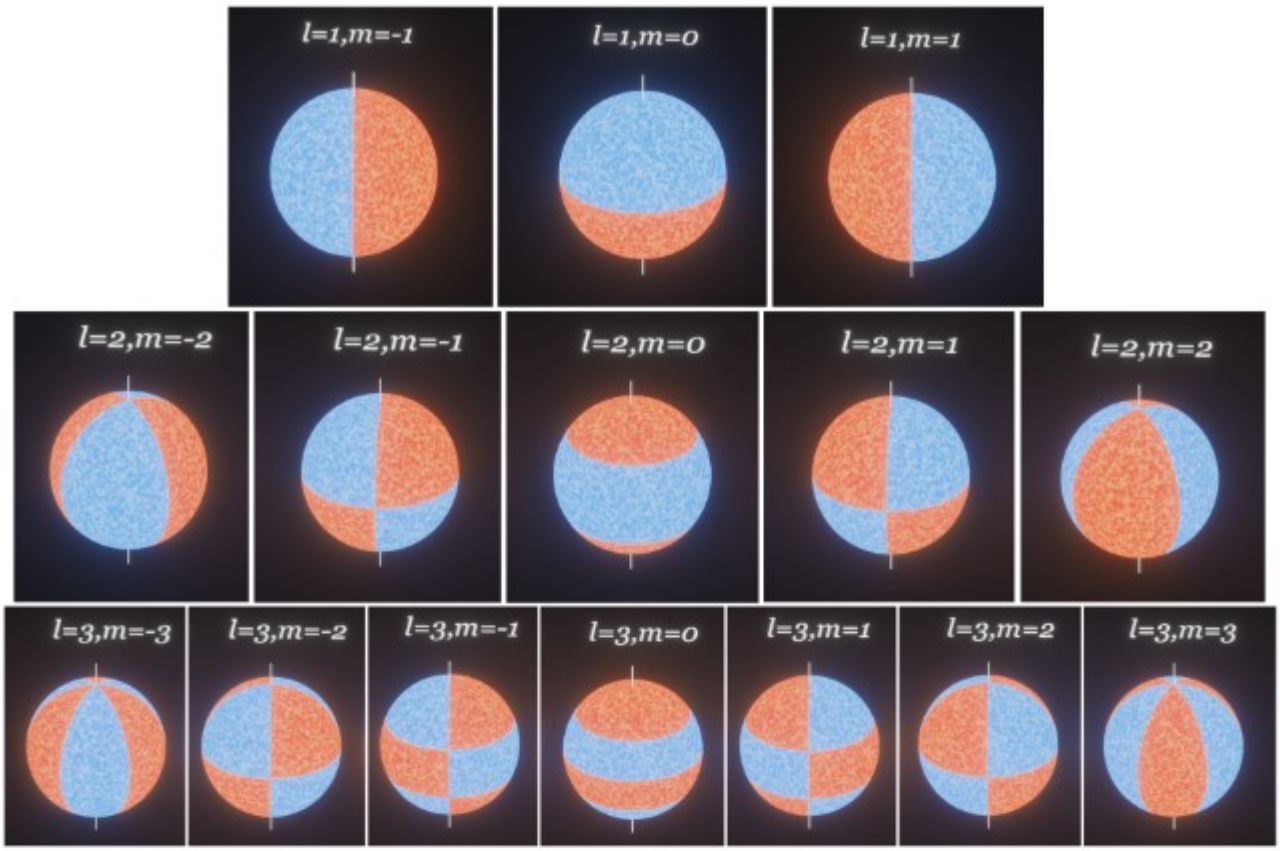

Figure 1.7: Modal degrees l of 1,2 and 3. Red and blue colors represent lower and higher temperatures, respectively.

One of our goals was to identify sdBV stars in both clusters, perform asteroseismic modeling to infer their interiors, and compare with sdBV stars in the Galactic field. The quality of the modeling is measured by a comparison of observed and calculated pulsation periods, which may, in principle, be performed easier when pulsation modes are identified, *i.e.* geometry of each mode is recognized. Stellar oscillations are described by three parameters, *i.e.* radial order (n) representing the number of radial nodes, modal degree (l) indicating the number of surface nodes, and azimuthal order (m) showing the number of longitudinal nodal lines, where m can range from -l to +l. We present examples of n, l and m values in Figures 1.6 and 1.7. Stellar disks of hot subdwarfs are too far away to see details of a pulsation geometry. Therefore, we utilized means that were recently widely applied to sdBV stars. These are rotationally split modes and asymptotic period spacings.

1.5.1 Rotationally split modes

Non-radial ($l>0$) modes of degree l have $2l+1$ components of $m = -l,\ldots,0,\ldots,+l$. In the absence of a rotation, these components have the same frequency. Stellar rotation lifts this degeneracy and shifts frequencies of $m \neq 0$ components. The separation between the adjacent components is indicative of the rotation period. The shift in the frequency due to the rotational splitting is given by

$$\Delta\nu_{n,l} = \frac{1 - C_{n,l}}{P_{\rm rot}} \tag{1.1}$$

$\Delta\nu_{n,l}$ is the frequency splitting for a given degree, while $C_{n,l}$ is the Ledoux constant which determines

the stability of convective zones in a star (Gough, 1986; Tassoul, 1980). When the $C_{n,l}$ is positive, convective zones are stable, indicating the absence of convection. Conversely, when the $C_{n,l}$ is negative, convective zones are unstable, indicating the presence of convective mixing. The value of $C_{n,l} \approx 0$ for p-modes (Charpinet et al., 2000), while for g-modes $C_{n,l}$ can be calculated using

$$C_{n,l} \approx (l^2 + l)^{-1} \tag{1.2}$$

A rotational splitting can be observed in both p- and g-modes. The inclination angle affects amplitudes of observed components of multiplets (Charpinet et al., 2011a), which may result in missing or reduced amplitudes of the split components. Regardless of the l value the rotational splitting for p-modes remains fairly constant. For g-modes of $l = 1$ the frequency splitting would be half of that for p-modes. Similarly, for $l = 2$ and $l = 3$, it would be 83.3% and 91.7%, respectively. As the modal degree increases the frequency splitting of g-modes approaches that of p-modes. Rotational multiplets are excellent for mode identification since they allow us to derive the modal degree based on the number of split components, often supported by the rotational splitting.

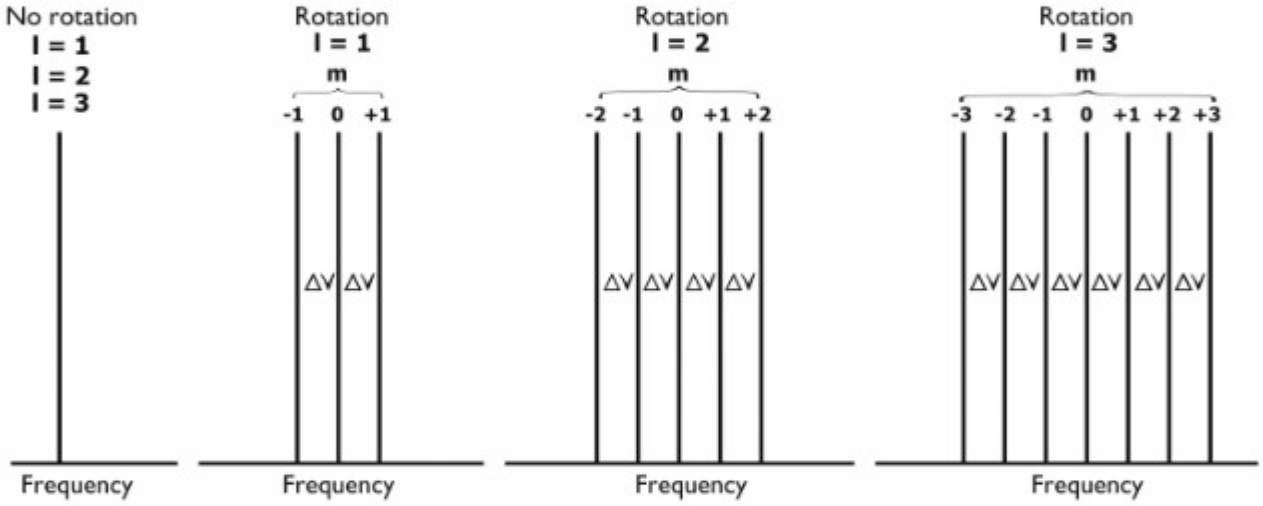

Figure 1.8: Schematic rotational multiplets of $l = 1$,2 and 3.

1.5.2 Asymptotic period spacing

The asymptotic period spacing relation describes the spacing between consecutive g-mode radial overtones, so pulsation modes of the same l and differing in n values. In the asymptotic limit $n \gg l$ the following formula is true

$$P_{l,n} = \frac{P_0}{\sqrt{l(l+1)}} n + \varepsilon \tag{1.3}$$

where P_0 is the period of the fundamental radial mode, while ε, according to Unno et al. (1979), is a small number. An asymptotic period spacing between two consecutive radial overtones, is given by the following equation

$$\Delta P_l = \frac{P_0}{\sqrt{l(l+1)}} \tag{1.4}$$

Reed et al. (2011) showed empirically that the average period spacing for dipole ($l = 1$) and

quadrupole ($l = 2$) g-modes in pulsating sdB stars is close to 250 sec and 144 sec, respectively. To estimate the common period spacing for modes of different modal degrees, the Kolmogrov-Smirnov (KS) test is commonly used. Asymptotic period spacing is commonly used to identify a modal degree and relative radial order of pulsation modes.

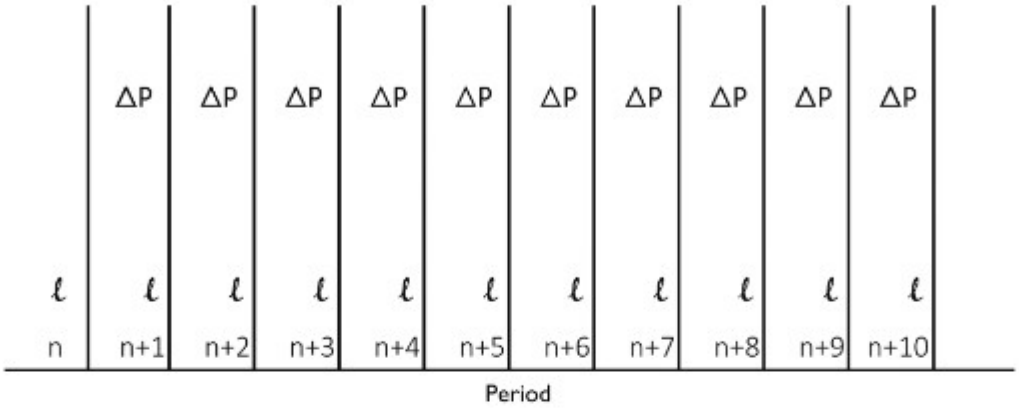

Figure 1.9: Schematic asymptotic period spacing for a modal degree l.

1.5.3 Pulsation mode identification

We used both means to perform a mode identification in B3, B4 and B5 (Sanjayan et al., 2022) (Paper I). We started with identification of rotationally split modes, and then we completed the period sequences using asymptotic period spacings. The majority of the modes were assigned to dipole and quadrupole modes. An échelle diagram is another representation of an asymptotic period spacing, which shows up in the diagram mostly as a vertical trend. We constructed échelle diagrams for B3, B4, and B5 (Paper I). All three stars show the expected vertical trend and a puzzling hook feature that was previously reported by Baran and Winans (2012). According to Charpinet et al. (2002), échelle diagrams provide insight into internal structures of stars and are useful for understanding diffusion and mode trapping. The authors found that trapping is expected every 2 000 sec in sdB stars.

We determined atmospheric parameters of those three sdB stars using spectroscopic observations taken with the HECTOSPEC instrument attached to the Multiple Mirror Telescope and available from archives[2]. All three sdBs were found to have temperatures between 23 500 – 25 300 K, and surface gravity $\log(g/\mathrm{cms}^{-2})$ between 5.31 – 5.51. A binary signature is clear in the time-series data of B4, while no signature of binary in photometric data is found in other hot subdwarf stars in this cluster. As we mentioned before such a detection was likely obtained in the spectroscopic data taken with the GMOS instrument.

Based on the rotational multiplets of B3, B4, and B5, we were able to directly determine the rotation periods of the stars to be 64.2(1.1), 9.196(33) and 71.0(1.8) d, respectively. In Figure 1.10 we show rotational periods as a function of effective temperatures. The diagram shows that hot subdwarfs with M dwarf and white dwarf companions are located at distinct areas. The first group shows shorter rotation periods, while the latter group shows longer periods. This is a consequence of a prior binary star evolution. This diagram could potentially serve as a tool for identifying binarity and even companions to hot subdwarfs based solely on two observables. It highlights an important role of a companion through a binary interaction in shaping the rotation periods of sdB stars. It should be

[2]https://lweb.cfa.harvard.edu/mmti/hectospec.html

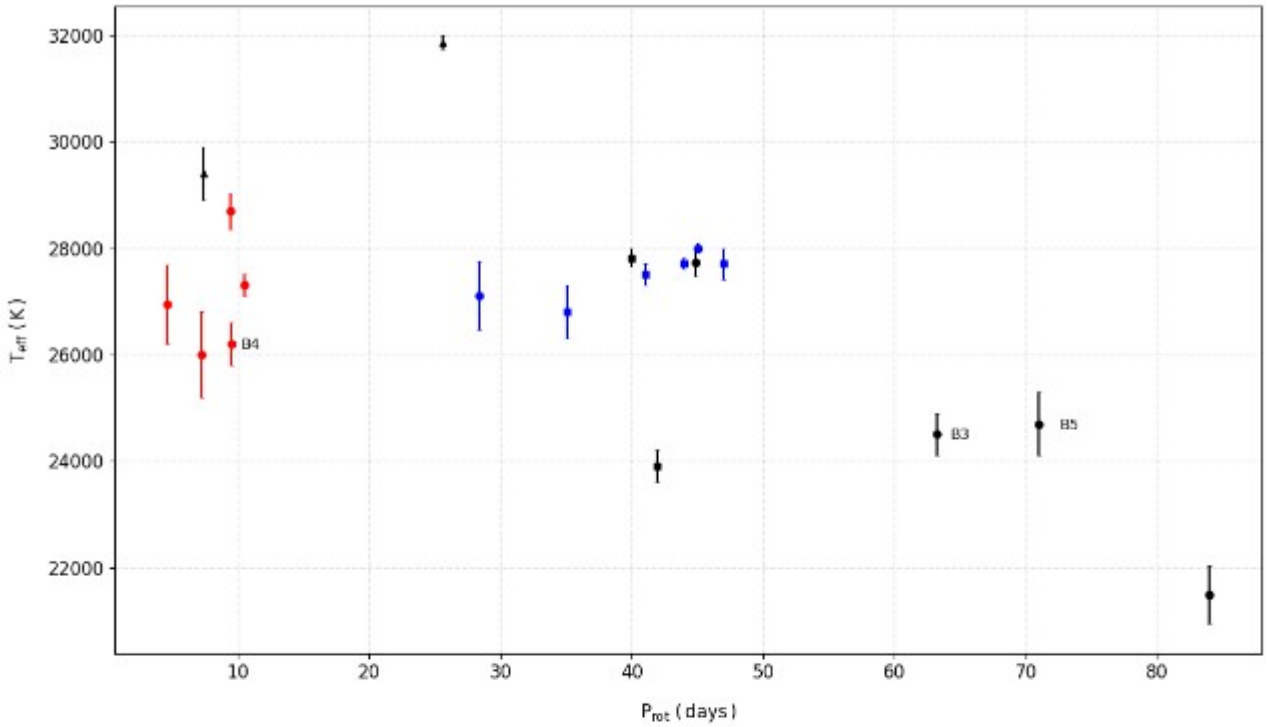

Figure 1.10: Rotation period vs effective temperature diagram for sdBV stars. Stars are plotted with symbols according to the pulsation content: g-modes (circles), hybrids with dominant g-modes (squares), hybrids with dominant p-modes (triangles), and their binary status: sdB+dM (red), sdB+WD (blue), unconfirmed (black).

noted, though, that eight stars have binarity status not cleared yet, hence the final interpretation of this diagram should be held off.

1.5.4 Theoretical models

Several studies toward seismic modeling to explore the interiors of hot subdwarf stars were published. They were performed using the forward modeling method (no prior constrains used) with static, structural models. These models allow for versatility and faster computations, although they can not fully reflect the prior evolutionary history of stellar configurations. The forward approach was applied to PG 1336-018 (Charpinet et al., 2008), Balloon 090100001 (Van Grootel et al., 2008), KPD 0629-0016 (Van Grootel et al., 2010a), KPD 1943+4058 (Van Grootel et al., 2010b), KIC 2697388 (Charpinet et al., 2011b), and EC 21494-7018 (Charpinet et al., 2019). The results obtained for PG 1336-018 were the first that proved the method useful. The mass of $0.459M_{\odot}$ and radius of $0.151R_{\odot}$ were derived. This result was inline with independent observations from Vučković et al. (2007). Modeling of Balloon 090100001 showed the star is in an advanced stage of evolution, *i.e.* at the post Terminal-Age EHB phase, with the mass of $0.432M_{\odot}$. In the case of KPD 0629-0016 the authors reported the mass of $0.471M_{\odot}$, the radius of $0.214R_{\odot}$, and the age of 42.6 Myr since the Zero-Age EHB (ZAEHB). For KPD 1943+4058, the mass of $0.496M_{\odot}$, radius of $0.203R_{\odot}$, and rather young age of 18.4 Myr since the ZAEHB, were reported. Modeling of KIC 2697388 provided no unique solution, with mass in the range of $0.452 - 0.463M_{\odot}$, radius of $0.198 - 0.203R_{\odot}$, and the age of less than 55 Myr since the ZAEHB. For EC 21494-7018, the authors reported a radius of $0.164R_{\odot}$, and a mass of $0.391M_{\odot}$. This mass may indicate that the sdB star was produced via a non-degenerate channel (Ostrowski et al., 2021).

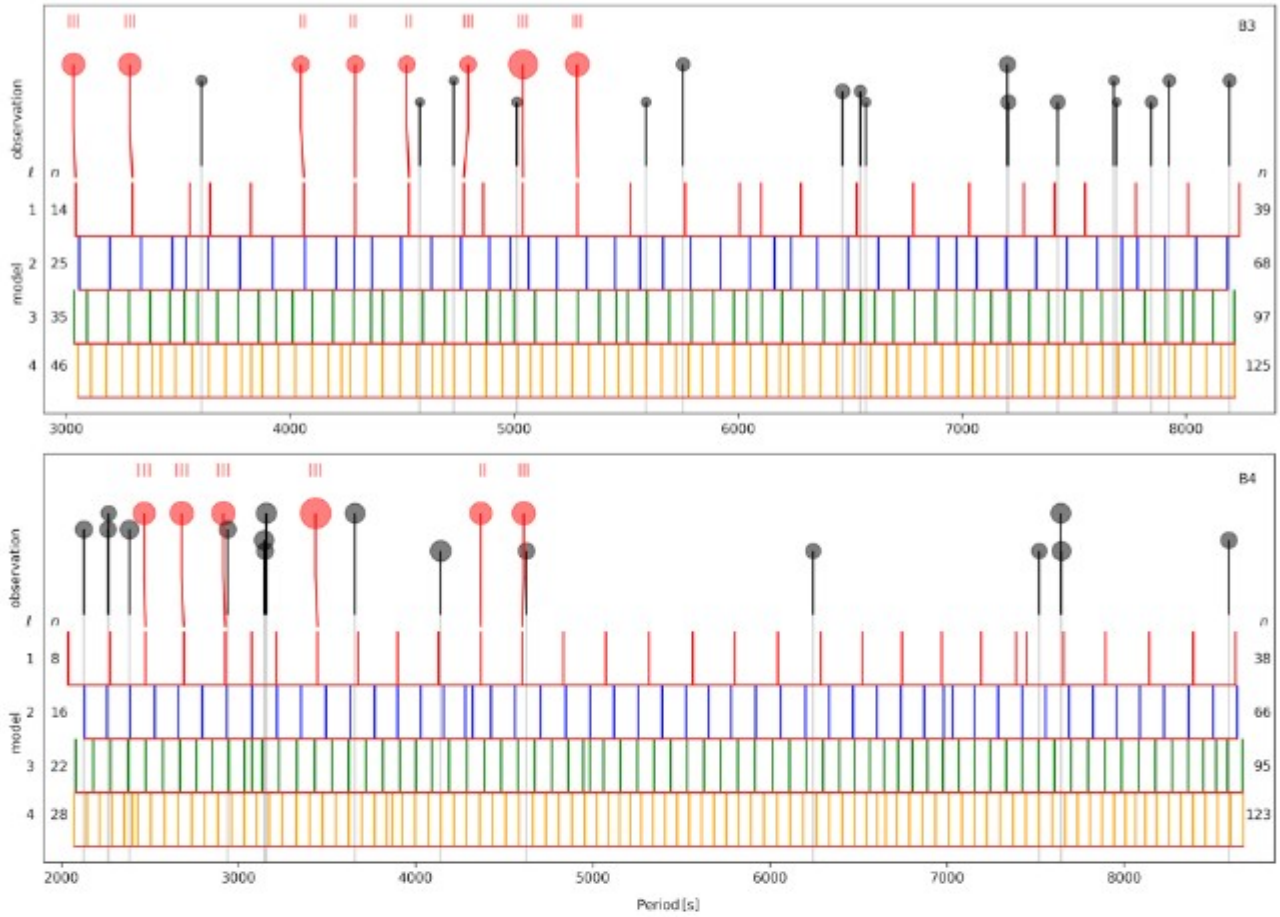

Figure 1.11: GYRE models that match the observed pulsation periods of central components in rotational multiplets in B3 (top panel) and B4 (bottom panel). Red filled circles represent detected dipole modes utilized in the period match, while the black ones represent detected periods that were not used. The size of a circle represents the amplitude of a pulsation mode. Vertical lines on top of red circles denote doublet or triplet detections. Red downward (from the circles) lines point at the nearest periods of dipole modes calculated from models.

The four latter stars were found to be young with more than 50% of central helium, Y_c, and of relatively low metallicities. Full exploitation of past evolution, and its influence on the hot subdwarf interiors and pulsating properties, can be possible with evolutionary codes, *e.g.* the Modules for Experiments in Stellar Astrophysics (MESA) code (Paxton et al., 2018) and the GYRE stellar evolution code (Townsend & Teitler, 2013).

It is essential to maintain the convective core to be a single and continuous region in order to maintain a stable energy transport mechanism. Some models show cores split into multiple fractions, disrupting the stable energy transport and leading to an unrealistic internal structure of a star (Ostrowski et al., 2021; Salaris & Cassisi, 2017). When the central helium abundance drops to about a few percent the occurrence of the breathing pulses becomes a challenge (Constantino et al., 2016). To address these and other complexities, advanced numerical algorithms should be implemented to accurately determine core boundaries, or adjustments, which should be made to the microphysics involved. Detailed insight into those issues can be found in a recent study reported by Ostrowski et al. (2021).

As a continuation of the work presented in Paper I, we performed a modeling effort of B3 and B4 and reported our results in Baran and Sanjayan (2023b)(Paper II). We also included two field

sdBV stars, KIC 2991403 and KIC 11159657, in our analysis. We utilized around 63 000 evolutionary models with the convective premixing scheme, calculated using the MESA and adiabatic pulsations using GYRE as a result of work reported by Ostrowski et al. (2021). Only central components of the rotational multiplets were used for a pulsation period match, since modal degrees obtained solely from the asymptotic period spacing do not guarantee reliable mode identification. To find the best match between the models and observations we adopted the following approach. First, we searched the entire grid of calculated periods, without any constraints on physical parameters. Then, we applied spectroscopic estimates of $T_{\rm eff}$ and $\log g$. Finally, for cluster members, we used age and metallicity constraints derived from previous works. As one would expect the best period match should be obtained in the last scenario, however the age and metallicity of the cluster may not necessarily be applicable to our individual cluster members since they reside in binaries. We show the result of our period match in the spectroscopically constrained case for B3 and B4 in Figure 1.11.

The results of our modeling show that B4 is 60.95 Myr since ZAEHB with 50% central helium left in its core. The radius and mass is 0.21 $R_\odot$ and 0.47 $M_\odot$, respectively. In the case of B3 we derived the radius of 0.25 $R_\odot$ and the mass of 0.14 $M_\odot$. The age of B3 was found to be around 55 Myr since ZAEHB with 50% central helium left in its core.

Our modeling of a field star, KIC 2991403, delivered the radius of 0.22 $R_\odot$, the mass of 0.47 $M_\odot$ and 10% central helium, which indicates advanced EHB stage, *i.e.* 120.3 – 121.9 Myr since the ZAEHB. For KIC 11179657 we derived the radius in the range 0.27 $R_\odot$, the mass of 0.48 $M_\odot$ and 10% helium left in the core. The age is in the range of 116.4 – 117.3 Myr since the ZAEHB.

1.6 In search of variable stars in NGC 6791

NGC 6791 is one of the OCs, which was extensively explored by means of photometry. Rucinski et al. (1996) found three detached binaries and a cataclysmic variable (CV) star with a notable three-day outburst. Mochejska et al. (2002) discovered 47 new low-amplitude variable stars, including several BY Dra-type stars, and two CV stars undergoing outbursts. Subsequently, Mochejska et al. (2003) reported the discovery of seven new variable stars characterized by prolonged and periodic flux variabilities. Kaluzny (2003) revisited archived data from Kaluzny and Rucinski (1993), and identified four additional variable stars. Bruntt et al. (2003) unveiled 22 new low-amplitude objects and confirmed 20 previously known variable stars. Hartman et al. (2005) detected 10 new variable stars, including one δ-Scuti pulsator and eight contact binaries. Mochejska et al. (2005) identified 14 new variable stars, including nine eclipsing binaries. de Marchi et al. (2007) identified 260 variables in the area of the NGC 6791, however the authors reported that not all of these stars are confirmed members of the cluster.

As a by-product of our search for pulsating hot subdwarfs, we reported a diverse population of variable stars in the area of NGC 6791 (Paper III). We found 278 variable stars in the *Kepler* superstamps exhibiting flux variability. The literature survey showed that 119 stars are newly found variable stars. The membership study of those 278 stars has revealed 129 stars to be cluster members. We collected spectroscopic observations of 111 stars from publicly available databases. To obtain atmospheric parameters we fitted spectra of 64 stars using the XT grid (Németh et al., 2012), while for the remainder we adopted the values from the literature. Using amplitude spectra and spectroscopic observations we classified our findings as 17 binary stars, 45 pulsators and 62 rotational variables, all of them being cluster members. Only five stars were not allocated to any of the variability types.

We further divided the binary stars into eclipsing, contact and active, as well as pulsators into sdB, solar-like, δ-Scuti, and semi-regular. Even if very long period (>90 days) variables with smooth flux variabilities may exist in this open cluster we did not expect to detect them. It is a consequence of our detrending applied to a quarter-long datasets.

1.7 In search of variable stars in NGC 6819

A photometric exploration was conducted also in NGC 6819. Lindoff (1971) reported the first irregular-type variable. Kaluzny and Shara (1988) discovered 11 variable stars, while Manteiga et al. (1989) found one BS star using radial velocity data. Kryachko (2001) identified two dwarf novae using photographic plates. Street et al. (2002) uncovered 25 variable stars and 13 suspected ones, and subsequently Street et al. (2003) found 11 stars with transiting events in a survey of 38,000 stars. Street et al. (2005) reported 141 variable stars, including eclipsing binaries of various types. Stello et al. (2010) conducted the first asteroseismic analysis of solar-like red giants. Talamantes et al. (2010) listed 14 binaries and one δ-Scuti pulsator from ground-based observations. Gosnell et al. (2012) discovered 12 X-ray sources in the cluster area using XMM Newton data.

Similarly to the search in NGC 6791, we reported our findings of variable stars in NGC 6819 in Sanjayan et al. (2023) (Paper IV). We found a total of 385 variable stars, including 128 cluster members. We reported 270 newly found variable stars. We marked eight pulsating hot subdwarf candidates and we collected spectroscopic data using the NOT. The analysis of our spectra revealed two δ-Scuti pulsators, which are cluster members. Additionally, one δ-Scuti and three γ-Dor, as well as one rotational and one unclassified variable, which are non-members, were revealed. We collected the archived spectra of 51 stars. We fitted spectra of 25 stars using the XT grid Németh et al. (2012), while we utilized the archived atmospheric parameters for 34 stars. We found a total of 69 stars exhibiting stellar oscillations of which 24 are cluster members, including 17 solar-like pulsators as well as two δ-Scuti and one γ-Dor pulsators. Detailed analysis of the solar-like pulsators is underway and will be published by Themessl (in prep), while the analysis of one active X-ray binary, two δ-Scuti and two γ-Dor stars has been already reported by Guzik et al. (2023). For the reason given in the previous section we found no variable stars with very long periods and a smooth flux variability.

1.8 Spectroscopic analysis

Spectroscopic data plays a crucial role in determining atmospheric parameters, including $T_{\rm eff}$, $\log g$ and chemical composition. A number of ground-based spectroscopic surveys available to the public were searched, such as APOGEE (Ahn et al., 2014; Majewski et al., 2017), SDSS (Blanton et al., 2017), LAMOST (Zhao et al., 2012), ESO (Gilmore et al., 2012; Randich et al., 2013), HECTOSPEC (Fabricant et al., 2005), and INT [3]. We observed a selected sample of variable stars using the NOT and the 3.5 m telescope at APO. Since the spectroscopic data that we collected comes from various archives and our own observations, they are very heterogeneous.

For cool stars with $T_{\rm eff} < 15\,000$ K, we applied interpolated Local Thermodynamic Equilibrium (LTE) synthetic spectra from the BOSZ (Bohlin et al., 2017) spectral library based on scaled solar metallicity with carbon and α-element enhancement. For hotter stars with $T_{\rm eff} > 15\,000$ K we applied

[3] http://www.ing.iac.es/Astronomy/telescopes/int/

non-LTE stellar atmosphere models and synthetic spectra with TLUSTY/SYNSPEC (Hubeny & Lanz, 1995; Hubeny & Lanz, 2017). In addition to calculating $T_{\rm eff}$ and $\log g$, we estimated the RV of the stars using XT grid procedure mentioned in Németh et al. (2012).

1.9 Cluster membership analysis

We used data from the *Gaia* mission (Gaia Collaboration et al., 2022), during which astrometry for over 1.8 billion stars have been collected. We applied a query tool in the `astropy` python package to download *Gaia* data. The package enables us to download all *Gaia* targets within a given radius. A number of parameters were used for the membership analysis, including parallax (ϖ), right ascension (α), declination (δ), proper motion in α (μ_α), and proper motion in δ (μ_δ). We used stars with parallaxes in the range of $0 < \varpi < 1$, and for which relative uncertainties of any of those five parameters listed above are smaller than 50%. The parallax offset was corrected using the corresponding `python zpt` package. We used a GMM implemented in `Python` by the `scikit-learn` library (Pedregosa et al., 2011) to determine the membership probabilities. Models based on GMM assume the star's astrometric parameters to be determined by finite Gaussian functions, and variational Bayesian inference with Dirichlet priors is used to determine the number of Gaussian functions (Ferguson, 1973). The centroid of Gaussian functions was optimized using the Expectation Maximization (EM) algorithm (Dempster et al., 1977). We accepted a star to be a cluster member if its membership probability is > 0.5.

We identified 2040 stars to be cluster members in NGC 6791 and 1971 stars in NGC 6819. For NGC 6791, during the time of our analysis, *Gaia* EDR3 data were the most recent resource available, which did not provide enough stars with RVs measured to allow us to determine the average RV of this cluster. During our analysis of NGC 6819, *Gaia* DR3 became available, and we found 126 stars from our sample with RVs estimated. We used RVs as a sixth parameter in the membership analysis. We found that adding the RV as an additional constraint in the GMM model does not cause a significant change in the membership probability, rather it improves its accuracy. Using the cluster members with probabilities higher than 90% we determined the average RV of NGC 6819 to be $+3.5(5)$ km/s.

To validate our membership determination, we compared our findings with those from previous literature surveys (Cantat-Gaudin et al., 2018; Gao, 2020). Our aim was to identify any discrepancies in the membership assignments and investigate possible reasons for them. Our analysis shows that most of the cluster members we identified match those from previous studies. However, some stars were left out because their astrometry was of low precision, while a fraction of some stars happened to be outside our search radius, more details and comparative study on cluster membership can be found in Paper III and Paper IV.

1.10 Color-magnitude diagrams of NGC 6791 and NGC 6819

We used cluster members to construct the CMD in the G magnitude and $B_p - R_p$ color. We fitted isochrones in the CMDs of both clusters. We downloaded the grid of isochrones from the MESA Isochrones and Stellar Tracks (MIST) project (Choi et al., 2016). We used the grid calculated in the *Gaia* absolute magnitudes with $V/V_{\rm critical} = 0$. The magnitudes are not extinction corrected. Recent studies (Carraro et al. (2006), Paper III) showed NGC 6791 to be 7 – 9 Gyr old and metal rich with metallicity [Fe/H] = +0.3 – +0.4 (Villanova et al., 2018), while NGC 6819 to be 2 – 3 Gyr (Anthony-Twarog et al., 2014) old and with [Fe/H] = -0.1 – +0.1 (Bragaglia et al., 2001; Lee-Brown et al., 2015).

We used these results to initially constrain our selection of the MIST models in order to minimize the computational time.

The fitting was performed using only stars in the MS, RGB, RC and Asymptotic Giant Branch (AGB) regions. We excluded a few binary stars, whose magnitudes and colors do not appear to be of single stars. Since evolutionary stages are not uniformly populated we weighted the G magnitudes and the B_p-R_p color with their variance. It effectively balanced the more densely populated MS region with the less populated RC and RGB regions. We applied a horizontal shift (G-M_G) and a vertical shift $E(B_p - R_p)$ to account for the distance and interstellar extinction.

For NGC 6791, we derived age of 8.91 Gyr and [Fe/H] = 0.26 – 0.28. We derived the interstellar extinction to be $A_G = 0.342$ mag and the distance to the cluster of 4134 pc. The distance estimate is comparable with the value derived from the *Gaia* parallaxes of cluster members, which is 4123(31) pc. For NGC 6819, we obtained the following parameters: age of 2.53(3) Gyr, [Fe/H] = -0.01(2), interstellar extinction $A_G = 0.388$, and the distance of 2300 pc. The distance estimate agrees with the one derived from the parallaxes of the cluster members, which is 2480(180) pc.

Using the T_{eff} and log g parameters from the best fitted models, we created the T_{eff} – log g diagrams (HRD). The majority of stars show consistent positions in both CMD and HRD, although there are outlying stars in the HRD, which may reflect limitations of our spectroscopic fits.

1.11 Other results

The observed minus calculated (O-C) diagrams were used to explore a variability of orbital periods in the binaries that we found in both clusters. We developed an eclipse timing tool to extract eclipses, determine their mid-times, and construct O-C diagrams. The mid-times were derived using a description provided by Kwee and van Woerden (1956). We used ephemerides derived from data we analyzed.

1.11.1 NGC 6791

An active eclipsing binary *Gaia* EDR3 2051105342091761536 (KIC 2437783) shows an orbital variation of 249 days (Fig. 4 of Paper III). A contact binary *Gaia* EDR3 2051294114497255936 shows an O-C variation with a period of around 900 days, while another contact binary *Gaia* EDR3 2051291361416937856 shows an O-C variation with a period of around 90 days. The O-C diagrams of all three stars are presented in Fig. 4 of Paper III. An eclipsing binary *Gaia* EDR3 2051288372129693440 shows a shallow secondary eclipse at phase around 0.65 (Fig. 2 of Paper III), which indicates an eccentric orbit, while a non-member binary *Gaia* EDR3 2051104826700758016 shows a secondary eclipse at phase around 0.95 (Figure 1.12). The latter system has the longest orbital period (196.34 days), and the highest eccentricity of the orbit, among all (member and non-member) binaries we found in the area of this cluster.

1.11.2 NGC 6819

The O-C analysis reveals that a contact binary *Gaia* DR3 2076394105234042496 shows an orbital period variability of around 1000 days (Fig. 6 of Paper IV). In addition, we found significant O-C variations in three non-member binaries. We estimated orbital periods of two eclipsing binaries, *Gaia* EDR3 2076298864347818624 and *Gaia* EDR3 2076392838230907264, to be 771.81 days and almost 414.55 days, respectively. We detected only two eclipses in the data of the former system hence the

period estimation still needs to be confirmed. If so, it would be the longest orbital period among all binary systems we found in our analysis. The latter system has an eccentric orbit with varying depths in the secondary eclipse. We found a non-member binary system *Gaia* EDR3 2076487671098665472 with an orbital period of 225.28 days, in a highly eccentric orbit. These three non-member binary systems are shown in Figure 1.13.

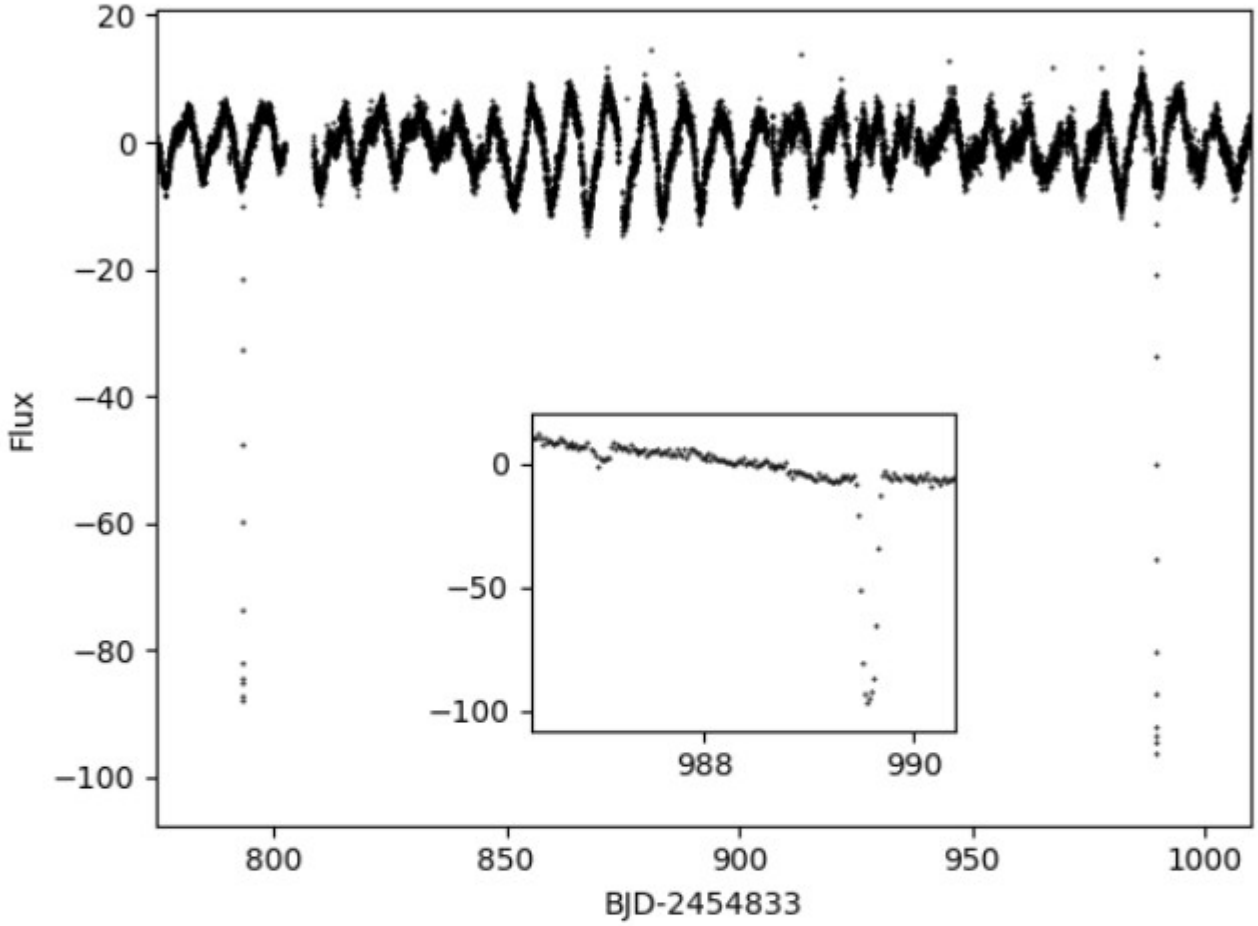

Figure 1.12: A close-up of time-series data of a non-member binary star in the area of NGC 6791, *Gaia* EDR3 2051104826700758016. The inset shows how close the secondary eclipse is to the primary eclipse, which reveals a highly eccentric orbit. An out-of-eclipse variation is prominent.

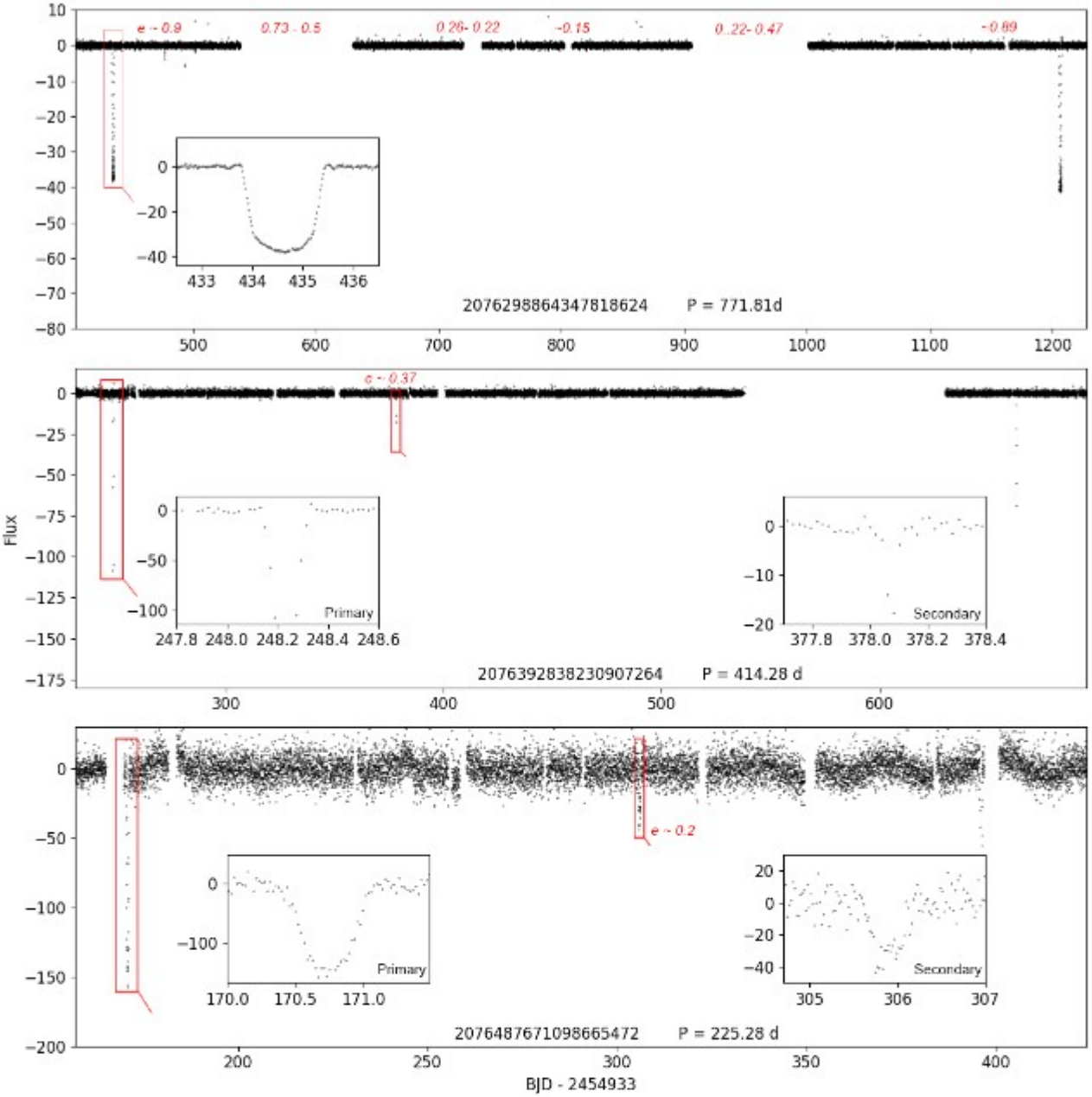

Figure 1.13: Close-ups of time-series data of three long-period binary stars in NGC 6819. *Gaia* EDR3 designations and orbital periods are given in each panel. A possible eccentricity of *Gaia* 2076298864347818624 is marked, assuming the secondary eclipse is missing because of the data gaps. A flux drop that may indicate an incomplete secondary eclipse at e~0.89 is also marked. For the other two stars, both types of eclipses are shown in inlets and rough estimations of eccentricities are provided.

1.12 Summary

We presented the results of our search for hot subdwarf pulsators within two open clusters NGC 6791 and NGC 6819, observed in the course of the *Kepler* mission. Below, we listed the significant results and caveats of our analysis.

1.12.1 Significant outcomes

- We confirmed three pulsating sdB stars in NGC 6791, while we found none in NGC 6819.
- We extended a list of detected pulsation periods in all three stars, including rotational multiplets and asymptotic period sequences, which we used toward mode geometry assignment and a rotation period estimation.
- Owing to spectroscopic observations we detected RV variations for three hot subdwarfs, members of NGC 6791, which indicate their possible binary status.
- We derived physical parameters and stellar interiors of four hot subdwarf pulsators, including two members of NGC 6791 and two field stars, for the first time utilizing evolutionary MESA and adiabatic GYRE models.
- The results of our modeling should help and encourage the scientific community to leverage further use of advanced MESA models towards evolutionary and stellar pulsation modeling of hot subdwarf pulsators.
- We found hundreds of new or previously known variable stars, most of them classified into three variable types and for many of them we derived spectroscopic parameters.
- We fitted isochrones and estimated age, metallicities and distances of both clusters. The distance estimates from the isochrone fitting are in agreement with the independent estimates from the *Gaia* parallaxes of cluster members.

1.12.2 Caveats

- A determination of spectroscopic parameters, which is instrument and atmospheric model dependent, influences seismic modeling.
- Cluster's parameters were not accepted to constrain seismic fitting.
- The evolutionary models we used are limited by the tip of the EHB branch, *i.e.* down to 10% of central helium, and they do not include a realistic hydrogen mass loss.
- The GYRE models we used are adiabatic.
- The grid resolutions for parameters such as mass of the hydrogen envelope, metallicity and central helium abundance could be larger, however it would come with the cost of more computational time needed.
- The metallicity of NGC 6791 members are not consistent.
- A population of pulsating hot subdwarf stars is not rich in open clusters, even those old ones, which hardly allows for a comparison between cluster and field counterparts.
- Spectroscopic estimates of variable stars we found during our survey are not coming from a uniform source, which can create a systematic shift between instruments and/or models used.

Bibliography

Ahn, C. P., Alexandroff, R., Allende Prieto, C., Anders, F., & et al. (2014). The Tenth Data Release of the Sloan Digital Sky Survey: First Spectroscopic Data from the SDSS-III Apache Point Observatory Galactic Evolution Experiment. *The Astrophysical Journal Supplement*, *211*(2), Article 17, 17. https://doi.org/10.1088/0067-0049/211/2/17

Altmann, M., Edelmann, H., & de Boer, K. S. (2004). Studying the populations of our Galaxy using the kinematics of sdB stars. *Astronomy and Astrophysics*, *414*, 181–201. https://doi.org/10.1051/0004-6361:20031606

Anthony-Twarog, B. J., Deliyannis, C. P., & Twarog, B. A. (2014). A uvbyCaHβ Analysis of the Old Open Cluster, NGC 6819. *The Astronomical Journal*, *148*(3), Article 51, 51. https://doi.org/10.1088/0004-6256/148/3/51

Baran, A., Oreiro, R., Pigulski, A., Pérez Hernández, F., & et al. (2009). The pulsating hot subdwarf Balloon 090100001: results of the 2005 multisite campaign. *Monthly Notices of the Royal Astronomical Society*, *392*(3), 1092–1105. https://doi.org/10.1111/j.1365-2966.2008.14024.x

Baran, A., Pigulski, A., Kozieł, D., Ogłoza, W., & et al. (2005). Multicolour photometry of Balloon 090100001: linking the two classes of pulsating hot subdwarfs. *Monthly Notices of the Royal Astronomical Society*, *360*(2), 737–747. https://doi.org/10.1111/j.1365-2966.2005.09066.x

Baran, A., & Sanjayan, S. (2023b). Sounding Interiors of Four Pulsating Subdwarf B Stars with Stellar Pulsations. *Acta Astronomica*, *73*(1), 21–34. https://doi.org/10.32023/0001-5237/73.1.2

Baran, A., Van Grootel, V., Østensen, R. H., Worters, H. L., & et al. (2023a). Short-period pulsating hot-subdwarf stars observed by TESS. I. Southern ecliptic hemisphere. *Astronomy and Astrophysics*, *669*, Article A48, A48. https://doi.org/10.1051/0004-6361/202244888

Baran, A., & Winans, A. (2012). Mode Identification of Three Pulsating Subdwarf B Stars via Multiplets and Period Spacing. *Acta Astronomica*, *62*(4), 343–355.

Battich, T., Miller Bertolami, M. M., Córsico, A. H., & Althaus, L. G. (2018). Pulsational instabilities driven by the $\in$ mechanism in hot pre-horizontal branch stars. I. The hot-flasher scenario. *Astronomy and Astrophysics*, *614*, Article A136, A136. https://doi.org/10.1051/0004-6361/201731463

Blanton, M. R., Bershady, M. A., Abolfathi, B., Albareti, F. D., & et al. (2017). Sloan Digital Sky Survey IV: Mapping the Milky Way, Nearby Galaxies, and the Distant Universe. *The Astronomical Journal*, *154*(1), Article 28, 28. https://doi.org/10.3847/1538-3881/aa7567

Bohlin, R. C., Mészáros, S., Fleming, S. W., Gordon, K. D., & et al. (2017). A New Stellar Atmosphere Grid and Comparisons with HST/STIS CALSPEC Flux Distributions. *The Astronomical Journal*, *153*(5), Article 234, 234. https://doi.org/10.3847/1538-3881/aa6ba9

Bragaglia, A., Tosi, M., Carretta, E., & Gratton, R. G. (2001). Metallicity of Old Open Clusters. In E. Vangioni-Flam, R. Ferlet, & M. Lemoine (Eds.), *Cosmic evolution* (p. 209). https://doi.org/10.1142/9789812810830_0047

Brown, T. M., Ferguson, H. C., & Davidsen, A. F. (1997). A Far Ultraviolet Analysis of the Stellar Populations in Six Elliptical and SO Galaxies. In M. Arnaboldi, G. S. Da Costa, & P. Saha (Eds.), *The nature of elliptical galaxies; 2nd stromlo symposium* (p. 220).

Brown, T. M., Ferguson, H. C., Stanford, S. A., & Deharveng, J.-M. (1998). Color-Luminosity Relations for the Resolved Hot Stellar Populations in the Centers of M31 and M32. *The Astrophysical Journal*, *504*(1), 113–138. https://doi.org/10.1086/306079

Bruntt, H., Grundahl, F., Tingley, B., Frandsen, S., & et al. (2003). A search for planets in the old open cluster NGC 6791. *Astronomy and Astrophysics*, *410*, 323–335. https://doi.org/10.1051/0004-6361:20031198

Cantat-Gaudin, T., Jordi, C., Vallenari, A., Bragaglia, A., & et al. (2018). A Gaia DR2 view of the open cluster population in the Milky Way. *Astronomy and Astrophysics*, *618*, Article A93, A93. https://doi.org/10.1051/0004-6361/201833476

Carraro, G., Villanova, S., Demarque, P., McSwain, M. V., & et al. (2006). NGC 6791: An Exotic Open Cluster or the Nucleus of a Tidally Disrupted Galaxy? *The Astrophysical Journal*, *643*(2), 1151–1159. https://doi.org/10.1086/500801

Charpinet, S., Brassard, P., Fontaine, G., Van Grootel, V., & et al. (2019). TESS first look at evolved compact pulsators. Discovery and asteroseismic probing of the g-mode hot B subdwarf pulsator EC 21494-7018. *Astronomy and Astrophysics*, *632*, Article A90, A90. https://doi.org/10.1051/0004-6361/201935395

Charpinet, S., Fontaine, G., Brassard, P., Chayer, P., & et al. (1997). A Driving Mechanism for the Newly Discovered Class of Pulsating Subdwarf B Stars. *The Astrophysical Journal Letters*, *483*(2), L123–L126. https://doi.org/10.1086/310741

Charpinet, S., Fontaine, G., Brassard, P., & Dorman, B. (1996). The Potential of Asteroseismology for Hot, Subdwarf B Stars: A New Class of Pulsating Stars? *The Astrophysical Journal Letters*, *471*, L103. https://doi.org/10.1086/310335

Charpinet, S., Fontaine, G., Brassard, P., & Dorman, B. (2000). Adiabatic Survey of Subdwarf B Star Oscillations. I. Pulsation Properties of a Representative Evolutionary Model. *The Astrophysical Journal Supplement*, *131*(1), 223–247. https://doi.org/10.1086/317359

Charpinet, S., Fontaine, G., Brassard, P., & Dorman, B. (2002). Adiabatic Survey of Subdwarf B Star Oscillations. III. Effects of Extreme Horizontal Branch Stellar Evolution on Pulsation Modes. *The Astrophysical Journal Supplement*, *140*(2), 469–561. https://doi.org/10.1086/339707

Charpinet, S., Fontaine, G., Brassard, P., Green, E. M., & et al. (2011a). A compact system of small planets around a former red-giant star. *Nature*, *480*(7378), 496–499. https://doi.org/10.1038/nature10631

Charpinet, S., Van Grootel, V., Fontaine, G., Green, E. M., & et al. (2011b). Deep asteroseismic sounding of the compact hot B subdwarf pulsator KIC02697388 from Kepler time series photometry. *Astronomy and Astrophysics*, *530*, Article A3, A3. https://doi.org/10.1051/0004-6361/201016412

Charpinet, S., Van Grootel, V., Reese, D., Fontaine, G., & et al. (2008). Testing the forward modeling approach in asteroseismology. II. Structure and internal dynamics of the hot B subdwarf

component in the close eclipsing binary system PG 1336-018. *Astronomy and Astrophysics*, *489*(1), 377–394. https://doi.org/10.1051/0004-6361:200809907

Charpinet, S., Giammichele, N., Zong, W., Van Grootel, V., & et al. (2018). Rotation in sdB stars as revealed by stellar oscillations. *Open Astronomy*, *27*(1), 112–119. https://doi.org/10.1515/astro-2018-0012

Choi, J., Dotter, A., Conroy, C., Cantiello, M., & et al. (2016). Mesa Isochrones and Stellar Tracks (MIST). I. Solar-scaled Models. *The Astrophysical Journal*, *823*(2), Article 102, 102. https://doi.org/10.3847/0004-637X/823/2/102

Constantino, T., Campbell, S. W., Lattanzio, J. C., & van Duijneveldt, A. (2016). The treatment of mixing in core helium burning models - II. Constraints from cluster star counts. *Monthly Notices of the Royal Astronomical Society*, *456*(4), 3866–3885. https://doi.org/10.1093/mnras/stv2939

Cooley, J. W., & Tukey, J. W. (1965). An algorithm for the machine calculation of complex fourier series. *Mathematics of Computation*, *19*, 297–301. https://doi.org/10.1090/S0025-5718-1965-0178586-1

Copperwheat, C. M., Morales-Rueda, L., Marsh, T. R., Maxted, P. F. L., & et al. (2011). Radial-velocity measurements of subdwarf B stars. *Monthly Notices of the Royal Astronomical Society*, *415*(2), 1381–1395. https://doi.org/10.1111/j.1365-2966.2011.18786.x

D'Cruz, N. L., Dorman, B., Rood, R. T., & O'Connell, R. W. (1996). The Origin of Extreme Horizontal Branch Stars. *The Astrophysical Journal*, *466*, 359. https://doi.org/10.1086/177515

de Marchi, F., Poretti, E., Montalto, M., Piotto, G., & et al. (2007). Variable stars in the open cluster NGC 6791 and its surrounding field. *Astronomy and Astrophysics*, *471*(2), 515–526. https://doi.org/10.1051/0004-6361:20077386

Dempster, A. P., Laird, N. M., & Rubin, D. B. (1977). Maximum likelihood from incomplete data via the em algorithm. *Journal of the Royal Statistical Society: Series B (Methodological)*, *39*(1), 1–22. https://doi.org/10.1111/j.2517-6161.1977.tb01600.x

Fabricant, D., Fata, R., Roll, J., Hertz, E., & et al. (2005). Hectospec, the MMT's 300 Optical Fiber-Fed Spectrograph. *Publications of the Astronomical Society of the Pacific*, *117*(838), 1411–1434. https://doi.org/10.1086/497385

Ferguson, T. S. (1973). A bayesian analysis of some nonparametric problems. *The Annals of Statistics*, *1*(2), 209–230. http://www.jstor.org/stable/2958008

Fontaine, G., Brassard, P., Charpinet, S., Green, E. M., & et al. (2012). A preliminary look at the empirical mass distribution of hot B subdwarf stars. *Astronomy and Astrophysics*, *539*, Article A12, A12. https://doi.org/10.1051/0004-6361/201118220

Gaia Collaboration, Vallenari, A., Brown, A. G. A., Prusti, T., & et al. (2022). Gaia Data Release 3: Summary of the content and survey properties. *arXiv e-prints*, Article arXiv:2208.00211, arXiv:2208.00211.

Gao, X. (2020). 5D memberships and fundamental properties of the old open cluster NGC 6791 based on Gaia -DR2. *Astrophysics and Space Science*, *365*(2), Article 24, 24. https://doi.org/10.1007/s10509-020-3738-2

Gilmore, G., Randich, S., Asplund, M., Binney, J., & et al. (2012). The Gaia-ESO Public Spectroscopic Survey. *The Messenger*, *147*, 25–31.

Gosnell, N. M., Pooley, D., Geller, A. M., Kalirai, J., & et al. (2012). An Unexpected Discovery in the Rich Open Cluster NGC 6819 Using XMM-Newton. *The Astrophysical Journal*, *745*(1), Article 57, 57. https://doi.org/10.1088/0004-637X/745/1/57

Gough, D. O. (1986). EBK Quantization of Stellar Waves. In Y. Osaki (Ed.), *Hydrodynamic and magnetodynamic problems in the sun and stars* (p. 117). https://ui.adsabs.harvard.edu/abs/1986hmps.conf..117G

Green, E. M., Fontaine, G., Reed, M. D., Callerame, K., & et al. (2003). Discovery of A New Class of Pulsating Stars: Gravity-Mode Pulsators among Subdwarf B Stars. *The Astrophysical Journal Letters*, *583*(1), L31–L34. https://doi.org/10.1086/367929

Green, R. F., Schmidt, M., & Liebert, J. (1986). The Palomar-Green Catalog of Ultraviolet-Excess Stellar Objects. *The Astrophysical Journal Supplement*, *61*, 305. https://doi.org/10.1086/191115

Guzik, J. A., Baran, A. S., Sanjayan, S., Németh, P., & et al. (2023). Variable Blue Straggler Stars in the Open Cluster NGC 6819 Observed in the Kepler Superstamp Field. *The Astronomical Journal*, *165*(5), Article 188, 188. https://doi.org/10.3847/1538-3881/acc0f0

Han, Z., Podsiadlowski, P., Maxted, P. F. L., Marsh, T. R., & et al. (2002). The origin of subdwarf B stars - I. The formation channels. *Monthly Notices of the Royal Astronomical Society*, *336*(2), 449–466. https://doi.org/10.1046/j.1365-8711.2002.05752.x

Han, Z. (2003). Binary Evolution – Problems and Applications. In S. Ikeuchi, J. Hearnshaw, & T. Hanawa (Eds.), *The proceedings of the iau 8th asian-pacific regional meeting, volume 1* (pp. 413–420). https://ui.adsabs.harvard.edu/abs/2003ASPC..289..413H

Hartman, J. D., Stanek, K. Z., Gaudi, B. S., Holman, M. J., & et al. (2005). Pushing the Limits of Ground-based Photometric Precision: Submillimagnitude Time-Series Photometry of the Open Cluster NGC 6791. *The Astronomical Journal*, *130*(5), 2241–2251. https://doi.org/10.1086/462405

Heber, U. (2009). Hot Subdwarf Stars. *Annual Review of Astronomy and Astrophysics*, *47*(1), 211–251. https://doi.org/10.1146/annurev-astro-082708-101836

Heber, U. (2016). Hot Subluminous Stars. *Publications of the Astronomical Society of the Pacific*, *128*(966), 082001. https://doi.org/10.1088/1538-3873/128/966/082001

Heber, U., Kudritzki, R. P., Caloi, V., Castellani, V., & et al. (1986). A spectroscopic study of HB stars in the galactic globular cluster NGC 6752. *Astronomy and Astrophysics*, *162*, 171–179.

Hubeny, I., & Lanz, T. (1995). Non-LTE Line-blanketed Model Atmospheres of Hot Stars. I. Hybrid Complete Linearization/Accelerated Lambda Iteration Method. *The Astrophysical Journal*, *439*, 875. https://doi.org/10.1086/175226

Hubeny, I., & Lanz, T. (2017). A brief introductory guide to TLUSTY and SYNSPEC. *arXiv e-prints*, Article arXiv:1706.01859, arXiv:1706.01859. https://doi.org/10.48550/arXiv.1706.01859

Humason, M. L., & Zwicky, F. (1947). A Search for Faint Blue Stars. *The Astrophysical Journal*, *105*, 85. https://doi.org/10.1086/144884

Kaluzny, J., & Rucinski, S. M. (1993). Discovery of 17 variable stars in the old open cluster NGC 6791. *Monthly Notices of the Royal Astronomical Society*, *265*, 34–42. https://doi.org/10.1093/mnras/265.1.34

Kaluzny, J., & Udalski, A. (1992). Photometric Study of the Old Open Cluster NGC 6791. *Acta Astronomica*, *42*, 29–47.

Kaluzny, J. (2003). Variable Yellow and Red Stragglers in the Old Open Cluster NGC 6791. *Acta Astronomica*, *53*, 51–62. https://doi.org/10.48550/arXiv.astro-ph/0303405

Kaluzny, J., & Shara, M. M. (1988). A CCD Survey for Contact Binaries in Six Open Clusters. *The Astronomical Journal*, *95*, 785. https://doi.org/10.1086/114677

Kilkenny, D., Koen, C., O'Donoghue, D., & Stobie, R. S. (1997). A new class of rapidly pulsating star - I. EC 14026-2647, the class prototype. *Monthly Notices of the Royal Astronomical Society*, *285*(3), 640–644. https://doi.org/10.1093/mnras/285.3.640

Kinemuchi, K., Barclay, T., Fanelli, M., Pepper, J., & et al. (2012). Demystifying Kepler Data: A Primer for Systematic Artifact Mitigation. *Publications of the Astronomical Society of the Pacific*, *124*(919), 963. https://doi.org/10.1086/667603

Kramer, M., Schneider, F. R. N., Ohlmann, S. T., Geier, S., & et al. (2020). Formation of sdB-stars via common envelope ejection by substellar companions. *Astronomy and Astrophysics*, *642*, Article A97, A97. https://doi.org/10.1051/0004-6361/202038702

Kryachko, T. V. (2001). New Dwarf Novae on Moscow Plates. *Information Bulletin on Variable Stars*, *5058*, 1.

Kwee, K. K., & van Woerden, H. (1956). A method for computing accurately the epoch of minimum of an eclipsing variable. *Bulletin of the Astronomical Institutes of the Netherlands*, *12*, 327.

Landsman, W., Bohlin, R. C., Neff, S. G., O'Connell, R. W., & et al. (1998). The Hot Stars of Old Open Clusters: M67, NGC 188, and NGC 6791. *The Astronomical Journal*, *116*(2), 789–800. https://doi.org/10.1086/300449

Lee-Brown, D. B., Anthony-Twarog, B. J., Deliyannis, C. P., Rich, E., & et al. (2015). Spectroscopic Abundances in the Open Cluster NGC 6819. *The Astronomical Journal*, *149*(4), Article 121, 121. https://doi.org/10.1088/0004-6256/149/4/121

Lindoff, U. (1971). A Late Type Variable in NGC 6819. *Information Bulletin on Variable Stars*, *606*, 1.

Majewski, S. R., Schiavon, R. P., Frinchaboy, P. M., Allende Prieto, C., & et al. (2017). The Apache Point Observatory Galactic Evolution Experiment (APOGEE). *The Astronomical Journal*, *154*(3), Article 94, 94. https://doi.org/10.3847/1538-3881/aa784d

Manteiga, M., Pickles, A. J., & Martinez-Roger, C. (1989). Blue stragglers and the binary hypothesis. *Astronomy and Astrophysics*, *210*, 66–77.

Maxted, P. F. L., Heber, U., Marsh, T. R., & North, R. C. (2001). The binary fraction of extreme horizontal branch stars. *Monthly Notices of the Royal Astronomical Society*, *326*(4), 1391–1402. https://doi.org/10.1111/j.1365-2966.2001.04714.x

Mochejska, B. J., Stanek, K. Z., & Kaluzny, J. (2003). Long-Term Variability Survey of the Old Open Cluster NGC 6791. *The Astronomical Journal*, *125*(6), 3175–3184. https://doi.org/10.1086/374993

Mochejska, B. J., Stanek, K. Z., Sasselov, D. D., & Szentgyorgyi, A. H. (2002). Planets in Stellar Clusters Extensive Search. I. Discovery of 47 Low-Amplitude Variables in the Metal-rich Cluster NGC 6791 with Millimagnitude Image Subtraction Photometry. *The Astronomical Journal*, *123*(6), 3460–3472. https://doi.org/10.1086/340695

Mochejska, B. J., Stanek, K. Z., Sasselov, D. D., Szentgyorgyi, A. H., & et al. (2005). Planets in Stellar Clusters Extensive Search. III. A Search for Transiting Planets in the Metal-rich Open Cluster NGC 6791. *The Astronomical Journal*, *129*(6), 2856–2868. https://doi.org/10.1086/430219

Moehler, S. (2001). Hot Stars in Globular Clusters: A Spectroscopist's View. *Publications of the Astronomical Society of the Pacific*, *113*(788), 1162–1177. https://doi.org/10.1086/323297

Moehler, S., Heber, U., & Rupprecht, G. (1997). Hot HB stars in globular clusters: physical parameters and consequences for theory III. NGC 6752 and its long blue vertical branch. *Astronomy and Astrophysics*, *319*, 109–121. https://doi.org/10.48550/arXiv.astro-ph/9607151

Moehler, S., Heber, U., Saffer, R., & Thejll, P. (1995). Hot Subdwarfs in Globular Clusters. *American Astronomical Society Meeting Abstracts*, *187*, Article 82.02, 82.02.

Moni Bidin, C., Moehler, S., Piotto, G., Momany, Y., & et al. (2009). A lack of close binaries among hot horizontal branch stars in globular clusters. M 80 and NGC 5986. *Astronomy and Astrophysics*, *498*(3), 737–751. https://doi.org/10.1051/0004-6361/200810579

Moni-Bidin, C. M. (2006). Spectroscopy of Hot Horizontal Branch Stars in Globular Clusters. *Revista Mexicana de Astronomia y Astrofisica Conference Series*, *26*, 174.

Napiwotzki, R., Karl, C. A., Lisker, T., Heber, U., & et al. (2004). Close binary EHB stars from SPY. *Astrophysics and Space Science*, *291*(3), 321–328. https://doi.org/10.1023/B:ASTR.0000044362.07416.6c

Németh, P., Kawka, A., & Vennes, S. (2012). A selection of hot subluminous stars in the GALEX survey - II. Subdwarf atmospheric parameters. *Monthly Notices of the Royal Astronomical Society*, *427*(3), 2180–2211. https://doi.org/10.1111/j.1365-2966.2012.22009.x

O'Connell, R. W. (1999). Far-Ultraviolet Radiation from Elliptical Galaxies. *Annual Review of Astronomy and Astrophysics*, *37*, 603–648. https://doi.org/10.1146/annurev.astro.37.1.603

Ostrowski, J., Baran, A. S., Sanjayan, S., & Sahoo, S. K. (2021). Evolutionary modelling of subdwarf B stars using MESA with the predictive mixing and convective pre-mixing schemes. *Monthly Notices of the Royal Astronomical Society*, *503*(3), 4646–4661. https://doi.org/10.1093/mnras/staa3751

Paxton, B., Schwab, J., Bauer, E. B., Bildsten, L., & et al. (2018). Modules for Experiments in Stellar Astrophysics (MESA): Convective Boundaries, Element Diffusion, and Massive Star Explosions. *The Astrophysical Journal Supplement*, *234*(2), Article 34, 34. https://doi.org/10.3847/1538-4365/aaa5a8

Pedregosa, F., Varoquaux, G., Gramfort, A., Michel, V., & et al. (2011). Scikit-learn: Machine learning in Python. *Journal of Machine Learning Research*, *12*, 2825–2830. https://doi.org/10.5555/1953048.2078195

Randich, S., Gilmore, G., & Gaia-ESO Consortium. (2013). The Gaia-ESO Large Public Spectroscopic Survey. *The Messenger*, *154*, 47–49.

Reed, M. D., Baran, A., Quint, A. C., Kawaler, S. D., & et al. (2011). First Kepler results on compact pulsators - VIII. Mode identifications via period spacings in g-mode pulsating subdwarf B stars. *Monthly Notices of the Royal Astronomical Society*, *414*(4), 2885–2892. https://doi.org/10.1111/j.1365-2966.2011.18532.x

Rucinski, S. M., Kaluzny, J., & Hilditch, R. W. (1996). A search for detached eclipsing binary systems in the oldest known open cluster NGC 6791. *Monthly Notices of the Royal Astronomical Society*, *282*(3), 705–712. https://doi.org/10.1093/mnras/282.3.705

Salaris, M., Weiss, A., & Percival, S. M. (2004). The age of the oldest Open Clusters. *Astronomy and Astrophysics*, *414*, 163–174. https://doi.org/10.1051/0004-6361:20031578

Salaris, M., & Cassisi, S. (2017). Chemical element transport in stellar evolution models. *Royal Society Open Science*, *4*(8), Article 170192, 170192. https://doi.org/10.1098/rsos.170192

Salgado, C., Moni Bidin, C., Villanova, S., Geisler, D., & et al. (2013). Spectroscopy of blue horizontal branch stars in NGC 6656 (M 22). *Astronomy and Astrophysics*, *559*, Article A101, A101. https://doi.org/10.1051/0004-6361/201321469

Sanjayan, S., Baran, A. S., Németh, P., & Kinemuchi, K. (2023). Variable Star Population in the Open Cluster NGC 6819 Observed by the Kepler Spacecraft. *Acta Astronomica*, *72*(4), 267–295. https://doi.org/10.32023/0001-5237/72.4.3

Sanjayan, S., Baran, A. S., Németh, P., Kinemuchi, K., & et al. (2022b). Variable Star Population in the Open Cluster NGC 6791 Observed by the Kepler Spacecraft. *Acta Astronomica*, *72*(2), 77–102. https://doi.org/10.32023/0001-5237/72.2.1

Sanjayan, S., Baran, A. S., Ostrowski, J., Németh, P., & et al. (2022). Pulsating subdwarf B stars in the oldest open cluster NGC 6791. *Monthly Notices of the Royal Astronomical Society*, *509*(1), 763–777. https://doi.org/10.1093/mnras/stab2985

Schuh, S., Huber, J., Dreizler, S., Green, E. M., & et al. (2006). Exciting new features in the frequency spectrum of the EC 14026 star HS 0702+6043. Simultaneous g-modes and p-modes in a sdB pulsator. *Memorie della Società Astronomica Italiana*, *77*, 480. https://ui.adsabs.harvard.edu/abs/2006MmSAI..77..480S

Stello, D., Basu, S., Bruntt, H., Mosser, B., & et al. (2010). Detection of Solar-like Oscillations from Kepler Photometry of the Open Cluster NGC 6819. *The Astrophysical Journal Letters*, *713*(2), L182–L186. https://doi.org/10.1088/2041-8205/713/2/L182

Street, R. A., Horne, K., Lister, T. A., Penny, A., & et al. (2002). Variable stars in the field of open cluster NGC 6819. *Monthly Notices of the Royal Astronomical Society*, *330*(3), 737–754. https://doi.org/10.1046/j.1365-8711.2002.05125.x

Street, R. A., Horne, K., Lister, T. A., Penny, A., & et al. (2005). Variable stars in the field of open cluster NGC 6819 - II. *Monthly Notices of the Royal Astronomical Society*, *358*(3), 795–812. https://doi.org/10.1111/j.1365-2966.2005.08751.x

Street, R. A., Horne, K., Lister, T. A., Penny, A. J., & et al. (2003). Searching for planetary transits in the field of open cluster NGC 6819 - I. *Monthly Notices of the Royal Astronomical Society*, *340*(4), 1287–1297. https://doi.org/10.1046/j.1365-8711.2003.06388.x

Sweigart, A. V. (1997). Effects of Helium Mixing on the Evolution of Globular Cluster Stars. *The Astrophysical Journal Letters*, *474*(1), L23–L26. https://doi.org/10.1086/310414

Talamantes, A., Sandquist, E. L., Clem, J. L., Robb, R. M., & et al. (2010). Bright Variable Stars in NGC 6819: An Open Cluster in The Kepler Field. *The Astronomical Journal*, *140*(5), 1268–1281. https://doi.org/10.1088/0004-6256/140/5/1268

Tassoul, M. (1980). Asymptotic approximations for stellar nonradial pulsations. *The Astrophysical Journal Supplement*, *43*, 469–490. https://doi.org/10.1086/190678

Thuillier, A., Van Grootel, V., Dévora-Pajares, M., Pozuelos, F. J., & et al. (2022). A search for transiting planets around hot subdwarfs. II. Supplementary methods and results from TESS Cycle 1. *Astronomy and Astrophysics*, *664*, Article A113, A113. https://doi.org/10.1051/0004-6361/202243554

Townsend, R. H. D., & Teitler, S. A. (2013). GYRE: an open-source stellar oscillation code based on a new Magnus Multiple Shooting scheme. *Monthly Notices of the Royal Astronomical Society*, *435*, 3406–3418. https://doi.org/10.1093/mnras/stt1533

Unno, W., Osaki, Y., Ando, H., & Shibahashi, H. (1979). Nonradial oscillations of stars. *University of Tokyo Press; Forest Grove, Ore., ISBS, Inc., 1979. 330 p.*

Van Grootel, V., Charpinet, S., Fontaine, G., Brassard, P., & et al. (2008). Testing the forward modeling approach in asteroseismology. I. Seismic solutions for the hot B subdwarf Balloon 090100001 with and without a priori mode identification. *Astronomy and Astrophysics*, *488*(2), 685–696. https://doi.org/10.1051/0004-6361:200809867

Van Grootel, V., Charpinet, S., Fontaine, G., Brassard, P., & et al. (2010b). *The Astrophysical Journal Letters*, *718*(2), L97–L101. https://doi.org/10.1088/2041-8205/718/2/L97

Van Grootel, V., Charpinet, S., Fontaine, G., Green, E. M., & et al. (2010a). Structural and core parameters of the hot B subdwarf KPD 0629-0016 from CoRoT g-mode asteroseismology. *Astronomy and Astrophysics*, *524*, Article A63, A63. https://doi.org/10.1051/0004-6361/201015437

Van Grootel, V., Pozuelos, F. J., Thuillier, A., Charpinet, S., & et al. (2021). VizieR Online Data Catalog: Search for transiting planets around sdBs (Van Grootel+, 2021). *VizieR Online Data Catalog*, Article J/A+A/650/A205, J/A+A/650/A205.

Villanova, S., Carraro, G., Geisler, D., Monaco, L., & et al. (2018). NGC 6791: A Probable Bulge Cluster without Multiple Populations. *The Astrophysical Journal*, *867*(1), Article 34, 34. https://doi.org/10.3847/1538-4357/aae4e5

Vučković, M., Aerts, C., Östensen, R., Nelemans, G., & et al. (2007). The binary properties of the pulsating subdwarf B eclipsing binary <ASTROBJ>PG 1336-018</ASTROBJ> (NY Virginis). *Astronomy and Astrophysics*, *471*(2), 605–615. https://doi.org/10.1051/0004-6361:20077179

Wang, B., & Han, Z. (2009). Companion stars of type Ia supernovae and hypervelocity stars. *Astronomy and Astrophysics*, *508*(2), L27–L30. https://doi.org/10.1051/0004-6361/200913326

Webbink, R. F. (1984). Double white dwarfs as progenitors of R Coronae Borealis stars and type I supernovae. *The Astrophysical Journal*, *277*, 355–360. https://doi.org/10.1086/161701

Zhao, G., Zhao, Y.-H., Chu, Y.-Q., Jing, Y.-P., & et al. (2012). LAMOST spectral survey — An overview. *Research in Astronomy and Astrophysics*, *12*(7), 723–734. https://doi.org/10.1088/1674-4527/12/7/002

Chapter 2

Paper I: Pulsating subdwarf B stars in the oldest open cluster NGC 6791

Abstract

We report results of our analysis of the *Kepler* super aperture LC data of the open cluster NGC 6791 to search for pulsating sdB stars. We checked all pixels and we found only three sdB stars to be pulsating, KIC 2569576 (B3), KIC 2438324 (B4) and KIC 2437937 (B5). These stars were known to be pulsators before, though we extended data coverage detecting more frequencies and features in their amplitude spectra, *i.e.* new multiplets and more complete period spacing sequences that we used for identifying geometry of the pulsation modes. The multiplet splittings were also used to derive rotation periods. The remaining known sdBs do not show any pulsation-related light variation down to our detection thresholds. We analyzed already existing spectroscopic observations taken with the HECTOSPEC at the MMT telescope in Smithsonian Arizona and with the GMOS at the Gemini North telescope, and fitted atmospheric parameters using the Balmer lines. Four stars, B3–B6, show atmospheric parameters that are consistent with g-mode dominated sdBs. We detected hints of radial velocity variability in B3, B5 and B6, indicating these three stars may be in binaries.

Monthly Notices of the ROYAL ASTRONOMICAL SOCIETY

MNRAS **509,** 763–777 (2022) https://doi.org/10.1093/mnras/stab2985
Advance Access publication 2021 October 19

Pulsating subdwarf B stars in the oldest open cluster NGC 6791

S. Sanjayan [1,2]★ A. S. Baran [1,3,4] J. Ostrowski [1] P. Németh [1,5,6] I. Pelisoli [7] R. Østensen,[1,4,8] J. W. Kern,[9] M. D. Reed [1,4] and S. K. Sahoo [1,2]

[1]*ARDASTELLA Research Group, Institute of Physics, Pedagogical University of Cracow, ul. Podchorążych 2, 30-084 Kraków, Poland*
[2]*Centrum Astronomiczne im. Mikołaja Kopernika, Polskiej Akademii Nauk, ul. Bartycka 18, 00-716 Warszawa, Polska*
[3]*Embry-Riddle Aeronautical University, Department of Physical Science, Daytona Beach, FL 32114, USA*
[4]*Department of Physics, Astronomy, and Materials Science, Missouri State University, Springfield, MO 65897, USA*
[5]*Astronomical Institute of the Czech Academy of Sciences, Fričova 298, CZ-251 65 Ondřejov, Czech Republic*
[6]*Astroserver.org, Fő tér 1, 8533 Malomsok, Hungary*
[7]*Department of Physics, University of Warwick, Coventry, CV4 7AL, UK*
[8]*Recogito AS, Storgaten 72, N-8200 Fauske, Norway*
[9]*Clemson University, Department of Physics and Astronomy, Clemson, SC 29631, USA*

Accepted 2021 October 12. Received 2021 October 11; in original form 2021 April 22

ABSTRACT

We report results of our analysis of the *Kepler* superaperture LC data of the open cluster NGC 6791 to search for pulsating sdB stars. We checked all pixels and we found only three sdB stars to be pulsating, KIC 2569576 (B3), KIC 2438324 (B4), and KIC 2437937 (B5). These stars were known to be pulsators before, though we extended data coverage detecting more frequencies and features in their amplitude spectra, i.e. new multiplets and more complete period spacing sequences that we used for identifying geometry of the pulsation modes. The multiplet splittings were also used to derive rotation periods. The remaining known sdBs do not show any pulsation-related light variation down to our detection thresholds. We analysed already existing spectroscopic observations taken with the HECTOSPEC at the MMT telescope in Smithsonian Arizona and with the Gemini Multi-Object Spectrograph at the Gemini North telescope, and fitted atmospheric parameters using the Balmer lines. Four stars, B3 – B6, show atmospheric parameters that are consistent with g-mode dominated sdBs. We detected hints of radial velocity variability in B3, B5, and B6, indicating these three stars may be in binaries.

Key words: asteroseismology – stars: oscillations – subdwarfs – galaxies: star clusters: general.

1 INTRODUCTION

Hot subdwarf B (sdB) stars are extreme horizontal branch objects. They consist of helium burning cores and very thin (<1 per cent in mass) hydrogen envelopes. SdB stars are compact objects with a typical mass of 0.47 $M_\odot$ (Fontaine et al. 2012), and surface gravity $\log(g/\mathrm{cm\,s^{-2}})$ of 5.0–5.8, hence their radii fall in a range of 0.1–0.3 $R_\odot$ (Heber 2016). The effective temperatures of sdB stars range between 20 000 and 40 000 K. It is generally accepted that sdB stars are descendants of low mass main-sequence stars (0.7–1.9 $M_\odot$), which have lost most of their hydrogen envelopes before the helium flash occurred (Heber 2016). Since the sdB stars have very thin (in mass) hydrogen envelopes, they are not able to sustain hydrogen shell burning, hence they will not evolve to the asymptotic giant branch but will go directly to the white dwarf cooling track, instead. The envelope can be removed during a binary evolution through common envelope ejection, Roche lobe overflow or white dwarf mergers (Han et al. 2002, 2003). The outcome of the two former cases becomes a binary system while of the latter a single star.

SdB stars became more interesting for study after pulsations were predicted and detected in these stars by Charpinet et al. (1997) and Kilkenny et al. (1997), respectively. Pulsating subdwarf B (sdBV) stars show two types of flux variation. The first, associated with short period pressure modes (p-modes), has pulsation periods of the order of minutes and amplitudes of pulsation modes reaching tens of mmag. The sdBVs showing p-modes are often called V361 Hya stars, after the prototype (Kilkenny et al. 1997). The second, associated with long period gravity modes (g-modes), has pulsation periods of the order of hours and amplitudes of pulsation modes below 10 mmag. The sdBVs showing g-modes are often called V1093 Her stars, after the prototype (Green et al. 2003). Some sdBV stars exhibit the hybrid phenomenon, where both p- and g-modes are present. Hybrids are sometimes referred to as DW Lyn stars, after the first hybrid sdBV detection (Schuh et al. 2006). Other hybrid sdBV are reported by Baran et al. (e.g. 2009); Reed et al. (e.g. 2014).

The *Kepler* spacecraft was launched in 2009, and observing for almost a decade, it has collected enormous amounts of photometric data of unprecedented quality. The first (original) *Kepler* mission lasted 1 460 days, during which 0.25 per cent of the sky was monitored. After two of the spacecraft's reaction wheels broke, the mission was reborn with its limited capabilities. During the second mission, called K2, *Kepler* observed along the ecliptic equator in so-

★ E-mail: sachusanjayan@gmail.com

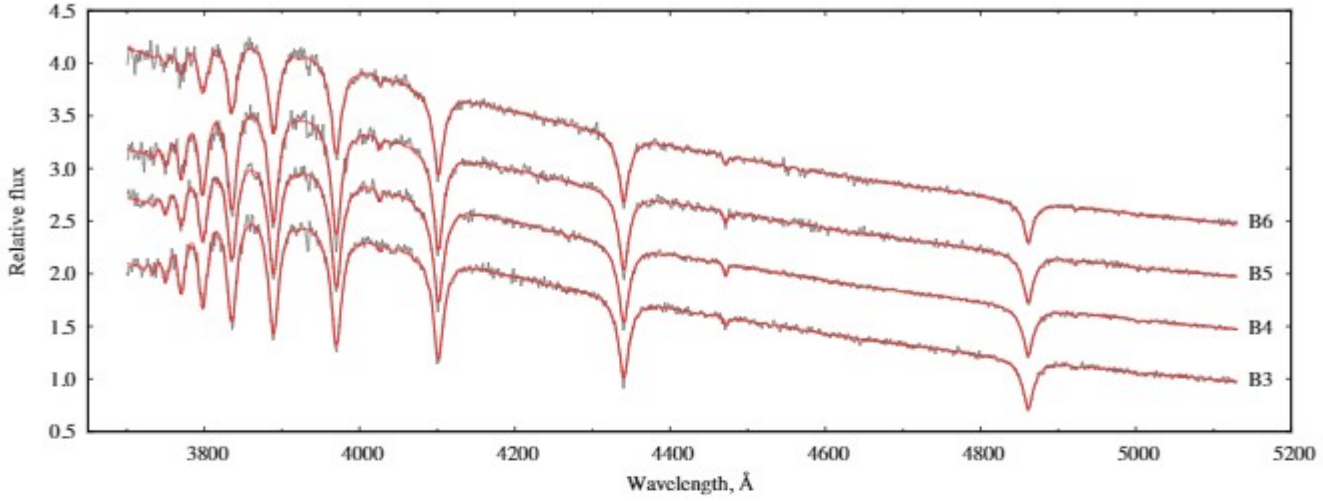

Figure 1. Best-fit TLUSTY/XTGRID non-LTE models for the four sdB stars in NGC 6791. The observed spectra have been re-calibrated to match the theoretical continuum.

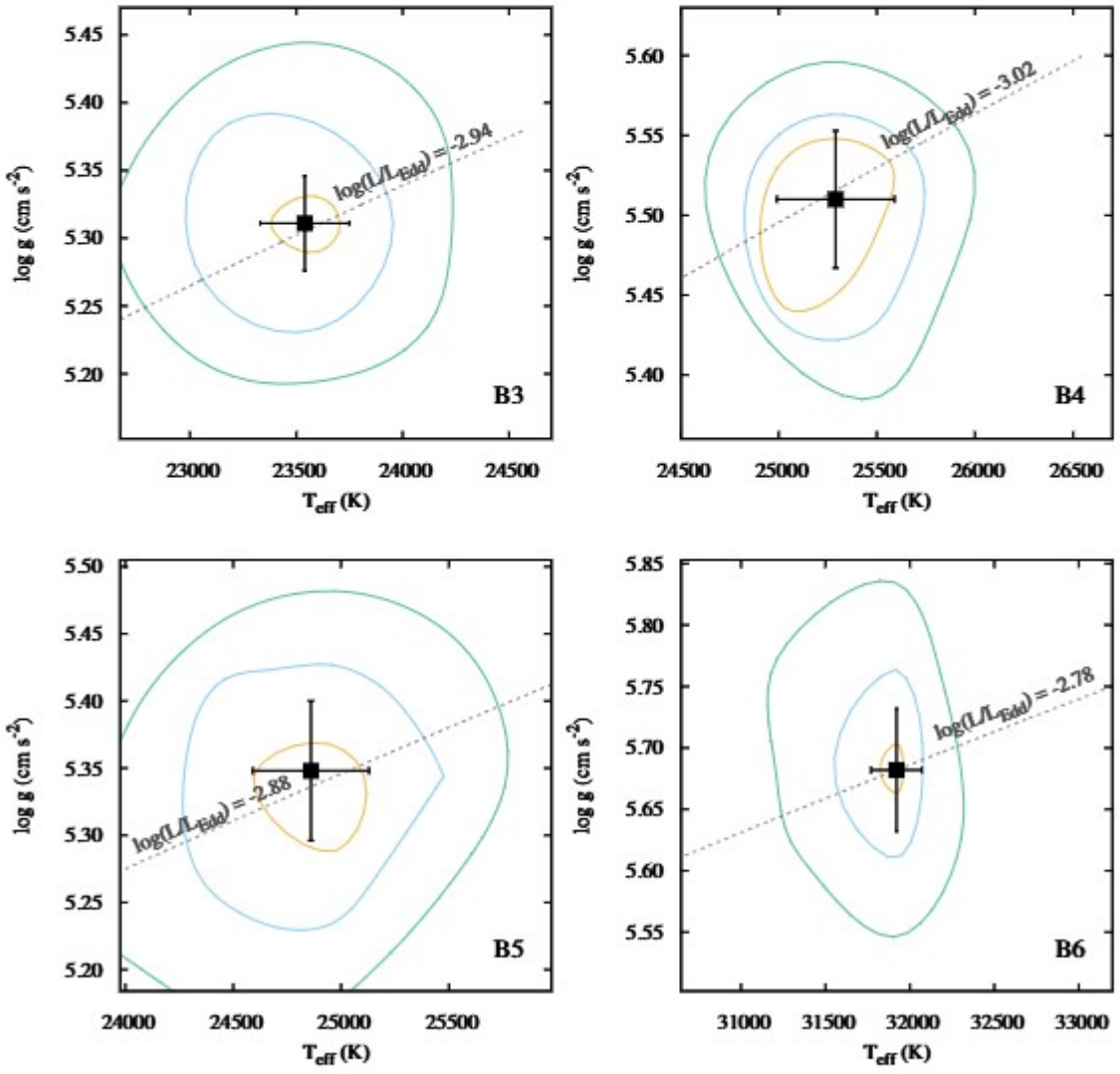

Figure 2. Atmospheric parameters for the four program stars from non-LTE TLUSTY/XTGRID models. The contours are calculated for 60, 90, and 99 per cent confidence around the solutions found by the fitting procedure. The adopted error bars correct for the asymmetries in the confidence regions.

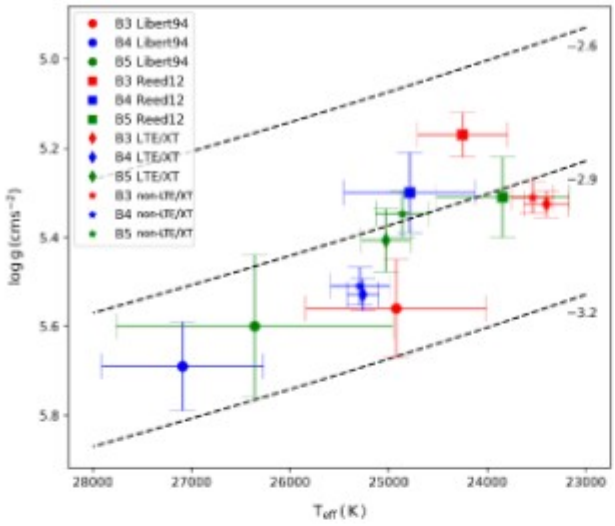

Figure 3. Atmospheric parameters of B3, B4, and B5 from Liebert et al. (1994) and Reed et al. (2012) in comparison with different values from the analyses in this paper. Three iso-luminosity curves are marked for Eddington luminosity fractions between $\log L/L_{\rm Edd} = -2.6$ and -3.2, representative of the theoretical EHB.

called campaigns, each lasting around 80 days. The engineering test campaign started in February 2014 followed by the first Campaign in May 2014. The K2 mission ended during Campaign 19. The total duration through all K2 campaigns is 1 695 days. During both missions data were stored in the short (58.85 s, SC) and long (1765.5 s, LC) cadences. During the original *Kepler* mission 18 sdBV stars have been detected. They revealed different features i.e. mode trapping (Østensen et al. 2014b), internal differential rotation (Foster et al. 2015), the Doppler beaming (Telting et al. 2012), unstable modes (Østensen et al. 2014a).

Two open clusters, NGC 6791 and NGC 6819, have been monitored by *Kepler* during the original mission in the so-called super-apertures. These are 20 x 100 pixel rectangles, which being contiguous, cover 0.22 by 0.22°, centered at the cores of the clusters. The data in super-apertures were collected in the LC mode only. In this paper, we report results of our search for sdBVs in one of the clusters, NGC 6791. This cluster is enigmatic in several ways. It is unusually massive (totalling around 4 000 solar masses, Carraro et al. 2006), about 1 kpc above the Galactic plane though it may have originated in the inner disc (Jílková et al. 2012), metal-rich with [Fe/H] from +0.3 to + 0.4 (determined only from its evolved stars, Villanova et al. 2018), despite its age of roughly 8 ± 1 Gyr (Carraro et al. 2006). This last enigma means that it does not fit any age metallicity relation for the Galactic disc and it is far above the disc where open clusters reside (King et al. 2005). It has an atypical white dwarf cooling curve which does not agree with the main sequence turn-off age (Bedin et al. 2005).

The goal of our work was to find all sdBV stars in NGC 6791, provide the mode identification of detected modes, derive parameters by means of asteroseismology, and compare them with parameters of field counterparts. We suspected that this high metallicity environment is a source of more efficient driving. In this paper, we limit our report to spectroscopic analysis and mode identification, while the results of our modelling will be published elsewhere. In addition, we identified blue-colour objects and analysed spectra of several of them that were found in a public archive.

2 SPECTROSCOPY

Using optical spectrophotometry, Kaluzny & Udalski (1992) have found seven blue-colour objects in NGC 6791. The authors used Cl∗ NGC 6791 KU Bx for designation, where x stands for a consecutive number. In the remainder of the paper, we will use a Bx format for short, i.e. KIC 2569576 (B3), KIC 2438324 (B4), KIC 2437937 (B5), KIC 2569583 (B6). Liebert, Saffer & Green (1994) have observed these stars spectroscopically with the 4.5 m Multiple Mirror Telescope (1979–1998) in Arizona and confirmed four of them to be hot subdwarf stars. New observations were taken by Reed et al. (2012), using the ALFOSC spectrograph mounted on the 2.56-m Nordic Optical Telescope to support their search for pulsating hot subdwarfs based on the first three months of Kepler data.

Blue stars in NGC 6791 were observed with the HECTOSPEC (Harvard CfA) spectrograph on the 6.5 m MMT telescope (1998) in Arizona, to calibrate for the instrumental response in a search program for optical counterparts of interacting X-ray binaries (van den Berg et al. 2013). We found these archived HECTOSPEC spectra for all four hot subdwarfs and measured a dispersion of 5.5 Å from the FWHM of well-exposed lines in the arc spectra. The signal-to-noise ratio (SNR) of the HECTOSPEC spectra in the 3800–5100 Å range are 67, 91, 62, and 70 per dispersion element for B3, B4, B5, and B6, respectively. The membership study of Gao (2020) suggests that all four hot subdwarfs are cluster members, which we confirm with our study (Section 3.1). Three of the four stars show a remarkable spectral similarity in Fig. 1, only B6 has a higher temperature and surface gravity.

2.1 Spectral analysis with XTGRID

We analysed the archival MMT/HECTOSPEC spectra with the steepest-descent chi-square minimization spectral analysis program XTGRID (Németh, Kawka & Vennes 2012) to determine $T_{\rm eff}$, log g, and nHe/nH. The fitting procedure is an interface to calculate non-LTE (non-Local Thermodynamic Equilibrium) stellar atmosphere models and synthetic spectra with TLUSTY/SYNSPEC (Hubeny & Lanz 1995, 2017), and fit observations. The theoretical models are matched to the observations with a piecewise normalization and the model parameters are varied iteratively along the steepest gradient of the global chi-square, until the fit converges on the best solution. The normalization method reduces the effects of the uncalibrated continuum flux and the fit is based on the relative strengths and profiles of the spectral lines. Our models included H, He, C, N, O, Ne, Mg, and Si opacities. Although the resolution and SNR of the HECTOSPEC spectra do not allow to measure metal abundances, the presence of metal opacities improve the model consistency. The fitting procedure iterated the models until the relative changes of all model parameters and the chi-square decreased below 0.1 per cent. Fig. 1 shows the best-fit non-LTE XTGRID models. The statistical errors for 60, 90, and 99 per cent confidence were evaluated in one dimension for abundances and include correlations for $T_{\rm eff}$ and log g (Fig. 2). XTGRID calculates upper and lower error bars independently, resulting in asymmetric errors, which were recalculated to symmetric error bars in this study.

We repeated the analysis assuming LTE conditions to estimate the effects of the non-LTE approximation on the spectral synthesis. No systematic trends have been found between the LTE and non-LTE results suggesting that non-LTE effects are low in this parameter range and random errors supersede the systematics among the different approaches. Higher quality spectra will be

Table 1. List of pulsating sdB stars in our analysis.

Name	Type	K_p [mag]	$T_{\rm eff}$ [K]	$\log(g/{\rm cm\,s^{-2}})$	$\log(N_{\rm He}/N_{\rm H})$	$P_{\rm memb}$	Reference[a]
B3	sdB	18.076	23 540(210)	5.311(35)	−2.73(23)	0.998	KU92,I.94,SS21
B4	sdB	18.267	25 290(300)	5.510(43)	−2.62(11)	0.998	KU92,I.94,SS21
B5	sdB	16.937	24 860(270)	5.348(52)	−2.46(12)	0.999	KU92,I.94,SS21

Note.[a] – SS21 – this work, KU92 – Kaluzny & Udalski (1992), I.94 – Liebert et al. (1994)

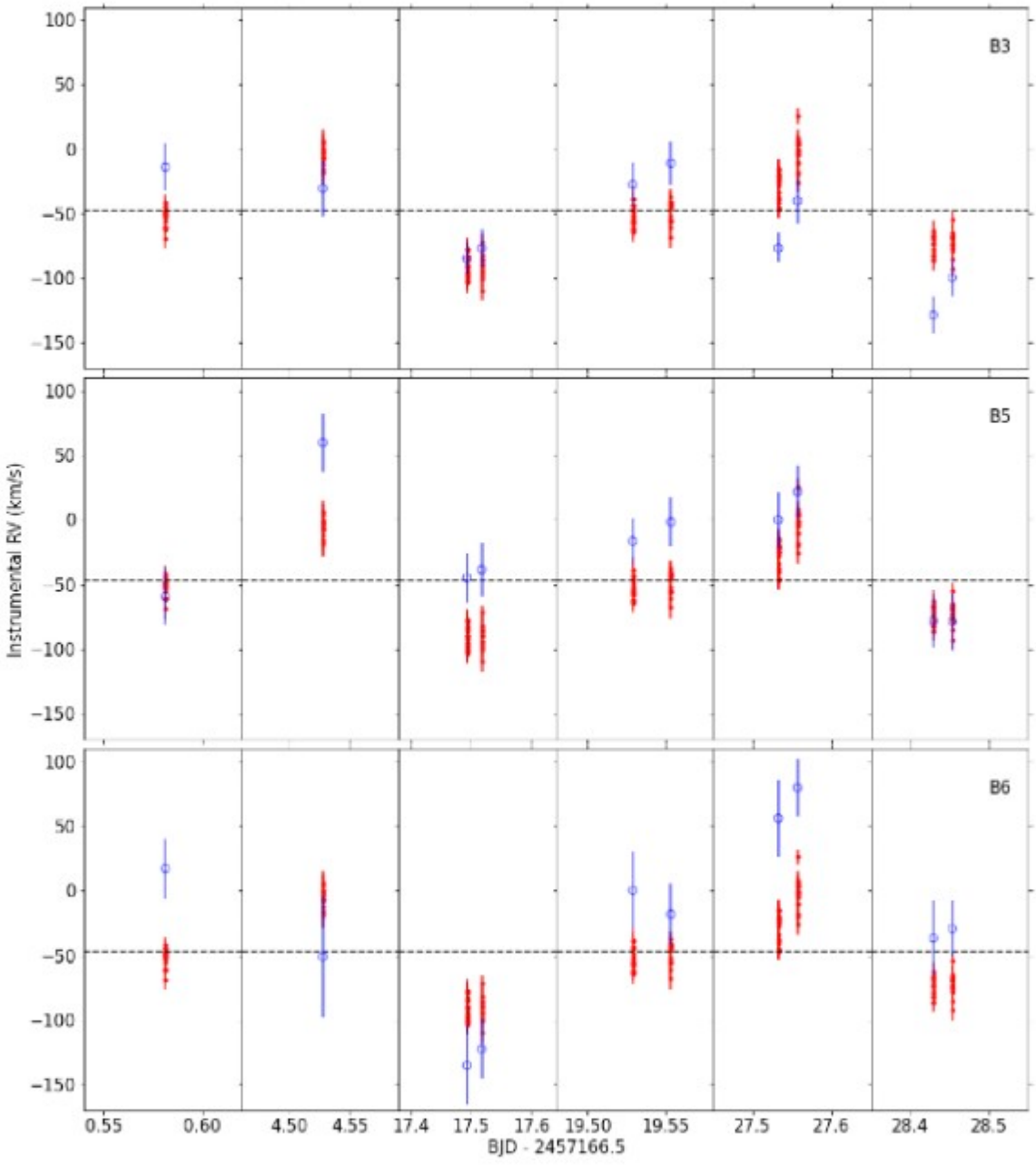

Figure 4. Instrumental radial velocities obtained from Gemini spectra. B3 (top panel), B5 (middle), and B6 (bottom) are shown as blue open circles, whereas the remaining cluster stars with Gemini spectra obtained with the same pointing are shown as red crosses. The dashed line is the cluster radial velocity of $-47.1 \pm 0.7\,{\rm km\,s^{-1}}$, determined by Bedin et al. (2006). The systematic shifts from this velocity are explained by the instrument flexure (hence, we emphasise that these are instrumental and not absolute radial velocities). It can be noted that our objects of interest show systematic shifts compared to the remaining cluster members.

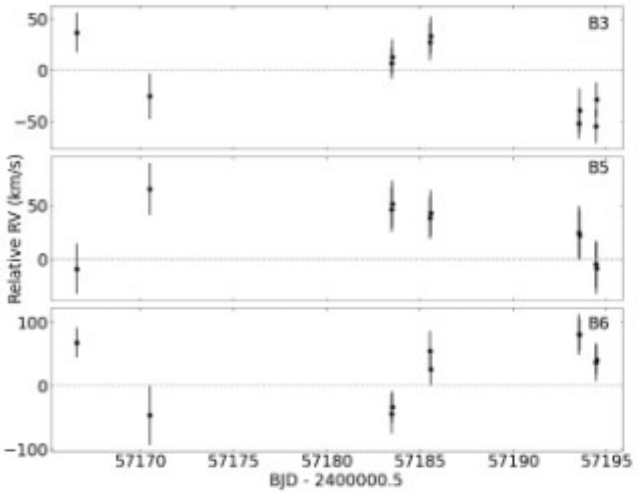

Figure 5. Radial velocities for B3 (top), B5 (middle), and B6 (bottom) relative to the cluster radial velocity. The radial velocity excesses suggest that these stars must have an internal motion within the cluster, which can be explained by binarity.

needed to explore such effects. We also show the iso-luminosity curves corresponding to the Eddington-luminosity fraction of the non-LTE solutions. Inconsistencies in the instrumental resolution, line broadening parameters and fitting approaches can increase the degeneracy between surface temperature and gravity, causing a shift of results along iso-luminosity curves. Such shifts are not observed among the solutions, suggesting the dominance of random, statistical errors. When our results are compared to past studies in Fig. 3 a better internal consistency can be outlined. While the results by Liebert et al. (1994) and Reed et al. (2012) are quite far from each other, the TLUSTY/XTGRID LTE and non-LTE results overlap and form a more compact set.

Table 1 lists the final non-LTE atmospheric parameters for each of the program stars. Atmospheric parameters of other hot cluster members that we derived in this work are listed in appendix Table A1.

2.2 Radial velocities

Multi-epoch spectra for NGC 6791 had been previously obtained with the Gemini Multi-Object Spectrograph (GMOS) at the Gemini North telescope, as part of GN-2014B-Q-11 programme. Data were obtained on seven different nights (20150524, 20150526, 20150528, 20150610, 20150612, 20150620, 20150621) using a grating with 1200 lines/mm and a central wavelength of 442 or 450 nm. During some nights, observations were taken with both configurations. Observations were executed in multi-object mode with a custom-designed mask with 35 slits. Among 35 targets three of our objects of interest, B3, B5, and B6, were assigned slits.

We downloaded these public spectra through the Gemini Science Archive,[1] with the goal of searching for radial velocity variability in B3, B5, and B6. The spectra were taken with an exposure time of 1700 s at a resolution of 1.1 Å. The S/N ratio are 39, 45, and 49, respectively for B3, B5, and B6. We processed the spectra using the `gemini` package in `pyraf`. We performed bias and background subtraction, flat-field correction, wavelength calibration, and extracted the spectra for each of the 35 stars in the GMOS field of view. Unfortunately, no arc lamps were taken at the same position as the observations. Due to instrument flexure, the dispersion function can vary significantly with pointing – we noticed shifts of more than 5 pixels for arc lamps taken on different nights – leading to a pointing-dependent wavelength solution. As a consequence, the lack of arc lamps taken immediately before or after the science observations implies that no absolute radial velocities can be obtained from these data.

We expect that the instrumental shifts resulting from the instrument flexure should be the same for all stars observed simultaneously with the same pointing. Hence, any star showing systematic shifts compared to the other cluster members must have an excess radial velocity compared to the cluster. We estimated the radial velocities for all 35 stars for all observed nights, with the exception of 20150526, for which no good wavelength solution can be obtained (for the other nights, we typically obtained wavelength solutions with RMS ≈ 0.5). We utilized the `rvsao` package[2] to obtain barycentric radial velocities through cross-correlation with template spectra (`xcsao` task). We downloaded the templates from the Sloan Digital Sky Survey,[3] corrected to zero radial velocity and air wavelengths, and we chose the template whose spectral type match each of the 35 stars the best. We show the result of the spectra processing in Fig. 4.

The obtained radial velocities suggest that B3, B5, and B6 show radial velocity excess compared to other cluster stars. We determine the average instrumental velocity using the other cluster stars, and then subtracted it from the velocities of B3, B5, and B6 to obtain velocities relative to the cluster (Fig. 5). These excesses in velocity shown by these three stars can only be explained if they show a motion with respect to the cluster motion, which can only be explained if they are binaries. We attempted to find orbital periods by performing a Lomb-Scargle periodogram of their relative velocities, but the window function prevents us from any unique period identification. Likely, they show periods of many days, since spectra taken on the same night show no significant shifts (as can be noted in Fig. 5). We cannot confirm this conclusion with photometry, since we found no significant peaks in the low frequency region of the amplitude spectra.

3 *KEPLER* PHOTOMETRIC AND *Gaia* ASTROMETRIC DATA

We downloaded the *Kepler* data of NGC 6791 from Mikulski Archive for Space Telescopes (MAST). We searched for a flux variation in each pixel of the data taken during quarters (Q) 2, 3, 4, and 5 only, since the location of stars on silicons repeats exactly every four quarters. First, we pulled out fluxes from a given pixel for each time stamp and created time-series data. We also analysed the SC of B3, B4, and B5 and selected either the SC or LC, whichever allowed for lower noise level in amplitude spectra. Next, we calculated amplitude spectra up to the Nyquist frequency, which equals 24 (LC) or 734 c/d (SC). Finally, we inspected the spectra by eye for any sign of variability. Large amplitude variations, mostly non-sinusoidal, e.g. eclipses, outbursts, were easily detected directly in the time-series data. In case of a positive detection, we defined target masks, either one-pixel or multiple-contiguous-pixels containing the same variability, in each of the Q 2 – 5 separately, and we applied these apertures to all quarters, 1 through 17. We prepared final light curves using both PYKE software (Kinemuchi et al. 2012) and our custom

[1] https://archive.gemini.edu/

[2] http://tdc-www.harvard.edu/iraf/rvsao/

[3] http://classic.sdss.org/dr5/algorithms/spectemplates/

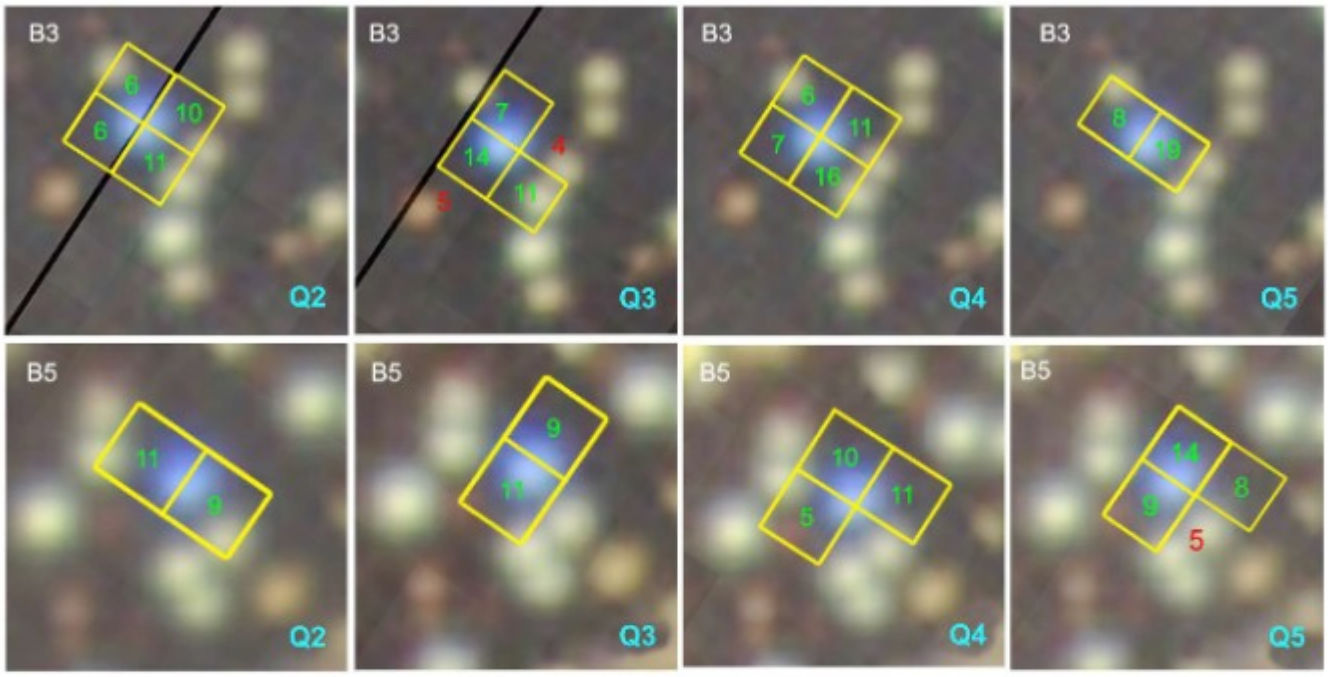

Figure 6. The target masks (yellow squares) defined in Q 2 – 5 for B3 (upper panels) and B5 (lower panels). The numbers in green and red denote the S/N ratio of the fluxes in given pixels. The black line shows the boundary between two adjacent super-apertures.

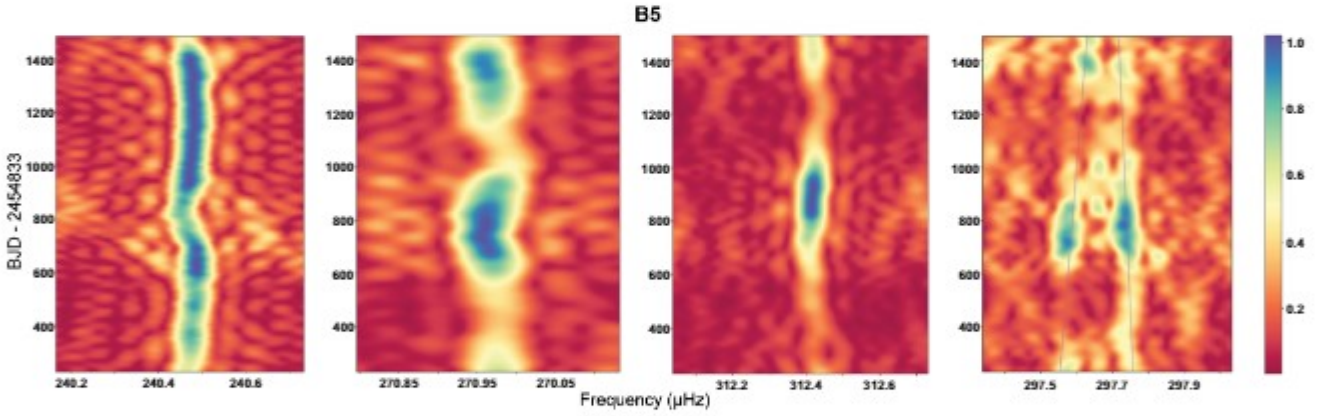

Figure 7. Sliding amplitude spectrum of B5 showing time evolution of selected frequencies. The rightmost panel shows convergence of two close frequencies 297.583 μHz and 297.735 μHz overtime.

scripts. We clipped the data using $3-5\,\sigma$ rule, depending on quarter and star. Then, we detrended data using cubic spline fits and finally, we normalized data by dividing by an average flux level, subtracting 1 and multiplied by 1000. The resultant flux is given in *parts per thousand* (ppt).

In this work, we focused on super-aperture LC data (Q 1 – 17) to lower the noise level in amplitude spectra by increasing the time coverage of the time-series data. We show the optimal apertures in Fig. 6. The apertures are formed by pixels with a flux variation of S/N ≥ 5, not including pixels that contain too much signal from neighbours, even though the S/N ratio is still ≥ 5. We note that our flux extraction does not account for neighbour contamination. Such photometry causes a median flux to be quarter dependent and the amplitudes of a flux variation are not realistic but arbitrarily normalized to Q1 median flux. B4 has been also observed in the SC mode during Q 6 – 17. These data are four quarters shorter in coverage but has 22 times the number of data points in LC, which provide a lower noise level in the amplitude spectrum, and we accepted the SC data for further analysis of B4. The all SC data set available now is longer than the data set analysed by Baran et al. (2012), and the flux delivered to the MAST is corrected for contamination making the amplitudes realistic.

We utilized parallaxes and proper motions from *Gaia* Early Data Release 3 for all *Gaia* targets within the tidal radius ≈ 23 arcmin (Platais et al. 2011) from the cluster center, RA = 19:20:51.3, DEC = +37:46:26, adopted from Kamann et al. (2019) to establish cluster membership. We used the *Gaia* EDR3 zero-point correction package available in PYTHON (Lindegren et al. 2021) to correct parallaxes. We included only stars with parallaxes between zero and one. Negative parallaxes are surely incorrect while stars closer than

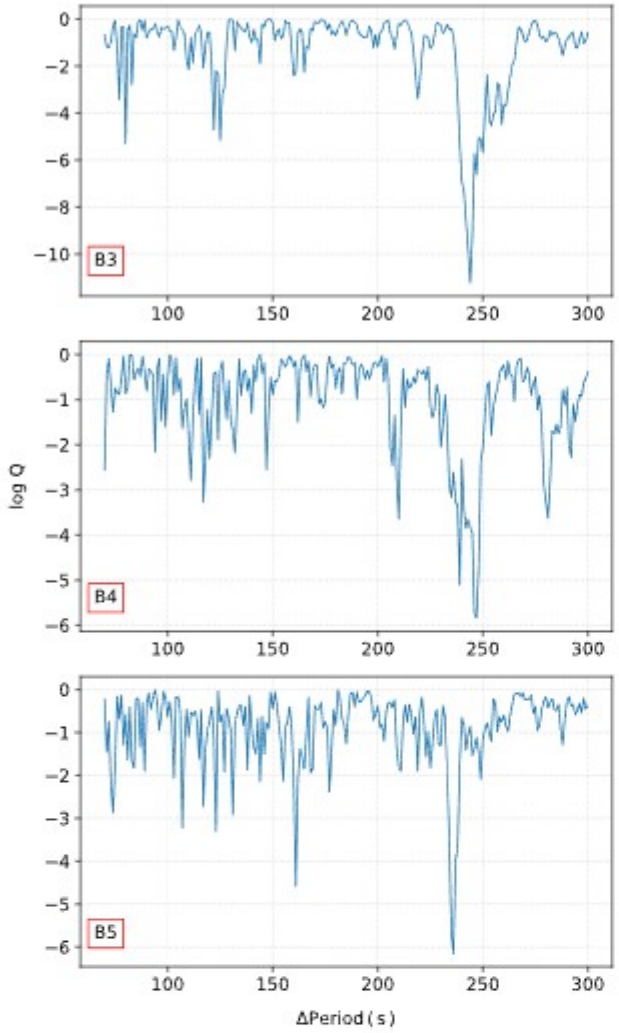

Figure 8. Kolmogrov-Smirnov test for B3, B4, and B5.

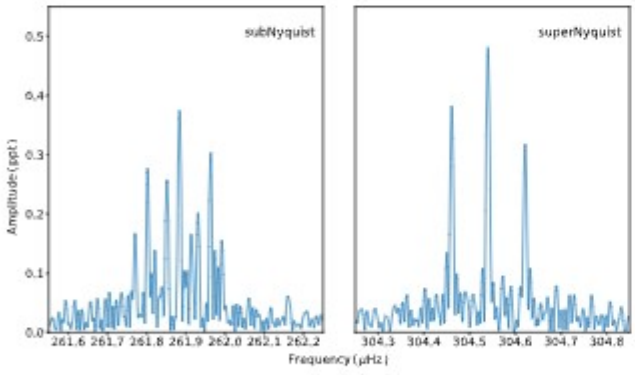

Figure 9. Comparison of peaks distribution in a multiplet detected in B3 in both the sub- and super-Nyquist regions.

1 kpc are too close to us to be cluster members. Since the *Gaia* data have limited precision, stars in dense environments may have relative errors of parallax bigger than 50 per cent. We rejected those targets from our analysis as well.

3.1 Cluster membership

To derive membership probabilities for B3, B4, and B5, as well as blue-colour targets (mentioned in Section 2), we employed variational Bayesian Gaussian Mixture Models with a Dirichlet process prior (Ferguson 1973) using *scikit–learn* machine learning library for the PYTHON programming language (Pedregosa et al. 2011). We calculated the probabilities using five parameters (5D), i.e. RA, DEC, PM_RA, PM_DEC, PARALLAX. Stars with P(5D) $\geq$ 0.5 are classified as almost certain members. The 5D probability of B3 is 0.998, of B4 is 0.998, and of B5 is 0.999, and we claim these stars are almost certain NGC 6791 members. The probabilities of other targets of our interest are also listed in Table A1 (Appendix A).

We found significant photometric variation in B3, B4, and B5, which were known to be pulsators before (Reed et al. 2012; Baran & Winans 2012) and according to our results, B3, B4, and B5 are the only sdBVs in NGC 6791. We list these three stars with $T_{\rm eff}$ and log g derived in this work in Table 1, and four other hot stars in Table A1. In the remainder of the paper, our focus is placed on the pulsation analysis of B3, B4, and B5.

3.2 Amplitude spectra

We used our custom scripts to calculate amplitude spectra and pre-white frequencies with significant amplitudes, i.e. above a detection threshold of 4.5σ, where σ is the mean noise level (Baran, Koen & Pokrzywka 2015). This is a very liberal threshold as it corresponds to a false alarm probability (FAP) of around 10 per cent, hence the peaks with amplitudes close to the threshold should be considered tentative. The pre-whitening is performed with the non-linear least-square method. The mean noise level is calculated from residual amplitude spectra. The 4.5σ detection threshold equals 0.085 ppt in B3, 0.1447 ppt in B4, and 0.0643 ppt in B5. We calculated FAP = 0.1 per cent for each star to be achieved at S/N of 5.23 (0.091 ppt) in B3, 5.63 (0.1827 ppt) in B4 and 5.16 (0.069 ppt) in B5.

We pre-whitened a few tens of frequencies in each star. All fit frequencies were checked against the list of artifacts reported by Baran (2013). In B3 and B4 most of the frequencies are pre-whitened with negligible residuals, which indicate stable amplitudes of the pulsation modes. In B5, some of the frequencies leave significant residuals, which we interpret as unstable frequencies or amplitudes of those modes. In Fig. 7, we present sliding amplitude spectra of five frequencies that significantly vary with time. We discuss it more in Section 3.3.3. In the right-most hand of Fig. 7, we show sliding amplitude spectra of two close frequencies f_{19} and f_{20} that may, in fact, be rotationally split and converge with time.

3.3 Mode identification

To make a preliminary mode identification, we used two features in amplitude spectra, a frequency splitting caused by stellar rotation and an asymptotic period spacing. Non-radial modes of degree ℓ have $2\ell + 1$ components of different m values, which are not distinguishable in the absence of rotation. Stellar rotation lifts this degeneracy. The corresponding m components are shifted in frequency according to the rotation rate, and a frequency shift is given by the following equations (Tassoul 1980; Gough 1986).

$$\Delta\nu_{n,\ell} = \frac{1 - C_{n,\ell}}{P_{\rm rot}}. \quad (1)$$

When the frequency shift is measured in an amplitude spectrum, a rotation period is estimated. $C_{n,\ell}$ is called the Ledoux constant.

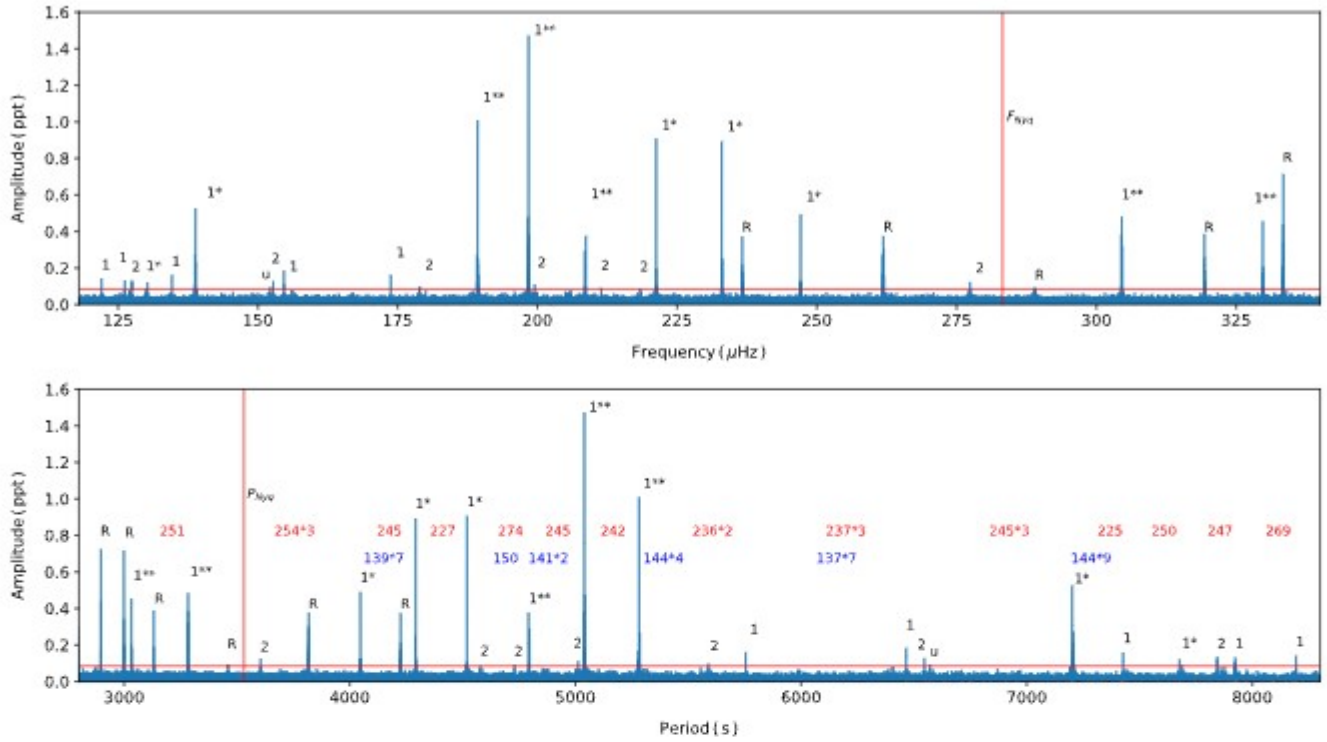

Figure 10. The amplitude spectrum of B3 in frequency (top panel) and period (bottom panel). The numbers above peaks denote modal degrees. '∗' (asterisk) denote doublets, while '∗∗' denote triplets. 'R' stands for reflections across Nyquist. The horizontal red line represents the detection threshold, defined as 4.5σ. The vertical red line marked as 'F_{Nyq}' shows the position of the Nyquist frequency, likewise 'P_{Nyq}' shows the position of the Nyquist frequency in the period domain. The red labels provide period spacing between adjacent dipole overtones, likewise blue labels for quadrupole overtones. Symbols 'u' stands for unidentified modes.

According to Charpinet et al. (2000), it is close to zero for p-modes, while for g-modes, it can be calculated from the following expression:

$$C_{n,\ell} \approx \left(\ell^2 + \ell\right)^{-1}. \tag{2}$$

In the asymptotic regime i.e. $n \gg \ell$, g-modes are evenly spaced in period. The periods of a given radial order and modal degree can be estimated from the following equation:

$$P_{\ell,n} = \frac{P_0}{\sqrt{\ell(\ell+1)}} n + \epsilon. \tag{3}$$

P_0 is the period of the fundamental radial mode, while ϵ, according to Unno et al. (1979), is a small number. Reed et al. (2011) showed empirically that the average period spacings for dipole and quadrupole g-modes in sdBV stars are close to 250 and 144 s, respectively.

To estimate a common period spacing for modes of different modal degrees, likewise Reed et al. (2011), we applied the Kolmogrov–Smirnov (KS) test. The result of our KS test application is shown in Fig. 8, and it clearly indicates that the most common period spacing is close to 250 s.

3.3.1 B3

Østensen et al. (2010) reported the effective temperature $T_{\rm eff} = 24\,250\,(459)$ K and surface gravity $\log(g/{\rm cm\,s^{-2}}) = 5.28\,(4)$. The latter overlaps, while the $T_{\rm eff}$, including errors, is different by 41 K (Table 1). These parameters place B3 in the $T_{\rm eff} - \log$ g diagram in the region of g-mode dominated sdBV stars. In fact, B3 has been discovered to be a sdBV star and analysed by Reed et al. (2012). They analysed 1-month of the SC data and reported 11 frequencies, including nine $\ell = 1$ frequencies. We used a detection threshold of 0.085 ppt, which is seven times better than achieved by Reed et al. (2012) and we detected 38 independent frequencies. We detected all frequencies but one detected by Reed et al. (2012). The exception is f3, which Reed et al. (2012) detected in the LC data only. Our closest frequency to f3 is f_{29}. We show an amplitude spectrum in Fig. 10. Following a discovery of an influence of the barycentric correction on peaks shapes by Baran et al. (2012) and an analytical derivation of the phenomenon by Murphy, Shibahashi & Kurtz (2013), we checked if any of the frequencies in an amplitude spectrum could originate from the super-Nyquist region. The influence is caused by an uneven sampling in the barycentric reference system, in which the time stamps are used. Such sampling makes the Nyquist vary over Kepler's orbit. In consequence, this changes the real sharp-shape signal into a blurred one across the Nyquist frequency. We show such an example in Fig. 9. A comparison of amplitudes in the sub- and super-Nyquist regions resulted in six frequencies, $f_{33} - f_{35}$ and $f_{36} - f_{38}$, originating beyond the Nyquist frequency. We also accepted two frequencies, f_{22} and f_{25}, which have S/N ratio a bit lower than 4.5σ. They are accepted because f_{22} is likely a middle component of a multiplet, while f_{25} fits an asymptotic sequence of $\ell = 2$ modes. We provide the list of all detected frequencies in Table 2.

We searched for multiplets and we found that 21 frequencies can be arranged into 8 multiplets with an average frequency splitting between multiplet members of 0.0901 (31) μHz. Frequencies f_4, f_5, and f_7, f_8 are also spaced roughly by this value but their profiles are not simple bell shapes making the estimation of the frequency

Table 2. List of fitted frequencies in B3. The 'u' symbol denotes unidentified.

ID	Frequency [μHz]	Period [s]	Amplitude [ppt]	S/N	n	l	m
f_1	122.04313(46)	8193.825(31)	0.142(15)	7.4	33	1	u
f_2	126.18748(48)	7924.716(30)	0.134(15)	7.0	32	1	u
f_3	127.47399(49)	7844.738(30)	0.133(15)	7.0	55	2	u
f_4	130.0544(8)	7689.090(44)	0.086(15)	4.5	31	1	−1
f_5	130.2518(5)	7677.436(31)	0.122(15)	6.4	31	1	1
f_6	134.63806(40)	7427.320(22)	0.163(15)	8.5	30	1	u
f_7	138.75596(25)	7206.897(13)	0.260(15)	13.6	29	1	−1
f_8	138.85834(13)	7201.584(6)	0.519(15)	27.1	29	1	0
f_9	152.1810(7)	6571.122(31)	0.091(15)	4.8	u	u	u
f_{10}	152.7512(5)	6546.592(22)	0.128(15)	6.7	46	2	u
f_{11}	154.66203(35)	6465.711(15)	0.184(15)	9.6	26	1	u
f_{12}	173.76970(40)	5754.743(13)	0.161(15)	8.4	23	1	u
f_{13}	178.9255(7)	5588.918(22)	0.092(15)	4.8	39	2	u
f_{14}	189.20814(24)	5285.185(7)	0.267(15)	13.9	21	1	−1
f_{15}	189.31946(6)	5282.0773(18)	1.009(15)	52.8	21	1	0
f_{16}	189.43405(48)	5278.882(13)	0.136(15)	7.1	21	1	1
f_{17}	198.32796(13)	5042.1534(33)	0.500(15)	26.2	20	1	−1
f_{18}	198.423399(44)	5039.7282(11)	1.478(15)	77.3	20	1	0
f_{19}	198.51785(18)	5037.3305(45)	0.367(15)	19.2	20	1	1
f_{20}	199.5218(6)	5011.984(16)	0.105(15)	5.5	35	2	u
f_{21}	208.48494(22)	4796.509(5)	0.293(15)	15.3	19	1	−1
f_{22}	208.5760(8)	4794.415(18)	0.081(15)	4.3	19	1	0
f_{23}	208.66842(17)	4792.2921(40)	0.379(15)	19.8	19	1	1
f_{24}	211.4113(7)	4730.115(16)	0.091(15)	4.8	33	2	u
f_{25}	218.3725(8)	4579.331(16)	0.083(15)	4.4	32	2	u
f_{26}	221.1824(6)	4521.155(13)	0.100(15)	5.2	18	1	−1
f_{27}	221.26361(7)	4519.4959(15)	0.909(15)	47.5	18	1	0
f_{28}	232.98206(7)	4292.1760(13)	0.900(15)	47.1	17	1	0
f_{29}	233.06906(24)	4290.5737(45)	0.266(15)	13.9	17	1	1
f_{30}	247.0106(5)	4048.410(8)	0.127(15)	6.6	16	1	−1
f_{31}	247.09599(13)	4047.0103(21)	0.496(15)	25.9	16	1	0
f_{32}	277.4081(5)	3604.797(7)	0.125(15)	6.6	25	2	u
f_{33}	304.46105(17)	3284.4924(19)	0.375(15)	19.6	13	1	−1
f_{34}	304.54017(14)	3283.6391(15)	0.478(15)	25.0	13	1	0
f_{35}	304.62135(21)	3282.7640(22)	0.315(15)	16.5	13	1	1
f_{36}	329.68961(37)	3033.1560(34)	0.176(15)	9.2	12	1	−1
f_{37}	329.76857(14)	3032.4297(13)	0.457(15)	23.9	12	1	0
f_{38}	329.84753(32)	3031.7038(29)	0.205(15)	10.7	12	1	1

splitting difficult. We identified these four frequencies as rotationally split but we decided not to estimate their splitting, and these two multiplets do not contribute to the average splitting cited above. We interpret the splitting to be caused by the rotation of an average period equals 64.2 (1.1) days. The splitting is not fixed between multiplets. It decreases as frequency increases (Fig. 11). The difference in rotation period calculated from the largest and smallest splitting is around 22.79 days. Since different radial overtones originate at different depths of a star, a differential rotation along the radius can be invoked as one of the explanations of this phenomenon. The study by Foster et al. (2015) shows a differential rotation inferred from different splittings of multiplets detected among g- and p-modes. It points at a different rotation rate of an envelope and a deeper stellar interior. In B3, a splitting difference is observed among g-modes only, hence the period difference may exist on a small radius scale. The splitting decrease can also be a consequence of small, but noticeable, dependence of the $C_{n,\ell}$ on the radial overtone.

The multiplet pattern allows us to identify a modal degree and an azimuthal order. A hint of what may be the average period spacing comes from the KS test shown in the top panel of Fig. 8. The K-S statistic Q describes the probability that the period spacing

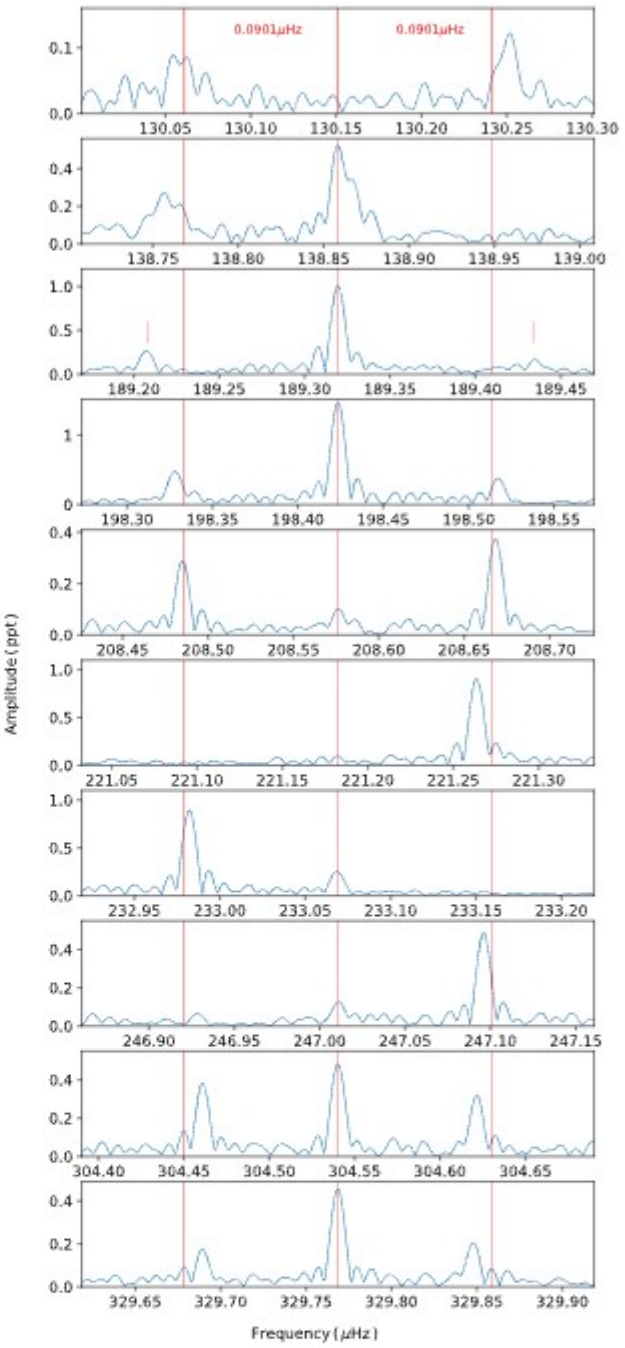

Figure 11. Multiplets of $\ell = 1$ modes we detected in B3. The splitting decreases as frequency increases.

is randomly distributed. The minimum value indicates a periodic spacing of around 245 s and we used it as a preliminary value to look for dipole overtones. After selection of best candidates for dipole modes, we assigned a relative radial order to each mode. Then, we applied a linear fit to relative radial order – period relation deriving an average spacing of 243.87 (87) s. We have not found enough quadrupole overtone candidates and we were unable to derive an independent estimation of the period spacing of $\ell = 2$ modes. We accepted a theoretical value of 140.80 (66) s, which is in relation to the period spacing of dipole modes by $1/\sqrt{3}$, and used it to search for other possible quadrupole modes. Owing to both multiplets and

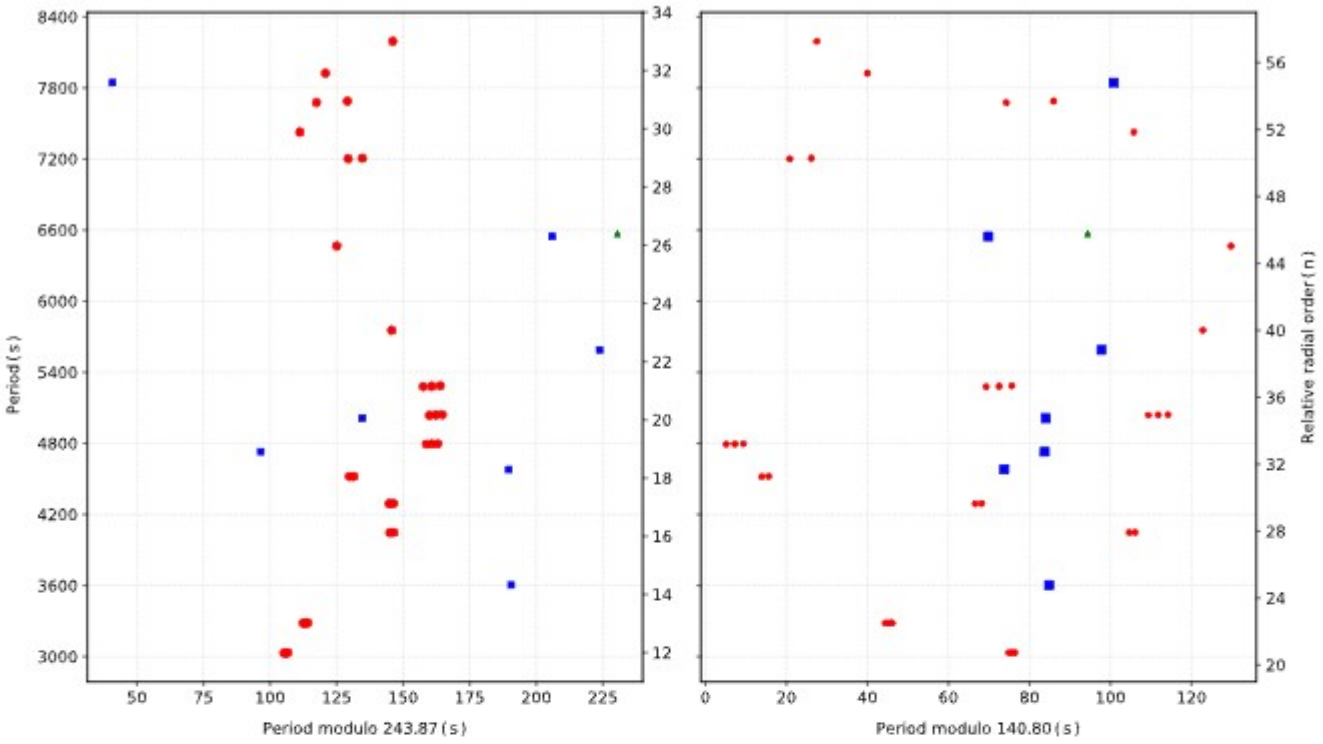

Figure 12. Échelle diagram for B3. The red dots represent the identified dipole modes, blue cubes represent identified quadrupole modes, and green triangles represent unidentified modes. The right y-axis shows relative radial orders.

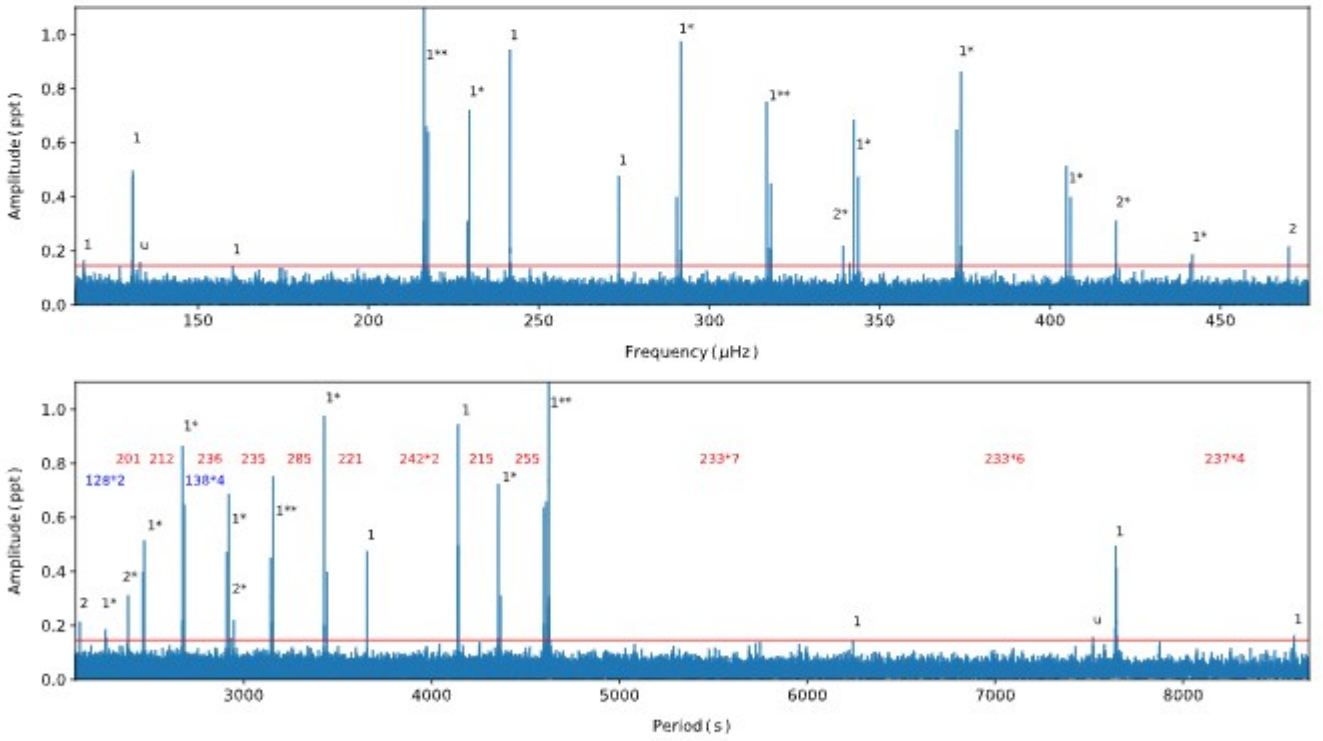

Figure 13. Same as in Fig. 10 but for B4.

Table 3. List of fitted frequencies in B4. The frequencies $f_{\rm orb}$ and $f_{\rm har}$ are due to the binarity.

ID	Frequency [μHz]	Period [s]	Amplitude [ppt]	S/N	n	l	m
$f_{\rm orb}$	29.044186(13)	34430.298(15)	12.056(28)	375.3	–	–	–
$f_{\rm har}$	58.088373	17215.149	1.936(28)	60.3	–	–	–
f_1	116.4050(11)	8590.70(8)	0.156(28)	4.9	36	1	u
f_2	130.82490(41)	7643.805(24)	0.409(28)	12.7	u	u	u
f_3	130.86402(34)	7641.520(20)	0.501(28)	15.6	32	1	u
f_4	132.9694(11)	7520.53(6)	0.155(28)	4.8	u	u	u
f_5	160.1687(12)	6243.418(47)	0.138(28)	4.3	26	1	u
f_6	216.2513(9)	4624.250(19)	0.197(28)	6.1	u	u	u
f_7	216.28353(10)	4623.5605(22)	1.649(28)	51.3	19	1	−1
f_8	216.89143(28)	4610.602(6)	0.609(28)	19.0	19	1	0
f_9	217.48776(27)	4597.960(6)	0.621(28)	19.3	19	1	1
f_{10}	229.0022(5)	4366.771(10)	0.318(28)	9.9	18	1	0
f_{11}	229.60627(23)	4355.2817(44)	0.723(28)	22.5	18	1	1
f_{12}	241.51669(18)	4140.5006(30)	0.951(28)	29.6	17	1	0
f_{13}	273.47895(36)	3656.5886(48)	0.469(28)	14.6	15	1	0
f_{14}	290.44230(43)	3443.025(5)	0.394(28)	12.3	14	1	−1
f_{15}	291.70969(17)	3428.0658(20)	0.976(28)	30.4	14	1	1
f_{16}	316.83457(22)	3156.2212(22)	0.758(28)	23.6	13	1	−1
f_{17}	317.4830(8)	3149.775(8)	0.208(28)	6.5	13	1	0
f_{18}	318.11065(36)	3143.5603(36)	0.467(28)	14.5	13	1	1
f_{19}	339.3322(8)	2946.964(7)	0.219(28)	6.8	21	2	−1
f_{20}	341.2395(11)	2930.493(9)	0.154(28)	4.8	21	2	1
f_{21}	342.42883(25)	2920.3149(21)	0.684(28)	21.3	12	1	−1
f_{22}	343.69197(35)	2909.5821(30)	0.478(28)	14.9	12	1	1
f_{23}	372.63000(26)	2683.6272(18)	0.656(28)	20.4	11	1	−1
f_{24}	373.89335(19)	2674.5595(14)	0.872(28)	27.2	11	1	1
f_{25}	404.77337(33)	2470.5182(20)	0.514(28)	16.0	10	1	−1
f_{26}	406.03713(42)	2462.8289(25)	0.403(28)	12.6	10	1	1
f_{27}	419.3760(5)	2384.4951(30)	0.314(28)	9.8	17	2	0
f_{28}	420.3858(12)	2378.767(7)	0.137(28)	4.3	17	2	1
f_{29}	441.1297(11)	2266.907(6)	0.153(28)	4.8	9	1	−1
f_{30}	441.7979(9)	2263.4784(46)	0.185(28)	5.8	9	1	0
f_{31}	470.0442(8)	2127.4596(35)	0.215(28)	6.7	15	2	u

period spacing, we assigned a modal degree and an azimuthal order of 37 frequencies. In the case of not all triplet components detection, we arbitrarily assigned the azimuthal orders of these components.

We calculated the échelle diagram (Fig. 12) using the average spacing of dipole (left hand) and quadrupole (right right) modes. The plots show ridges of modes that meander roughly straight up. The numbers denote the relative radial orders of identified modes. The échelle diagram for dipole modes shows a side bump between 3000 and 7000 s. This feature is similar to the one already reported by Baran & Winans (2012) and becomes characteristic of the sdB interior. According to (Charpinet et al. 2013a, b, 2014) the feature could be caused by strong diffusion inside the stars.

3.3.2 B4

B4 is a binary system containing a sdBV star and a main sequence companion with the orbital period of 9 h 33 min 50 s. The effective temperature and surface gravity of the system reported by Østensen et al. (2010) is $T_{\rm eff} = 24\,786\,(665)$ K and $\log(g/{\rm cm\,s^{-2}}) = 5.50\,(7)$, respectively, both values in agreement with our estimates (Table 1). The pulsation properties have been extensively studied by Baran & Winans (2012). The authors used the longest data set at the time, which was Q5 – 9 data. Using a detection threshold of 0.21 ppt, they reported 19 pulsation frequencies and two related to binarity.

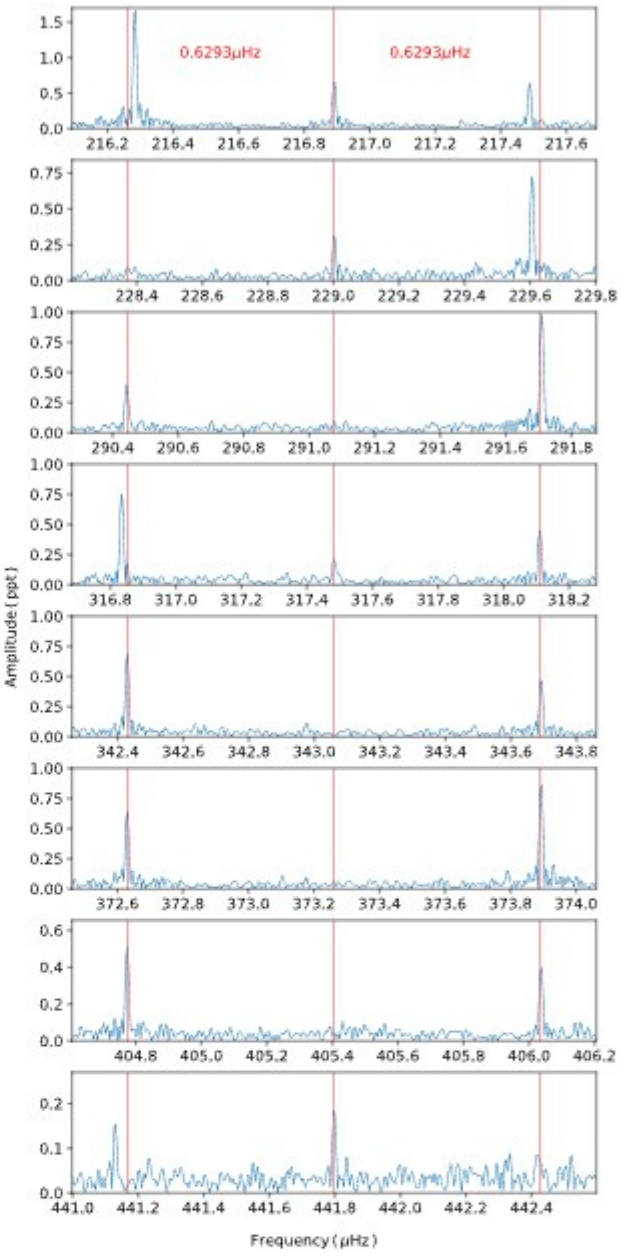

Figure 14. Multiplets of $\ell = 1$ modes we detected in B4.

We show an amplitude spectrum calculated from the SC data in Fig. 13. The detection threshold equals 0.145 ppt, lower by 30 per cent as compared to Baran & Winans (2012). We found 33 frequencies in the g mode region, including two caused by binarity. The $f_{\rm har}$ is the first harmonic of the binary frequency and was not fit, but assumed precisely twice the $f_{\rm orb}$, instead. We show the full list of frequencies in Table 3. The list includes all the frequencies detected by Baran & Winans (2012).

Searching for multiplets, we found 18 frequencies to be split by the average splitting of 0.6293 (45) μHz. These frequencies form six $\ell = 1$ multiplets. Likewise in B3, we assumed these multiplets are caused by stellar rotation of the period of 9.196 (33) days. We found consistent splitting among four $\ell = 2$ candidates. The average frequency splitting of quadrupole modes is 0.972 (15) μHz and the

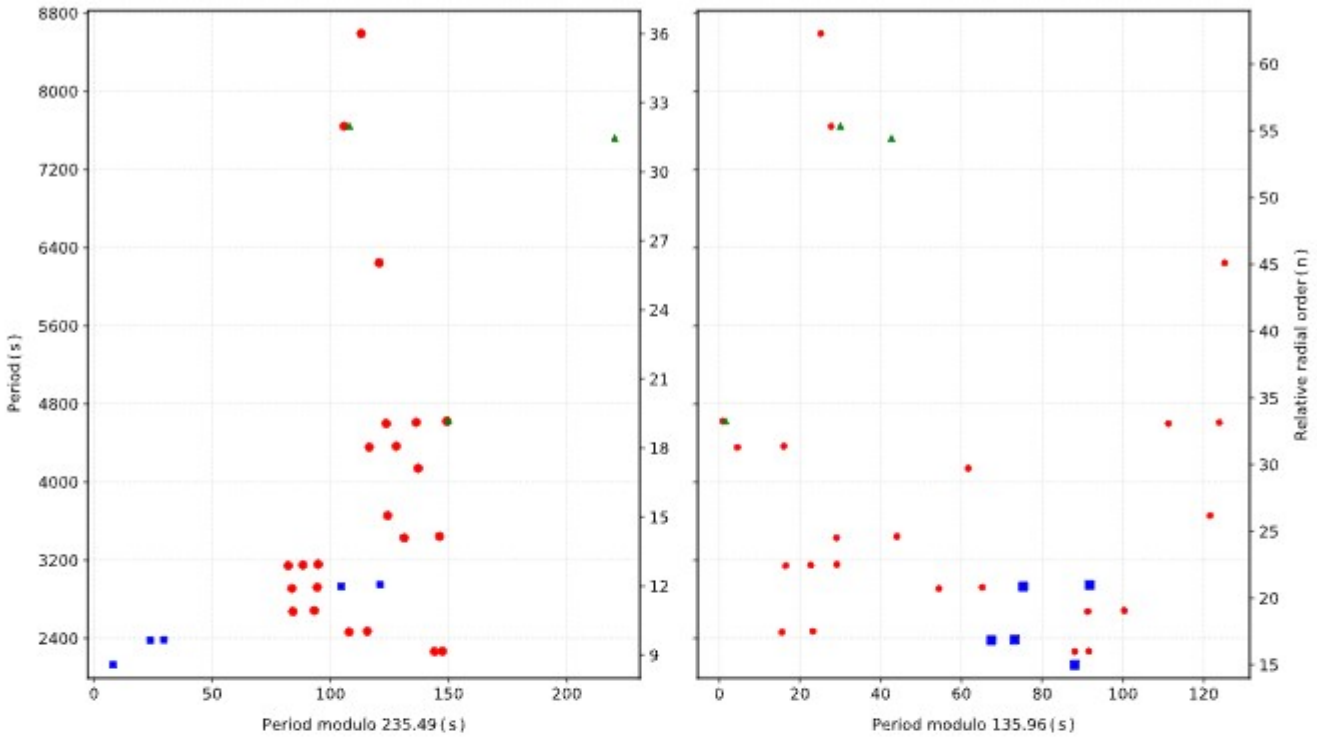

Figure 15. Same as Fig. 12 but for B4.

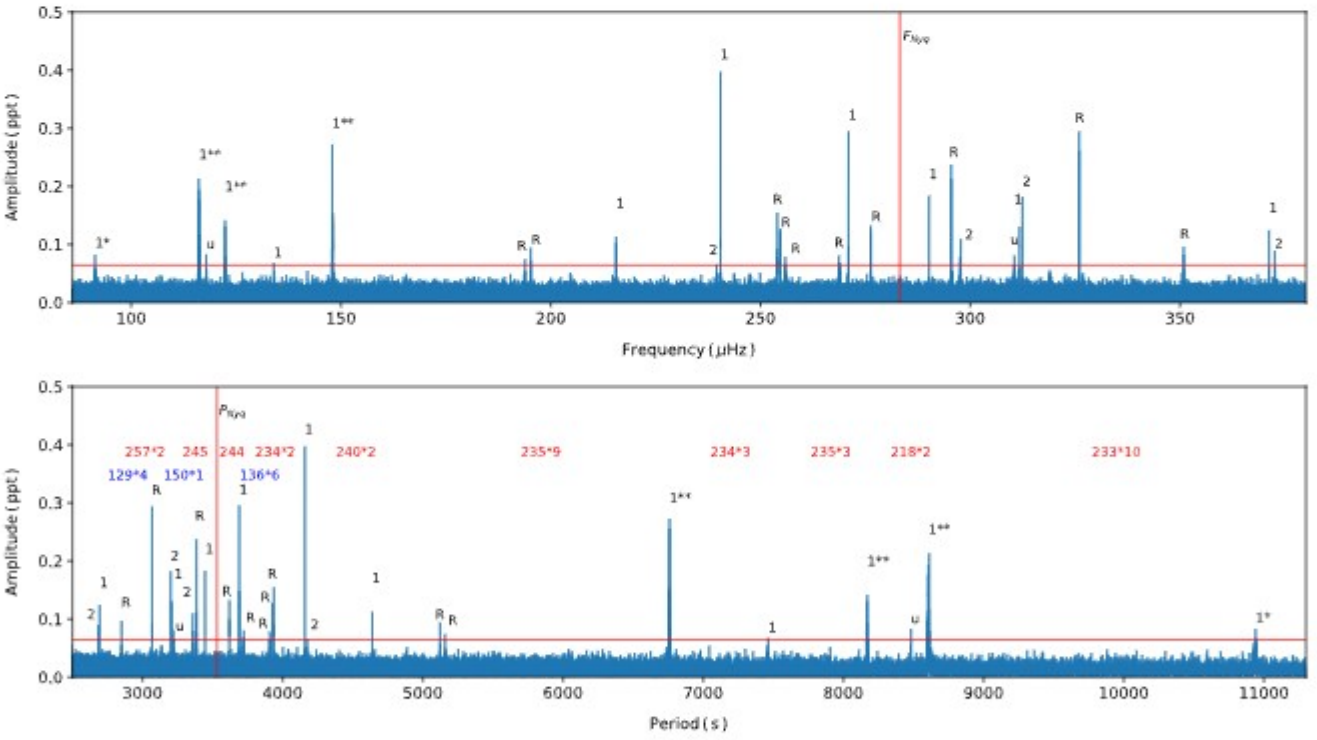

Figure 16. Same as in Fig. 10 but for B5.

corresponding rotation period equals 10.12 (14) days. Surprisingly, six out of eight $\ell = 1$ multiplets are doublets. Side components in doublets suggest a specific inclination of the sdB star, i.e. a pole-on orientation, however, central components in two $\ell = 1$ multiplets break the rule (fig. A.5 of Charpinet et al. 2011). We show dipole multiplets in Fig. 14. The splitting changes with frequency, which can also be an indication of the $C_{n,\ell}$, or rotation period variation, as discussed in the case of B3.

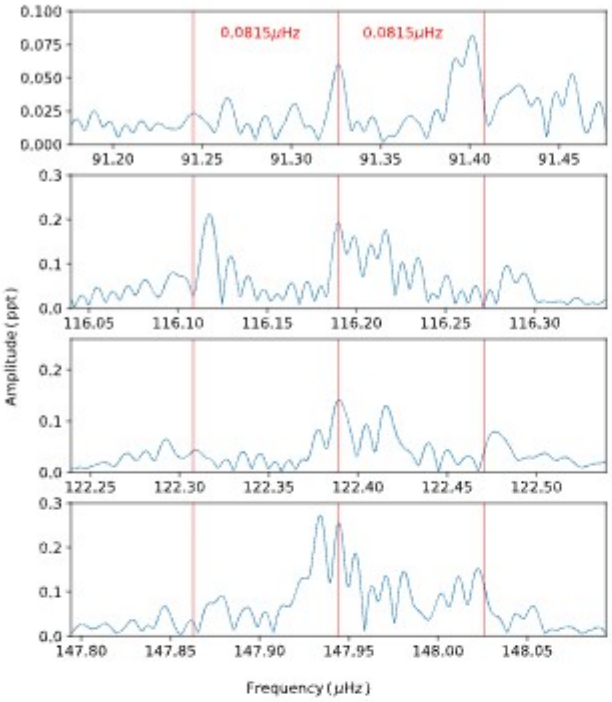

Figure 17. Selection of blurred-profile frequencies we detected in B5.

The KS test (Fig. 8) indicates a spacing near 250 s. We selected those modes, which are roughly spaced by this value, and we derived the precise average period spacing of 235.49 (71) s for dipole modes. Since the quadrupole overtone sequence is not numerous, we estimated the average period spacing of those modes using the relation likewise in B3, to be 135.96 (54) s, and we searched for quadrupole overtones spaced by this value. We list the assignment of the relative radial order, modal degree and the azimuthal order in Table 3. The échelle diagram, shown in Fig. 15, was calculated for dipole (left hand) and quadrupole (right hand) modes. We identified only three of the latter modes with all of them between 2000 and 3000 s. The échelle for dipole modes is quite vertical with a side bump between 3000 and 7500 s, likewise B3 and other sdBVs reported by Baran & Winans (2012). There may be another side bump below 3000 s, however, such short period g-modes are not too common among sdBVs, so any claim on its common appearance cannot be yet justified. It was also detected only in KIC 2438324 (Baran & Winans 2012).

3.3.3 B5

Østensen et al. (2010) reported B5 as a sdB star with $T_{\rm eff}$ = 23 844 (676) K and a surface gravity $\log(g/{\rm cm\,s^{-2}}) = 5.31$ (9). Our estimate of the surface gravity (Table 1) is in agreement with the one reported above, while $T_{\rm eff}$ differs by 70 K, including errors. The Kepler data of B5 were first studied by Reed et al. (2012). The authors found B5 to be sdBV star and detected four frequencies. We achieved the detection threshold of 0.064 ppt, which is 6.5 times better than the one used by Reed et al. (2012), and we detected 26 frequencies, including all four frequencies detected by Reed et al. (2012). We list all detected frequencies in Table 4. Likewise in B3, we checked which frequencies may originate beyond the Nyquist frequency and we found seven of these. We show the amplitude spectrum of B5 in Fig. 16.

Table 4. List of fitted frequencies in B5.

ID	Frequency [μHz]	Period [s]	Amplitude [ppt]	S/N	n	l	m
f_1	91.3268(9)	10949.69(11)	0.056(11)	4.1	46	1	0
f_2	91.4014(6)	10940.75(8)	0.077(11)	5.6	46	1	1
f_3	116.11708(24)	8611.997(18)	0.210(11)	15.2	36	1	−1
f_4	116.19014(27)	8606.582(20)	0.187(11)	13.6	36	1	0
f_5	116.2844(6)	8599.604(42)	0.088(11)	6.4	36	1	1
f_6	117.8895(6)	8482.517(46)	0.078(11)	5.6	u	u	u
f_7	122.2930(8)	8177.09(5)	0.064(11)	4.6	34	1	−1
f_8	122.38929(37)	8170.650(25)	0.134(11)	9.7	34	1	0
f_9	122.4773(6)	8164.781(42)	0.079(11)	5.7	34	1	1
f_{10}	133.9872(8)	7463.399(45)	0.062(11)	4.5	31	1	u
f_{11}	147.87944(50)	6762.265(23)	0.100(11)	7.2	28	1	−1
f_{12}	147.93372(18)	6759.784(8)	0.277(11)	20.1	28	1	0
f_{13}	148.02275(31)	6755.718(14)	0.159(11)	11.5	28	1	1
f_{14}	215.57111(45)	4638.840(10)	0.109(11)	7.9	19	1	u
f_{15}	239.5441(9)	4174.596(15)	0.056(11)	4.1	30	2	u
f_{16}	240.47627(13)	4158.4145(22)	0.390(11)	28.2	17	1	u
f_{17}	270.97091(17)	3690.4330(24)	0.286(11)	20.7	15	1	u
f_{18}	290.16990(27)	3446.2568(33)	0.180(11)	13	14	1	u
f_{19}	297.5827(6)	3360.411(7)	0.078(11)	5.6	u	u	u
f_{20}	297.73493(44)	3358.6922(50)	0.112(11)	8.1	24	2	u
f_{21}	310.4975(8)	3220.637(9)	0.060(11)	4.3	u	u	u
f_{22}	311.72740(38)	3207.9310(39)	0.129(11)	9.3	13	1	u
f_{23}	312.41728(28)	3200.8473(29)	0.176(11)	12.7	23	2	u
f_{24}	371.19904(41)	2693.9725(29)	0.122(11)	8.8	11	1	u
f_{25}	372.5513(6)	2684.1939(41)	0.088(11)	6.3	19	2	u
f_{26}	372.6264(8)	2683.653(6)	0.063(11)	4.6	u	u	u

The shapes of the peaks in B5 are very messy. It is an indication of the amplitude/frequency instability. Non-coherent peaks have been also detected by Østensen et al. (2014a) who invoked a termohaline convection as a possible explanation. We show a few examples of non-coherent peaks using sliding amplitude spectra in Fig. 7. Three left hand show single frequencies, while the right most hand shows a region of 297.7 μHz. In this region, we find two frequencies, which may converge in time. It is possible that these two frequencies are split modes. Pre-whitening of non-coherent frequencies leaves significant residuals and detecting other neighbouring frequencies is more difficult, if possible at all. A search for multiplets is also more difficult. Multiplet components which are of low amplitudes, may be smeared by unstable amplitude/frequencies, causing their S/N to drop below the detection threshold and leading to null detection.

We found 11 frequencies that show similar splitting ($f_{1,2}$, $f_{3,4,5}$, $f_{7,8,9}$, $f_{11,12,13}$) and we present them in Fig. 17. However, the profiles of the peaks are so messy that we are unable to estimate the real frequencies, particularly of the central components. Given the complexity of the profiles, and the requirement of precise and long time-series data, we expect a confirmation of those multiplets with additional data may be hardly possible. If the interpretation of the splitting is correct, then the value is in a range of splittings we detected in other sdBV stars. The average splitting is 0.0815 (41) μHz, which translates to 71.0 (1.8) days rotation period. During our pre-whitening of the messy regions, we fit the highest peaks, which may not be a correct choice, hence the value of the splitting and the rotation period is only a rough estimate. We list the assignment of the modal degree and the azimuthal order in Table 4. Only four frequencies were not identified.

The KS test points at the period spacing close to 240 s. We selected frequencies spaced nearly by this value and derived a more precise average value of 235.33 (61) s for dipole modes. The theoretical

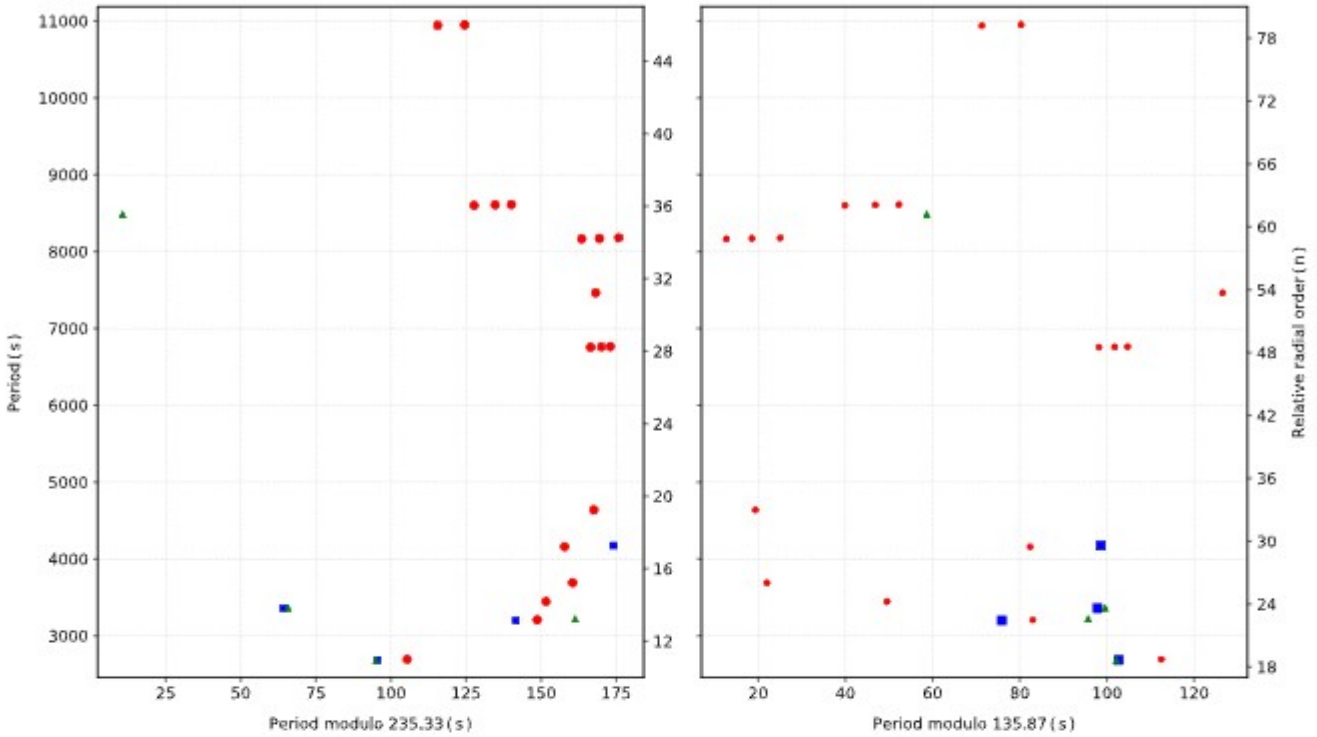

Figure 18. Same as Fig. 15 but for B5.

estimate of the average period spacing of quadrupole modes is 135.87 (46) s, which is consistent with the fit value we derived from just a few detected $\ell = 2$ modes, equalling 135.9 (1.9) s. The assignment of the three parameters describing the mode geometry is included in Table 4.

We calculated the échelle diagram for dipole and quadrupole modes and we present it in Fig. 18. In the left hand, the dipole modes are lined up along a side bump that is common among sdBVs (Baran & Winans 2012). This bump may be even wider in the case of B3 and B4, reaching 11 000 s on the long end of the period range. The right hand shows only four quadrupole modes, which group at the short end, instead.

4 SUMMARY

In this work, we presented results of our photometric and spectroscopic data analysis of sdBV stars located in the open cluster NGC 6791. We analysed MMT/HECTOSPEC spectra available in the public databases and derived the atmospheric parameters using NLTE models of stellar atmospheres. We analysed medium resolution multi epoch spectra of B3, B5, and B6 taken with the Gemini/GMOS, also downloaded from the public database. These spectra were used for constraining radial velocities and we found that B3, B5, and B6 show an excess as compared to other stars in the cluster. Our results suggest that the stars have a peculiar motion with respect to the motion of the entire cluster, which may possibly be due to companions in the star's systems. Using astrometry from *Gaia* EDR3, we calculated the membership probabilities of sdBs. We confirmed B3, B4, and B5 are cluster members with more than 99 per cent likelihood. We also analysed spectra of four other hot stars that we found to be cluster members but show no photometric variability. We provide our estimates of the atmospheric parameters of these stars.

Although we did a thorough search for variable stars in the cluster using the *Kepler* data, we detected stellar pulsations only in three sdBs B3, B4, and B5. These three stars have been analysed previously, however, we obtained extended time coverage, and therefore, higher quality of the data, which allow us to confirm already reported frequencies in the g-mode region and to detect additional ones. We found rotationally split modes and estimated the rotation periods of all three sdB stars. We used these split modes along with the asymptotic overtone sequences to describe mode geometry. We assigned most of the detected frequencies to either dipole or quadrupole modes. Since the quadrupole mode sequences are very short we were unable to calculate the reduced period diagrams and search for any trapped mode candidates likewise found by Østensen et al. (2014b) or Uzundag et al. (2017). The échelle diagrams for all three stars show a side bump that has been previously reported by e.g. Baran & Winans (2012). This feature can be a consequence of a characteristic sdB interior and may be very useful diagnostic tool of evolutionary modelling. For B4, observed in the SC mode, we also searched for p-modes but detected none above the detection threshold.

ACKNOWLEDGEMENTS

Financial support from the National Science Centre under projects No. UMO-2017/26/E/ST9/00703 and UMO-2017/25/B/ST9/02218 is acknowledged. Calculations have been carried out using resources provided by Wroclaw Centre for Networking and Supercomputing (http://wcss.pl), grant No. 265. P. Németh acknowledges support from the Grant Agency of the Czech Republic (GACR 18-20083S). This research has used the services of www.Astroserver.org under reference F668BE. I. Pelisoli acknowledges support from the UK's Science and Technology Facilities Council (STFC), grant ST/T000406/1.

DATA AVAILABILITY

The photometric datasets were derived from the MAST in the public domain archive.stsci.edu. The spectroscopic observations were downloaded from the MMT public archive available at https://oirsa.cfa.harvard.edu/search/ and Gemini Science Archive accessible at https://archive.gemini.edu/gaia. The astrometry was collected by the ESA mission *Gaia* and is accessible at https://www.cosmos.esa.int/gaia.

REFERENCES

Baran A. S., 2013, AcA, 63, 203
Baran A. S., Winans A., 2012, AcA, 62, 343
Baran A. et al., 2009, MNRAS, 392, 1092
Baran A. S. et al., 2012, MNRAS, 424, 2686
Baran A. S., Koen C., Pokrzywka B., 2015, MNRAS, 448, L16
Bedin L. R., Salaris M., Piotto G., King I. R., Anderson J., Cassisi S., Momany Y., 2005, ApJ, 624, L45
Bedin L. R., Piotto G., Carraro G., King I. R., Anderson J., 2006, A&A, 460, L27
Carraro G., Villanova S., Demarque P., McSwain M. V., Piotto G., Bedin L. R., 2006, ApJ, 643, 1151
Charpinet S., Fontaine G., Brassard P., Chayer P., Rogers F. J., Iglesias C. A., Dorman B., 1997, ApJ, 483, L123
Charpinet S., Fontaine G., Brassard P., Dorman B., 2000, ApJS, 131, 223
Charpinet S. et al., 2011, Nature, 480, 496
Charpinet S., Van Grootel V., Brassard P., Fontaine G., Green E. M., Randall S. K., 2013a, European Physical Journal Web of Conferences, Vol. 43, EDP Sciences, p. 4005
Charpinet S., Van Grootel V., Brassard P., Fontaine G., 2013b, Precision Asteroseismology Proceedings of the International Astronomical Union Symposium, Vol. 301, Cambridge University Press, Cambridge, p. 397
Charpinet S., Brassard P., Van Grootel V., Fontaine G., 2014, Meetings on Hot Subdwarf Stars and Related Objects, Vol. 481, Astronomical Society of the Pacific, San Francisco, p. 179
Ferguson T. S., 1973, Ann. Stat., 1, 209
Fontaine G., Brassard P., Charpinet S., Green E. M., Randall S. K., Van Grootel V., 2012, A&A, 539, A12
Foster H. M., Reed M. D., Telting J. H., Østensen R. H., Baran A. S., 2015, ApJ, 805, 94
Gao X., 2020, Ap&SS, 365, 24
Gough D. O., 1986, in Osaki Y., ed., Hydrodynamic and Magnetodynamic Problems in the Sun and Stars,University of Tokyo Press, Tokyo, p. 117
Green E. M. et al., 2003, ApJ, 583, L31
Han Z., Podsiadlowski P., Maxted P. F. L., Marsh T. R., Ivanova N., 2002, MNRAS, 336, 449
Han Z., Podsiadlowski P., Maxted P. F. L., Marsh T. R., 2003, MNRAS, 341, 669
Heber U., 2016, PASP, 128, 082001
Hubeny I., Lanz T., 1995, ApJ, 439, 875
Hubeny I., Lanz T., 2017, preprint (arXiv:1706.01937)
Jílková L., Carraro G., Jungwiert B., Minchev I., 2012, A&A, 541, A64
Kaluzny J., Udalski A., 1992, AcA, 42, 29
Kaluzny J., Stanek K. Z., Garnavich P. M., Challis P., 1997, ApJ, 491, 153
Kamann S., Bastian N. J., Gieles M., Balbinot E., Hénault-Brunet V., 2019, MNRAS, 483, 2197
Kilkenny D., Koen C., O'Donoghue D., Stobie R. S., 1997, MNRAS, 285, 640
Kinemuchi K., Barclay T., Fanelli M., Pepper J., Still M., Howell S. B., 2012, PASP, 124, 963
King I. R., Bedin L. R., Piotto G., Cassisi S., Anderson J., 2005, AJ, 130, 626
Liebert J., Saffer R. A., Green E. M., 1994, AJ, 107, 1408
Lindegren L. et al., 2021, A&A, 649, A4
Murphy S. J., Shibahashi H., Kurtz D. W., 2013, MNRAS, 430, 2986
Németh P., Kawka A., Vennes S., 2012, MNRAS, 427, 2180
Østensen R. H. et al., 2010, MNRAS, 409, 1470
Østensen R. H., Reed M. D., Baran A. S., Telting J. H., 2014a, A&A, 564, L14
Østensen R. H., Telting J. H., Reed M. D., Baran A. S., Nemeth P., Kiaeerad F., 2014b, A&A, 569, A15
Pedregosa F. et al., 2011, J. Mach. Learn. Res., 12, 2825
Platais I., Cudworth K. M., Kozhurina-Platais V., McLaughlin D. E., Meibom S., Veillet C., 2011, ApJ, 733, L1
Reed M. D. et al., 2011, MNRAS, 414, 2885
Reed M. D., Baran A., Østensen R. H., Telting J., O'Toole S. J., 2012, MNRAS, 427, 1245
Reed M. D., Foster H., Telting J. H., Østensen R. H., Farris L. H., Oreiro R., Baran A. S., 2014, MNRAS, 440, 3809
Schuh S., Huber J., Dreizler S., Heber U., O'Toole S. J., Green E. M., Fontaine G., 2006, A&A, 445, L31
Stetson P. B., Bruntt H., Grundahl F., 2003, PASP, 115, 413
Tassoul M., 1980, ApJS, 43, 469
Telting J. H. et al., 2012, A&A, 544, A1
Unno W., Osaki Y., Ando H., Shibahashi H., 1979, University of Tokyo Press; Forest Grove, Ore., ISBS, Inc., p. 330
Uzundag M., Baran A., Østensen R., Reed M., Telting J., Quick B., 2017, A&A, 597, 95
van den Berg M., Verbunt F., Tagliaferri G., Belloni T., Bedin L. R., Platais I., 2013, ApJ, 770, 98
Villanova S., Carraro G., Geisler D., Monaco L., Assmann P., 2018, ApJ, 867, 34

APPENDIX A:

Table A1. List of other hot and non-pulsating stars in our analysis that we found to be almost certain NGC 6791 members (Section 3.1), and have spectroscopic estimates derived in this work (Section 2.1). The probability membership for B7 and SBG 644 has been calculated without PM_RA. The spectral analysis of B2 is from the SDSS observation while others are from the HECTOSPEC observations.

Name	Type	K_p [mag]	$T_{\rm eff}$ [K]	$\log(g/{\rm cm\,s^{-2}})$	$\log(N_{\rm He}/N_{\rm H})$	$P_{\rm memb}$	Reference[a]
B6	sdB	15.443	31 920(150)	5.682(50)	−2.50(13)	0.991	KU92,L94,SS21
B2	sdO	17.177	48 920(1210)	5.164(34)	−1.80(14)	0.999	KU92,O10,SS21
B7	CV	17.068	35 510(1110)	6.72(18)	−3.80(35)	0.993	K97,SS21
SBG 644	A0V	19.138	10 950(60)	4.437(46)	−2.84(97)	0.931	S03,SS21

Note.[a] – SS21 – this work, KU92 – Kaluzny & Udalski (1992), O10 – Østensen et al. (2010), L94 – Liebert et al. (1994), K97 – Kaluzny et al. (1997), S03 – Stetson, Bruntt & Grundahl (2003).

This paper has been typeset from a TEX/LATEX file prepared by the author.

Chapter 3

Paper II: Sounding Interiors of Four Pulsating Subdwarf B Stars with Stellar Pulsations

Abstract

We present the results of asteroseismic modeling of four pulsating sdB stars KIC 2438324, KIC 2569576, KIC 2991403 and KIC 11159657. We used fully evolutionary models and this is the first attempt of seismic modeling of sdB stars using the MESA models and GYRE. We adopted an already reported list of periods identified with dipole modes. Additionally, we used two spectroscopic parameters, *i.e.*$T_{\rm eff}$ and $\log g$, and, only for KIC 2438324 and KIC 2569576, we used cluster parameters, *i.e.* total age and metallicity, to further filter the outcome of matching observed and theoretical pulsation periods. In the case of a spectroscopically constrained approach only for KIC 2438324 we derived a unique solution. For two stars we derived unique input parameters except the hydrogen and progenitor mass, respectively for KIC 2569576 and KIC 2991403. All input parameters except the convective core and progenitor masses are unique for KIC 11179657. Except for KIC 11179657, our fits, measured by a relative period difference ($\Delta P/P$), are well within 1%. These results sound very promising and more asteroseismic modeling of sdB stars should be done in future.

doi: 10.32023/0001-5237/73.1.2

ACTA ASTRONOMICA
Vol. **73** (2023) pp. 21–34

Sounding Interiors of Four Pulsating Subdwarf B Stars with Stellar Pulsations

A. Baran[1,2,3] and S. Sanjayan[1,4]

[1] ARDASTELLA Research Group
[2] Astronomical Observatory, University of Warsaw, Al. Ujazdowskie 4, 00-478 Warszawa, Poland
[3] Department of Physics, Astronomy, and Materials Science, Missouri State University, Springfield, MO 65897, USA
[4] Nicolaus Copernicus Astronomical Centre, Bartycka 18, 00-716 Warszawa, Poland

Received March 18, 2023

ABSTRACT

We present the results of asteroseismic modeling of four pulsating sdB stars KIC 2438324, KIC 2569576, KIC 2991403 and KIC 11159657. We used fully evolutionary models and this is the first attempt of seismic modeling of sdB stars using the MESA models and GYRE. We adopted an already reported list of periods identified with dipole modes. Additionally, we used two spectroscopic parameters, *i.e.*, $T_{\rm eff}$ and $\log g$, and, only for KIC 2438324 and KIC 2569576, we used cluster parameters, *i.e.*, total age and metallicity, to further filter the outcome of matching observed and theoretical pulsation periods. In the case of a spectroscopically constrained approach we derived a unique solution only for KIC 2438324. For two stars we derived unique input parameters except for the hydrogen and progenitor mass, respectively for KIC 2569576 and KIC 2991403. All input parameters except for the convective core and progenitor masses are unique for KIC 11179657. Except for KIC 11179657, our fits, measured by a relative period difference ($\Delta P/P$), are well within 1%. These results sound very promising and more asteroseismic modeling of sdB stars should be done in future.

Key words: *Stars: evolution – Stars: interiors – subdwarfs – Stars: oscillations*

1. Introduction

Subdwarf B stars (sdB) are identified with core-helium burning stars. According to Fontaine *et al.* (2012), 68.3% of sdB stars have masses between 0.439 $M_\odot$ and 0.501 $M_\odot$, with a median being 0.471 $M_\odot$ (also known as a canonical mass). Subdwarf B stars are hot and compact with effective temperature $T_{\rm eff} = 20\,000 - 40\,000$ K and surface gravity $\log g$ [cgs] $= 5.0-5.8$ (Heber 2016). A unique feature of sdB stars, which differs them from classical horizontal branch stars, is a very low-mass hydrogen envelope, $M_{\rm env} < 0.01$ $M_\odot$ (Heber 1986, Saffer *et al.* 1994). Such envelope is unable to sustain a hydrogen-burning shell, which could lift the

stars to the asymptotic giant branch. After the helium in the core is exhausted sdB stars evolve directly to the white dwarf cooling track (Dorman *et al.* 1993). To remove the hydrogen envelope a few evolutionary channels have been proposed (Han *et al.* 2002, 2003). The mass loss resulting from interactions between binary components may probably be dominant, since about two third of sdB stars are members of binary systems (Maxted *et al.* 2001). Evolutionary channels leading to single sdB stars include mergers, hot-flashes and substellar companions (Mengel, Norris and Gross 1976, D'Cruz *et al.* 1996, Han *et al.* 2002, 2003, Miller Bertolami *et al.* 2008, Fontaine *et al.* 2012, Charpinet *et al.* 2018).

Stellar pulsations are commonly observed in many sdB stars. Pulsations in pressure (p) modes in sdB stars were predicted by Charpinet *et al.* (1996) and first observationally detected by Kilkenny *et al.* (1997), whereas the gravity (g) modes in sdB stars were detected by Green *et al.* (2003). Typical periods of p-mode sdB pulsators are of the order of minutes, while periods of g-mode sdB pulsators are of the order of hours (Heber 2016). Both p- and g-modes in sdB stars are driven by the κ-mechanism efficiently working owing to the metal opacity bump (Charpinet *et al.* 1996, 1997, Fontaine *et al.* 2003). Seismic modeling was applied to probe the internal structure of sdB stars and allowed determination of the convective core masses of four g-mode pulsators: $M_{\rm core} = 0.22 \pm 0.01$ M$_\odot$ (KPD 0629-0016, Van Grootel *et al.* 2010a), $M_{\rm core} = 0.28 \pm 0.01$ M$_\odot$ (KPD 1943+4058, Van Grootel *et al.* 2010b), $M_{\rm core} = 0.274^{+0.008}_{-0.010}$ M$_\odot$ or $M_{\rm core} = 0.225^{+0.011}_{-0.016}$ M$_\odot$ (KIC 2697388, Charpinet *et al.* 2011), and $M_{\rm core} = 0.198 \pm 0.010$ M$_\odot$ (EC 21494-7018, Charpinet *et al.* 2019). The masses of the first three stars are close to the canonical value, whereas of the fourth one has significantly lower mass, $M_{\rm sdB} = 0.391 \pm 0.009$ M$_\odot$. The solutions for these four stars point to rather young models with central helium abundance in the range of $Y_c \approx 0.8-0.5$. All of the seismic studies of sdB stars were performed using the forward modeling method (Charpinet *et al.* 2008, Van Grootel *et al.* 2008) with static, structural models, which are complete hydrostatic stellar structures in thermal equilibrium (*e.g.*, Brassard and Fontaine 2008, 2009, Charpinet *et al.* 2019). The advantages of static models compared to evolutionary models are higher versatility, faster computations, and possibility to explore more structural configurations. The structure of static models is inspired by full evolutionary calculations. However, many static configurations are not realistic from an evolutionary point of view.

The core-helium-burning phase is very challenging for evolutionary calculations, particularly because of the complex behavior of the physical quantities, such as opacity, temperature, density, etc. The most common problems in the models are determining the boundaries of the convective core (aka splitting of the convective core) that leads to an unrealistic structure of a star (*e.g.*, Paczyński 1970, Castellani *et al.* 1971, Eggleton 1972, Dorman and Rood 1993, Salaris and Cassisi 2017) or the occurrence of breathing pulses, which are most likely numerical artifacts and not realistic features of stellar evolution (*e.g.*, Caputo *et al.* 1989, Dorman and

Rood 1993, Constantino *et al.* 2016, 2017). There is also a discrepancy between the masses of convective cores of sdB stars derived from structural and fully evolutionary models, where the latter yield significantly lower values. The proposed solutions that attempt to mitigate these problems involve additional mixing that helps to increase the size of the core, such as semiconvection or overshooting (Sweigart 1987, Dorman and Rood 1993), taking advantage of an element diffusion that also allows the core to grow (Michaud *et al.* 2007), introduction of more sophisticated algorithms to determine core boundaries (*e.g.*, the predictive mixing scheme and the convective pre-mixing scheme, Paxton *et al.* 2018, 2019), or changes to microphysics. A comprehensive discussion on this subject can be found in Schindler *et al.* (2015) or, more recently, in Ostrowski *et al.* (2021).

The goal of this paper is to report the current capabilities and limitations of seismic modeling of sdB stars using fully evolutionary models calculated with the MESA code, and adiabatic pulsation periods calculated with the GYRE code. We aim to use the grid of models with a reliable internal structure to reproduce the observed periods of four g-mode dominated sdB pulsators: KIC 2569576 and KIC 2438324 (Sanjayan *et al.* 2022a), as well as KIC 2991403 and KIC 11179657 (Baran and Winans 2012).

The structure of this paper is as follows. In Section 2, we describe the setup of the calculated grid of models. Section 3 discusses the results of our seismic modeling and is followed by conclusions presented in Section 4.

2. Grid of Models

A grid of evolutionary models was calculated using publicly available and open source code MESA (Modules for Experiments in Stellar Astrophysics, Paxton *et al.* 2011, 2013, 2015, 2018, 2019), version 11701. Our goal was to find models with realistic internal structure and correct behavior of quantities such as radiative gradient, crucial for the proper modeling of mixed regions. In this section, we present the short overview of the models. The detailed description of the physics and algorithms applied to calculate them can be found in the paper by Ostrowski *et al.* (2021), in which thoroughly explored MESA models of sdB stars are presented.

The models were calculated for progenitors with masses, M_i, in the range of 1.0–1.8 $M_\odot$ and a 0.005 $M_\odot$ step, as well as metallicities, Z in the range of 0.005–0.035 and a 0.005 step. The latter represents the percentage of a star's mass attributed to elements that are heavier than hydrogen. We follow the [Fe/H] notation from Németh *et al.* (2012), where $[\mathrm{Fe/H}] = \log(Z/Z_\odot)$. We adopted the solar metallicity $Z_\odot = 0.0142$. The initial helium abundance was determined by the linear enrichment law, $\Delta Y/\Delta Z = 1.5$. The protosolar helium abundance, $Y_{\odot,\,\mathrm{protosolar}} = 0.2703$, and the mixture of metals were adopted from Asplund *et al.* (2009). The progenitors were evolved to the tip of the red giant branch where most of the hydrogen has been removed before the helium ignition, leaving only a

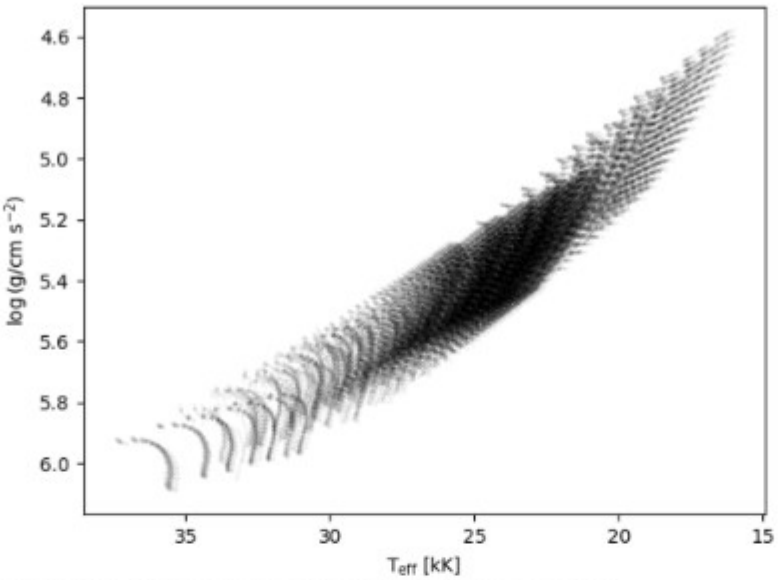

Fig. 1. Grid of evolutionary models on the EHB calculated with the MESA.

residual hydrogen envelope on top of the helium core. The envelope masses, M_{env}, are in the range of 0.0001–0.0030 $M_{\odot}$, with a step of 0.0001 $M_{\odot}$, and in the range of 0.003–0.010 $M_{\odot}$, with a step of 0.001 $M_{\odot}$. The models were relaxed to an equilibrium state and evolved until the depletion of helium in the core. We show the grid of evolutionary models in Fig. 1.

The convective pre-mixing scheme was applied, which is a novel algorithm introduced to the MESA code to solve problems with determination of convective boundaries (Paxton *et al.* 2019). Ostrowski *et al.* (2021) showed that the convective premixing scheme ensures the correct and expected behavior of radiative gradient at the border of the convective core (Gabriel *et al.* 2014). The use of the algorithm in sdB models leads to formation of partially-mixed semi-convective region on top of the convective core. Following Ostrowski *et al.* (2021), the core of an sdB model was defined as a combination of the fully-mixed convective core and a partially-mixed semi-convective region. Such a combined mixed region has a smooth structure and a mass higher than what would be obtained from a model with only the standard Ledoux criterion.

The adiabatic pulsation models were calculated using the GYRE code, version 5.2 (Townsend and Teitler 2013, Townsend *et al.* 2018, Goldstein and Townsend 2020). The pulsation models were calculated for evolutionary models with central helium abundance, Y_c, in the range of 0.9–0.1, with a step of 0.05. The models with $Y_c < 0.1$ were not considered because of the occurrence of the breathing pulses, which are currently an unavoidable side effect of using the convective premixing scheme (Ostrowski *et al.* 2021).

3. Period Fitting

The calculated grid consists of 63 113 models with pulsation modes calculated up to a modal degree of $\ell = 4$. We used a goodness-of-fit function, which delivers a difference between observed and calculated periods:

$$S^2 = \frac{1}{N_o} \sum_{i=1}^{N_o} \left(P_o^i - P_c^i\right)^2, \tag{1}$$

where P_o is an observed period, P_c is a calculated period, and N_o is the number of periods used. The smallest S^2 value indicates the best fit. For our consideration we accepted all fits up to 1.5 times the minimum value of S^2.

Table 1

Periods of the central components of multiplets used in our fitting

	KIC 2438324	KIC 2569576	KIC 2991403	KIC 11179657
	P_o^i [sec]			
1	2263.4784(46)	3032.4297(13)	2709.9847(25)	2709.807(12)
2	2466.6735(18)	3283.6391(15)	2986.6839(10)	2965.8311(34)
3	2679.0934(13)	4047.0103(21)	3239.084(11)	3239.849(12)
4	2914.9485(24)	4292.1760(13)	3512.2355(24)	3513.349(8)
5	3149.775(8)	4519.4959(15)	3781.5923(17)	3777.025(50)
6	3435.5454(35)	4794.415(18)	4337.3974(35)	4840.46(6)
7	4366.771(10)	5039.7282(11)	5123.517(9)	5109.267(9)
8	4610.602(6)	5282.0773(18)	6362.558(8)	5362.571(9)
9		7201.584(6)		6612.32(18)
10		7683.263(42)		6835.44(9)

To find the best match between the models and observations we adopted the following approach. First, we searched the entire grid of calculated periods, without any constraints on physical parameters. Then, we applied spectroscopic estimates of $T_{\rm eff}$ and $\log g$. Finally, but only available to cluster members, we used age and metallicity constraints derived from previous works. Since our calculated periods are based on adiabatic calculations we have no information on the driving efficiency of specific pulsation modes. Using all detected periods without prior mode identification would easily lead to a solution biased toward the highest modal degrees to be the best matches, since as the modal degree increases the period spacing among consecutive same-degree overtones decreases. We decided not to consider such an approach. Instead, we chose previously reported multiplets to be the only periods fitted. We listed all periods fitted in a given star in Table 1. Since we do not consider rotation in our calculated periods, only the central components were used, however, as we tested it, the difference in periods between consecutive components

is too small to make a difference in a period fitting. Therefore, a misidentification of central components does not influence our final conclusions.

3.1. KIC 2438324

KIC 2438324 is a binary system containing a pulsating sdB star and a main-sequence companion (Baran and Winans 2012). The authors detected 21 frequencies, including two identified with the binarity, and identified seven dipole modes using rotational splitting and the expected period spacing between consecutive radial overtones. The spectroscopic parameters reported by Sanjayan *et al.* (2022a) are $T_{\rm eff} = 25\,290(300)$ K and $\log g$ [cgs] $= 5.510(43)$. In addition, this star is a member of an unusual open cluster, NGC 6791, which does not fit any age-metallicity relation for the Galactic disk and is located about 1 kpc above the Galactic plane, where the majority of open clusters reside (Jílková *et al.* 2012). Despite its rather old age of 8(1) Gyr (Carraro *et al.* 2006), the cluster is metal rich with [Fe/H] in the range of 0.3–0.4 (Villanova *et al.* 2018). Recently Sanjayan *et al.* (2022b) reported the age of 8.91 Gyr and the [Fe/H] of 0.26–0.28, the latter being lower than the estimate reported by Villanova *et al.* (2018).

The most recent analysis based on the longest coverage was presented by Sanjayan *et al.* (2022a). The authors detected 31 frequencies that can be attributed to g-mode pulsations in the sdB component. In addition, two frequencies related to the binarity were also reported. For our analysis, we selected eight central components of triplets (Table 3 in Sanjayan *et al.* 2022a) and we listed them in Table 1. We show the results of our period fitting in Table 2. The top part includes models derived solely based on the selected periods. No other constraints were used. The solutions satisfying the $1.5\,S^2$ criterion point at a fairly consistent model with an exception of two input parameters. The mass of the hydrogen envelope, which ranges between 0.005 $M_\odot$ and 0.006 $M_\odot$, and the mass of a progenitor, which ranges from 1.30 $M_\odot$ to 1.65 $M_\odot$. The range of the former is the step of this parameter in the grid of models. The star seems to be a canonical mass hot subdwarf with the 0.14 $M_\odot$ convective core and it has 55% of the central helium left. In the next step we applied the spectroscopic constraints, *i.e.*, the effective temperature and surface gravity. In this approach we derived a unique solution. The solution is similar to, but it does not overlap with, those derived in the previous approach. It also does not fit the age of the cluster as it is younger compared to estimates reported by Carraro *et al.* (2006) and Sanjayan *et al.* (2022b). We marked the model we derived in the spectroscopically constrained approach in the top panel of Fig. 2. The quality of the fit measured by $\Delta P/P$ is 0.51%, where ΔP denotes a sum of absolute differences between observed and modeled periods.

We also tried the opposite approach. We searched for a model that overlaps with the cluster age and metallicity cited by Carraro *et al.* (2006), Villanova *et al.* (2018) or Sanjayan *et al.* (2022b), and delivers the smallest S^2. The model is presented in Table 3 and it indicates an sdB star with 30% central helium burned during the

T a b l e 2

Models of four stars that meet the 1.5 S^2 criterion

star	KIC 2438324	KIC 2569576	KIC 2991403	KIC 11179657
			unconstrained	
M_{core} [$M_\odot$]	0.14	0.14	0.13–0.14	0.13–0.14
M_{sdB} [$M_\odot$]	0.47	0.47	0.46–0.48	0.46–0.47
M_{env} [10^{-3} $M_\odot$]	0.5–0.6	0.3	0.1–6.0	0.1
Y_c	0.55	0.55	0.10–0.30	0.10–0.35
Fe/H	0.24	0.15	0.15–0.39	0.32–0.39
T_{eff} [K]	26 000–26 500	29 340	18 900–32 500	25 500–35 500
log g [cgs]	5.538–5.561	5.720	4.78–5.79	5.34–5.82
R [$R_\odot$]	0.19	16.35	0.14–0.47	0.14–0.24
L [$L_\odot$]	15.36–15.56	0.16	18.60–20.83	16.76–22.33
M_i [$M_\odot$]	1.30–1.65	1.25	1.05–1.75	1.30–1.80
Age [Myr][a]	52.73–53.64	52.08	84.0–135.7	87.7–137.6
Age [Gyr]	2.3–5.4	5.86	2.1–11.0	1.9–5.9
$\Delta P/P$ [%]	0.35–0.43	0.17	0.25–0.37	0.19–0.28
			constrained by spectroscopy	
M_{core} [$M_\odot$]	0.14	0.14	0.14	0.14–0.15
M_{sdB} [$M_\odot$]	0.47	0.47	0.47	0.48
M_{env} [10^{-3} $M_\odot$]	0.7	2.2–2.4	1.0	2.2
Y_c	0.50	0.50	0.10	0.10
Fe/H	0.32	0.15	-0.16	-0.16
T_{eff} [K]	25 200	23 460–23 690	27 300	25 200–25 300
log g [cgs]	5.476	5.310–5.330	5.41	5.26
R [$R_\odot$]	0.21	0.25	0.22	0.27
L [$L_\odot$]	15.38	17.43–17.45	24.92–25.27	25.92–26.11
M_i [$M_\odot$]	1.25	1.05	1.70–1.75	1.25–1.45
Age [Myr][a]	60.95	55.06–55.13	120.3–121.9	116.4–117.3
Age [Gyr]	6.57	10.97	1.6–1.7	2.9–4.7
$\Delta P/P$ [%]	0.51	0.25–0.30	0.37–0.39	1.23–1.73

Periods are listed in Table 1. The top part represents fitting without any constraints except for the selected periods used. The bottom part represents period fitting with two constraints, T_{eff} and log g.
[a] – denotes stellar age since the Zero-Age Extreme Horizontal Branch.

EHB. The spectroscopic estimates fully agree with our observations. We stress, however, that the age of the cluster represents a single star evolution timescale, while KIC 2438324 is a binary system. A mass transfer in the binary system affects the evolutionary timescale as compared to a single star scenario. Therefore, the age of the cluster may not be a fortunate choice to constrain our model selection. To avoid a bias caused by uncertain application of the age of the cluster we repeated the same experiment taking into account sole cluster metallicity. The model that meets our criteria the best is very similar to the one we obtained in the previous scenario. It should be noted, though, that expecting the metallicity in models to be realistic implies that we assumed the MESA treats diffusion throughout stellar

evolution realistically. Stellar interior is similar in these two scenarios, but the progenitor mass and so the evolutionary timescale are different. Both models agree with spectroscopic estimates derived from observations.

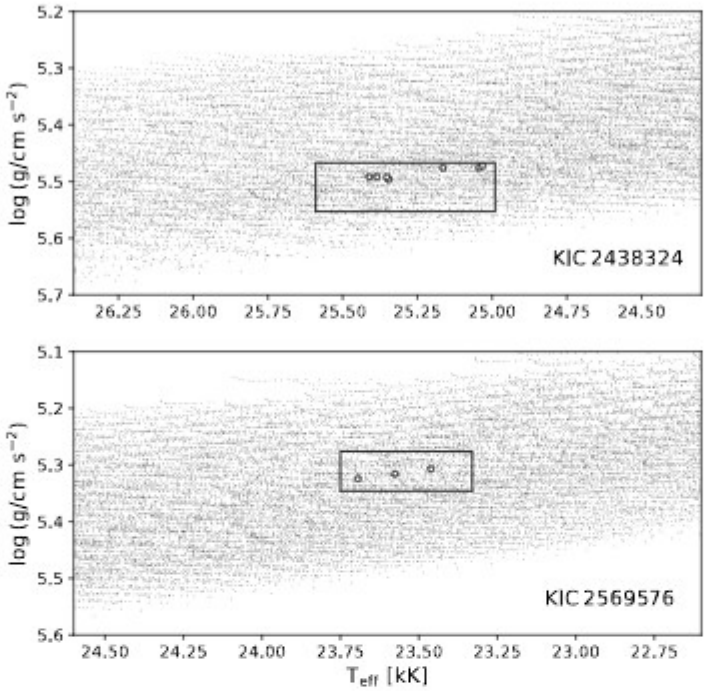

Fig. 2. A close-up of the grid of evolutionary models (dots) with the solutions identified in the spectroscopically constrained approach (circles) for KIC 2438324 (*top panel*) and KIC 2569576 (*bottom panel*).

3.2. KIC 2569576

KIC 2569576 was found to be a pulsating sdB star by Reed *et al.* (2012) based on one month short cadence Kepler data. The authors detected 11 frequencies and identified nine dipole modes using the expected period spacing between consecutive radial overtones. No multiplets have been identified. Sanjayan *et al.* (2022a) analyzed long cadence data span over Quarters 1–17, *i.e.*, 47 months, which is the longest coverage analyzed thus far. Such a coverage is much longer that a typical rotation period reported for sdB stars, *i.e.*, 40 d, and, indeed, the authors reported a detection of eight rotationally split modes, specifically triplets. In total, 38 frequencies were detected and attributed to g-mode pulsations. For our analysis, we accepted all 10 central components of triplets (Table 3 in Sanjayan *et al.* 2022a). We list periods of the central components in Table 1. To constrain our period fitting we used the spectroscopic parameters reported by Sanjayan *et al.* (2022a),

i.e., $T_{\rm eff} = 23\,540(210)$ K and $\log g$ [cgs] $= 5.311(35)$. Likewise for KIC 2438324, this star is also a member of the open cluster NGC 6791, hence we made an attempt to use cluster parameters as constraints in the period fitting.

We present the results of the period fitting in Table 2. In the top part we include a solution derived without constraints except for the selected periods that we used. It is a consistent model, however it does not overlap with the spectroscopic estimates. In the bottom panel we include solutions limited to those that are satisfactory with the $T_{\rm eff}$ and $\log g$ estimates. In this approach, we derived a set of solutions that, among the input parameters, differ only in the envelope mass. The models are close to the cluster age of 8.91 Gyr, however older by 23%. These models represent a star that is half way through its core-helium burning. The metallicity is lower than the one derived by Sanjayan *et al.* (2022b). This model does not agree with the cluster's two parameters, the age and metallicity. According to Sanjayan *et al.* (2022a), KIC 2569576 is likely a binary system, which can make our period fitting a subject to the same caveat as explained for KIC 2438324. We marked all models we derived in the spectroscopically constrained approach in the bottom panel of Fig. 2. The quality of the fit measured by $\Delta P/P$ is between 0.25 and 0.30%.

In the following approach, likewise for KIC 2438324, we searched for a model that fits the cluster age and metallicity, and delivers the smallest S^2. First, we used both cluster parameters, the age and metallicity. The models that, in both scenarios, meet our criteria are shown in Table 3. Comparing the spectroscopic estimates with observations, the surface gravity agrees in both scenarios, while the effective temperature agrees only in the latter one. The models also differ in stellar interiors. The progenitor mass is very different between scenarios.

3.3. KIC 2991403

KIC 2991403 was identified as an sdB star residing in a binary system with a main sequence M dwarf by Østensen *et al.* (2010). The authors reported spectroscopic estimates of $T_{\rm eff} = 27\,300(200)$ K and $\log g$ [cgs] $= 5.43(3)$, which we used in our work to constrain a model selection. In addition, the authors detected a flux variation caused by a reflection effect and pulsations identified as gravity modes. The most recent, and based on the longest time coverage, analysis was presented by Baran and Winans (2012). The authors detected 40 frequencies, including two identified as a binary frequency and its harmonic. The remaining 38 frequencies were explained by stellar pulsations. Eight $\ell = 1$ multiplets were identified and we used the central components of all of them for our period fitting.

We show the result of our period fitting in Table 2. In the unconstrained approach we derived quite a variety of solutions. Neither of the input parameters is uniquely determined. The age, since the Zero-Age Extended Horizontal Branch (ZAEHB), varies between 84.0 Myr and 135.7 Myr. The metallicity is quite rich, specifically, at least 0.15. The envelope mass is anything between 0.0001 $M_\odot$ and

Table 3

Same as in Table 2, but only for the cluster members and using age and metallicity to constrain solutions

	KIC 2438324		KIC 2569576	
	Age and Fe/H	Fe/H	Age and Fe/H	Fe/H
$M_{\rm core}$ [$M_\odot$]	0.14	0.14	0.13	0.13
$M_{\rm sdB}$ [$M_\odot$]	0.46	0.46	0.46	0.46
$M_{\rm env}$ [10^{-3} $M_\odot$]	0.7	0.7	1.1	0.9
$Y_{\rm c}$	0.7	0.7	0.35	0.25
Fe/H	0.39	0.39	0.39	0.39
$T_{\rm eff}$ [K]	25 200	25 200	22 430	23 560
$\log g$ [cgs]	5.552	5.553	5.321	5.318
L [$L_\odot$]	13.02	12.90	16.47	16.71
R [$R_\odot$]	0.19	0.19	0.25	0.25
$M_{\rm i}$ [$M_\odot$]	1.20	1.45	1.20	1.80
Age [Myr][a]	27.51	27.98	87.39	111.87
Age [Gyr]	7.73	3.90	7.79	1.94

0.006 $M_\odot$, while the progenitor mass represents almost the entire grid size. A quite different result, mostly in metallicity, we derived for the spectroscopically constrained approach. Other parameters seem to be either unique or in narrow ranges, and are included in the solutions derived in the previous approach. In this approach we derived a model, which represents a star that has only 10% of the central helium indicating its late evolution during the core-helium burning (the age since ZAEHB is around 121 Myr). The evolutionary phase is well constrained. The hydrogen envelope is only 0.1 % of the solar mass, the star is of canonical mass and has a 0.14 $M_\odot$ convective core. We marked all models we derived in the spectroscopically constrained approach in the top panel of Fig. 3. The quality of the fit measured by $\Delta P/P$ is between 0.37% and 0.39%.

3.4. TIC 11179657

TIC 11179657 was found to be an sdB star by Østensen *et al.* (2010). The authors reported the effective temperature and surface gravity to be $T_{\rm eff} = 26\,000(800)$ K and $\log g$ [cgs] $= 5.14(13)$, respectively, which we utilized in our period fitting for the spectroscopically constrained approach. A flux variation caused by the reflection effect and stellar pulsations was also reported. Baran and Winans (2012) delivered an analysis of the longest time-series reporting 45 frequencies, including two caused by the reflection effect. The authors identified 10 $\ell = 1$ and one $\ell = 2$ multiplets. In our period fitting we utilized only the central components of triplets.

We present the results of our period fitting in Table 2. In the unconstrained approach, similarly to the previous star, we derived neither a unique solution nor

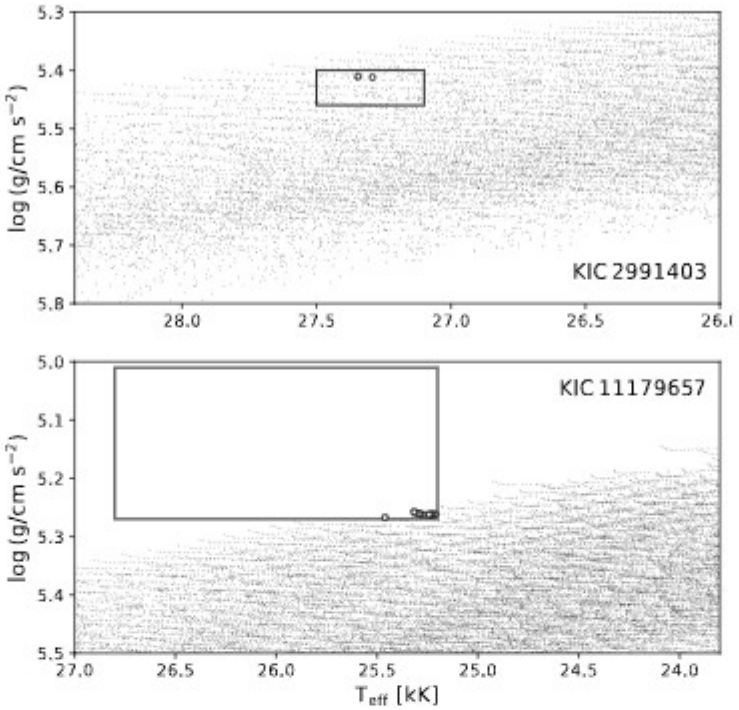

Fig. 3. Same as in Fig. 2 but for KIC 2991403 (*top panel*) and KIC 11179657 (*bottom panel*).

narrow ranges of parameters. The helium content is anything between 0.1 and 0.35, while the progenitor mass is between 1.30 $M_\odot$ and 1.80 $M_\odot$. These solutions do not even indicate any preferred evolutionary stage of the star. More constrained solutions are derived when spectroscopic estimates are used. The hydrogen envelope mass, helium content and metallicity are uniquely derived. This model represents a star with the helium in the core mostly exhausted (10% left), low metallicity ($Fe/H = -0.16$) and the hydrogen envelope with only 0.1% of the total mass. The progenitor mass and so the age is not well constrained. However, the progenitor is not more massive than 1.45 $M_\odot$. The star seems to be metal-poor and at the end of its EHB evolution. We marked all models we derived in the spectroscopically constrained approach in the top panel of Fig. 3. We stress, however, that the spectroscopic estimates place this star well above the models in our grid. Only a small part of the error box overlaps with the grid. It means that the only available models that will satisfy the spectroscopic constraints will represent late-EHB stars, and this can also influence the total range of parameters of models. Our hunch is that either the spectroscopic fit does not provide too precise estimates or the star is not an EHB star, which resulted from a single star evolution, and that is why its location does not fit our grid too well. The quality of the fit measured by $\Delta P/P$ is between 1.23% and 1.73% and is the poorest among all stars analyzed in this work, which may be caused by spectroscopic estimates to be off the grid.

4. Summary and Conclusions

We presented our results of pulsation period fitting for four pulsating sdB stars. Two stars belong to an open cluster, NGC 6791, and the pulsation periods were recently reported by Sanjayan *et al.* (2022a). The authors claim that all four sdBs they found in the cluster, including KIC 2438324 and KIC 2569576, are residing in binary systems. Two other stars presented in this work are field sdB stars, but also residing in binary systems. Binarity affects the evolutionary timescale as compared to a single star evolution in which case the age of NGC 6791 was derived by Sanjayan *et al.* (2022b). It means that for KIC 2438324 and KIC 2569576 the cluster age may not serve as a reliable constraint in our period fitting. We used spectroscopic estimates reported in previous works to constrain our period fitting.

The grid of models we used were calculated based on a work presented by Ostrowski *et al.* (2021). The grid consists of 63 113 models of hot subdwarf stars with pulsation modes up to modal degree of four, however according to a preliminary mode identification reported in the literature, only a selection of dipole modes was used in our period fitting.

As a result of our analysis we arrived at the following conclusions:

- The solutions we derived are spectroscopic estimates sensitive, which means that the estimates are crucial toward period fitting and proper model selection.
- In the case of the spectroscopically constrained approach we derived either unique or narrow ranges of models. The mass of the convective core, hydrogen envelope and total mass, central helium, which gives the age since the ZAEHB, and metallicity are well constrained.
- All models represent canonical mass hot subdwarfs (Fontaine *et al.* 2012) with consistent mass of the convective core.
- Since two cluster stars we analyzed are members of binary systems, the age of NGC 6791 is likely not serving as a reliable constraint.

The material in this paper is subject to a number of caveats:

- Spectroscopic estimates are subject to large uncertainties, which cover a large portion of the grid of models and cause a degeneracy of solutions, *e.g.*, parameters can vary but provide comparable quality of a period fit.
- We only considered adiabatic pulsation periods, which do not allow us to limit the period fitting to the driven modes only. A driving mechanism of g-modes in hot subdwarfs is far from being fully understood, and quantitative non-adiabatic asteroseismology, *i.e.*, selecting only modes that are driven, has not been yet ever done.

- The evolutionary tracks cover the EHB evolution only up to the tip, where 10% of central helium is left in the core. It means that our solutions will be limited to the EHB evolution and will not cover late EHB and post-EHB evolutionary stages.

- The models represent only a single star evolution and that is why cannot be described by precise estimates of the total age.

Even though the results we presented here are not yet satisfactory, we consider our work to be an important step toward advancing the potential of asteroseismic analysis to derive the interiors of sdB stars. We used the most advanced MESA models currently available and our results can serve as a motivation for improving the MESA code as concerns helium burning phase and to be able to apply non-adiabatic period calculations in GYRE. In addition, more pulsating sdB stars, for which observed periods were preliminary identified (at least partially), should be analyzed seismically to obtain more thorough conclusions on how satisfactory our current application of the MESA and GYRE is, identify caveats and mitigate them in future evolutionary modeling. The possible, but computationally expensive, improvement may include an increase of a grid's resolution, particularly in Y_c, but also in M_{env} and Z. If the current problems calculating reliable evolutionary models with implemented radiative levitation are sorted out, non-adiabatic pulsation models would help to constrain the period fitting much better than it is currently possible.

Acknowledgements. We thank Jakub Ostrowski for helping us at the early stage of this manuscript preparation, and Valerie Van Grootel for valuable comments, which have significantly improved the quality of the manuscript. This work was financially supported by the National Science Centre grants UMO-2017/26/E/ST9/00703 and UMO-2017/25/B/ST9/02218. Calculations were carried out using resources provided by Wroclaw Centre for Networking and Supercomputing (*http://wcss.pl*), grant No. 265.

REFERENCES

Asplund, M., Grevesse, N., Sauval, A.J., and Scott, P. 2009, *ARA&A*, **47**, 481.
Baran, A.S., and Winans, A. 2012, *Acta Astron.*, **62**, 343.
Brassard, P., and Fontaine, G. 2008, *ASP Conf. Ser.*, **392**, 261.
Brassard, P., and Fontaine, G. 2009, *Journal of Physics: Conference Series*, **172**, 2009.
Caputo, F., Castellani, V., Chieffi, A., Pulone, L., and Tornambe, A. 1989, *ApJ*, **340**, 241.
Carraro, G., Villanova, S., Demarque, P., *et al.* 2006, *ApJ*, **643**, 1151.
Castellani, V., Giannone, P., and Renzini, A. 1971, *Ap&SS*, **10**, 355.
Charpinet, S., Fontaine, G., Brassard, P., and Dorman, B. 1996, *ApJ*, **471**, L103.
Charpinet, S., Fontaine, G., Brassard, P., *et al.* 1997, *ApJ*, **483**, L123.
Charpinet, S., Van Grootel, V., Reese, D., *et al.* 2008, *A&A*, **489**, 377.
Charpinet, S., Van Grootel, V., Fontaine, G., *et al.* 2011, *A&A*, **530**, A3.

Charpinet, S., Giammichele, N., Zong, W., *et al.* 2018, *Open Astronomy*, **27**, 112.
Charpinet, S., Brassard, P., Fontaine, G., *et al.* 2019, *A&A*, **632**, A90.
Constantino, T., Campbell, S.W., Lattanzio, J.C., and van Duijneveldt, A. 2016, *MNRAS*, **456**, 3866.
Constantino, T., Campbell, S.W., and Lattanzio, J.C., 2017, *MNRAS*, **472**, 4900.
Dorman, B., and Rood, R.T. 1993, *ApJ*, **409**, 387.
Dorman, B., Rood, R.T., and O'Connell, R.W. 1993, *ApJ*, **419**, 596.
D'Cruz, N.L., Dorman, B., Rood, R.T., and O'Connell R.W. 1996, *ApJ*, **466**, 359.
Eggleton, P.P. 1972, *MNRAS*, **156**, 361.
Fontaine, G., Brassard, P., Charpinet, S., *et al.* 2003, *ApJ*, **597**, 518.
Fontaine, G., Brassard, P., Charpinet S., *et al.* 2012, *A&A*, **539**, A12.
Gabriel, M., Noels, A., Montalbán, J., and Miglio, A. 2014, *A&A*, **569**, A63.
Goldstein, J., and Townsend, R.H.D. 2020, *ApJ*, **899**, 116.
Green, E.M., Fontaine, G., Reed, M.D., *et al.* 2003, *ApJ*, **583**, L31.
Han, Z., Podsiadlowski, P., Maxted, P.F.L., Marsh, T.R., and Ivanova, N. 2002, *MNRAS*, **336**, 449.
Han, Z., Podsiadlowski, P., Maxted, P.F.L., and Marsh, T.R. 2003, *MNRAS*, **341**, 669.
Heber, U. 1986, *A&A*, **155**, 33.
Heber, U. 2016, *PASP*, **128**, 082001.
Jilkovaá, L., Carraro, G., Jungwiert, B., and Minchev I. 2012, *A&A*, **541**, A64.
Kilkenny, D., Koen, C., O'Donoghue, D., and Stobie, R.S. 1997, *MNRAS*, **285**, 640.
Maxted, P.F.L., Heber, U., Marsh, T.R., and North, R.C. 2001, *MNRAS*, **326**, 1391.
Mengel, J.G., Norris, J., and Gross, P.G. 1976, *ApJ*, **204**, 488.
Michaud, G., Richer, J., and Richard, O. 2007, *ApJ*, **670**, 1178.
Miller Bertolami M.M., Althaus, L.G., Unglaub, K., and Weiss, A. 2008, *A&A*, **491**, 253.
Németh, P., Kawka, A., and Vennes, S. 2012, *MNRAS*, **427**, 2180.
Østensen, R.H., Silvotti, R., Charpinet, S., *et al.* 2010, *MNRAS*, **409**, 1470.
Ostrowski, J., Baran, A.S, Sanjayan, S., and Sahoo, K.S. 2021, *MNRAS*, **503**, 4646.
Paczyński, B. 1970, *Acta Astron.*, **20**, 195.
Paxton, B., Bildsten, L., Dotter, A., *et al.* 2011, *ApJS*, **192**, 3.
Paxton, B., Cantiello, M., Arras, P., *et al.* 2013, *ApJS*, **208**, 4.
Paxton, B., Marchant, P., Schwab, J., *et al.* 2015, *ApJS*, **220**, 15.
Paxton, B., Schwab, J., Bauer, E.B., *et al.* 2018, *ApJS*, **234**, 34.
Paxton, B., Smolec, R., Schwab, J. *et al.* 2019, *ApJS*, **243**, 10.
Reed, M.D., Baran, A., Østensen, R.H., Telting, J., and O'Toole, S.J. 2012, *MNRAS*, **427**, 1245.
Salaris, M., and Cassisi, S. 2017, *Royal Society Open Science*, **4**, 170192.
Saffer, R.A., Bergeron, P., Koester, D., and Liebert, J. 1994, *ApJ*, **432**, 351.
Sanjayan, S. Baran, A.S., Ostrowski, J., *et al.* 2022a, *MNRAS*, **509**, 763.
Sanjayan, S., Baran, A.S., Németh, P., *et al.* 2022b, *Acta Astron.*, **72**, 77.
Schindler, J.-T., Green, E.M., and Arnett, W.D., 2015, *ApJ*, **806**, 178.
Sweigart, A.V. 1987, *ApJS*, **65**, 95.
Townsend R.H.D., and Teitler S.A. 2013, *MNRAS*, **435**, 3406.
Townsend R.H.D., Goldstein J., and Zweibel E.G. 2018, *MNRAS*, **475**, 879.
Van Grootel, V., Charpinet, S., Fontaine, G., *et al.* 2008, *A&A*, **488**, 685.
Van Grootel, V., Charpinet, S., Fontaine, G., Green, E.M., and Brassard, P. 2010a, *A&A*, **524**, A63.
Van Grootel, V. Charpinet, S., Fontaine, G., *et al.* 2010b, *ApJ*, **718**, L97.
Villanova, S., Carraro, G., Geisler, D., Monaco, L., and Assmann P. 2018, *ApJ*, **867**, 34.

Chapter 4

Paper III: Variable Star Population in the Open Cluster NGC 6791 Observed by the *Kepler* Spacecraft

Abstract

We present the list of variable stars we found in the *Kepler* superstamp data covering approximately 9 arcminutes from the central region of NGC 6791. We classified the variable stars based on the variability type and we established their cluster membership based on the available *Gaia* Early Data Release 3 astrometry, by means of the Bayesian Gaussian mixture models. In total we found 278 variable objects, among which 17 binaries, 45 pulsators, 62 rotational and five unclassified variables are cluster members. The remaining 28 binaries, 25 pulsators, 83 rotational, four unclassified and nine unidentified variables are either not members or their membership is not established. In the case of eclipsing binaries we calculated the mid-times of eclipses and derived ephemerides. We searched for eclipse timing variation by means of the observed minus calculated diagrams. Only three objects show significant orbital period variation. Independently of a report published just recently by Colman et al.(2022) we found 119 new variables. We used isochrones calculated within the MIST project and derived the age (8.91 Gyr), average distance (4134 pc) and iron content [Fe/H] (0.26-0.28), of NGC 6791. Using the cluster members with membership probabilities greater than 0.9, we calculated the distance to the cluster of 4123(31) pc, which agrees with the result from our isochrone fitting.

doi: 10.32023/0001-5237/72.2.1

ACTA ASTRONOMICA
Vol. **72** (2022) pp. 77–102

Variable Star Population in the Open Cluster NGC 6791 Observed by the Kepler Spacecraft

S. Sanjayan[1,2], A. S. Baran[1,3,4], P. Németh[1,5,6], K. Kinemuchi[7,8], J. Ostrowski[1] and S. K. Sahoo[1,2]

[1] ARDASTELLA Research Group, Institute of Physics, Pedagogical University of Cracow, ul. Podchorążych 2, 30-084 Kraków, Poland
[2] Centrum Astronomiczne im. Mikołaja Kopernika, Polskiej Akademii Nauk, ul. Bartycka 18, 00-716 Warszawa, Polska
[3] Embry-Riddle Aeronautical University, Department of Physical Sciences, Daytona Beach, FL 32114, USA
[4] Department of Physics, Astronomy, and Materials Science, Missouri State University, Springfield, MO 65897, USA
[5] Astroserver.org, Fő tér 1, 8533 Malomsok, Hungary
[6] Astronomical Institute of the Czech Academy of Sciences, Fričova 298, CZ-251 65 Ondřejov, Czech Republic
[7] Department of Astronomy, New Mexico State University, Box 30001, MSC 4500, Las Cruces, NM 88003, USA
[8] Apache Point Observatory, 2001 Apache Point Road, P.O. Box 59, Sunspot, NM 88349-0059

Received April 15, 2022

ABSTRACT

We present the list of variable stars we found in the Kepler superstamp data covering approximately 9′ from the central region of NGC 6791. We classified the variable stars based on the variability type and we established their cluster membership based on the available Gaia Early Data Release 3 astrometry, by means of the Bayesian Gaussian mixture models. In total we found 278 variable objects, among which 17 binaries, 45 pulsators, 62 rotational and five unclassified variables are cluster members. The remaining 28 binaries, 25 pulsators, 83 rotational, four unclassified and nine unidentified variables are either not members or their membership is not established. In the case of eclipsing binaries we calculated the mid-times of eclipses and derived ephemerides. We searched for eclipse timing variation by means of the observed minus calculated diagrams. Only three objects show significant orbital period variation. Independently of a recently published report, we found 119 new variables. We used isochrones calculated within the MIST project and derived the age (8.91 Gyr), average distance (4134 pc) and iron content [Fe/H] (0.26–0.28), of NGC 6791. Using the cluster members with membership probabilities greater than 0.9, we calculated the distance to the cluster of 4123(31) pc, which agrees with the result from our isochrone fitting.

Key words: *open clusters and associations: individual: NGC 6791 – binaries: general – Stars: oscillations – Stars: rotation*

1. Introduction

NGC 6791 has been first described as a metal rich cluster by Baade (1931) and listed as an old open cluster by King (1964). The authors provided no age estimations. Kinman (1965) presented a detailed comparative study of color–magnitude diagrams (CMD) of NGC 6791 along with other two open clusters, M 67 (4 Gyr) and NGC 188 (6.8 Gyr). From the first photometric observations in the $B-V$ color, Harris and Canterna (1981) determined a reddening of $E(B-V) = 0.13$ mag. According to the recent studies NGC 6791 is 7–9 Gyr old (Chaboyer *et al.* 1999, Carraro *et al.* 2006, Basu *et al.* 2011), and it has a mass of around 4000 $M_{\odot}$ (Kaluzny and Udalski 1992, Carraro *et al.* 2006, Platais *et al.* 2011, Tofflemire *et al.* 2014). The cluster is located ≈ 8000 pc from the Galactic center and 1000 pc above the Galactic plane. According to some hypotheses the cluster may have formed in the bulge of the Galaxy and radially migrated to its current location (Jilkova *et al.* 2012, Villanova *et al.* 2018). The distance to the cluster is approximately 3614 pc, which was estimated for the first time by Stetson *et al.* (2003) from the de-reddened distance modulus of $(m-M)_0 \approx 12.79$ mag. The authors derived $E(B-V) = 0.09$ mag. According to Villanova *et al.* (2018) NGC 6791 is a super metal-rich cluster with $[\mathrm{Fe/H}] = +0.3 - +0.4$. Geisler *et al.* (2012) showed that NGC 6791 has multiple stellar populations, which makes the cluster chemically peculiar. NGC 6791 has an anomalous horizontal branch with a red clump (RC) region. Liebert *et al.* (1994) found a group of extreme horizontal branch members using spectrophotometry of blue targets observed by Kaluzny and Udalski (1992). The age of the cluster predicts that it should have a rich population of cooling white dwarfs, hence Bedin *et al.* (2005) observed the cluster using the Hubble Space Telescope up to $m_{\mathrm{F606W}} \approx 28.5$ mag. They found the white dwarf luminosity function to give a peak at 27.4 mag, which corresponds to an age of 2.5 Gyr. Such an estimate does not agree with the age derived from the main sequence (MS) or red giant branch (RGB) population (Chaboyer *et al.* 1999, Carraro *et al.* 2006). Thus far, these studies show the cluster is very unusual. A more detailed study is required to constrain the age and metal abundances for understanding the formation and evolution of NGC 6791. A clear picture of the cluster could be achieved by deriving an entire population of variable stars and analysis of components of the stars to find their ages and chemical abundances.

NGC 6791 has been a subject of extensive search for variable stars. Kaluzny and Udalski (1992) and Kaluzny and Rucinski (1993) did an extensive photometric survey finding 17 variable stars which includes 8 contact binaries, two blue stragglers and one binary consisting of a hot subdwarf B star. Rucinski *et al.* (1996) found three detached binaries and one cataclysmic variable (CV) star exhibiting a three day outburst. As a part of search for planets in stellar clusters, Mochejska *et al.* (2002) found 47 new low amplitude variable stars. The authors reported several BY Dra type and two outbursting CV stars, confirming the CV found by Rucinski *et al.* (1996). Mochejska *et al.* (2003) reported seven new variable stars with a

long and periodic flux variation. Kaluzny (2003) found four new variable stars by reanalyzing archived data from Kaluzny and Rucinski (1993). A search for transiting events by giant planets reported by Bruntt *et al.* (2003) yielded 22 new low amplitude objects along with 20 previously known variable stars. Using a high precision time-series photometry, Hartman *et al.* (2005) detected 10 new variable stars including one δ-Scuti type star and 8 contact binaries. Mochejska *et al.* (2005) detected 14 more variable stars and reported 9 eclipsing binaries. Using a high precision photometry in the Johnson *V*-band, de Marchi *et al.* (2007) detected 260 variables in the cluster area, although not all stars are members of the cluster.

From the launch in 2009, for almost 10 years the Kepler spacecraft has served mankind by providing very precise and almost continuous photometric measurements (Koch *et al.* 2010). The Kepler has observed more than five hundred thousand stars during its entire mission time. The Kepler mission was completed in two phases. During the first mission, Kepler observed 0.25% of the sky in the direction of Cygnus and Lyra constellation for 1460 d. The mission was reborn as K2 (second mission) after the second reaction wheel failed. K2 mission made 80 d observing campaigns along the ecliptic equator, which lasted 1695 d (Howell *et al.* 2014). During both missions, the observations were obtained using two different exposures, 30 min for the long cadence (LC) and 1 min for the short cadence (SC) mode (Koch *et al.* 2010, Borucki *et al.* 2010, Caldwell *et al.* 2010, Thompson *et al.* 2016). During the first mission, four open clusters were inside the Kepler field of view, NGC 6791, NGC 6819, NGC 6811 and NGC 6866. Two of the open clusters, NGC 6791 and NGC 6819, were observed by using the so-called LC superstamps.

Recently, Colman *et al.* (2022) presented light curves of KIC stars obtained from the Kepler superstamp data. The authors used an image subtraction method to derive light curves of all Kepler cataloged targets. They identified variability in 239 out of 5342 stars they extracted light curves of. The number of new variables is not given. We stress that our work has been performed simultaneously to, yet independently from, Colman *et al.* (2022) and contains additional analysis. By comparing our results with results of Colman *et al.* (2022), we have noticed that the authors applied a very strong detrending policy removing either eclipses or out-of-eclipse variations in binaries or variations in other objects that we claim to be variables.

In Section 2 we present a brief description of the Kepler data and method used for obtaining the light curves of variable objects. In Section 3, we present a spectroscopic study of the variable stars found in this project using either archived spectra from public surveys or our own data. In Section 4, we describe the method of deriving the membership probabilities of our new variable star findings. In Section 5, we report individual variable star cluster members divided into variability classes. The field variable counterparts are listed in Tables 5–8. In Section 6, we present the result of isochrone fitting.

2. Kepler Photometry

We downloaded the Kepler superstamp data of NGC 6791 from the Mikulski Archive for Space Telescopes (MAST*). The data are 20×100 pixel boxes piled up in two contiguous 10 box stacks. The field of view of all pixels is $800'' \times 800''$ and covers the most central part of the cluster. The superstamps data were collected in the LC mode. The pixel scale of an individual square pixel is $4''$. The data were collected over 1460 d and are split into 18 quarters.

We searched for a flux variation by extracting fluxes for all time stamps in individual pixels for each of the quarters Q 2–5. Then, a Fourier transform of the time-series data was performed in each pixel and each quarter separately. The pixels showing peaks (representing signal) in the amplitude spectra were selected. Signals that were identified with artifacts, either reported by Baran (2013) or those found in this project, were discarded. We combined all contiguous pixels showing the same signal and defined an optimal aperture of pixels. To keep the solar cells exposed to the sunlight, every quarter the spacecraft rolled 90°, hence, with each quarterly rotation of the spacecraft, our targets landed on different CCD chips. This positioning caused different target images, and consequently, different optimal apertures (Bryson *et al.* 2010). Fortunately, every four quarters the images and apertures were the same, so we have defined the apertures only in four quarters, *i.e.*, Q 2–5, and propagate them to the corresponding quarters (*e.g.*, Q 2, 6, 10, 14). Next, using the optimal apertures for all targets showing flux variation we used PyKE software (Kinemuchi *et al.* 2012) to pull out the fluxes and correct them for instrumental artifacts by means of Co-trending Basis Vectors. Finally, using our custom scripts, we clipped the data at 4.5σ, detrended using spline fits, and normalized them to parts per thousand (ppt). The variable stars discovered in our work will be presented in Section 5.

3. Spectroscopy

We searched for spectra in the literature of all variables we detected. We found optical or infrared spectra for 111 objects in the archives of APOGEE (Ahn *et al.* 2014, Majewski *et al.* 2017), SDSS (Blanton *et al.* 2017), LAMOST (Zhao *et al.* 2012), ESO (Gilmore *et al.* 2012, Randich *et al.* 2013), and the HECTOSPEC (Fabricant *et al.* 2005) surveys. All spectra with $T_{\rm eff} < 15\,000$ K were modeled with interpolated local thermal equilibrium (LTE) synthetic spectra drawn from the BOSZ (Bohlin *et al.* 2017) spectral library to determine the fundamental atmospheric parameters. The BOSZ library was calculated for scaled solar metallicity with carbon and α-element enhancement. Therefore, individual abundance patterns cannot be investigated with our method.

*https://archive.stsci.edu/

Our fitting procedure (XTGRID; Németh *et al.* 2012) is based on a steepest-gradient chi-square minimizing method, which was originally developed to model hot stars. To improve its performance for cool stars, we added a grid-search preconditioning to the procedure. We step through a set of models to search for the best starting model for the steepest-descent part. Next, the descent part takes over in driving the fit and converges on the best solution. Once a convergence is achieved, the procedure explores the parameter errors by stepping through a set of points around the best solution. If a better solution is found during error calculations, then the procedure returns to the descent part, and hence pushing the solution toward the global minimum. XTGRID fits the radial velocity and projected rotation velocity of each spectra along with the stellar surface parameters, such as the effective temperature ($T_{\rm eff}$), surface gravity ($\log g$) and abundances.

In addition, the procedure accesses photometric data from the VizieR Photometry Viewer[†], distance data from the Gaia EDR3 database, and extinction values from the NED online services. The spectroscopic surface parameters combined with these measurements allow us to reduce systematics and derive absolute stellar parameters, such as mass, radius, and luminosity. An anti-correlation is observed between $T_{\rm eff}$ and [Fe/H]. Fortunately, the spectral energy distribution (SED) helps in resolving this bias by restricting the $T_{\rm eff}$. Another bias is observed in surface gravity, in particular below $T_{\rm eff} = 4000$ K. At such low temperatures, the spectrum is insensitive to the surface gravity. When the spectral coverage is very limited, we could not determine an accurate value for $\log g$. We do not report atmospheric parameters for such stars.

The archival spectroscopic data are very inhomogeneous. Consequently, high resolution spectra (*e.g.*, obtained with ESO instruments) with a short wavelength coverage are more suitable for radial velocity measurements, while low resolution spectra (*e.g.*, from the SDSS and LAMOST surveys) can provide more consistent atmospheric parameters, but less precise velocities. Some ESO spectra cover only 5300–5600 Å range at a resolution of $R = 20\,000$, and only weak spectral features are visible. For such spectra, at a relatively low signal-to-noise ratio (SNR), the fitting procedure increases the projected rotation above 100 km/s, which decreases the radial velocity accuracy. In general, low SNR spectra limit our analysis the most, while crowding in dense stellar fields and a limited spectral coverage affects the parameter determination.

4. Cluster Membership

We used Gaia astrometry to determine the membership probabilities of all variable stars we found. We used five parameters, *i.e.*, equatorial coordinates α and δ, proper motions μ_α and μ_δ, and parallax π (further called five astrometric parameters). First, we adopted/estimated mean values of these parameters. The cluster

[†] *http://vizier.u-strasbg.fr/vizier/sed/*

center has been taken from Kamann *et al.* (2019) to be at $\alpha_{2000} = 19^h20^m51\overset{s}{.}3$ and $\delta_{2000} = +37°46'26''$. Next, we downloaded Gaia Early Data Release 3 (EDR3) (Gaia collaboration *et al.* 2016, 2021) data for all stars within a tidal radius of $23'$ (Platais *et al.* 2011). The area contains 36 647 targets accessible to our analysis. However, we filtered out dubious targets with parallaxes to be negative or greater than $1''$or relative uncertainties for any of the proper motion or parallax values to be greater than 50%. A cluster environment, particularly toward the center, is very dense, which can lead to unrealistic or imprecise estimates of these three parameters (μ_α, μ_δ, π). In addition, we limited our sample to targets for which the zero point offset corrections of parallax have been applied (Lindegren *et al.* 2021). After filtering and correcting for the parallax zero offset, we ended up with 11 466 targets.

To determine the membership probabilities, we used the Bayesian Gaussian Mixture Models (GMM) using scikit–learn python toolkit (Pedregosa *et al.* 2011). The GMM assumes each data point to be a combination of finite Gaussian functions, in which the number of these functions is determined using a variational Bayesian inference model with Dirichlet process prior (Ferguson 1973). We performed 10 000 iterations using the Expectation-Maximization algorithm (Dempster *et al.* 1977), and we derived membership probabilities for each target in our sample based on all five astrometric parameters. In the case of targets that we found variables in the superstamp area, we estimated their membership probabilities regardless of precision of their five astrometric parameters. If the uncertainties were larger than 50%, we considered corresponding parameters to be error-free, while the negative parallaxes were ignored and only four astrometric parameters were used.

To strengthen the probability, the radial velocity of individual stars can also be used. However, they need to be corrected for the effects of binarity, rotation, and pulsations. Different instruments differ in instrumental calibration which often bias the radial velocity (RV) estimates. Since we did not conduct one single survey that could provide us with consistent RV estimations, we decided not to use RVs for the membership analysis. Since binarity and rotation affects the measurement of intrinsic motion, we expect the RVs will be random values and, as it will be seen in Section 5, the values in Tables 1–3, confirm our suspicion. We expected the most consistent estimates for single solar-like pulsators, since their oscillation motion on the surface is of a very small amplitude. In fact, in only three cases the RVs are far from the average cluster value (-47.46 ± 1.08 km/s, Carrera *et al.* 2019), since the stars may belong to binary systems. On the other hand, RVs that are consistent indicate that the stars are likely single or the orbital motion (if any) is very slow or the spectra were taken when both stars were aligned with the observer's line-of-sight. The RVs of the solar-like stars that are unlikely to be members (Table 6) are not close to the cluster average and seem to confirm their field membership, unless they are in binaries.

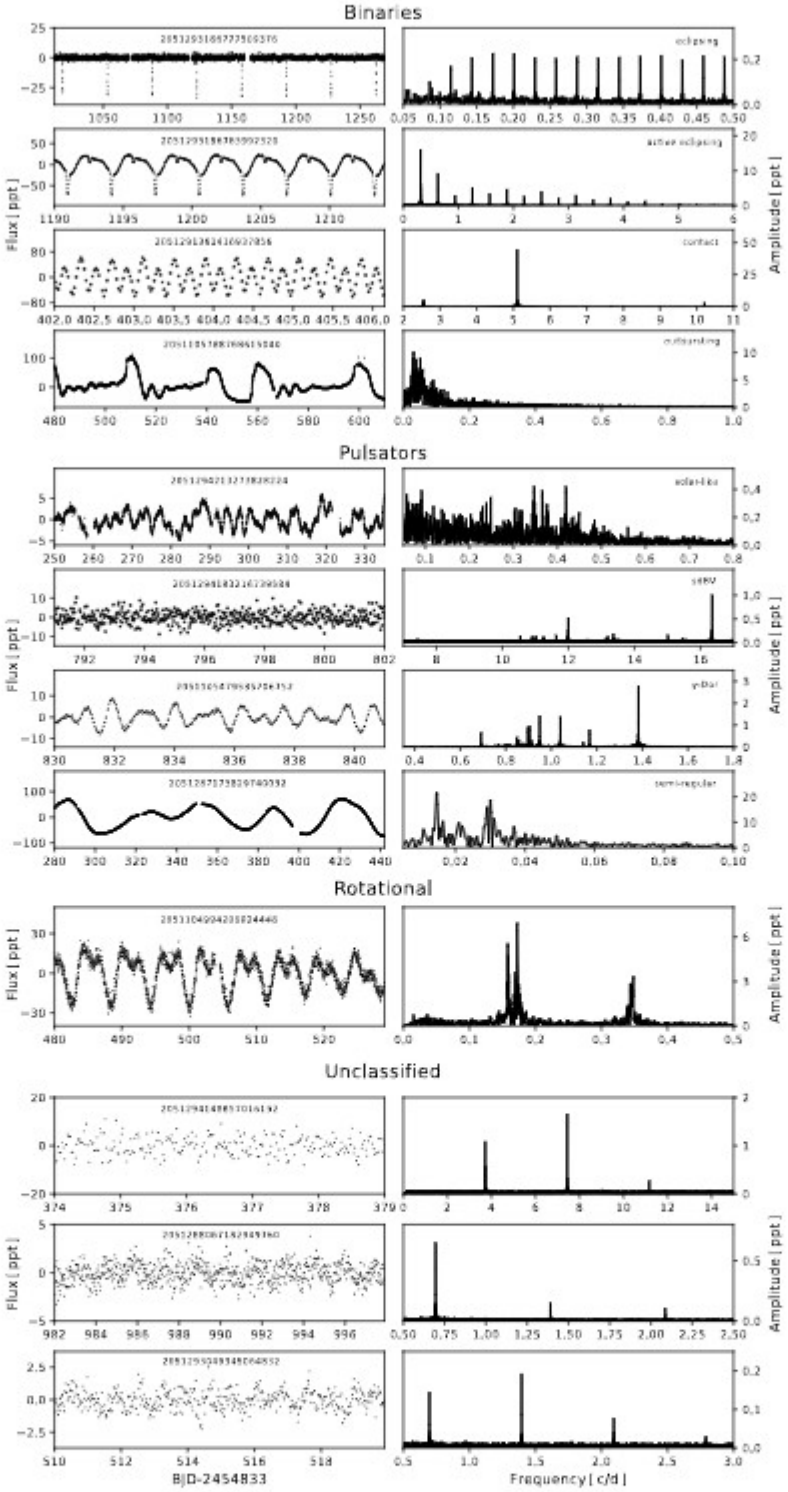

Fig. 1. Examples of light curves and corresponding amplitude spectra of a zoo of variable stars in the open cluster NGC 6791.

5. A Zoo of Variable Stars

In total, we found 278 variable objects in the superstamp area. Our sample contains cluster members as well as foreground and background stars. In Section 4, we provided details on a membership analysis. Our prime focus is on the members of NGC 6791. The non-members and objects with unknown membership status, as a consequence of a lack of the Gaia astrometry, are listed in Tables 5–8. Their variability is classified the same way as for the cluster members.

Based on flux variations, we classified the stars into three main variability types, *i.e.*, eclipsing, pulsating, and rotating stars. The first two types are further split into specific classes. Five stars remained unclassified. Their light curves show variations that we are unable to unambiguously identify as one of the three types listed. These objects show flux variations which can origin in *e.g.*, a reflection effect, ellipsoidal variation or a rotation of a spotted star. These stars have typically low amplitude flux variations. In Fig. 1 we present examples of light curves and their corresponding amplitude spectra for each type and a selection of classes of variable stars we found.

5.1. Binary Systems

We selected binary stars with sharp eclipses typical for semi- and detached systems. Some eclipsing systems show additional out-of-eclipse variation, which can be caused by a chromospheric activity, and we call them "active" eclipsing. We identified contact systems, which are characterized by a continuous flux change and typical for W UMa stars. Another class contains outbursting stars, which we associate with binaries experiencing a rapid mass transfer causing sudden eruptions, *e.g.*, novae, dwarf novae, nova-like variables. We stress that our classification is not based on radial velocities. Some of the stars may not be classified correctly, *e.g.*, a smoothly continuous and small amplitude flux changes may be misidentified with rotational variables. However, the flux change over the course of observations is not modulated (see explanation in Section 5.3) or they can be long-period pulsating stars. In Fig. 2 we present the phased light curves of three stars that we consider new discoveries. The sample includes all the classes of binary stars we identified in the superstamp data. We found 17 binaries to be cluster members (Table 1), 28 binaries are field objects, including two binaries for which we could not establish membership due to the lack of Gaia astrometry data (Table 5). For binary systems their membership has been derived based on all five astrometric parameters. The majority of binaries in the cluster are main sequence (MS) stars with just two exceptions, assuming the position of the latter in the CMD is correct. Gaia EDR3 2051105720053889536 is a post-MS star on its early ascent of the red giant branch (RGB), while Gaia EDR3 2051293186783992320 is located below the RGB, which can be explained by an incorrect color index or pre-MS evolutionary status. Among the member counterparts, five are eclipsing, six active eclipsing, five contact, and one outbursting stars.

Table 1

List of binary stars that are cluster members

Gaia EDR3	KIC	P_{orb} [d]	T_0 [BJD]	G [mag]	CMD	HRD	T_{eff} [K]	log g	RV [km/s]	[Fe/H]	Ref
				eclipsing							
2051287203888386688	2436378 [10L]	8.531633(8)	2 454 969.2757(8)	19.031	MS$^+$	–	–	–	–	–	–
2051288372129693440	2569175 [2]	43.499395(21)	2 455 041.61331(38)	18.383	MS	RGB	5 620(40)	3.517(18)	−65.8(4)	−0.67(9)	2*
2051292980625561216	2437149 [12,0L]	18.7986285(37)	2 454 971.02807(16)	17.480	MS	MS−MS	5 100(900)	4.5(4)	−80.9(9)	−0.25(25)	2*
2051293083698347008	2437482 [2]	17.551175(14)	2 454 966.9452(7)	18.210	MS	RGB	4 860(50)	3.042(20)	−67.5(5)	−0.48(15)	1*
2051293186777509376	2437041 [2]	34.859569(14)	2 454 979.90568(33)	18.055	MS	MS	6 360(40)	4.58(7)	−57.0(8)	−0.42(11)	2*
				active eclipsing							
2051105342091761536	2437783 [4L]	7.453112(10)	2 454 964.7652(11)	18.391	MS	BS	7 160(50)	3.60(8)	−20.1(6)	−0.82(9)	2*
2051105548255223680	2438490 [4L]	3.3157657(10)	2 454 967.85556(27)	17.887	MS$^+$	HB	5 410(90)	2.87(7)	−62.2(12)	−0.68(15)	2*
2051105784476572032	2438061 [1,13L]	4.8858826(16)	2 454 965.01144(28)	17.721	MS	HB	5 220(30)	2.197(10)	−46.5(45)	0.42(22)	1*
2051293186783992320	2437060 [4L]	3.1871038(8)	2 454 969.04204(21)	16.989	RGB	MS	5 270(20)	4.253(45)	−59.6(7)	−0.445(47)	1*
2051294423734919552	2569494 [1,5L]	1.5232747(12)	2 454 965.3339(7)	17.288	MS	MS	5 580(50)	4.06(6)	−116(8)	−0.36(11)	1*
2051295351447975168	2570480 [2]	0.7349394(16)	2 454 964.9628(18)	19.340	MS$^+$	HB	5 870(160)	2.34(11)	41.2(30)	−0.14(7)	2*
				contact							
2051105543955885696	2438413 [2]	0.31754621(10)	2 454 964.63952(27)	18.281	MS	RGB	5 380(100)	3.347(38)	−34.70(13)	−0.631(46)	2*
2051105720053889536	2438148 [2]	0.29468323(11)	2 454 964.79285(30)	16.612	RGB	–	–	–	–	–	–
2051291361416937856	2568950 [2]	0.3917614(15)	2 454 964.91341(33)	17.555	MS	MS/RGB	5 300(20)	3.926(20)	−39.50(10)	−1.131(26)	1*
2051293324222974976	2569965 [2]	0.325587259(49)	2 454 964.71162(13)	17.510	MS$^+$	MS	5 380(20)	4.46(8)	−63(6)	−0.36(8)	1*
2051294114497255936	2569630 [2]	0.31265938(26)	2 454 964.7815(7)	16.964	MS	MS	5 620(50)	4.030(56)	−41(2)	−0.14(9)	1*
				outbursting							
2051105788768615040	2438114 [4L]	32.27	–	18.192	blue of MS$^+$	blue of MS	27 000(5 000)	7.3(6)	−34(25)	−1(1)	1*

The stars that we consider newly detected variables are marked in bold. The superscripts in the KIC column denote if the data are available on the MAST: X stands for no data, L and S stand for the LC and SC data, respectively, and the numbers represent a total number of quarters the date were taken in. CMD refers to a position in the CMD (MS – main sequence, RGB – red giant branch, BS – blue straggler, AGB – asymptotic giant branch, RC – red clump, HB – horizontal branch, EHB – extreme horizontal branch). HRD refers to a position in the T_{eff}, log g diagram. The $^+$ symbol indicates that not all five astrometric parameters were used in the membership analysis. The Ref column refers to the source of the spectra, *i.e.*, 1 – HECTOSPEC, 2 – ESO, 3 – LAMOST, 4 – SDSS and 5 – APOGEE. The * indicates that the atmospheric parameters are derived in this work.
HECTOSPEC – *https://oirsa.cfa.harvard.edu*, ESO – *http://archive.eso.org*, APOGEE – *https://www.sdss.org/dr16/irspec*, LAMOST – *http://dr6.lamost.org*, SDSS – *http://skyserver.sdss.org/dr16*

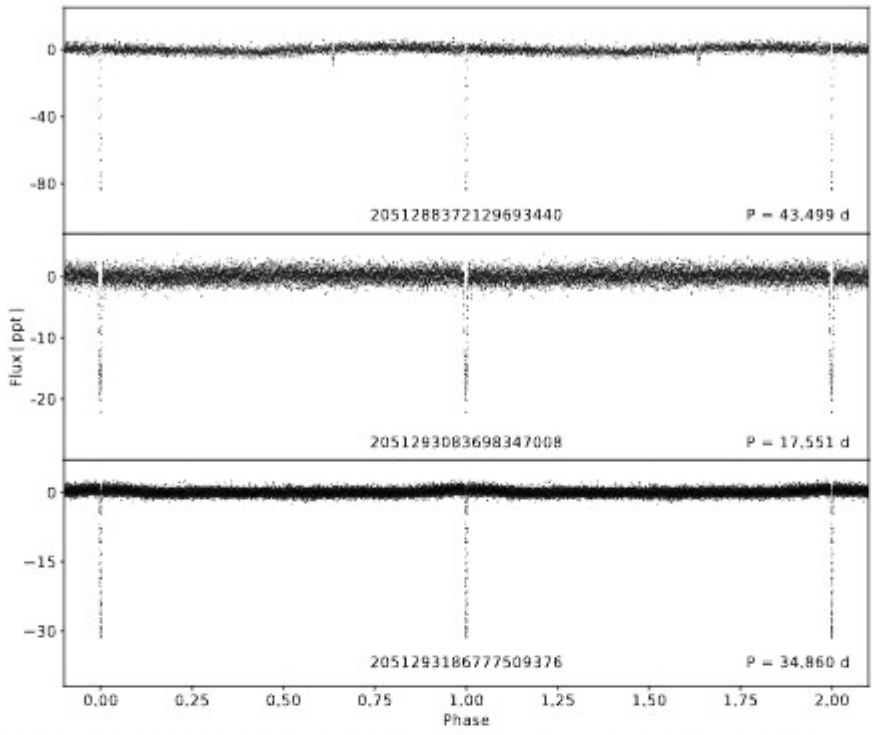

Fig. 2. Phased light curves of three newly discovered binary star members of NGC 6791.

Since the objects considered in this section are binaries, magnitudes and color indices used in the top panel of Fig. 3 and $T_{\rm eff}$ and $\log g$ in the top panel of Fig. 6 (this figure will be explained in Section 6) may be averages of all components in a specific binary system and may not indicate a proper location of individual stars in the CMD. If the average location in the CMD diagram is in the well defined regions, *e.g.*, MS or RGB, we can expect the components are of similar properties (or a secondary component is not detectable in our data), and the average is not far from single star values (unless the binary components are much different but the shift is only along a given evolutionary stage, *e.g.*, along the RGB branch). If the location is outside those regions, *e.g.*, below MS or RGB, then the individual components in a binary system are not alike, *e.g.*, WD + MS, and the average will be somewhere between a WD track and the MS (as is the case for Gaia EDR3 2051105788768615040). For this same reason, the RV of binaries is typically different from the average RV of a cluster. We expect the orbital RV to be dominating. There are only one exception with the RV being close to the average cluster value. In the case of Gaia EDR3 2051105784476572032 the spectrum could have been taken during the eclipse or it is a spectroscopic single-line binary.

We estimated the mid-times of eclipses or, in the case of non-eclipsing systems, a minimum of a light variation by means of the method described in Kwee

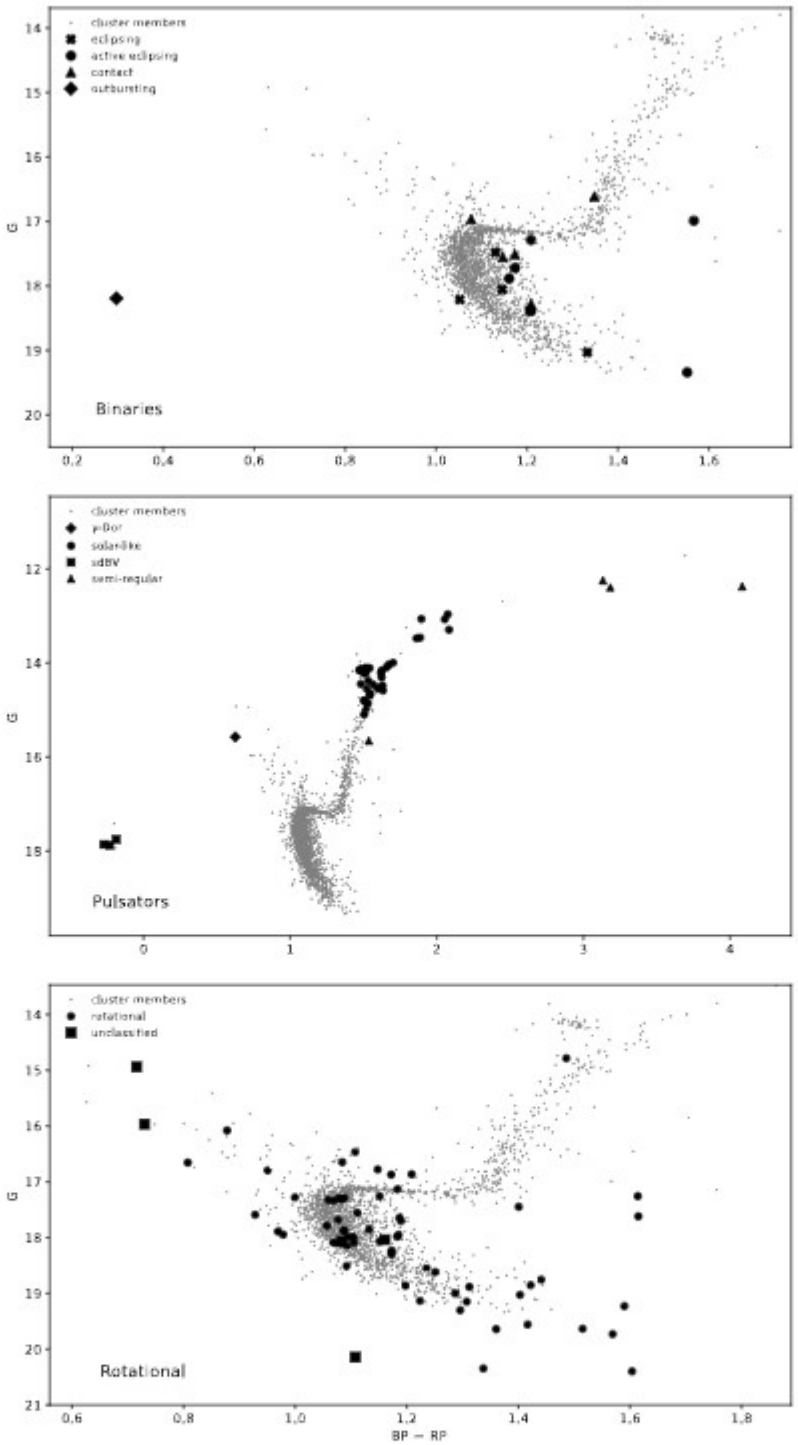

Fig. 3. CMD for NGC 6791. We listed variable stars such as binaries, pulsators and rotational cluster members in the *top, middle and bottom panels*, respectively. Unclassified stars are plotted in the *bottom panel*.

and van Woerden (1956). We used the mid-times to derive the ephemeris, *i.e.*, a reference epoch, defined as the first mid-time in a given dataset, and an orbital period for each binary system we found. We provided estimates of these two parameters in Table 1 and Table 5. The exceptions are systems for which the data are very noisy, not allowing us to derive precise mid-times, and outbursting stars. For these systems we reported only rough estimates (arbitrarily adopted two decimal places for precision) of their orbital periods, derived from the Fourier amplitude spectra. The ephemerides were used to calculate the $O-C$ diagrams to check on the orbital period variation. For most of the stars the $O-C$ diagrams do not show any significant period variation. The exceptions are shown in Fig. 4. Gaia EDR3 2051294114497255936 (the top panel in Fig. 4) shows quite a large amplitude period variation with only one full cycle covered. These two $O-C$ diagrams are constructed based on an average primary and secondary eclipses. Gaia EDR3 2051105342091761536 (the bottom panel in Fig. 4) shows cyclic variations of the orbital period derived solely from primary eclipses. To explain a periodic change an additional body in the system can be invoked. To test this hypothesis and, if confirmed, to constrain the parameters of those bodies, RV time-series data are required.

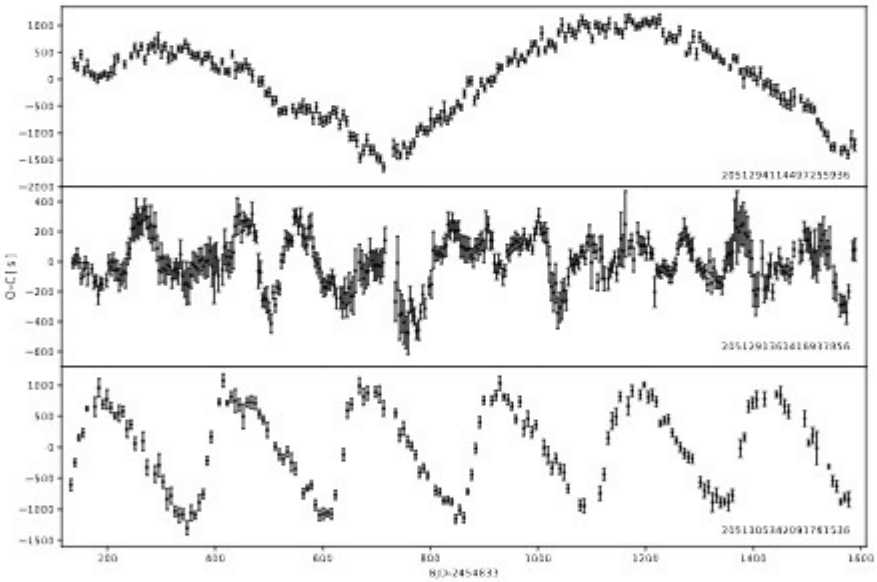

Fig. 4. $O-C$ diagrams for three binary systems that show variation of the orbital period.

5.2. Pulsators

We found 70 objects that show an intrinsic variability caused by stellar oscillations. We identified the following types of pulsators, *i.e.*, δ Scuti and γ-Dor, solar-like along the RGB, RR Lyr, pulsating hot subdwarf B stars (sdBV) on the

EHB, and semi-regular along the RGB and AGB. In Table 2 we show only the cluster member counterpart, while the field pulsators are listed in Table 6.

Among the cluster members we found one blue straggler, 36 solar-like pulsators (10 being RC objects, while 26 are still on the RGB), three sdBVs and five semi-regular giants. We analyzed the pulsation component in the solar-like counterpart, and the results will be published elsewhere. The analysis of the only three sdBVs we found in NGC6791 has already been reported by Sanjayan *et al.* (2022). Among sdBVs only Gaia EDR3 2051105509596144768 is a known binary star. The RV is likely influenced by orbital motion. The other two sdBVs also show different RVs from the cluster average, which may be an indication of their binary nature. Sanjayan *et al.* (2022) reported on the time-series spectroscopy (their Fig. 4), which indicates a RV variation. The RVs of other pulsators we found to be members of NGC 6791 are close to the average value, with only a few exceptions. For instance, Gaia EDR3 2051293255503478528 shows a much faster motion, but the quality flag of the spectra suggests a possible contamination. We do not have resources to sort out these inconsistency cases. Perhaps the explanation of these cases is an additional RV component either of a binary or a rotational nature. In the case of other objects the RV confirms their membership and a single nature. We are aware that their spectra could have been taken while their orbital RV is negligible, but we consider it to be a less likely case. As in the case of binaries, the location of pulsators in the CMD (the middle panels of Fig. 3 and 6) may still be influenced by binary components.

5.3. Rotational Variables

We defined rotational type as stars showing modulated flux variation. Such variation is caused by the presence of migrating spots on the surface, which contribute to a flux modulation as a star rotates. The rotational variables can mimic other types of variability, *e.g.*, ellipsoidal or contact binaries, and high-amplitude radially pulsating stars. We stress that our identification may not be ideal for rotational variable stars. We assumed that binaries show none or negligible modulation of a flux variation. This modulated variation can be verified by either a light curve shape or a profile of peaks in amplitude spectra. A complex profile indicates either period or amplitude change. Objects showing light curves with modulated flux variation have been classified as rotational variables.

We found a total of 145 rotational variables out of which 62 are cluster members and are listed in Table 3. The field counterpart is listed in Table 7. Likewise among binaries, there is no Gaia astrometry for four rotational variables and they are also listed in Table 7. We show the CMD location of members in the bottom panel of Fig. 3. The members occupy mostly the MS region, with three exceptions being the RGB objects and three exceptions being BS objects. Likewise in the case of binaries and pulsators, their true location may be influenced by binarity.

Table 2

List of cluster members showing pulsations

Gaia EDR3	KIC	G [mag]	CMD	HRD	$T_{\rm eff}$ [K]	log g	RV [km/s]	[Fe/H]	Ref
				γ-Dor					
2051105479535706752	2438249 [17L]	15.573	BS	BS	6 980(90)	3.636(84)	−56.7(9)	−0.15(13)	2*
				solar-like					
2051098710667044608	2297384 [17L]	14.204	RC	RC	4 512(91)	2.460(28)	−45.71(17)	0.400(7)	5
2051099260422933632	2437539 [17L]	14.545	RGB	RGB	4230(30)	2.353(10)	−39.9(4)	−0.57(7)	2*
2051099329142406400	2437240 [17L]	14.648	RGB	RGB	4 380(70)	3.116(17)	−45.5(3)	−0.12(13)	2*
2051104586182496000	2438462 [12L]	14.586	RGB	RGB	4 240(80)	2.020(23)	−45.71(37)	−0.39(7)	2*
2051105135938204160	2437507 [17L]	14.032	RGB	RGB	4 262(80)	2.160(46)	−47.504(21)	0.400(7)	5
2051105135938218624	2437698 [17L]	14.191	RC	RC	4 521(93)	2.370(28)	−45.25(6)	0.400(8)	4
2051105239017444992	2437564 [17L]	14.226	RC	RC	4 515(99)	2.400(29)	−48.53(11)	0.400(9)	5
2051105342096702080	2437804 [17L]	14.110	RC	RC	4 459(97)	2.350(27)	−45.367(23)	0.400(9)	5
2051286795872609920	2436209 [17L]	14.802	RGB	RGB	4 498(103)	2.650(45)	−47.91(45)	0.400(9)	5
2051287002031072768	2437164 [12L]	14.157	RC	RC	4 300(50)	2.515(10)	−48.26(37)	−0.58(13)	2*
2051287070750544128	2436900 [17L]	14.456	RGB	RGB	4 428(101)	2.500(45)	−47.92(8)	0.400(9)	5
2051287242549228032	2436608 [10L]	14.446	RGB	RGB	4 500(50)	2.254(35)	−45.5(15)	−0.07(7)	2*
2051287311268703232	2436543 [12L]	14.120	RC	–	–	–	–	–	–
2051287311268706432	2436540 [17L]	14.856	RGB	RGB	4 473(104)	2.560(46)	−48.13(14)	0.400(10)	4
2051288067183227008	2436417 [17L]	14.104	RC	–	–	–	–	–	–
2051288135902691840	2436332 [17L]	14.302	RGB	RGB	4 360(60)	3.445(20)	−47.54(30)	−0.07(12)	2*
2051288170262450816	2436458 [17L]	14.532	RGB	RGB	4 250(30)	2.602(10)	−46.36(30)	−0.24(11)	2*
2051291228279110912	2435987 [17L]	14.529	RGB	RGB	4 428(98)	2.490(46)	−44(4)	0.400(9)	5
2051292877546340864	2437340 [17L]	13.462	RGB	RGB	4 058(82)	1.660(43)	−45.0(8)	0.300(9)	5
2051293083704792960	2437444 [17L]	13.998	RGB	RGB	4 105(66)	2.35(11)	−56(4)	0.12(6)	3
2051293118064539520	2437496 [17L]	13.069	RGB	RGB	3 920(67)	1.350(45)	−47.8(7)	0.300(7)	5
2051293118064542976	2437653 [17L]	15.090	RGB	RGB	4 559(97)	2.710(48)	−47(1)	0.400(8)	5
2051293152424246912	2436884 [10L]	13.476	RGB	RGB	4 061(83)	1.670(43)	−44.482(34)	0.300(9)	4
2051293186784001152	2437103 [17L]	14.378	RGB	RGB	4 500(50)	3.356(41)	−48.6(15)	0.002(92)	2*
2051293221143724032	2436824 [17L]	14.478	RGB	–	–	–	–	–	–
2051293221143725952	2436814 [17L]	14.209	RGB	–	–	–	–	–	–
2051293255503469184	2436912 [17L]	14.181	RC	RC	4 330(90)	2.140(46)	−45.75(42)	0.300(8)	4
2051293255503478528	2437040 [17L]	14.158	RGB	RGB	3 760(50)	2.955(27)	−81.7(8)	0.003(10)	5*
2051293319920668160	2569935 [17L]	13.065	RGB	RGB	4 032(65)	1.500(46)	−47.90(8)	0.400(6)	5
2051293599100902016	2570518 [17L]	14.683	RGB	RGB	4 509(89)	2.600(49)	−48.68(8)	0.300(7)	5
2051293977058270592	2436732 [17L]	14.135	RC	RGB	4 300(100)	2.60(7)	−44.9(2)	−0.36(8)	2*
2051294045777739520	2569360 [17L]	14.093	RGB	RGB	4 287(86)	2.180(46)	−46.44(47)	0.300(8)	5
2051294114497261952	2569618 [17L]	14.797	RGB	RGB	4 486(103)	2.650(46)	−45.75(9)	0.400(9)	5
2051294213273828224	2569624 [x]	12.965	RGB	RGB	3 896(62)	1.300(45)	−44.98(7)	0.300(6)	5
2051294251936167424	2569204 [11L]	13.293	RGB	RGB	3 967(77)	1.430(43)	−47.909(11)	0.300(8)	5
2051297275593144192	2569055 [17L]	14.173	RC	RC	4 543(97)	2.450(29)	−46.881(12)	0.400(8)	5
				sdBV					
2051105509596144768	2438324 [35S,12L]	17.859	EHB	EHB	25 290(300)	5.510(43)	−90(3)	−2.62(11)	6
2051105754408746880	2437937 [1S,1L]	17.878	EHB	EHB	24 860(270)	5.348(52)	−75(6)	−2.46(12)	6
2051294183216739584	2569576 [12S,5L]	17.752	EHB	EHB	23 540(210)	5.311(35)	−28(4)	−2.73(23)	6
				semi-regular					
2051105101578558464	2438151 [17L]	15.655	RGB	MS	5 420(60)	3.912(19)	−50.0(15)	−0.10(9)	1*
2051105616974709504	2438421 [17L]	12.246	AGB	AGB	3 555(57)	0.510(43)	−46.540(46)	0.200(8)	5
2051287002031070208	2437171 [17L]	12.394	AGB	AGB	3 540(56)	0.610(42)	−47.11(16)	0.300(8)	5
2051287173829740032	2436324 [8L]	12.373	AGB	AGB	3 332(53)	0.270(41)	−49.315(19)	0.200(10)	5
2051292976324527232	2437317 [17L]	14.939	RGB	–	–	–	–	–	–

See footnote of Table 1 for explanation. Ref 6 refers to Sanjayan *et al.* (2022).

Table 3

List of cluster members showing rotational variability

Gaia EDR3	KIC	P_{orb} [d]	G [mag]	CMD	HRD	T_{eff} [K]	log g	RV [km/s]	[Fe/H]	Ref
2051099015605500672	2297584[X]	18.02	18.299	MS+	–	–	–	–	–	–
2051104757981275264	2438685[X]	7.78	17.256	RGB	MS	5 500(50)	4.953(20)	−44.8(44)	0.47(15)	1*
2051104891118311040	2437994[X]	1.85	19.228	MS+	–	–	–	–	–	–
2051104891120796672	2437990[X]	13.15	19.148	MS+	–	–	–	–	–	–
2051104959840285696	2437791[X]	15.28	18.067	MS+	–	–	–	–	–	–
2051104964139549824	2437941[X]	10.12	17.944	MS	–	–	–	–	–	–
2051104994200024448	2438113[X]	5.80	17.288	MS	–	–	–	–	–	–
2051105097281783040	2438031[X]	8.28	17.591	MS	MS	5 810(40)	4.216(34)	−62.3(23)	−0.158(47)	1*
2051105131636983808	2437646[X]	13.23	17.558	MS	–	–	–	–	–	–
2051105234715895552	2437707[X]	11.00	17.867	MS	MS	6 080(30)	4.641(35)	−47.8(48)	0.60(14)	1*
2051105273377206784	2437801[X]	7.19	18.508	MS+	MS	5 380(70)	4.111(26)	−65.30(10)	−0.40(10)	1*
2051105342091728384	2437761[X]	11.81	19.001	MS	–	–	–	–	–	–
2051105372154852736	2437849[6Z]	11.02	16.863	MS	MS	5 260(50)	3.923(16)	−51.7(14)	−0.31(11)	1*
2051105372154855552	2437944[X]	1.96	18.543	MS+	–	–	–	–	–	–
2051105372157195264	–	2.45	19.556	MS+	MS	5480(50)	4.835(21)	−56(4)	0.45(17)	1*
2051105578318626304	2438569[X]	7.00	17.279	MS	MS	5 970(50)	4.295(20)	−69.2(15)	0.32(14)	1*
2051105612675379968	2438390[X]	3.80	17.987	MS	–	–	–	–	–	–
2051105685689315968	2438129[X]	16.58	17.853	MS	–	–	–	–	–	–
2051105784484742144	2570443[X]	2.20	17.643	MS	MS	5 610(50)	4.298(20)	−133.2(45)	−0.62(30)	1*
2051105818833811584	2438344[X]	7.74	18.616	MS+	–	–	–	–	–	–
2051105857492894592	2570649[X]	13.36	17.293	MS	–	–	–	–	–	–
2051105921913036160	2570622[X]	9.57	19.026	MS+	–	–	–	–	–	–
2051105926212896512	2570559[X]	1.32	20.343	MS+	–	–	–	–	–	–
2051107055787471104	2438631[X]	7.36	19.729	MS+	–	–	–	–	–	–
2051287002024520064	–	10.86	19.640	MS+	–	–	–	–	–	–
2051287066449451136	2436942[X]	9.26	18.098	MS	–	–	–	–	–	–
2051287066449464064	2436959[X]	2.65	18.852	MS+	–	–	–	–	–	–
2051287070744003456	2436969[X]	7.92	19.132	MS+	RGB	4 500(50)	3.09(8)	−45.0(8)	−0.155(20)	2*
2051287242549232384	2436767[X]	12.32	17.309	MS	MS	5 690(50)	4.163(20)	−43.2(57)	0.148(33)	1*
2051287895379273088	2436011[X]	10.00	19.632	MS+	–	–	–	–	–	–
2051288372119657728	2569185[X]	13.43	17.258	MS	MS	5 660(50)	4.117(34)	−97.9(35)	−0.08(10)	1*
2051288376420896384	2569162[X]	5.90	18.088	MS	–	–	–	–	–	–
2051291262638872192	2568864[X]	14.42	17.618	MS	MS	5 370(30)	4.78(10)	−61.5(42)	0.58(27)	1*
2051291503157017472	2568685[X]	19.87	17.342	MS	–	–	–	–	–	–
2051292873245240192	2437350[X]	16.82	17.885	MS	MS	5 790(50)	4.913(20)	−74.3(15)	0.13(8)	1*
2051292911906089728	2437521[X]	11.27	17.987	MS+	–	–	–	–	–	–
2051293946259301504	2437092[3Z]	3.20	18.145	MS+	MS	4 700(100)	4.619(50)	−78(1)	−1.87(6)	1*
2051293014978876672	2437584[X]	5.90	18.486	+	–	–	–	–	–	–
2051293083704791040	2437354[9Z]	7.21	16.465	MS	MS	5 580(50)	4.391(20)	−55.6(8)	−0.413(46)	2*
2051293113776412416	2437613[X]	11.05	17.787	MS	–	–	–	–	–	–
2051293148133456896	2437062[X]	8.82	17.133	RGB	–	–	–	–	–	–
2051293152424243968	2436909[X]	12.00	16.778	MS	MS	5 640(40)	4.654(21)	−69.3(26)	−0.203(17)	1*
2051293186783997056	–	9.63	18.232	MS+	–	–	–	–	–	–
2051293186784004096	2437238[X]	4.00	16.079	BS	BS	5 880(30)	3.546(23)	−48.0(4)	−0.34(8)	2*
2051293255503480320	2437079[X]	5.81	16.794	BS	–	–	–	–	–	–
2051293289863230720	2437338[X]	1.24	16.655	BS	–	–	–	–	–	–
2051293319934813184	2569984[X]	12.50	17.704	MS	–	–	–	–	–	–
2051293358583014528	2569763[4Z]	8.29	16.648	MS	MS/RGB	5 510(20)	3.788(49)	−38.6(5)	−0.397(48)	2*
2051293392942762240	2569825[X]	0.48	18.754	MS+	MS	5 000(50)	4.86(15)	−86.3(7)	0.02(14)	1*
2051293427302195584	2437884[X]	3.23	16.871	MS+	MS	5 930(20)	4.048(26)	−43.9(3)	−0.44(10)	2*
2051293530375009920	2570217[X]	5.55	17.891	MS	MS	5 760(20)	4.49(7)	−62.4(23)	0.07(8)	1*
2051293663519464192	2570420[X]	19.96	17.951	MS	–	–	–	–	–	–
2051293977053182592	2436790[X]	9.61	18.861	MS	MS	4 990(80)	4.832(25)	−169(3)	−0.356(15)	1*
2051294007116759808	2569597[X]	7.17	18.091	MS+	–	–	–	–	–	–
2051294148851985536	–	9.66	20.397	MS+	–	–	–	–	–	–
2051294148857020160	2569767[X]	2.40	17.323	MS+	–	–	–	–	–	–
2051294217574157440	–	4.92	19.300	MS+	–	–	–	–	–	–
2051294251931077888	2569279[X]	1.14	18.883	MS+	–	–	–	–	–	–
2051294281994746880	2569324[X]	10.90	17.983	MS	–	–	–	–	–	–
2051294286296294528	2569334[X]	6.29	17.447	MS	MS	5 330(20)	4.220(25)	−47.4(23)	0.15(8)	1*
2051294797390943872	2569591[X]	14.89	17.679	MS	–	–	–	–	–	–
2051296176081696768	2570281[12Z]	14.42	14.785	RGB	–	–	–	–	–	–

See footnote of Table 1 for explanation. Ref 6 refers to Sanjayan *et al.* (2022).

5.4. Unclassified and Unidentified Variables

In the case of nine objects, we were unable to unambiguously classify them according to the three types described above. The amplitude of a flux variation is low and it is not clear if the variation remains stable over time. The latter indicates that it is not unlikely these stars may be rotational variables. We leave a definite classification for further analysis, preferentially if based on better quality data. Five members of the cluster are listed in Table 4 and they are plotted in the bottom panel of Fig. 3, while four non-members are listed in Table 8.

While checking the pixel content we found signals in the amplitude spectra, associated with optical detections found in Pan-STARRS data (Chambers *et al.* 2016, Flewelling *et al.* 2020) survey that do not have any designations. We classified the signal to a proper variability type and estimated its period. We show the list of these unidentified objects in Table 9. Since the stars are not listed in the Gaia catalog, we are unable to estimate their membership. At three locations on the silicons (last three coordinates listed), we detected a signal in the amplitude spectra, however, we are unable to associate these coordinates with any optical objects in the Pan-STARRS survey. In addition, the last two signals listed may be of the same origin, though the coordinates are different. This result indicates that these three signals listed are residual signals of some other variable stars in the Kepler field of view that were spread over the silicons. We consider the signals detected at those three specific locations on the detector to be artifacts and not real sources.

T a b l e 4

List of cluster members with unclassified variability

Gaia EDR3	KIC	Period [d]	G [mag]	CMD	HRD
2051105269075634176	2437760[X]	0.44	18.064	MS	–
2051288067182949760	2436421[8L]	1.44	14.937	BS	–
2051291498855854208	2568724[X]	0.63	20.141	MS$^+$	–
2051293049345064832	2437745[X]	1.43	15.968	BS	–
2051294148857016192	2569676[X]	0.27	18.037	MS$^+$	–

See footnote of Table 1 for explanation.

6. The Distance and Age Estimation

We downloaded a grid of isochrones given in the Gaia photometric system from the MESA Isochrones and Stellar Tracks (MIST) project (Choi *et al.* 2016, Dotter 2016). The current version of MIST is 1.2. The MESA version 7503 was employed to calculate isochrones. We selected $V/V_{\rm crit} = 0$. The grid covers age in a logarithmic scale between 9.8 and 10.3 with a step of 0.01, while [Fe/H] was between 0.20 and 0.45 with a step of 0.01.

Table 5

List of binary stars that are not cluster members

Gaia EDR3	KIC	P_{orb} [d]	T_0 [BJD]	G [mag]	T_{eff} [K]	log$g$	RV [km/s]	[Fe/H]	Ref
			eclipsing						
2051104826700758016	2438661[K]	196.34051(1)	2 455 037.21466(43)	16.449	–	–	–	–	–
2051105131638986752	–	23.878352(36)	2 454 967.0873(12)	19.782	–	–	–	–	–
2051107128803742336	2438562[K]	10.406512(6)	2 454 965.58747(47)	19.369	6 220(130)	2.864(51)	–49(4)	–1.29(17)	2*
2051287311268711168	2436579[K]	9.287153(22)	2 454 971.1134(18)	19.613	–	–	–	–	–
2051291739386261248	2568780[K]	3.5316020(11)	2 454 964.71245(25)	19.913	–	–	–	–	–
2051292907615354240	2437452[15,17Z]	14.4699358(24)	2 454 974.81692(14)	17.286	6 170(50)	4.26(9)	–92.1(6)	–0.86(9)	2*
2051293079414230912	2437505[10Z]	21.476420(11)	2 454 982.26244(40)	18.324	4 920(50)	3.25(6)	–19.6(30)	–0.25(19)	1*
2051293118063233408	2437675[K]	1.75	–	21.175	–	–	–	–	–
2051294629893394176	2569880[K]	0.51323254(22)	2 454 964.60382(35)	17.866	–	–	–	–	–
			active eclipsing						
2051104586182512128	2438502[4,16Z]	8.35905(26)	2 455 005.2748(14)	16.216	5 563(234)	4.17(37)	–14(5)	0.37(22)	3
2051104684959920896	2438464[K]	0.43657907(7)	2 454 964.92853(13)	19.443	4 310(50)	4.169(20)	41(16)	–0.91(6)	1*
2051286761512868992	2436203[K]	2.06	–	14.328	–	–	–	–	–
2051288170257319808	–	3.7024382(14)	2 454 968.16622(31)	20.135	–	–	–	–	–
2051288372119654528	2569138[K]	0.88305272(12)	2 454 964.71084(11)	19.205	–	–	–	–	–
2051293599094508032	–	2.8516350(19)	2 454 967.1274(6)	20.335	–	–	–	–	–
			contact						
2051105543955885312	2438471[K]	0.27345629(34)	2 454 964.8195(11)	19.527	4 300(50)	3.92(7)	3.9(9)	–1.354(25)	1*
2051288269040355584	2436044[K]	0.24533697(21)	2 454 964.6646(7)	19.452	–	–	–	–	–
2051286417915483392	2297170[K]	0.3664306(6)	2 455 002.6182(13)	17.797	–	–	–	–	–
2051287070750548736	2437038[17Z]	0.267678275(46)	2 454 964.58218(14)	16.149	–	–	–	–	–
2051291228279113216	2435971[17Z]	0.27182769(8)	2 454 964.81810(25)	16.276	–	–	–	–	–
2051291468797350528	2568971[17Z]	5.088522(10)	2454966.2350(17)	13.081	–	–	–	–	–
2051293530381417856	2570289[17Z]	0.279027932(31)	2 454 964.57880(1)	15.781	–	–	–	–	–
2051295076563264000	2570552[K]	0.28417822(44)	2 454 964.5913(13)	20.279	–	–	–	–	–
2051295454527201792	2570460[K]	0.2659879(15)	2 454 964.61531(47)	18.689	–	–	–	–	–
2051296313520692864	2708123[K]	0.302184513(81)	2 454 964.69239(22)	17.742	–	–	–	–	–
2051297374371300992	2569082[K]	0.33401898(23)	2 454 964.8252(6)	17.579	5 750(50)	4.052(15)	–38.30(54)	–1.069(20)	1*
2051297477460338304	–	0.2690446(1)	2 454 964.7175(30)	20.838	–	–	–	–	–
			outbursting						
2051287203888388736	2436450[15,17Z]	35.71	–	19.884	–	–	–	–	–

See caption of Table 1 for explanation. Targets with no astrometry available, hence with no membership established, are denoted in italic.

At least 50% of the stars are expected to be in binary systems. The observed magnitude of a given target may include the flux contribution from all companions and not a single star, which shifts the position of the target in the CMD. Therefore, we excluded outlying stars where their positions in the CMD are uncertain. For the fit, we only kept the MS, RGB and RC stars. We included magnitude uncertainties as weights in the fit, which prevented the MS targets from over-fitting. The RC and RGB targets, even though less numerous, are brighter, and hence also remains significant in the fit.

The MIST synthetic isochrones are given in absolute magnitudes, and we selected no extinction. To account for a distance and a non-vacuum environment, in our fit, we included a shift $(m-M)$ in the Gaia G magnitude and in B_p-R_p color. The best-fit isochrones point to a narrow range of age and [Fe/H]. The age is 8.91 Gyr, while [Fe/H] is between 0.26 and 0.28. The apparent distance modulus $(m-M)$ equals 13.424 mag, while $E(B_p-R_p)$ from 0.165 mag to 0.176 mag. We show the fits in Fig. 5. Based on the extinction curve from Cardelli *et al.* (1989), Bressan *et al.* (2012) showed a rough relation between extinction in the Gaia G band and $E(B_p-R_p)$, which is $A_G \approx 2\cdot E(B_p-R_p)$. Taking the average of

Table 6

List of pulsators that are not cluster members

Gaia EDR3	KIC	G [mag]	$T_{\rm eff}$ [K]	log$g$	RV [km/s]	[Fe/H]	Ref
			δ-Scuti				
2051098981244205056	2297728 [15,18Z]	9.929	6 888(25)	3.680(40)	−37(7)	0.272(22)	3
2051107369321426432	2570760 [18Z]	13.459	–	–	–	–	–
			solar-like				
2051098710667526912	2297357 [1Z]	12.115	–	–	–	–	–
2051099054264914048	2437622 [12Z]	15.583	–	–	–	–	–
2051099329142404480	2437207 [X]	18.731	–	–	–	–	–
2051104105146054784	2297793 [17Z]	13.626	4 085(81)	1.430(52)	−83.615(30)	−0.300(10)	5
2051104139506469760	2438094 [17Z]	15.322	4 060(50)	1.11(15)	−84.7(6)	−1.14(8)	2*
2051104861060304640	2437816 [17Z]	13.958	4 229(77)	2.090(47)	0.400(7)	−47.27(9)	5
2051105720053903232	2438289 [10Z]	14.384	–	–	–	–	–
2051105857492905600	2570715 [7Z]	12.678	4 713(84)	2.330(36)	−3.30(7)	−0.200(7)	5
2051107369321441920	2570794 [10Z]	15.158	–	–	–	–	–
2051286520994706432	2436457 [18Z]	13.245	4 969(24)	3.015(39)	−19.14(4)	−0.422(22)	3
2051286933311578112	2436680 [10Z]	15.187	–	–	–	–	–
2051288445140366464	2569078 [10Z]	13.650	4 418(90)	2.290(49)	−5.428(56)	0.200(8)	5
2051291434437586304	2568912 [9Z]	12.859	4 701(95)	3.01(6)	−7.122(55)	−0.100(8)	5
2051291567575397120	2568656 [X]	15.618	–	–	–	–	–
2051291571876502912	2568654 [11Z]	13.140	4 301(83)	2.07(5)	−73.155(12)	0.100(8)	5
2051291674955780992	2568888 [10Z]	14.131	4 387(100)	2.070(51)	−58.47(23)	−0.100(11)	5
2051291949833615104	2568575 [5Z]	13.407	4 501(50)	2.55(8)	−2.26(4)	0.181(48)	3
2051293118064546944	2437692 [15Z]	11.203	4 817(86)	2.610(38)	−12.780(24)	0.200(6)	5
2051293702180102144	2570002 [X]	13.628	–	–	–	–	–
2051294320655654912	2569137 [10Z]	13.630	4 298(102)	1.71(6)	−194.10(44)	−0.800(16)	5
2051295282728537216	2570696 [2Z]	13.620	4 461(80)	2.13(6)	−11.38(9)	−0.300(8)	5
			RRLyr/BLBoo				
2051294934839887872	2569850 [X]	20.426	–	–	–	–	–
			semi-regular				
2051105032859063424	2438242 [X]	16.817	4 511(99)	2.660(47)	−47.85(8)	0.400(9)	4

See caption of Table 1 for explanation.

$E(B_{\rm p}-R_{\rm p}) = 0.171$ mag and using this relation, we derived $A_{\rm G} = 0.342$ mag. Subtracting $A_{\rm G}$ from $(m-M)$ we find the true distance modulus of 13.082 mag, which gives the distance to the cluster of 4134 pc. We also derived distance from the parallaxes of the cluster members with probability membership at least 90% and the relative parallax uncertainty of smaller than 10%, which equals 4123(31) pc. The distance estimated from the isochrone fit lies well within the uncertainty of the distance estimations from the cluster parallax. The cluster age we derived from the isochrone fit is also comparable to the age reported by Choi *et al.* (2018).

To verify the correctness of the spectroscopic fits we also engaged isochrones in $T_{\rm eff}$ and log$g$ plane (HRD). We used the isochrones for the age and the average metallicity, which we derived from the isochrone fitting in the CMD. Then, we overplotted the isochrones with our variable stars from Tables 1–3, for which $T_{\rm eff}$ and log$g$ are listed. The column HRD in Tables 1–3 describes the location of a

T a b l e 7

List of rotational variables that are not cluster members

Gaia EDR3	KIC	Period [d]	G [mag]	$T_{\rm eff}$ [K]	log g	RV [km/s]	[Fe/H]	Ref
2051098951180105088	–	1.33	20.929	–	–	–	–	–
2051099088624172928	2297416 [K]	2.66	20.201	–	–	–	–	–
2051099187404218752	2436945 [K]	4.58	16.735	–	–	–	–	–
2051104139500783744	–	0.64	20.943	–	–	–	–	–
2051104139505811328	2297846 [K]	13.40	14.901	–	–	–	–	–
2051104272645525760	2438284 [K]	2.63	19.629	–	–	–	–	–
2051104272645529472	–	1.53	20.277	–	–	–	–	–
2051104276944815744	2438272 [18L]	11.48	13.173	–	–	–	–	–
2051104586182508928	2438513 [15S,17L]	13.27	13.939	5 652(125)	4.51(8)	−35.74(33)	0.000(10)	5
2051104753679401728	2438740 [K]	0.42	19.653	–	–	–	–	–
2051104826696024832	–	1.06	20.370	–	–	–	–	–
2051104925480543616	2437773 [K]	0.51	19.083	6 070(110)	2.9(1)	8(4)	−0.54(15)	2*
2051105062917626624	2437959 [K]	15.27	17.987	–	–	–	–	–
2051105067218772096	2437888 [8L]	10.34	14.730	6 120(80)	4.93(5)	16.42(37)	−0.39(12)	2*
2051105067218785280	2438003 [18L]	0.70	13.025	7 132(30)	4.102(50)	3(10)	−0.22(3)	3
2051105135933158144	–	3.99	20.627	–	–	–	–	–
2051105239017448448	2437649 [K]	7.62	16.377	–	–	–	–	–
2051105273377200384	2437789 [K]	16.61	17.023	–	–	–	–	–
2051105303437700224	2437984 [K]	4.70	19.703	–	–	–	–	–
2051105307736986496	2437996 [17L]	14.61	13.887	5 753(37)	4.60(6)	−38(5)	0.104(35)	3
2051105410811376640	2438305 [K]	7.01	19.692	–	–	–	–	–
2051105823133141888	2438376 [K]	11.44	17.788	–	–	–	–	–
2051105926207653504	–	5.11	20.540	–	–	–	–	–
2051106063646757888	2438861 [K]	1.48	19.672	–	–	–	–	–
2051107124503872256	2438516 [K]	5.13	18.313	5 150(50)	4.773(27)	−36.9(15)	0.64(30)	1*
2051107472400670720	2570846 [17L]	10.82	15.313	–	–	–	–	–
2051107541120138752	2570736 [K]	1.61	18.428	–	–	–	–	–
2051286997729896832	–	0.86	19.542	–	–	–	–	–
2051287066448488192	–	1.62	19.279	4 850(50)	4.871(40)	−112.4(1)	−0.15(12)	1*
2051287139470009088	2436635 [17L]	1.17	15.989	4 445(291)	4.09(45)	−76(6	−0.32(27)	3
2051287547485746432	2436206 [K]	8.25	17.626	–	–	–	–	–
2051288032823472128	2436274 [K]	4.58	18.220	–	–	–	–	–
2051288101537860992	–	3.39	20.539	–	–	–	–	–
2051288165961197952	2436416 [K]	3.99	19.859	–	–	–	–	–
2051288445135225472	2569015 [K]	1.32	20.103	–	–	–	-	–
2051290919041461632	2435889 [K]	14.47	16.670	–	–	–	–	–
2051291434437576320	2568884 [K]	10.50	18.224	–	–	–	–	–
2051291468792223104	–	7.37	20.190	–	–	–	–	–
2051291571876503424	2568672 [K]	18.09	16.477	–	–	–	–	–
2051292976335015296	2437180 [K]	4.07	17.907	–	–	–	–	–
2051292980625560448	2437292 [K]	5.51	18.356	–	–	–	–	–
2051292980625569792	2437234 [17L]	24.10	13.153	–	–	–	–	–
2051293014978879744	2437723 [K]	1.17	18.608	–	–	–	–	–
2051293014985313152	2437469 [K]	9.85	19.161	–	–	–	–	–
2051293014985313792	2437574 [K]	11.683	17.183	5 650(50)	4.5(8)	−45.0(3)	0.05(7)	1*
2051293049338645504	–	1.97	20.310	–	–	–	–	–
2051293083704793856	2437359 [17L]	16.91	14.598	–	–	–	–	–
2051293152424251648	2436988 [K]	4.69	20.213	–	–	–	–	–
2051293221143720832	2436808 [K]	4.94	16.764	–	–	–	–	–
2051293255503475200	2436958 [K]	4.50	20.342	–	–	–	–	–
2051293289863227520	2437329 [16L]	11.67	15.925	–	–	–	–	–
2051293358577984768	–	1.55	20.049	–	–	–	–	–
2051293388640138880	–	8.48	20.028	–	–	–	–	–

Table 7

Concluded

Gaia EDR3	KIC	Period [d]	G [mag]	$T_{\rm eff}$ [K]	log g	RV [km/s]	[Fe/H]	Ref
2051293496015260416	2570182 ^{X}	1.99	18.719	–	–	–	–	–
2051293530375018112	–	4.27	20.832	–	–	–	–	–
2051293599094510848	2570536 ^{17L}	10.03	14.507	–	–	–	–	–
2051293839619440640	2570259 ^{15,1L}	3.84	16.128	–	–	–	–	–
2051293908333956352	2570154 ^{X}	6.39	18.171	5380(50)	4.004(20)	−68.6(36)	0.12(8)	1*
2051293942698672000	2570258 ^{X}	7.40	16.852	–	–	–	–	–
2051293942698685056	2570313 ^{X}	1.39	19.449	–	–	–	–	–
2051293972756992384	2436621 ^{X}	7.58	18.758	–	–	–	–	–
2051293977053154688	2436734 ^{X}	1.59	20.187	–	–	–	-	–
2051294011418019072	2436852 ^{X}	3.31	18.871	–	–	–	–	–
2051294080137491968	2569421 ^{X}	13.51	18.689	–	–	–	–	–
2051294114495072896	–	3.54	20.960	–	–	–	–	–
2051294148851973888	2569675 ^{X}	5.24	20.253	–	–	–	–	–
2051294148857011712	2569737 ^{14L}	13.54	16.109	–	–	–	–	–
2051294492454406272	2569431 ^{X}	2.49	17.007	–	–	–	–	–
2051294664251895808	–	4.90	21.163	–	–	–	–	–
2051294728671468672	2569908 ^{X}	6.32	16.820	–	–	–	–	–
2051294831750674944	2569761 ^{X}	1.99	20.008	–	–	–	–	–
2051294870413630208	2569467 ^{X}	9.78	15.965	–	–	–	–	–
2051295007845559552	–	6.08	20.344	–	–	–	–	–
2051295007845583744	–	1.80	21.103	–	–	–	–	–
2051295488886958592	2570555 ^{X}	6.35	16.869	–	–	–	–	–
2051295557606451456	2570581 ^{X}	16.52	16.997	–	–	–	–	–
2051296652817037056	2707961 ^{X}	8.00	18.949	–	–	–	–	–
2051297516106367232	–	2.65	21.041	–	–	–	–	–
2051297962788050816	2707771 ^{X}	0.73	18.021	–	–	–	–	–
2051298031507519616	2707692 ^{X}	2.50	19.376	–	–	–	–	–
2051299474616582912	2707858 ^{X}	0.91	20.076	–	–	–	–	–
2051297275593155328	2569073 ^{X}	14.66	14.236	–	–	–	–	–
2051293255496998912	–	9.00	19.651	–	–	–	–	–

See caption of Table 1 for explanation.

Table 8

List of unclassified variables that are not cluster members

Gaia EDR3	KIC	Period [d]	G [mag]	$T_{\rm eff}$ [K]	log g	RV [km/s]	[Fe/H]	Ref
2051104654901977984	2438433 ^{X}	0.93	20.356	–	–	–	–	–
2051105307732052864	2438028 ^{2L}	0.06	20.639	3470(50)	3.842(47)	−48.80(30)	0.09(10)	1*
2051288337759883648	2436293 ^{X}	0.20	18.578	–	–	–	–	–
2051293736533447424	2570195 ^{X}	0.77	20.856	–	–	–	–	–

See caption of Table 1 for explanation.

Table 9

List of equatorial coordinates that are associated with superstamp pixels showing signal in their amplitude spectra

α_{2000}	δ_{2000}	Period [d]	Type
$19^h20^m51^s.72$	$+37^\circ47'45''.4$	1.10	rotational
$19^h20^m53^s.56$	**$+37^\circ47'05''.4$**	1.20	eclipsing
$19^h20^m56^s.85$	**$+37^\circ47'43''.2$**	2.40	rotational
$19^h20^m31^s.99$	**$+37^\circ47'42''.4$**	0.41	binary
$19^h20^m45^s.84$	**$+37^\circ47'04''.1$**	3.07	rotational
$19^h20^m47^s.82$	**$+37^\circ42'18''.2$**	0.68	rotational
$19^h21^m03^s.71$	**$+37^\circ44'17''.6$**	11.68	rotational
$19^h20^m51^s.85$	**$+37^\circ39'51''.5$**	9.21	solar-like
$19^h20^m32^s.77$	$+37^\circ43'23''.8$	0.15	binary
$19^h20^m44^s.47$	$+37^\circ40'51''.5$	5.73	rotational
$19^h20^m46^s.46$	$+37^\circ40'18''.9$	5.73	rotational

In the case of the last three positions listed, we found no optical objects that could be a source of the signal.

given star in the HRD. If the location agrees with the one in CMD, we can expect the spectroscopic fit is likely correct and we obtained an agreement for the majority of stars. It should be noted that the scatter in the HRD is larger, hence some objects may have not been allocated properly. There are clear exceptions, eight among binaries, two among pulsators and two among rotational variables. These cases should be treated with caution.

7. Summary

We presented a search for variable stars in the Kepler superstamp data. All available pixels were searched, by means of a Fourier amplitude spectrum, and contiguous optimal apertures for each object that shows a significant flux variation were defined. The coordinates of these optimal apertures were matched with optical counterparts using Pan-STARRS. In total, we detected 278 variable stars. We cross-matched our variable star sample with those reported in the literature and found 16 variable stars reported by Kaluzny and Rucinski (1993), four by Rucinski *et al.* (1996), 23 by Mochejska *et al.* (2002), six by Mochejska *et al.* (2003), four by Kaluzny (2003), 15 by Bruntt *et al.* (2003), seven by Mochejska *et al.* (2005), one by Hartman *et al.* (2005) and 33 by de Marchi *et al.* (2007).

We found 240 stars having KIC designations, out of which 140 stars do not have data delivered to the MAST. A variability of 119 stars was not known prior to

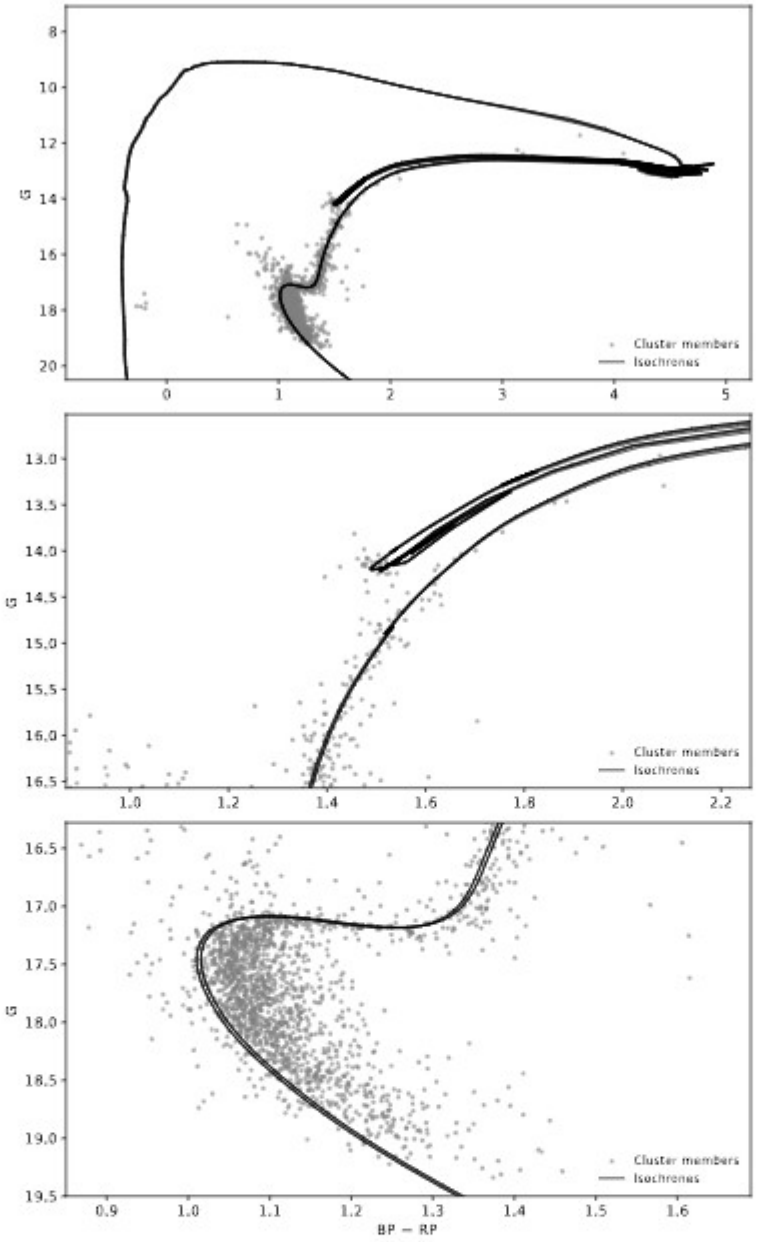

Fig. 5. CMD of NGC 6791, showing the best MIST isochrone fits. The *top panel* shows the overall diagram, while the *middle panel* shows the red clump region and the *bottom panel* shows the main-sequence region.

our analysis. These stars are marked in bold in Tables 1–8, including the first nine objects listed in Table 9. Just recently, and independently of our work, Colman *et al.* (2022) reported light curves of stars with a KIC designation. However, the authors

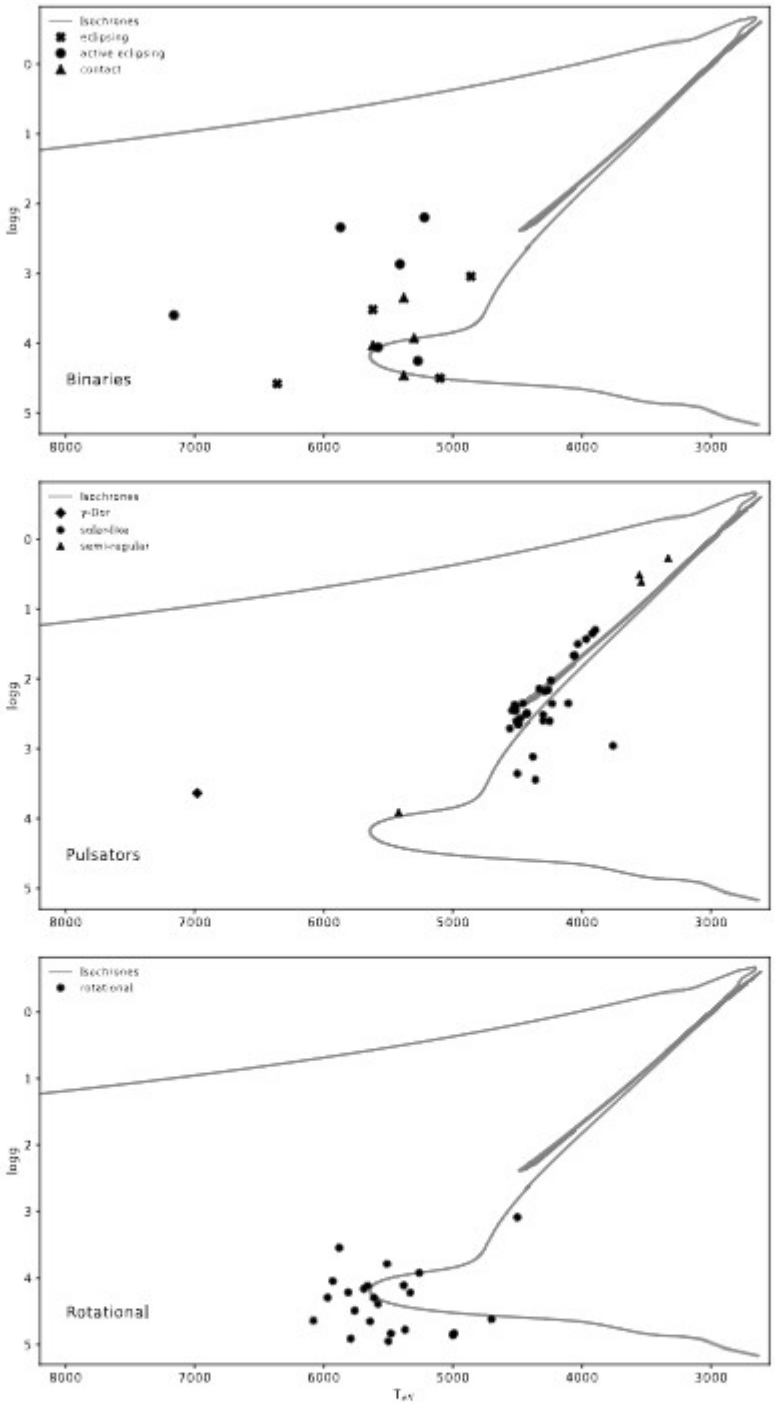

Fig. 6. $T_{\rm eff}-\log g$ diagram showing the cluster members with atmospheric parameters derived in this work. The *top, middle* and *bottom panels* show binary, pulsating and rotational stars, respectively. The isochrones represent the best MIST fits in $T_{\rm eff}$ and $\log g$ coordinates.

did not specify which stars were found variables, only reporting a total number of 239 variables. Even accounting for this report, which is limited to the KIC stars only, we can consider 26 variable stars having no KIC designation (including seven objects marked in bold), to be new detections. No ground-based work on the detection of the variability of these 26 stars was reported, either.

Using Gaia EDR3 astrometry, we calculated the membership probabilities for all variable stars in our sample by applying Bayesian Gaussian mixture models. A star is considered to be a cluster member if the probability is higher than 50%. In total, we found 129 variable stars that are cluster members: 17 binary systems, 45 pulsators, 62 rotationally and five unclassified variables. The locations of these cluster variable stars in the CMD diagram were estimated and indicate the evolutionary status of cluster members. In the CMD, a majority of our variable stars are located in the MS. Solar-like pulsators are mostly located in the RGB and RC, while semi-regular variables are located in the RGB and AGB. In addition there are five BS and three EHB stars in the CMD.

In the case of binary systems, we estimated mid-times of eclipses and derived ephemerides. We calculated the $O-C$ diagrams and checked for any orbital period variation. Only three binary systems show significant period variation. However, its nature is not confirmed. The solar-like counterpart has been a subject of a detailed analysis of its pulsation content, and the results will be published elsewhere. The analysis of three sdBVs has already been reported by Sanjayan *et al.* (2022). The rotational variables are not subject to our detailed analysis. This type of variables can be very useful toward gyrochronology.

We utilized public and archived spectra for 111 variable stars. Spectra for 64 stars were fitted with XTGRID, while for the remainder of the sample, we adopted the fit values from the surveys. We derived $T_{\rm eff}$, $\log g$, [Fe/H] and RVs. Our spectral analysis was able to recover consistent stellar parameters from very diverse spectroscopic data. This consistency is reflected by the similar distribution of stars in the CMD and HRD. The most significant limiting factor on the parameter determination was the low SNR of some spectra, while the spectral coverage and crowding in dense fields played less significant roles. We found that the metallicity is not consistent among the cluster members and it is still unclear what causes it. If the inconsistency is real a possible explanation would be the presence of multiple stellar populations within the cluster as mentioned by Geisler *et al.* (2012). To confirm this hypothesis a uniform spectroscopic survey is required.

MIST isochrones were fit to our CMD comprised of cluster members, including our variable star population. From our best three fits, we derived a metallicity range of 0.26 to 0.28 and the age of NGC 6791 to be 8.91 Gyr. Our age estimate agrees with the values reported by *e.g.*, Choi *et al.* (2018). The average distance estimate from the distance modulus is 4134 pc which overlaps with our independent estimate of 4123(31) pc we derived from the Gaia astrometry.

Acknowledgements. Financial support from the National Science Centre under projects No. UMO-2017/26/E/ST9/00703 and UMO-2017/25/B/ST9/02218 is acknowledged. PN acknowledges support from the Grant Agency of the Czech Republic (GAČR 22-34467S). The Astronomical Institute in Ondřejov is supported by the project RVO:67985815. This paper includes data collected by the Kepler mission and obtained from the MAST data archive at the Space Telescope Science Institute (STScI). Funding for the Kepler mission is provided by the NASA Science Mission Directorate. STScI is operated by the Association of Universities for Research in Astronomy, Inc., under NASA contract NAS 5-26555. This work has made use of data from the European Space Agency (ESA) mission Gaia (https://www.cosmos.esa.int/gaia), processed by the Gaia Data Processing and Analysis Consortium (https://www.cosmos.esa.int/web/gaia/dpac/consortium). Funding for the DPAC has been provided by national institutions, in particular the institutions participating in the Gaia Multilateral Agreement. This research has made use of the NASA/IPAC Extragalactic Database (NED), which is operated by the Jet Propulsion Laboratory, California Institute of Technology, under contract with the National Aeronautics and Space Administration. This research has used the services of *www.Astroserver.org* under reference XZR329. We thank the anonymous referee for valuable comments, which have significantly improved the quality of the manuscript.

REFERENCES

Ahn, C.P., Alexandroff, R., Allende P.C., *et al.* 2014, *ApJS*, **211**, 17.
Baade, W. 1931, *Astron. Nachr.*, **243**, 303.
Baran, A. 2013, *Acta Astron.*, **63**, 203.
Basu, S., Grundahl, F., Stello, D.*et al.* 2011, *ApJ*, **729**, L10.
Bedin, L.R., Salaris, M., Piotto, G. *et al.* 2005, *ApJ*, **624**, L45.
Blanton, M.R., Bershady, Matthew A., *et al.* 2017, *AJ*, **154**, 28.
Bohlin, R.C., Mészáros, S., Fleming, S.W., *et al.* 2017, *AJ*, **153**, 234.
Borucki, W.J., Koch, D., Basri, G., *et al.* 2010, *Science*, **327**, 977.
Bressan, A.M., Marigo, P., Girardi, L., *et al.* 2012, *MNRAS*, **427**, 127.
Bryson, S.T., Tenenbaum, P., Jenkins, J.M., *et al.* 2010, *ApJ*, **713**, L97.
Bruntt, H., Grundahl, F., Tingley, B., *et al.* 2003, *A&A*, **410**, 323.
Caldwell, D.A., Kolodziejczak, J.J. Van Cleve, J.E., *et al.* 2010, *ApJ*, **713**, 92.
Cardelli, J.A., Clayton, G.C., Mathis, J.S., *et al.* 1989, *ApJ*, **345**, 245.
Carraro, G., Villanova, S., Demarque, P., *et al.* 2006, *AJ*, **643**, 1151.
Carrera, R., Bragaglia, A., Cantat-Gaudin, T., *et al.* 2019, *A&A*, **623**, A80.
Chaboyer, B., Green, E.M., and Liebert, J. 1999, *AJ*, **117**, 1360.
Chambers, K.C., Magnier, E.A., Metcalfe, N., *et al.* 2016, arXiv1612.05560.
Choi, J., Dotter, A., Conroy, C., *et al.* 2016, *ApJ*, **823**, 102.
Choi, J., Conroy, Ch. Ting, Y.-S.*et al.* 2018, *ApJ*, **863**, 65.
Colman, I.L.,Bedding, T.R., Huber, D., Kjeldsen, H. 2022, *ApJS*, **258**, 39.
de, Marchi, F., Poretti, E., Montalto, M., *et al.* 2007, *A&A*, **471**, 515.
Dempster, A.P., Laird, N.M., and Rubin, D.B. 1977, *Journal of the Royal Statistical Society*, **39**, 1.
Dotter, A. 2016, *ApJS*, **222**, 8.
Fabricant, D., Fata, R., Roll, J., *et al.* 2005, *PASP*, **117**, 1411.

Ferguson, T.S. 1973, *The Annals of Statistics*, **1**, 209.
Flewelling, H.A., Magnier, E.A., Chambers, K.C., *et al.* 2020, *ApJS*, **251**, 7.
Gaia Collaboration, Prusti, T., de Bruijne, J.H.J., *et al.* 2016, *A&A*, **595**, A1.
Gaia Collaboration, Brown, A.G.A., Vallenari, A., *et al.* 2021, *A&A*, **649**, A1.
Geisler, D., Villanova, S., Carraro, G., *et al.* 2012, *ApJ*, **756**, L40.
Gilmore, G., Randich, S., Asplund, M., *et al.* 2012, *The, Messenger*, **147**, 25.
Harris, W.E., and, Canterna, R. 1981, *AJ*, **86**, 1332.
Hartman, J.D., Stanek, K.Z., Gaudi, B.S., Holman, M.J., and McLeod, B.A. 2005, *AJ*, **130**, 2241.
Howell, S.B., Sobeck, Ch., Haas, M., *et al.* 2014, *PASP*, **126**, 398.
Jilkova, L., Carraro, G., Jungwiert, B., and Minchev, I. 2012, *A&A*, **541**, 64.
Kaluzny, J. 2003, *Acta Astron.*, **53**, 51.
Kaluzny, J.and, Rucinski, S.M. 1993, *MNRAS*, **265**, 34.
Kaluzny, J.and, and Udalski, A. 1992, *Acta Astron.*, **42**, 29.
Kamann, S., Bastian, N.J., Gieles, M., Balbinot, E., and Henault-Brunet, V. 2019, *MNRAS*, **483**, 2197.
Kinemuchi, K., Barclay, T., Fanelli, M., *et al.* 2012, *PASP*, **124**, 963.
King, I.R. 1964, *Royal Observatory Bulletin*, **82**, 106.
Kinman, T.D. 1965, *ApJ*, **142**, 655.
Koch, D.G., Borucki, William J., Rowe, J.F., *et al.* 2010, *ApJ*, **713**, 79.
Kwee, K., and van Woerden, H. 1956, *Bulletin of the Astronomical Institutes of the Netherlands*, **12**, 327.
Liebert, J., Saffer, R.A., and Green, E.M. 1994, *AJ*, **107**, 1408.
Lindegren, L., Bastian, U., Biermann, M., *et al.* 2021, *A&A*, **649**, A4.
Majewski, S.R., Schiavon, Ricardo P., Frinchaboy, P.M., *et al.* 2017, *AJ*, **154**, 94.
Mochejska, B.J., Stanek, K.Z., Sasselov, D.D., *et al.* 2005, *AJ*, **129**, 2856.
Mochejska, B.J., Stanek, K.Z., and Kaluzny, J. 2003, *AJ*, **125**, 3175.
Mochejska, B.J., Stanek, K.Z., Sasselov, D.D., and Szentgyorgyi, A.H. 2002, *AJ*, **123**, 3460.
Németh, P., Kawka, A., and Vennes, S. 2012, *MNRAS*, **427**, 2180.
Pedregosa, F., Varoquaux, G., Gramfort, A., *et al.* 2011, *Journal of Machine Learning Research*, **12**, 2825.
Platais, I., Cudworth, K.M., Kozhurina-Platais, V., *et al.* 2011, *AJ*, **733**, 1.
Randich, S., Gilmore, G., Gaia-ESO Consortium, *et al.* 2013, *The, Messenger*, **154**, 47.
Rucinski, S.M., Kaluzny, J., and Hilditch, R.W. 1996, *MNRAS*, **282**, 705.
Sanjayan, S., Baran, A.S., Ostrowski, J., *et al.* 2022, *MNRAS*, **509**, 763-777.
Stetson, P.B., Bruntt, H., and Grundahl, F. 2003, *PASP*, **115**, 413.
Thompson, S., Fraquelli, D., Van, Cleve, J., and Caldwell, D. 2016, Kepler Science Document KDMC-10008-006, id. 9.
Tofflemire, B.M., Gosnell, N.M., Mathieu, R.D., and Platais, I. 2014, *AJ*, **148**, 61.
Villanova, S., Carraro, G., Geisler, D., Monaco, L., and Assmann, P. 2018, *ApJ*, **867**, 34.
Zhao, G., Zhao, Y.-H., Chu, Y.-Q., Jing, Y.-P., and Deng, L.-C 2012, *Research in Astronomy and Astrophysics*, **12**, 7.

Chapter 5

Paper IV: variable Star Population in the Open Cluster NGC 6819 Observed by the *Kepler* Spacecraft

Abstract

We present the list of variable stars we found in the *Kepler* superstamp data covering approximately nine arcminutes from the central region of NGC 6819. This is a continuation of our work presented by Sanjayan et al.(2022a). We classified the variable stars based on the variability type and we established their cluster membership based on the available *Gaia* Data Release 3 astrometry. Our search revealed 385 variable stars but only 128 were found to be cluster members. In the case of eclipsing and contact binaries we calculated the mid-times of eclipses and derived ephemerides. We searched for eclipse timing variation using the observed minus calculated diagrams. Only five objects show significant orbital period variation. We used isochrones calculated within the MESA Isochrones and Stellar Tracks project and derived the average age (2.54 Gyr), average distance (2.3 kpc) and iron content [Fe/H] = -0.01(2), of NGC 6819. We confirm this distance by the one derived from *Gaia* astrometry of the cluster members with membership probabilities greater than 0.9.

doi: 10.32023/0001-5237/72.4.3

ACTA ASTRONOMICA
Vol. **72** (2022) pp. 267–295

Variable Star Population in the Open Cluster NGC 6819 Observed by the Kepler Spacecraft

S. Sanjayan[1,2], A. S. Baran[1,3], P. Németh[1,4,5] and K. Kinemuchi[6,7]

[1] ARDASTELLA Research Group
[2] Centrum Astronomiczne im. Mikołaja Kopernika, Polskiej Akademii Nauk, ul. Bartycka 18, 00-716 Warszawa, Poland
[3] Astronomical Observatory, University of Warsaw, Al. Ujazdowskie 4, 00-478 Warszawa, Poland
[4] Astroserver.org, Fötér 1, 8533 Malomsok, Hungary
[5] Astronomical Institute of the Czech Academy of Sciences, Fričova 298, CZ-251 65 Ondřejov, Czech Republic
[6] Department of Astronomy, New Mexico State University, Box 30001, MSC 4500, Las Cruces, NM 88003, USA
[7] Apache Point Observatory, 2001 Apache Point Road, P.O. Box 59, Sunspot, NM 88349-0059

Received November 22, 2022

ABSTRACT

We present the list of variable stars we found in the Kepler superstamp data covering approximately nine arcminutes from the central region of NGC 6819. This is a continuation of our work presented by Sanjayan *et al.* (2022a). We classified the variable stars based on the variability type and we established their cluster membership based on the available Gaia Data Release 3 astrometry. Our search revealed 385 variable stars but only 128 were found to be cluster members. In the case of eclipsing and contact binaries we calculated the mid-times of eclipses and derived ephemerides. We searched for eclipse timing variation using the observed minus calculated diagrams. Only five objects show significant orbital period variation. We used isochrones calculated within the MESA Isochrones and Stellar Tracks project and derived the average age (2.54 Gyr), average distance (2.3 kpc) and iron content [Fe/H]=-0.01(2), of NGC 6819. We confirm this distance by the one derived from Gaia astrometry of the cluster members with membership probabilities greater than 0.9.

Key words: *open clusters and associations: individual: NGC 6819 – Stars: variables: general*

1. Introduction

In the notes of Caroline Herschel (Hoskin 2005), NGC 6819 was listed in the class of nebulae and star clusters found between θ Lyr and δ Cyg. Early study was mostly focused on photometry that allowed for construction of a color–magnitude diagram (CMD) and to estimate the age of the cluster. Detecting only a weak

nebula in photographic plates from the Palomar Observatory Sky Survey (POSS-I), King (1964) added NGC 6819 to the list of open clusters that may be old, which made the cluster exceptional as open clusters were considered to be young objects. The first photometry of 38 stars in the field of the cluster were done by Purgathofer (1966) who used the original plates from Barnard (1931). From a CMD Burkhead (1971) pointed out that the main sequence turnoff (MSTO) region of NGC 6819 is near to that of M67 hence both clusters have comparable ages, however no age of the latter was reported. Later Lindoff (1972) and Auner (1974) observed the cluster in the $B-V$ color. They compared the MSTO and red giant branch (RGB) with other older clusters and predicted that the age of the cluster is at least 2.5 Gyr. From the theoretical isochrones Rosvick and Vandenberg (1998) reported an age of 2.4 Gyr, which is in agreement with the age 2.3(2) Gyr estimated by Anthony-Twarog *et al.* (2014). Rosvick and Vandenberg (1998) suggested that red clump (RC) stars are the descendants of blue stragglers (BS), given that NGC 6819 has a confirmed BS population. Kalirai *et al.* (2001) estimated a total mass of the cluster to be 2600 $M_{\odot}$.

Many researchers undertook a search for a variable content in the area of the cluster. We compared our findings with the results reported in most of the following papers. Barkhatova and Vasilevsky (1967) conducted the first attempt to detect variable stars in NGC 6819 with a null result. A variable of the irregular type was reported for the first time by Lindoff (1971). As a result of search for contact binaries Kaluzny and Shara (1988) made the first significant discovery by detecting 11 variable stars but none of them were reported to be a contact binary. Manteiga *et al.* (1989) used RV data of stars in the area of the cluster and detected only one RV variable BS. Kryachko (2001) discovered two dwarf novae in the cluster area. A survey by Street *et al.* (2002) revealed 25 variable stars and 13 suspected variable stars in the area of NGC 6819. Street *et al.* (2003) did an extended search for planetary transits by analyzing data of 38 000 stars in the area of NGC 6819, and they found 11 stars with transiting events. Street *et al.* (2005) reported a detection of 141 variable stars, including 53 eclipsing binaries, eight RS CVn variables, 70 rotational stars, 13 long period variables and five variables of other types. Stello *et al.* (2010) reported the first asteroseismic analysis of solar-like red giants in the cluster. Additional ground-based observations were taken by Talamantes *et al.* (2010) in the area of NGC 6819 and they listed 14 binaries and one δ Scuti pulsator. Using the XMM Newton data, Gosnell *et al.* (2012) made an unexpected discovery of 12 X-ray sources in the cluster area.

A time-series photometry of the cluster variable population allowed for an independent determination of a distance modulus and cluster age. Balona *et al.* (2013) used 129 rotational variables in NGC 6819 to study the relation between the period and $B-V$ color, and they derived cluster age of about 2.5 Gyr. Basu *et al.* (2011) estimated the distance modulus of $(m-M)_0 \approx 11.85$ mag and reddening $E(B-V) \approx 0.15$ mag using asteroseismic analysis of red giant stars in the cluster.

The authors estimated the distance to the cluster to be 2344(24) pc. According to Salaris *et al.* (2004), NGC 6819 is located in the halo of the Milky Way and 300 pc above the galactic plane.

Spectroscopic observations allowed for determination of the motion in the Galaxy and the cluster metallicity. Using only seven cluster members, Friel *et al.* (1989) derived the mean cluster radial velocity (RV) of $-7(13)$ km/s. A more precise estimation of 2.34(5) km/s was reported by Hole *et al.* (2009). Ak *et al.* (2016) reported that the cluster has a slightly eccentric orbit with the eccentricity (e) of 0.06 and has the orbital period of 142 Myr. According to Bragaglia *et al.* (2001), the cluster has a super solar metallicity of $[\mathrm{Fe/H}] = +0.09(3)$, while Lee *et al.* (2015) pointed to a sub solar metallicity of $[\mathrm{Fe/H}] = -0.02(2)$.

Stellar clusters are studied through their members, hence it is essential to identify cluster members. Below, we present a historical progress of a member hunt in NGC 6819. Sanders (1972) used the relative proper-motion of 189 stars in the cluster area and found 88 probable cluster members. Using RV measurements from the WIYN open cluster study XXIV, Hole *et al.* (2009) established membership of 913 stars in the cluster area, finding 437 targets to have probabilities greater than 50%. Stello *et al.* (2011) determined membership probability of 61 stars using asteroseismic analysis and found 50 members. Platais *et al.* (2013) derived 2314 stars with more than 50% membership probability among 15 750 stars located in the cluster area. The authors used data from the WIYN open cluster study LV. Gao *et al.* (2015) established 537 cluster members by means of RVs and proper motion data. Zhang *et al.* (2015) presented membership studies of 80 stars using RVs from the Large Sky Area Multi-Object Fibre Spectroscopic Telescope (LAMOST) survey. Sampedro *et al.* (2017) determined the membership probability of 1074 stars using the United States Naval Observatory (USNO) CCD Astrograph Catalog (UCAC4). The first membership analysis using Gaia astrometry was done by Cantat-Gaudin *et al.* (2018), who found 1915 members. The cited works revealed many confirmed cluster members derived by means of RVs, proper motions, and seismic analysis. In Section 4 we present a comparison of the results of the membership studies reported by Cantat-Gaudin *et al.* (2018) with our results.

To increase the efficiency of the detection of all variable star populations in the cluster area, we undertook an analysis of all Kepler superstamp data of NGC 6819. The variable stars should in future serve the purpose of deriving the most precise parameters of the cluster, through binary star, asteroseismic and gyrochronology studies. In addition, Gaia data of the cluster members were used toward the cluster age and distance derivation. This is a continuation of our previous work on NGC 6791 presented by Sanjayan *et al.* (2022a). Recently, Colman *et al.* (2022) presented the light curves of KIC targets observed in the Kepler superstamps of NGC 6819 using an image subtraction technique. We stress that the method and analysis presented in this work is independent of the one presented in Colman *et al.* (2022).

In Section 2, we present a short description of the Kepler mission and data processing in order to obtain the light curves of variable stars. In Section 3, we present our analysis of spectra taken at Nordic Optical Telescope (NOT), Apache Point Observatory (APO) and other spectra we found in public databases *i.e.*, LAMOST survey, Apache Point Observatory Galactic Evolution Experiment (APOGEE) survey, MMT Hectospec 300 optical fiber fed spectrograph survey, and Apache Point Observatory 3.5-meter telescope survey. In Section 4, we invoke the Gaia astrometric parameters of variable stars we detected to establish their cluster membership. In Section 5, we report the zoo of variable stars we found in the area of NGC 6819. In Section 6, we present the results of the MIST (MESA Isochrones and Stellar Tracks) isochrones fitting to estimate the age of and the distance to NGC 6819.

2. Kepler Photometry

During the original Kepler mission four open clusters (NGC 6791, NGC 6819, NGC 6811, NGC 6866) were continuously observed. NGC 6791 and NGC 6819 were observed in the so-called "superstamps", which were used for observing multiple targets in crowded fields. The central most parts NGC 6791 and NGC 6819 were covered during Quarters (Q) 1–17. In the first part of our work, we reported a detailed study of the Kepler superstamps of NGC 6791 (Sanjayan *et al.* 2022a).

We downloaded the Kepler superstamp data of NGC 6819 from the Mikulski Archive for Space Telescopes (MAST*). The data are 20×100 pixel boxes piled up in two contiguous 10 box stacks. The field of view of all pixels is $800'' \times 800''$ and covers the central most part of the cluster. The superstamps data are collected in the long cadence mode, lasting 30 min. The pixel scale is $4''$. The data were collected over 1460 days and are split into 18 quarters.

We searched for a flux variation by extracting fluxes for all time stamps in individual pixels for each of the quarters Q2–5. Next, a Fourier transform of the time-series data was performed in each pixel and each quarter separately. The pixels showing peaks (representing signal) in the amplitude spectra were selected. Signals that were identified with artifacts, either reported by Baran (2013) or those found in this project, were discarded. The optimal apertures are formed by contiguous pixels showing the same flux variation of $S/N \geq 5$, not including pixels that contain too much signal from neighbors, even though the S/N ratio is still ≥ 5. Examples of optimal apertures can be seen in Fig. 6 of Sanjayan *et al.* (2022b). To keep the solar cells facing sunlight, every quarter the spacecraft rolled 90°, hence, with each quarterly rotation of the spacecraft, our targets landed on different CCD silicons. One CCD silicon covering the area of NGC 6819 had failed prior to Q6 data collection, which caused quarterly data gaps during Q6,10 and 14. Using the optimal apertures for all targets showing flux variation, we used PyKE software (Kinemuchi *et al.* 2012) to pull out the fluxes and correct them for instrumental

*https://archive.stsci.edu/

artifacts by means of Co-trending Basis Vectors. Finally, using our custom scripts, we clipped the data at 4.5σ, detrended using spline fits, and normalized them to parts per thousand (ppt). The variable stars detected in our work are presented in Section 5.

3. Spectroscopy

Using the Astrophysical Research Consortium's 3.5 m telescope at APO, we obtained spectra for five stars. The spectra were collected from the Dual Imaging Spectrograph (DIS), using the B1200 and R1200 grating. In the blue channel, the grating was centered at 4300 Å and had a wavelength range of 1240 Å, while for the red channel, the grating was centered at 6400 Å and had a range of 1160 Å. The linear dispersions were 0.62 Å/pix in the blue and 0.58 Å/pix in the red. The magnitude range of the stars were 14.08 to 18.70 in the Johnson V, and for one object, the Gaia G magnitude was 17.39. The spectra were reduced and extracted using standard IRAF single slit spectroscopic techniques (Tody 1986, 1993). We observed the spectra of eight pulsating variable stars with the 2.56 m NOT using ALFOSC spectrograph. In these spectra, we measured a dispersion of 2.2 Å from the full width at the half maximum of the lines in the arc spectra and a signal-to-noise ratio of ≈ 100 in the range of wavelengths 4950–5300 Å. For a number of targets we found spectra in the publicly available archives (links can be found in Table 1). HECTOSPEC (Fabricant *et al.* 2005) operates at a resolution of approximately $R \approx 1000-2000$, LAMOST (Zhao *et al.* 2012) offers low-resolution spectra with a resolution of around $R \approx 1800$, while APOGEE (Ahn *et al.* 2014, Majewski *et al.* 2017) covers the H-band (1.51–1.70 μm) with a resolution of approximately $R \approx 22\,500$.

We followed the fitting procedures from Németh *et al.* (2012) in using XTGRID. The χ-square minimizing steepest-descent procedure fits an observation with interpolated ATLAS 9 models, calculated in local thermodynamic equilibrium, drawn from the spectral library of Bohlin *et al.* (2017). Atmospheric parameters were derived by iteratively applying successive approximations of synthetic spectra to the observations. We interpolated in effective temperature ($T_{\rm eff}$), surface gravity ($\log g$) and scaled solar metallicity ([M/H]) space, and also fitted the radial velocity with respect to synthetic spectra. Iterations were pursued until the variation of surface parameters and the χ-square decreased below 0.5%. Uncertainties of parameters were determined by changing [M/H] and radial velocities in one dimension until the statistical limit for 60% confidence was reached. The correlations between $T_{\rm eff}$ and $\log g$ were considered by the procedure. To avoid local minima the fitting procedure returns to the global minimization if a better solution is found during these calculations. Further details of the analysis methods are presented in Section 3 of Sanjayan *et al.* (2022a). Fig. 1 shows the best-fit BOSZ/XTGRID model to the NOT/ALFOSC observation of KIC 5113357.

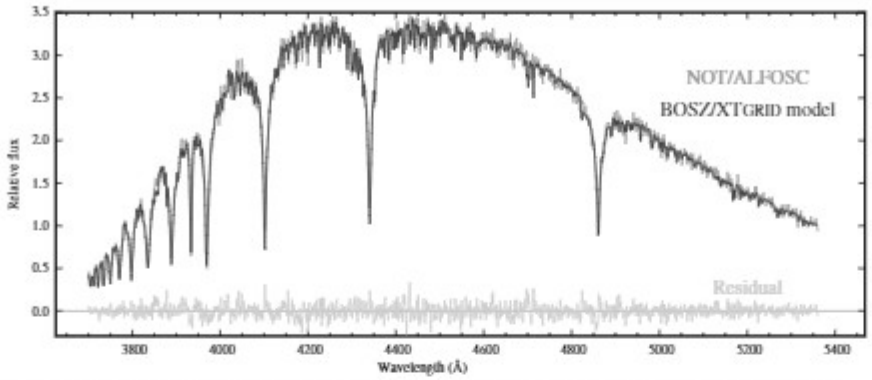

Fig. 1. Best-fit BOSZ/XTGRID model to the NOT/ALFOSC observation of KIC 5113357.

4. Cluster Membership

Our goal was to use the Gaia Data Release 3 (DR3) astrometry to estimate the membership probability of all variable stars we found in this work. We downloaded astrometric data of over 36 000 stars from the Gaia DR3 catalog (Gaia Collaboration *et al.* 2022). We selected the stars in the area of NGC 6819, defined by the cluster center $\alpha_{2000} = 19{:}41{:}17.2$ and $\delta_{2000} = +40{:}11{:}18$ (Kamann *et al.* 2019) and a tidal radius of $23'$ (Kalirai *et al.* 2001). The membership analysis was done using five astrometric parameters, position (α and δ in equatorial coordinates), proper motion (μ_α and μ_δ) and, parallax π. To establish the membership of our variable stars we followed the method used and described in Sanjayan *et al.* (2022a). It employs variational Bayesian inference model with Dirichlet process prior (Ferguson 1973) using scikit–learn library in Python (Pedregosa *et al.* 2011). We found 1971 Gaia targets to be cluster members, including 128 variable stars. A CMD of 15 636 stars that were used in our analysis is presented in Fig. 2. The majority of stars we found to be members of NGC 6819 nicely mark the main sequence, red giant branch as well as BS and RC regions.

We compared 1527 stars identified as the cluster members with a membership probability at least 0.7, reported by Cantat-Gaudin *et al.* (2018), with members found in our analysis. We found 1482 stars to be cluster members. Of the remaining 45 stars, we found 19 to be outside our search radius, we excluded two stars due to high uncertainty in the parallax and proper motion, while we found 24 stars not to be members.

RV data in the Gaia DR3 allow us to enhance the membership analysis for some of the stars in our sample. However, the data can be contaminated by binarity, rotation and pulsation effects. The data need to be free of these effects before applying to the membership analysis to obtain a reliable solution. We preliminarily assumed the Gaia DR3 RV data are clean of those effects and we used a RV as a sixth parameter in our analysis. We recalculated the membership probability of 821 stars for which we collected the RV data, deriving 126 cluster members.

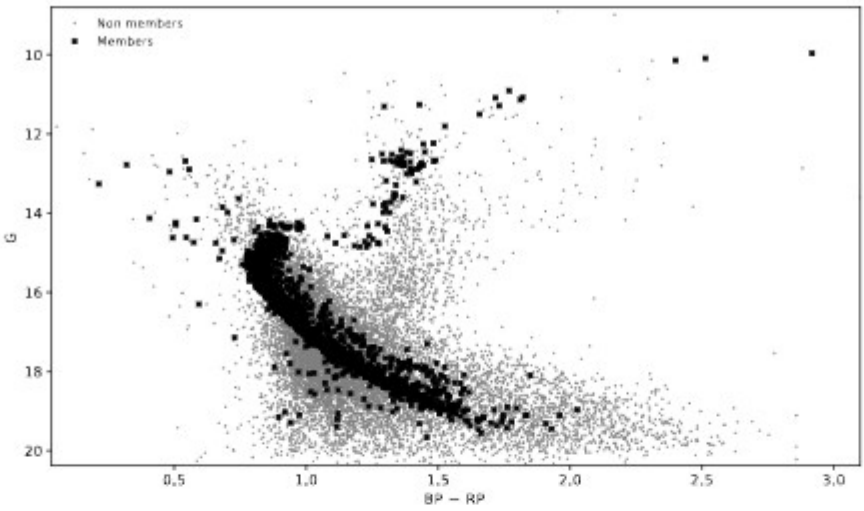

Fig. 2. CMD of all stars included in our analysis.

The membership of these 126 stars has not changed after using the RV data. This outcome validates either our assumption that RVs have no additional effects or any such effects do not affect the membership analysis. Using the RV data of these 126 cluster members we estimated the average radial velocity of the cluster to be +3.5(5) km/s.

5. A Zoo of Variable Stars

In total, we found 385 variable stars in the area of NGC 6819. The observed variability is classified based on the light curve shape and the periods estimated from an amplitude spectrum. We distinguished three main variability types, *i.e.*, binaries, pulsators and rotational. In addition, we listed several cases of unclassified and unidentified sources. Below we discuss each group of the flux variation. The cluster members and non members are listed in separate tables. For each type of variability we provide a number of newly detected variables.

We used amplitude spectra calculated from the light curves to classify pulsators into solar-like, δ Scuti, γ Dor, and semi-regular variables. Stars with a periodic flux variation but showing additional flux modulation are classified as rotational stars. A sample of the light curves with corresponding amplitude spectra for each type of variability and specific classes we detected in this analysis is presented in Fig. 3.

We stress that our variability classification is subject to a number of caveats, which we have discussed in Sanjayan *et al.* (2022a) presenting similar work on NGC 6791. Therefore the location of targets, especially binaries, in the CMDs and our RV estimates should be considered with caution.

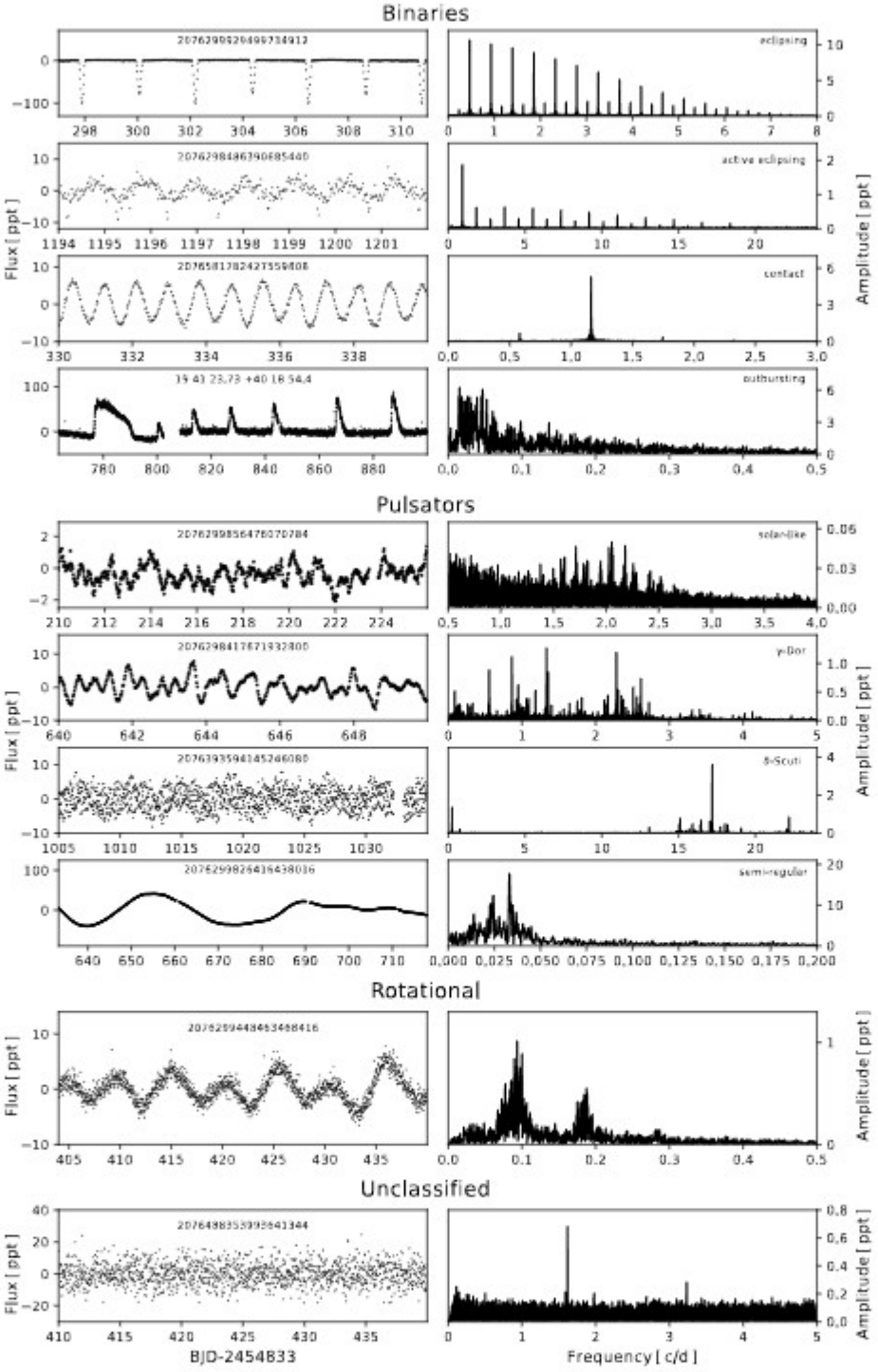

Fig. 3. Sample of the light curves and amplitude spectra for different types and classes of variable stars in the area of NGC 6819.

5.1. Binary Variables

We detected 59 binaries which included members, non members, and eight stars that are not associated with any Gaia targets, and hence their membership was not determined. From the phased light curves, we classified binaries into four classes, eclipsing, active eclipsing, contact and outbursting. We found 15 eclipsing systems with sharp eclipses and no out-of-eclipse variation. There are two members, 12 non-members, and one with no membership established. Eclipsing binaries with additional out-of-eclipse variation, likely caused by chromospheric activity, are called active eclipsing and we found eight members, 10 non-members and one with no membership established. The contact binaries are identified with systems showing light curves characteristics of W UMa system and we found seven members, 10 non-members and three with no membership established. Typical orbital periods of contact binaries are known not to be longer than 1 day so three stars may not be properly classified. Our classification is phenomenological, hence additional spectroscopic RV data may re-classify these objects. We found five outbursting stars, which we assumed to be binaries. Two of them are non-members while three have no membership established yet. In total we found 30 new variable binaries, including six cluster members, 17 field counterparts and seven with membership undetermined yet. We list the cluster members in Table 1, non-members in Table 5, while stars with no membership determined in Table 9. In Fig. 4 we present only phased light curves of the NGC 6819 member binaries that we found to be new discoveries. In a CMD shown in the top panel of Fig. 5, the majority of the binaries are located on the MS, while six are in the MSTO region. The latter ones can provide an independent estimate of the cluster age, if parameters are derived for individual components. As it was explained in Sanjayan *et al.* (2022a) the positions of binaries in the CMD should be treated with caution.

We identified five outbursting stars, which may possibly be associated with eruptions caused by a mass transfer. None of the outbursting stars were found to be members of the cluster. Gaia DR3 2076392906942365568 was reported as an X-ray cataclysmic variable during the XMM Newton survey by Gosnell *et al.* (2012).

Using the eclipses in eclipsing systems and the light maxima in contact binaries, we estimated the mid-times by means of the method described in Kwee and van Woerden (1956). We used the mid-times to derive ephemerides, which are reported in Table 1 and 5. For a few cases we provided only rough estimates of periods, which is caused by a low precision of data. In two cases we detected single eclipses only. To search for an orbital period variation we calculated Observed minus Calculated ($O-C$) diagrams. We found significant orbital period variations in five binaries, including only one cluster member (Fig. 6). In two cases, KIC 5112759 and KIC 5113461, the variations may look sinusoidal caused by an additional body in these systems. The other three cases are not easy to interpret.

Table 1

List of binary stars that are cluster members

Gaia DR3	KIC	P_{orb} [days]	T_0 [BJD]	G [mag]	CMD	HRD	T_{eff} [K]	log *g*	RV [km/s]	[Fe/H]	Ref
eclipsing											
2076300062631198208	5024475[X]	0.35461351(48)	2 454 964.3935(11)	16.950	MS	–	–	–	–	–	–
2076298864347818624	5024447[14L]	771.8122(14)	2 455 267.6048(10)	14.933	MS	–	–	–	–	–	–
active eclipsing											
2076300101298442368	5112456[X]	1.04163866(35)	2 454 965.06811(26)	16.943	MS	MS	5 660(200)	4.36(1)	0(13)	−0.439(31)	4*
2076299929499734912	5024292[15,4L]	4.3010306(16)	2 454 967.449238(30)	15.001	MS	–	–	–	–	–	–
2076299826420588288	5024450[15,11L]	3.0518491(12)	2 455 185.42743(27)	14.985	MS	–	–	–	–	–	–
2076487121349914752	5023948[15,9L]	3.64930727(38)	2 455 465.83818(6)	14.991	MS	–	–	–	–	–	–
2076299169277916160	5024064[X]	2.05541020(25)	2 454 965.97867(10)	18.528	MS	–	–	–	–	–	–
2076298486390685440	5024364[X]	1.089253(5)	2 454 965.8187(39)	16.982	MS	–	–	–	–	–	–
2076393422338668800	5113176[X]	2.504898870(38)	2 454 964.84980(12)	18.973	MS	–	–	–	–	–	–
2076392838230907264	5024980[X]	414.54921(33)[e]	2 455 081.23049(61)	17.427	MS	–	–	–	–	–	–
contact											
2076581713708050176	5112407[X]	0.366025967(25)	2 454 964.90170(5)	16.415	MS	MS	5620(50)	4.345(37)	65(3)	−1.15(8)	1*
2076299792060826496	5024624[X]	0.30321101(8)	2 454 964.70244(22)	17.097	MS	MS	5590(20)	4.865(23)	26(2)	−0.430(23)	1*
2076299448463338368	5023989[X]	0.26367746(8)	2 454 964.78122(23)	19.508	–+	–	–	–	–	–	–
2076581782427559808	5112708[X]	1.7195289(19)	2 454 965.2048(9)	14.915	MS	–	–	–	–	–	–
2076394105234042496	5112759[X]	0.25622643(8)	2 454 964.66578(25)	17.788	MS	MS	4650(30)	4.184(28)	15(5)	−0.67(7)	1*
2076389608415499392	5025105[X]	1.5747014(35)	2 454 965.1646(19)	15.286	MS	–	–	–	–	–	–
2076300066938740096	5112693[X]	0.211752(1)	2 454 964.59610(38)	16.828	MS	–	–	–	–	–	–

The newly discovered variables are marked in bold in the Gaia DR3 column. The data availability from MAST is denoted in the superscript of the KIC ID, where X means no data, L and S stands for the LC and SC data, respectively. The numbers before the letters represent how many quarters of data are available. CMD refers to the position in the color-magnitude diagram (MS – main sequence, MSTO – main sequence turn off, RGB – red giant branch, BS – blue straggler, AGB – asymptotic giant branch, RC – red clump, HB – horizontal branch, EHB – extreme horizontal branch). The superscript [e] of the period denotes significantly eccentric orbit. The superscript + of the CMD indicates that not all five astrometric parameters were used in the membership analysis. HRD refers to a position in the T_{eff}, log *g* diagram. The source of the spectra is marked in the Ref column, *i.e.*, 1 – HECTOSPEC, 2 – NOT, 3 – LAMOST, 4 – APO35, and 5 – APOGEE. The * indicates that the atmospheric parameters are derived in this work.

HECTOSPEC – *https://oirsa.cfa.harvard.edu*, APOGEE – *https://www.sdss.org/dr16/irspec*, LAMOST – *http://dr6.lamost.org*, APO 35 – *https://www.apo.nmsu.edu*

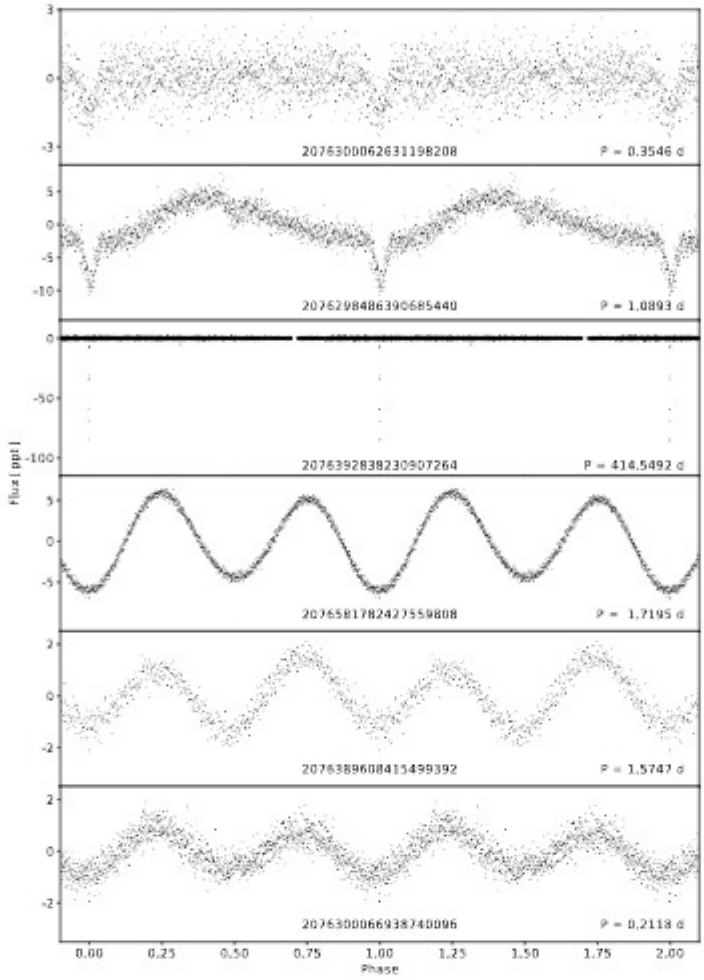

Fig. 4. Phased light curves of newly found cluster member binaries. See Table 1 for details.

5.2. Pulsators

We found a flux variation in 69 stars, which we interpreted as stellar oscillations and we separated the following classes, solar-like, δ Scuti, γ Dor and semi-regular pulsators. We found 24 pulsating cluster members including 17 solar-like, three δ Scuti, one γ Dor and three semi-regular. The field counterpart includes, 34 solar-like, two δ Scuti, six γ Dor and three semi-regular pulsators. In total we found 32 new variable pulsators, including two cluster members and 30 field counterparts. We present the pulsating cluster members in Table 2 and the field counterpart in Table 6. The location of the former group in the CMD is shown in the middle panel of Fig. 5. A detailed analysis of solar-like and δ Scuti/γ Dor pulsators will be reported by Themessl *et al.* (in preparation) and Guzik *et al.* (2023), respectively.

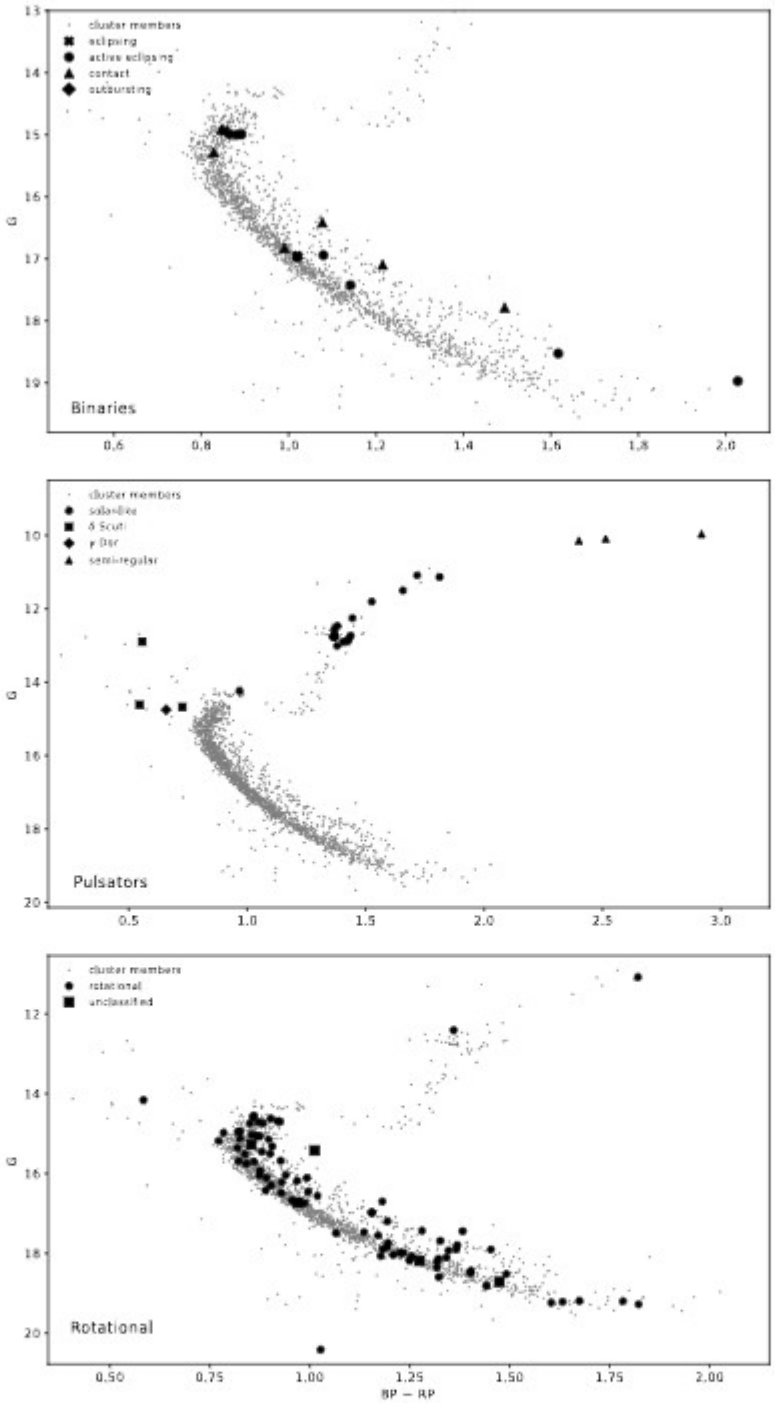

Fig. 5. CMD of NGC 6819. Binaries, pulsators and rotational/unclassified cluster members are marked in the *top, middle* and *bottom panels*, respectively.

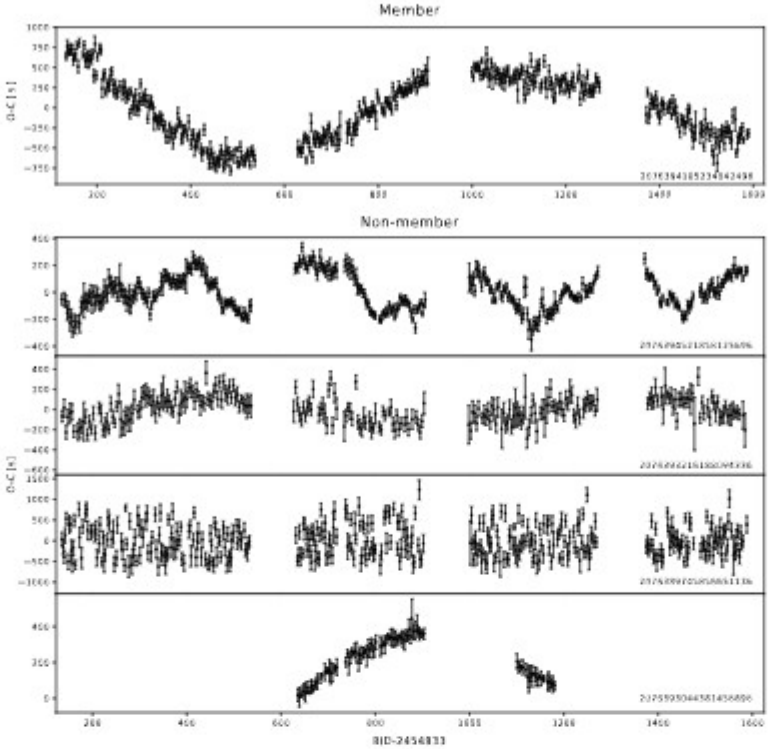

Fig. 6. $O-C$ diagrams of four contact and one active eclipsing systems showing significant orbital period variations. Gaia DR3 numbers are given in the bottom right corners.

The majority of pulsating cluster members are located on the RGB, six are the RC objects, while four δ Scuti and γ Dor objects seems to be located in the BS region. The semi-regular pulsators are the asymptotic giant branch (AGB) objects.

Since this work is also a part of our search for pulsating extreme horizontal branch stars, we specifically looked for any flux variation that is characteristic of pulsating hot subdwarfs identified in NGC 6791 and reported by Sanjayan *et al.* (2022ab). Hot subdwarfs can be formed through either a degenerate or a non-degenerate channel. The former channel works only for progenitor masses up to around 2.2 $M_{\odot}$. Such stars need significantly less time than 2.5 Gyr to settle down onto the HB and even to reach the end of the white dwarf (WD) cooling tracks, becoming too faint to be detected. The latter channel is available for progenitors more massive than around 2.2 $M_{\odot}$. Given the age of the cluster, stars with masses in a range of 1.5–1.6 $M_{\odot}$ had enough time to evolve to the HB and, if most of the hydrogen is lost, to become hot subdwarfs. More massive stars could have evolved to become post-HB stars (the most massive ones can now be very cool WDs and too faint to be seen), while less massive stars are still on the RGB or the MS, if less massive than 1.45 $M_{\odot}$. Our consideration leads to a conclusion that the CMD of NGC 6819 should be well populated with stars all the way from the MS to the WD stage. This is not what we can see in Fig. 5. There is neither the WD nor

the extreme HB populations. We stress that our consideration is based on a single star evolutionary time scale. Binary channels contributing either to a mass loss or a merger event can extend the time scale significantly, which could explain a lack of the hot subdwarf population in this cluster.

Table 2

List of cluster members showing pulsations

Gaia DR3	KIC	G [mag]	CMD	HRD	$T_{\rm eff}$ [K]	log g	RV [km/s]	[Fe/H]	Ref
				solar-like					
2076488427020005632	5111940[14Z]	13.005	RGB	RGB	4771(92)	2.79(11)	2.964(71)	0.200(28)	5
2076581919866484224	5112401[15Z]	12.562	RC	RC	4842(92)	2.65(11)	2.488(60)	0.200(27)	5
2076487872957025408	5112387[15Z]	12.776	RC	RC	4839(92)	2.85(11)	2.80(22)	0.200(28)	5
2076581713708596352	5112481[15Z]	14.239	RGB	RGB	4152(69)	1.66(8)	−1.664(80)	0.000(25)	5
2076487838597288320	5112373[15Z]	12.755	RC	RC	4821(92)	2.73(11)	2.29(51)	0.200(28)	5
2076300101298433792	5024297[14Z]	12.896	RGB	–	–	–	–	–	–
2076299792060819328	5024583[14Z]	12.732	RGB	RGB	4687(92)	2.55(11)	1.9843(34)	0.200(27)	5
2076299856476070784	5024511[X]	12.256	RGB	–	–	–	–	–	–
2076394659297111552	5113061[15Z]	11.088	RGB	RGB	4221(92)	1.67(11)	2.56(11)	0.100(26)	5
2076581816787312896	5112744[15Z]	12.890	RGB	RGB	4691(92)	2.63(11)	2.7996(89)	0.100(28)	5
2076393937742523904	5112730[15Z]	12.719	RC	RC	4823(92)	2.72(11)	1.350(75)	0.200(27)	5
2076393692914035456	5112786[15Z]	11.502	RGB	RGB	4308(92)	1.86(11)	3.824(45)	0.100(27)	5
2076393869023076608	5112948[14Z]	12.833	RGB	RGB	4766(92)	2.68(11)	3.588(24)	0.200(27)	5
2076393765943846656	5112938[14Z]	12.762	RC	RC	4842(92)	2.69(11)	1.328(28)	0.200(27)	5
2076393624194561152	5024750[15Z]	11.806	RGB	RGB	4501(92)	2.11(11)	2.177(27)	0.100(27)	5
2076299860780325504	5024601[14Z]	12.465	RC	–	–	–	–	–	–
2076298761268676352	5024851[15Z]	11.136	RGB	RGB	4159(92)	1.60(11)	6.23(23)	0.100(26)	5
				δ Scuti					
2076299826420542080	5024468[X]	12.898	BS	BS	7770(50)	4.38(10)	−14(2)	−0.2(1)	2*
2076299482823088000	5024084[15,14Z]	14.674	BS	–	–	–	–	–	–
2076393594145246080	5113357[X]	14.613	BS	BS	7270(50)	3.70(5)	65(3)	−0.53(10)	2*
				γ Dor					
2076298417671932800	5024455[15,14Z]	14.751	BS	–	–	–	–	–	–
				semi-regular					
2076299826416438016	5024470[X]	9.964	AGB	–	–	–	–	–	–
2076582950658667264	5199859[15Z]	10.143	AGB	AGB	3828(92)	1.00(11)	2.1875	−0.200(27)	5
2076394728016615680	5113517[1Z]	10.091	AGB	–	–	–	–	–	–

See caption of Table 1 for explanation.

5.3. Rotational Variables

Stars showing modulated periodic flux variations are classified as rotational variables. Such a flux modulation can also be verified by amplitude spectra showing complex peak profile, as a consequence of amplitude/frequency variation. The rotational variability is usually identified with migrating star spots on the stellar surface. Our classification of rotational variables may not always be correct, since it can be mimicked *e.g.*, by small amplitude ellipsoidal variability or unstable long-period pulsations. Light curves showing stable periodic flux variations are classified as binaries, since we do not expect non migrating star spots.

Table 3

List of cluster members showing rotational variability

Gaia DR3	KIC	Period [days]	G [mag]	CMD	HRD		T_{eff} [K]	log g	RV [km/s]	[Fe/H]	Ref
2076489148574565888	5112059[X]	22.3010	17.901	MS	–	–	–	–	–	–	–
2076489217294036352	5199551[X]	23.1662	17.495	MS	–	–	–	–	–	–	–
2076488942416130688	5112104[305,11Z]	5.6490	14.593	MSTO	–	–	–	–	–	–	–
2076488869389772800	5112151[X]	18.5003	18.812	MS	–	–	–	–	–	–	–
2076492034792541952	5111815[145]	3.5750	14.948	MS	–	–	–	–	–	–	–
2076488495739451136	5111800[X]	3.8679	15.181	MS	–	–	–	–	–	–	–
2076488770617529088	5112068[X]	15.9215	14.982	MS	–	–	–	–	–	–	–
2076488152142173312	5112298[X]	2.3639	15.688	MS	–	–	–	–	–	–	–
2076488319633886336	5111907[X]	15.7120	18.175	MS	–	–	–	–	–	–	–
2076488289581014400	5111849[15,2Z]	5.9651	14.551	MSTO	–	–	–	–	–	–	–
2076488147835261696	5112257[X]	19.5174	18.594	MS	–	–	–	–	–	–	–
2076488903749503104	5112187[X]	19.6927	19.217	MS[f]	–	–	–	–	–	–	–
2076487945983692672	5112173[X]	7.1660	16.702	MS	–	–	–	–	–	–	–
2076487568026522880	5111983[X]	6.1842	17.794	MS	–	–	–	–	–	–	–
2076300135658207232	5112512[X]	5.5446	16.422	MS	–	–	–	–	–	–	–
2076300131350662912	5112490[X]	7.5360	16.452	MS	–	–	–	–	–	–	–
2076393972102236800	5112566[X]	11.0660	17.832	MS	–	–	–	–	–	–	–
2076487808537778688	–	0.9752	19.236	MS	–	–	–	–	–	–	–
2076300101298445184	5112431[X]	5.2943	16.739	MS	–	–	–	–	–	–	–
2076300066938738176	5112630[X]	4.4602	15.141	MS	–	–	–	–	–	–	–
2076300131353981312	5112536[X]	0.6732	17.686	MS	–	–	–	–	–		
2076300101298455168	5112519[X]	5.9061	17.900	MS	–	–	–	–	–	–	–
2076300101299126912	5112434[X]	5.0307	14.740	MSTO	–	–	–	–	–	–	–
2076393903382760576	5112677[X]	7.1078	14.707	MSTO	–	–	–	–	–	–	–
2076299826420536320	5024456[14Z]	3.2313	11.079	RGB	RGB		4062(69)	1.49(8)	1.383(76)	0.000(25)	5
2076487082683547008	5023857[X]	11.5019	18.360	MS[f]	–	–	–	–	–	–	–
2076300066938722176	5024480[X]	4.1951	15.679	MS	–	–	–	–	–	–	–
2076299585902316416	5024114[X]	11.9194	15.754	MS	–	–	–	–	–	–	–
2076299723341297920	5024318[X]	3.7930	15.516	MS	–	–	–	–	–	–	–
2076299929499804288	5024287[15,1Z]	7.1699	14.623	MS	–	–	–	–	–	–	–
2076299963859447936	5024151[X]	45.9273	14.157	BS	–	–	–	–	–	–	–
2076299448463468416	5023967[X]	10.6964	16.676	MS	–	–	–	–	–	–	–
2076299757701068800	5024600[X]	3.9612	16.221	MS	–	–	–	–	–	–	–
2076299723341302272	5024403[X]	5.0020	15.704	MS	–	–	–	–	–	–	–
2076299036142588032	5024760[X]	2.4474	16.043	MS	–	–	–	–	–	–	–
2076299753393405312	5024526[X]	8.0142	18.520	MS	–	–	–	–	–	–	–
2076299688981553280	5024365[15,1Z]	7.4463	14.700	MSTO	–	–	–	–	–	–	–
2076299001786815104	5024641[14Z]	5.6497	14.742	MSTO	–	–	–	–	–	–	–
2076298963119414912	5024756[X]	21.7471	17.979	MS	–	–	–	–	–	–	–
2076298417671212800	5024491[X]	4.0566	16.486	MS	–	–	–	–	–	–	–
2076298310287835776	4936866[X]	20.9493	17.739	–	–	–	–	–			
2076582465319137792	5200072[X]	10.0885	18.497	MS	–	–	–	–	–	–	–
2076581851136420608	–	0.2074	20.413	MS[f]	–	–	–	–	–	–	–
2076396171125625984	5200422[14Z]	5.1932	14.950	MS	–	–	–	–	–	–	–
2076581675044794112	5112589[X]	7.3381	17.476	MS	–	–	–	–	–	–	–
2076394075181506688	5112866[X]	0.4869	17.434	MS	–	–	–	–	–	–	–
2076394006454008320	5112675[X]	4.3123	16.720	MS	–	–	–	–	–	–	–
2076394006461998336	5112698[X]	3.6742	15.321	MS	–	–	–	–	–	–	–
2076393903382776576	5112699[X]	2.3101	15.925	MS	–	–	–	–	–	–	–
2076393869023084288	5112979[11Z]	23.2479	15.034	MS	–	–	–	–	–	–	–
2076394002154821632	5112736[X]	21.9286	18.039	MS	–	–	–	–	–	–	–

Table 3

Concluded

Gaia DR3	KIC	Period [days]	G [mag]	CMD	HRD		T_{eff} [K]	log g	RV [km/s]	[Fe/H]	Ref
2076393933435330688	5112777[X]	5.9733	17.445	MS	–	–		–	–	–	–
2076393899075931904	5112682[X]	8.7219	19.198	MS[I]	–	–		–	–	–	–
2076393800303612032	5113045[X]	22.2631	15.054	MS	–	–		–	–	–	–
2076393903382776704	5112710[X]	19.6045	15.451	MS	–	–		–	–	–	–
2076393697224343296	5112781[X]	2.6031	18.105	MS	–	–		–	–	–	–
2076393869023085440	5113010[X]	1.4268	15.357	MS	–	–		–	–	–	–
2076394178252904320	5113076[X]	13.3217	18.439	MS	–	–		–	–	–	–
2076393319267340288	5113478[X]	0.8781	16.560	MS	–	–		–	–	–	–
2076393662865120256	5112908[X]	4.7402	16.980	MS	MS		5500(30)	4.47(7)	18(2)	-0.43(9)	1*
2076393731584598528	5112852[X]	4.5927	16.185	MS	–	–		–	–	–	–
2076393628504856448	5024697[X]	3.3347	16.109	MS	–	–		–	–	–	–
2076393692914036608	5112741[14L]	17.6960	12.408	RC	RC		4814(107)	2.64(17)	-38(5)	-0.08(10)	3
2076393044389353984	5113099[X]	23.3089	17.201	MS	–	–		–	–	–	–
2076393765944335104	5113001[14L]	6.5676	14.687	MSTO	–	–		–	–	–	–
2076393662865120256	5112908[X]	2.9060	16.980	MS	–	–		–	–	–	–
2076393284907576960	5113426[X]	7.3628	18.081	MS	–	–		–	–	–	–
2076393147460788864	5113295[11L]	28.6162	16.112	MS	RGB		5420(400)	3.5(5)	-34(6)	1.5(5)	1*
2076392838230907392	5024988[X]	5.4480	15.502	MS	–	–		–	–	–	–
2076392868287903872	5024774[X]	2.8742	17.551	MS	–	–		–	–	–	–
2076392872590614784	5024751[X]	3.4953	17.904	MS	–	–		–	–	–	–
2076390295610350464	5113519[X]	10.9769	17.991	MS	–	–		–	–	–	–
2076392730841568640	5025077[X]	21.7111	17.929	MS	–	–		–	–	–	–
2076392975669885568	5113165[X]	6.4769	16.297	MS	–	–		–	–	–	–
2076392799560963584	–	20.2391	19.278	MS[I]	–	–		–	–	–	–
2076389711494716800	5025150[X]	6.3577	15.074	MS	–	–		–	–	–	–
2076389878983223808	5025470[X]	22.1879	18.216	MS	–	–		–	–	–	–
2076300066938729856	5112574[X]	1.6160	16.045	MS	–	–		–	–	–	–
2076393800295734144	5113026[X]	20.8330	18.069	MS	–	–		–	–	–	–
2076298967427112448	5024801[X]	1.8472	15.123	MS	–	–		–	–	–	–
2076488049055863936	–	6.8456	19.194	MS	–	–		–	–	–	–
2076299856472624128	–	17.8793	18.135	MS	–	–		–	–	–	–

See caption of Table 1 for explanation.

In total, we found 233 variable stars showing rotational variability, which makes them the most abundant variable population in NGC 6819. There are 82 cluster members (Table 3), 136 field counterparts (Tables 7), and 15 stars with no membership established (Table 9). The periods of rotational variables are in a wide range of 0.2–45 d. Cross matching our list of rotational variables with the International Variable Star Index (VSX) catalog, we found 15 rotational variables to be of BY Dra type, while KIC 5112508 is a rotating X-ray binary reported by Gosnell *et al.* (2012). In summary, we found 185 new variable rotating stars, including 70 cluster members, 100 field counterparts and 15 with membership undetermined yet. The location of the cluster members in the CMD is shown in the bottom panel of Fig. 5.

5.4. Unclassified and Unidentified Variables

In the case of 24 stars, we were unable to classify their variability types. The data are either not precise or it is not too clear if the shape of a light curve remains stable over time. The latter argument is essential to distinguish between binaries and rotational variables. An example of a light curve in an unclassified group is presented in the bottom panel of Fig. 3. We identified five variables to be cluster members, 18 non-members and one with membership undetermined, and they are listed in Tables 4, 8 and 9, respectively. All field stars, four members and the one with no membership, are new variables detected in this work. The newly discovered variable KIC 5023913 exhibits low frequency pulsations, similar to solar-like ones, and is positioned near the MS on the CMD. However, it cannot be classified as a solar-like pulsator due to the limited sampling of the Kepler long cadence data, which is insufficient to detect MS pulsation occurring beyond the Nyquist limit. KIC 5112843 shows two close frequencies with high amplitudes, which translates into beating in a light curve. The star may be a binary system, as discussed by Guzik *et al.* (2023), however it does not fit into any of our four binary classes. We leave such cases for future investigation. The location of the cluster members in the CMD is shown in the bottom panel of Fig. 5.

We found signals in amplitude spectra, associated with optical counterparts in the Pan-STARRS (Chambers *et al.* 2016, Flewelling *et al.* 2020) survey that do not have Gaia designations. Only one star has a custom designation and was reported in the past. The remainder of the stars are given by coordinates. We classified the signal to a proper variability type and estimated its period. These stars were included in the counts of the variability types discussed in the previous subsections. We show the list of these unidentified objects in Table 9. Since the stars are not listed in the Gaia catalog, we are unable to estimate their membership.

T a b l e 4

List of cluster members with unclassified variability

Gaia DR3	KIC	Period [days]	G [mag]	CMD	HRD		$T_{\rm eff}$ [K]	log g	RV [km/s]	[Fe/H]	Ref
2076488353993641344	5111986^{X}	0.6185	18.188	MS	–	–	–	–	–	–	–
2076299306716922752	5024211^{X}	1.1752	18.711	MS	–	–	–	–	–	–	–
2076393765943855744	5112994^{X}	1.0031	16.729	MS	–	–	–	–	–	–	–
2076299414103588224	5023913^{X}	18.3197	15.274	MS	–	–	–	–	–	–	–
2076393731584598400	5112843^{X}	0.1743	15.422	MS	RGB		5600(50)	4.37(5)	42(1)	−1.4(1)	2*

See caption of Table 1 for explanation.

Table 5

The list of binary stars in the field that are not cluster members or no memberships derived

Gaia DR3	KIC	P_{orb} [days]	T_0 [BJD]	G [mag]	T_{eff} [K]	log$g$	RV [km/s]	[Fe/H]	Ref
			eclipsing						
2076487671098665472	–	225.27602919(47)[e]	2455003.738545(5)	19.596	–	–	–	–	–
2076299757701057920	–	38.857349(27)[e]	2454997.2392(6)	19.489	–	–	–	–	–
2076298898703420416	–	0.42517143(28)	2454971.20746(53)	20.682	–	–	–	–	–
2076297657449418880	5023984[2]	single-eclipse	2455008.4490(24)	18.400	–	–	–	–	–
2076298417671214464	5024527[2]	30.564505(25)[e]	2454986.35489(57)	15.876	5910(200)	4.736(22)	−75(14)	−0.68(13)	4*
2076583294245566720	–	2.8083498(28)	2454967.2876(7)	20.461	–	–	–	–	–
2076583839713435776	5200364[2]	0.206879465(16)	2454964.58302(7)	19.420	–	–	–	–	–
2076394590569930240	–	0.8907258(10)	2454965.42331(9)	20.064	–	–	–	–	–
2076394178252936704	5113146[1,2,12]	18.789711(29)	2456216.94558(19)	19.193	–	–	–	–	–
2076390123803775104	5025294[1,12]	5.462678(18)[e]	2455021.8935(23)	13.246	–	–	–	–	–
2076390119501429120	5025349[2]	50.71339(6)[e]	2454967.2679(10)	18.897	–	–	–	–	–
2076298692545230848	–	single-eclipse	2455156.9573(25)	19.816	–	–	–	–	–
			active eclipsing						
2076487495009192064	5023833[2]	1.5995032(46)	2454965.0930(26)	19.173	–	–	–	–	–
2076487495000121216	5023832[2]	0.357122835(39)	2454964.69840(9)	19.523	–	–	–	–	–
2076487293141296640	5023901[2]	318.7285(20)[e]	2455009.7943(50)	19.557	–	–	–	–	–
2076487636738867328	–	0.4169454(7)	2454965.2280(24)	19.745	–	–	–	–	–
2076394006453983488	–	3.0224820(6)	2454964.98930(15)	20.519	–	–	–	–	–
2076487254481737728	5024077[2]	0.932208699(49)	2454965.28509(44)	13.984	16860(230)	5.79(16)	6(5)	−4(2)	4*
2076299276660357760	5024146[2]	0.787121288(48)	2454964.73835(41)	15.588	5810(200)	4.03(1)	−13(9)	−0.45(27)	4*
2076393284907582464	5113407[2]	13.826433(5)[e]	2454975.78903(29)	18.049	–	–	–	–	–
2076393044381456896	5113053[1,2,12]	3.1850900(12)	2455466.35322(11)	20.230	–	–	–	–	–
2076394639289386880	5200325[2]	5.3159294(28)[e]	2454969.74506(27)	17.393	5380(200)	5.04(8)	−40(13)	−0.81(15)	4*
			contact						
2076489182934321920	5199669[2]	0.75895896(42)	2454964.903723(46)	15.226	–	–	–	–	–
2076488285274150784	5111817[2]	0.28994151(7)	2454964.73887(21)	19.638	–	–	–	–	–
2076487739818143360	–	0.28136943(9)	2454964.71482(27)	20.462	–	–	–	–	–
2076298452030939392	5024283[2]	0.33846178(5)	2454964.58443(13)	18.044	–	–	–	–	–
2076298314587607040	–	0.223753315(41)	2454964.56924(15)	20.089	–	–	–	–	–
2076394521858125696	5112917[2]	0.29314610(6)	2454964.66198(17)	16.878	–	–	–	–	–
2076393697224860544	5112791[2]	0.9816957(5)	2454964.78683(42)	14.669	–	–	–	–	–
2076393216188094336	5113461[2]	0.275128153(42)	2454964.73810(13)	19.632	–	–	–	–	–
2076389745856651136	5025261[1,12]	2.171411(7)	2454966.95452(29)	12.296	–	–	–	–	–
2076487454939938816	5023779[2]	0.1963	–	17.826	–	–	–	–	–
			outbursting						
2076392906942365568	–	–	–	20.427	–	–	–	–	–
2076392902640277632	5024812[2]	–	–	16.431	–	–	–	–	–

See caption of Table 1 for explanation. Targets with no astrometry, hence no membership established, are denoted in *italic*.

6. The Distance and Age Estimation

We downloaded a grid of isochrones given in the Gaia photometric system from the MIST project (Choi *et al.* 2016, Dotter 2016). The current version of MIST is 1.2. The MESA version 7503 was employed to calculate isochrones. We selected $V/V_{\rm crit} = 0$. The grid covers age in a logarithmic scale between 9.1 and 9.6 with a step of 0.01 and the iron content [Fe/H] from -0.1 to $+0.1$ with a step of 0.01.

For the fit, we only kept the MS, RGB and RC stars. However, in case of binary systems, the observed magnitude may include the flux contribution from all companions and not a single star, which shifts the position of a system in the CMD. To avoid biased magnitudes, we excluded outlying stars by considering their positions in the CMD as uncertain. We included magnitude uncertainties as weights in the fit, which prevented the MS targets from over-fitting. The RC and RGB targets, even though less numerous, are brighter, and hence remain significant in the fit.

The MIST synthetic isochrones are given in absolute magnitudes, and we selected no extinction. We applied a shift $(m - M)$ in the Gaia G magnitude and $B_p - R_p$ color to account for the extinction. The isochrones that fit the best are defined by two consecutive values of the age and, for each age, the same three [Fe/H] values. This solution is quite common in astrophysical modeling. The fitting shows a degeneration of solutions in which a pair of different age and [Fe/H] val-

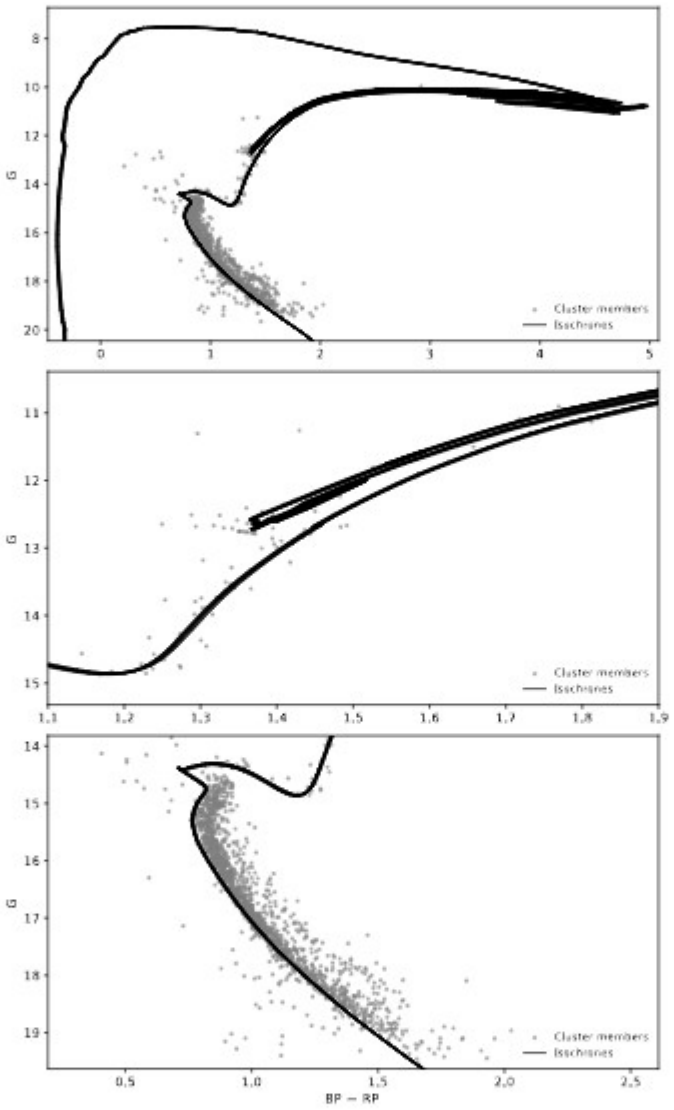

Fig. 7. CMD of NGC 6819, showing the best MIST isochrone fits. The *top panel* shows the overall diagram, while the middle panel shows the red clump region and the bottom panel shows the main-sequence region.

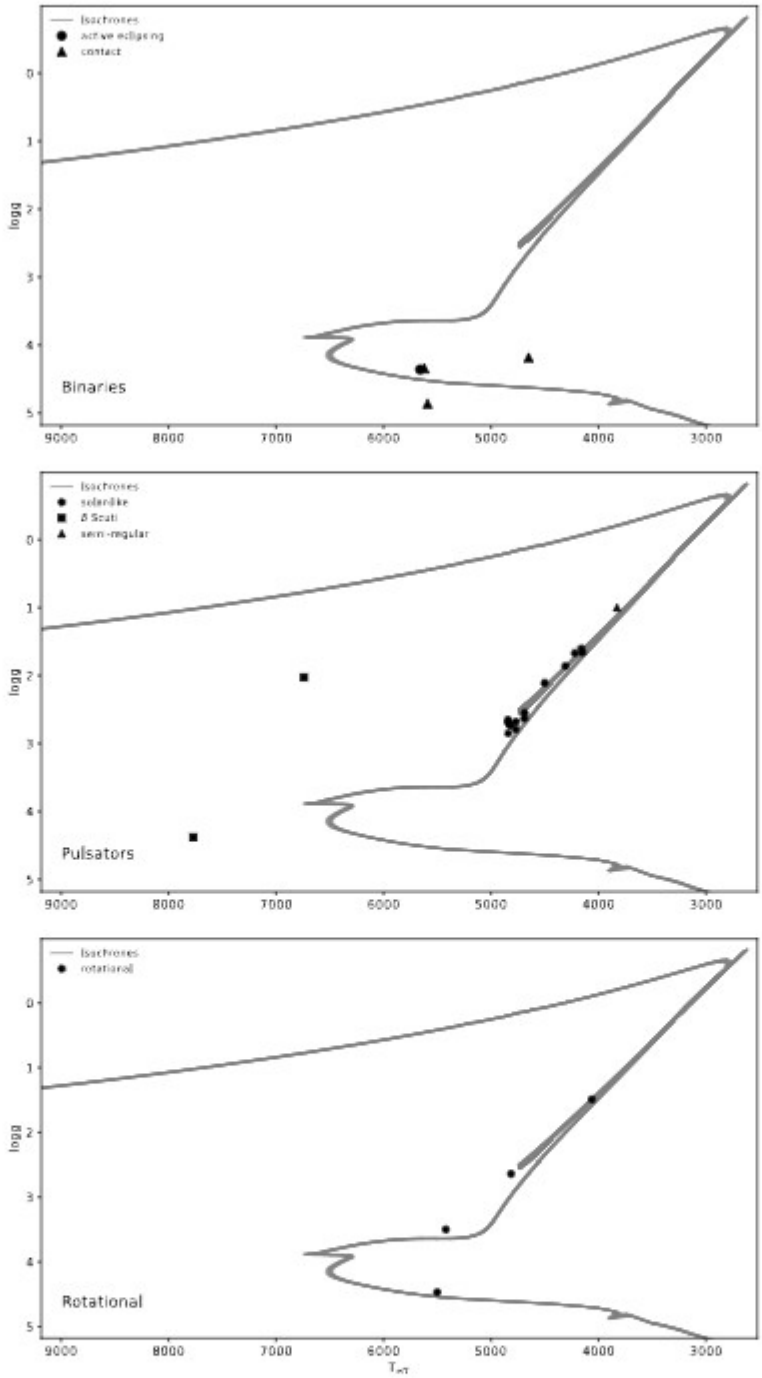

Fig. 8. $T_{\rm eff}$ – log$g$ diagram showing the cluster members with atmospheric parameters derived in this work. The *top, middle* and *bottom panels* show binary, pulsating and rotating stars, respectively. The isochrones represent the best MIST fits in the CMD plotted in $T_{\rm eff}$ and log$g$ space.

ues compensate by providing similar quality fits. We have determined the age to be 2.54(3) Gyr and [Fe/H] to be $-0.01(2)$. The apparent distance modulus $(m-M)$ equals 12.20 and $E(B_p-R_p)$ to be 0.195(10). We show the best isochrone fits in Fig. 7.

For the Gaia DR3 cluster members $E(B_p-R_p)$ and interstellar extinction in the G band, the A_G form a linear relation $A_G = 2\cdot E(B_p-R_p)$. Averaging the parameters from the best models we obtain $E(B_p-R_p) = 0.194$ mag, which corresponds to $A_G = 0.388$ mag. Subtracting A_G from $(m-M)$ we find the true distance modulus of 11.812, which gives the distance to the cluster of 2.3 kpc.

We also derived distance from the parallaxes of the cluster members with probability membership higher than 90% and the relative parallax uncertainty smaller than 10%, which equals 2.48(18) kpc. The distance measurements from parallaxes and isochrone fits are in agreement to each other, and the age and [Fe/H] derived in our work is comparable to the results reported by Choi *et al.* (2018).

We also plotted isochrones in the $T_{\rm eff}$ and $\log g$ plane (HRD) shown in Fig. 8. We used the isochrones for the age and [Fe/H], which we derived from the isochrone fitting in the CMD. We over-plotted the isochrones with our variable stars from Tables 1–3, for which $T_{\rm eff}$ and $\log g$ are listed. The column HRD in Tables 1–4 describes the location of a given star in the HRD. If the location agrees with the one in the CMD, we can expect the spectroscopic fit is likely correct. We obtained an agreement in all but two cases. One of the exceptions is a rotational variable KIC 5113295. In both cases, as the CMD shows, the gravity of MS stars is around 4.5.

7. Summary

We presented a search for variable stars in the Kepler superstamp data of NGC 6819. Individual pixels were searched, by means of a Fourier amplitude spectrum, and contiguous apertures for each object that shows a significant flux variation were defined. The coordinates of these optimal apertures were matched with optical counterparts using the Pan-STARRS survey. In total, we detected 385 variable stars. We searched the literature for variable stars reported prior to our work, and we found that 27 variable stars were reported by Street *et al.* (2002), eight by Street *et al.* (2005), one from the All Sky Automated Survey (ASAS) catalog by Pigulski *et al.* (2009), 75 from VSX by Watson *et al.* (2006), 21 from General Catalog of Variable Stars (GCVS) and from New Catalog of Variable Stars (NSV) by Samus (2017). We found 306 stars having KIC designations, out of which 226 stars do not have any data delivered to the MAST. For 270 stars, their variable nature was unknown prior to our analysis. These stars are marked in bold in Tables 1–9.

Using Gaia DR3 astrometry, we calculated the membership probabilities for all variable stars in our sample by applying Bayesian Gaussian mixture models. We considered a star to be a cluster member if its membership probability is higher

Table 6

List of pulsators in the field that are not cluster members or no memberships derived

Gaia DR3	KIC	G [mag]	T_{eff} [K]	log g	RV [km/s]	[Fe/H]	Ref
			solar-like				
2076489251653787904	5199605[3L]	11.496	4250(50)	3.00(5)	0.2(1)	−0.19(3)	5*
2076488495739440128	5111767[6L]	13.641	4524(130)	2.66(20)	−49(3)	0.20(12)	3
2076488804977149568	5111987[14L]	14.949	–	–	–	–	–
2076488117782408192	5112211[X]	14.424	–	–	–	–	–
2076488014703171328	5112103[X]	14.804	–	–	–	–	–
2076488598818838400	5111863[X]	14.886	–	–	–	–	–
2076488873696651264	5112156[X]	15.403	–	–	–	–	–
2076487945983698432	5112169[15,15L]	10.864	6283(11)	3.927(18)	39(4)	0.155(9)	3
2076300135658208384	5112558[10L]	14.112	–	–	–	–	–
2076299963859543680	5024196[X]	13.291	–	–	–	–	–
2076299895139970816	5024238[X]	13.612	–	–	–	–	–
2076299585902315264	5024100[X]	13.609	–	–	–	–	–
2076299688981538944	5024290[X]	15.275	–	–	–	–	–
2076298967427099136	5024773[3L]	14.325	–	–	–	–	–
2076298761268662016	5024804[X]	15.290	–	–	–	–	–
2076299139225684096	5024043[15L]	12.779	4762(92)	2.70(11)	2.82(14)	−0.10(3)	5
2076298280232974976	4936972[X]	13.597	–	–	–	–	–
2076296837123206912	4936825[4L]	13.144	–	–	–	–	–
2076582916298933888	5199930[3L]	11.893	4260(50)	1.94(5)	0.2(3)	-0.25(9)	5*
2076582503982578944	5200146[1L]	11.611	4069(144)	2.15(23)	−20(3)	−0.22(14)	3
2076582297823683712	5200223[X]	14.140	–	–	–	–	–
2076582366543185664	5200359[X]	13.118	–	–	–	–	–
2076394693656870400	5200392[X]	14.772	–	–	–	–	–
2076582362237411712	5200367[X]	13.063	–	–	–	–	–
2076581919866487808	5112421[X]	15.505	–	–	–	–	–
2076582263463928064	5200143[X]	15.564	–	–	–	–	–
2076394418778961024	5113246[X]	14.720	–	–	–	–	–
2076393899075590528	5112672[X]	16.690	–	–	–	–	–
2076393594145243136	5113371[X]	14.452	–	–	–	–	–
2076392700791972992	5025162[15L]	12.623	–	–	–	–	–
2076392769511450368	5025101[2L]	13.003	4404(74)	2.73(12)	−60(4)	0.10(7)	3
2076389711494720640	5025168[X]	14.392	–	–	–	–	–
2076392563352990208	5025060[X]	14.124	–	–	–	–	–
2076392528993243008	5025021[6L]	12.842	4675(92)	2.65(11)	38.86(46)	0.100(28)	5
			δ Scuti				
2076298211512787328	5024570[X]	16.935	7760(60)	3.926(24)	27.1(8)	-0.57(7)	2*
2076395896247722496	5200521[15,15L]	11.182	5810(32)	3.535(53)	−10(6)	0.276(30)	3
			γ Dor				
2076487632439073408	5024090[X]	19.103	–	–	–	–	–
2076582602761996672	5200181[X]	17.216	7150(50)	4.80(5)	−5.6(7)	−0.46(9)	2*
2076394315699722368	5113250[14L]	14.439	5430(50)	3.0(1)	−51(2)	−0.65(7)	2*
2076390192533257216	5025464[15L]	13.122	7182(30)	4.078(50)	−7(9)	−0.243(28)	3
2076392627762286336	5025047[X]	18.250	6930(40)	3.35(7)	45(5)	−0.40(7)	2*
2076389642775246080	5025234[15L]	13.285	–	–	–	–	–
			semi-regular				
2076487808546982784	5112438[15L]	10.602	3715(69)	0.94(8)	−38.40(34)	−0.400(29)	5
2076298829988110976	5024699[15L]	11.600	3500	1	−45.9053(69)	−0.5	5
2076392632072463232	5025003[15L]	8.011	–	–	–	–	–

See captions of Tables 1 and 5 for explanation.

Table 7

List of rotational variables that are not cluster members or no memberships derived

Gaia DR3	KIC	Period [days]	G [mag]	T_{eff} [K]	log g	RV [km/s]	[Fe/H]	Ref
2076489006828963200	–	4.2194	20.192	–	–	–	–	–
2076491656835399552	5111748[K]	2.2534	14.809	–	–	–	–	–
2076488972469006720	–	4.3523	19.439	–	–	–	–	–
2076491588108521600	5111658[K]	11.2363	18.431	–	–	–	–	–
2076489212987407872	5199564[K]	3.4612	18.809	–	–	–	–	–
2076488976768870656	–	4.0641	19.688	–	–	–	–	–
2076491656828123904	–	11.6758	19.207	–	–	–	–	–
2076489109908182400	–	1.8813	20.143	–	–	–	–	–
2076489079855048320	5111878[K]	5.2625	16.775	–	–	–	–	–
2076492030485722880	5111830[K]	3.1613	18.914	–	–	–	–	–
2076488835030026752	5112025[K]	6.1208	18.934	–	–	–	–	–
2076491656835403776	5111760[K]	6.7188	15.758	–	–	–	–	–
2076491519396420864	5111722[K]	2.3987	19.046	–	–	–	–	–
2076491618168829184	5111737[K]	2.1654	16.894	–	–	–	–	–
2076488873696743936	5112157[14L]	27.9330	15.165	–	–	–	–	–
2076488873696744064	5112117[14L]	13.6986	14.966	–	–	–	–	–
2076488835038990976	5112066[K]	11.1315	18.715	–	–	–	–	–
2076488633178431232	5111890[14L]	8.2095	13.851	–	–	–	–	–
2076488427020146176	5111932[14L]	1.4345	12.215	6556(16)	4.216(27)	−19(5)	−0.133(15)	3
2076488628871828992	5111870[K]	5.1734	18.803	–	–	–	–	–
2076488152135136256	–	0.9692	20.024	–	–	–	–	–
2076488113482225920	5112203[K]	24.0132	17.997	–	–	–	–	–
2076488731950773760	5112036[K]	4.4587	17.976	–	–	–	–	–
2076488495732070016	5111802[K]	14.2002	19.035	–	–	–	–	–
2076488461379688448	5111755[K]	26.8169	12.863	–	–	–	–	–
2076488014703180416	5112144[K]	26.8614	17.006	–	–	–	–	–
2076488491432593024	5111774[K]	20.2080	17.369	–	–	–	–	–
2076488427019997568	5111912[K]	19.7522	16.803	–	–	–	–	–
2076488044756006528	5112226[K]	3.1371	19.372	–	–	–	–	–
2076487945983706880	5112224[K]	7.7540	16.816	–	–	–	–	–
2076487602386283520	5112061[K]	0.3031	16.601	–	–	–	–	–
2076487872957580544	5112420[K]	10.1352	18.165	–	–	–	–	–
2076581644988572160	5112508[1L]	0.7502	15.189	–	–	–	–	–
2076487907323097600	5112158[K]	1.2659	18.122	–	–	–	–	–
2076487705465511936	5024046[K]	7.2570	15.464	–	–	–	–	–
2076487357561147264	5023750[K]	7.2731	18.786	–	–	–	–	–
2076300135658196864	5112483[14L]	62.8479	11.401	–	–	–	–	–
2076487636746036736	5024079[14L]	20.000	15.152	–	–	–	–	–
2076487739825262976	5112228[14L]	21.0838	14.138	5653(133)	4.67(0.22)	−3(6)	−0.02(13)	3
2076581640685054208	5112520[K]	15.1677	17.561	–	–	–	-	–
2076300032574913920	–	0.5615	20.904	–	–	–	-	–
2076487258788897792	5024021[K]	1.0110	19.549	–	–	–	-	–
2076487293141276672	5023904[K]	32.5945	20.454	–	–	–	-	–
2076487190069384960	5023844[K]	5.4594	19.614	–	–	–	-	–
2076487190061988608	–	0.1887	20.733	–	–	–	-	–
2076487151403028224	–	3.5949	19.612	–	–	–	-	–

Table 7

Continued

Gaia DR3	KIC	Period [days]	G [mag]	T_{eff} [K]	log g	RV [km/s]	[Fe/H]	Ref
2076299860780304512	5024541[A]	7.4085	15.600	–	–	–	-	–
2076299895135780224	5024204[A]	0.5714	19.901	–	–	–	-	–
2076299551542571264	5024070[A]	16.2968	13.604	3883(92)	0.73(11)	−84.49(29)	−0.500(31)	5
2076299890832483584	5024233[A]	6.4642	18.150	–	–	–	–	–
2076299895139968000	5024215[14L]	4.4271	13.396	6491(42)	4.12(7)	−27(7)	0.01(40)	3
2076299860776267136	5024529[A]	12.5097	17.884	–	–	–	–	–
2076299895135748864	5024202[11L]	2.9086	17.612	–	–	–	–	–
2076299757697024128	–	6.3272	18.758	–	–	–	–	–
2076299654617645056	–	1.2605	19.506	–	–	–	–	–
2076299684674005504	5024300[A]	6.6880	17.767	–	–	–	–	–
2076299345384113536	5023985[15L]	6.5381	13.453	–	–	–	–	–
2076299482818776704	–	10.6186	19.999	–	–	–	–	–
2076299753396856576	5024581[A]	3.9925	18.570	–	–	–	–	–
2076299207945181824	5024254[14L]	34.9997	13.878	–	–	–	–	–
2076299242304936192	5024335[A]	6.0531	15.292	–	–	–	–	–
2076299139225682688	5024055[A]	7.1974	15.755	–	–	–	–	–
2076298726908910336	5024794[A]	28.2478	15.957	–	–	–	–	–
2076298722601233792	5024811[A]	2.2620	15.734	–	–	–	–	–
2076298589469925632	5024647[A]	8.3029	15.259	–	–	–	–	–
2076298795628342912	5024515[A]	4.7317	16.948	–	–	–	–	–
2076298310284438656	4936870[A]	3.8084	17.681	–	–	–	–	–
2076298314587586304	4936842[A]	0.7882	16.477	–	–	–	–	–
2076298486386442112	5024389[A]	2.3891	20.433	–	–	–	–	–
2076582607061342336	5200184[13L]	7.5913	15.584	–	–	–	–	–
2076582534038273920	5200034[A]	3.8284	19.555	–	–	–	–	–
2076582946355475968	–	13.7111	19.060	–	–	–	–	–
2076582843276554240	–	7.8372	20.120	–	–	–	–	–
2076582607061335936	5200185[11L]	3.7272	15.565	–	–	–	–	–
2076584118889853696	5200273[A]	6.5349	16.913	4390(60)	3.25(3)	−46(1)	−0.18(13)	1*
2076583908425657472	5200352[A]	6.6710	18.897	–	–	–	–	–
2076582087361668608	5199996[A]	6.4674	19.317	–	–	–	–	–
2076582538341833344	5200036[A]	21.9286	16.748	–	–	–	–	–
2076582018642530432	5112402[10L]	4.8263	17.044	–	–	–	–	–
2076582362237425920	5200342[A]	5.8353	18.743	–	–	–	–	–
2076582465319431296	5200038[11L]	2.6316	15.154	–	–	–	–	–
2076582259160998400	–	4.8721	19.985	–	–	–	–	–
2076582057294883200	5112553[15L]	5.2427	13.055	5812(27)	4.595(44)	−35(4)	0.135(25)	3
2076396166816178176	5200463[A]	0.7563	19.301	–	–	–	–	–
2076581812488757632	5112718[A]	2.0447	18.446	–	–	–	–	–
2076581679348337152	5112646[A]	12.5816	14.484	–	–	–	–	–
2076394517550928640	–	6.1322	19.448	–	–	–	–	–
2076394414469300096	5113282[A]	1.4962	18.000	–	–	–	–	–
2076394345749739264	–	0.3484	20.151	4503(92)	2.25(11)	−27.92(44)	−0.100(28)	5
2076394277037190656	5113103[A]	5.3265	18.427	–	–	–	–	–
2076394246980225280	5113042[A]	12.1961	16.138	–	–	–	–	–

Table 7
Concluded

Gaia DR3	KIC	Period [days]	G [mag]	T_{eff} [K]	log g	RV [km/s]	[Fe/H]	Ref
2076394075181511296	5112921[K]	1.040	15.961	–	–	–	–	–
2076394040821761792	5112865[K]	8.1032	15.741	–	–	–	–	–
2076394109541233536	5112796[K]	1.0060	17.176	–	–	–	–	–
2076394105234044032	5112746[K]	4.5372	18.790	–	–	–	–	–
2076395071614000512	5113378[13L]	24.4924	15.524	–	–	–	–	–
2076394173950795136	–	3.5243	19.318	–	–	–	–	–
2076393869023082240	5113011[K]	10.1982	14.427	–	–	–	–	–
2076393834655370240	–	8.6988	19.625	–	–	–	–	–
2076393456700278656	–	3.7551	20.610	–	–	–	–	–
2076393903374713856	5112711[K]	8.4417	17.731	–	–	–	–	–
2076393491065999360	5113306[K]	1.9503	18.317	–	–	–	–	–
2076393353627026944	5113228[14L]	4.9268	12.332	4030(92)	1.19(11)	-6.277(22)	-0.100(28)	5
2076393795993621376	5113037[K]	2.6187	20.041	–	–	–	–	–
2076393658557409792	5024787[14L]	12.7227	17.924	–	–	–	–	–
2076392765201345280	5025129[K]	9.5598	17.830	–	–	–	–	–
2076392872590618112	–	7.2291	19.511	–	–	–	–	–
2076393250540210432	5113521[K]	0.9759	18.448	–	–	–	–	–
2076393211878004096	5113452[K]	0.7334	18.605	–	–	–	–	–
2076393113108873344	5113418[K]	12.8024	17.779	–	–	–	–	–
2076393108798746752	5113384[K]	1.3900	17.050	–	–	–	–	–
2076392971359814528	5113140[K]	7.9415	18.691	–	–	–	–	–
2076392838230901632	5024960[K]	9.2894	15.874	–	–	–	–	–
2076392872582614144	–	17.6075	18.606	–	–	–	–	–
2076390192531117440	5025475[K]	5.4480	17.747	–	–	–	–	–
2076390055084332672	5025381[K]	5.8275	19.118	–	–	–	–	–
2076389604105250560	5025159[K]	3.3906	19.053	–	–	–	–	–
2076390020724772736	5025605[K]	12.1848	18.306	–	–	–	–	–
2076389711494726272	5025195[K]	13.1484	18.311	–	–	–	–	–
2076390050781929472	5025372[K]	0.9905	18.329	–	–	–	–	–
2076392559042768896	5025092[K]	4.4708	19.278	–	–	–	–	–
2076488942409044864	–	1.4495	–	–	–	–	–	–
2076581988577868032	–	3.9648	21.031	–	–	–	–	–
2076488049065148288	5112292[K]	1.9006	16.004	–	–	–	–	–
2076487739818146048	–	3.8497	21.192	–	–	–	–	–
2076487224431395712	–	2.2195	20.442	–	–	–	–	–
2076581919858187136	–	7.4127	20.923	–	–	–	–	–
2076581748057139456	–	17.6544	21.159	–	–	–	–	–
2076487464947285248	5023707[K]	0.9582	15.199	–	–	–	–	–
2076392941302191616		0.6279	20.924	–	–	–	–	–
2076394620627810432	5200435[K]	0.6398	18.505	–	–	–	–	–
2076394384411491712	5113161[K]	2.2842	19.132	–	–	–	–	–
2076491588108524160	5111658[K]	1.3542	16.277	4470(60)	4.572(57)	-89(1)	-0.76(6)	2*
2076491588108524160	–	1.9159	17.492	–	–	–	–	–
2076298310287835776	4936866[K]	1.3921	18.014	–	–	–	–	–
2076390123803764352	–	3.9365	15.646	–	–	–	–	–

See captions of Table 1 and 5 for explanation.

Table 8

List of unclassified variables that are not identified as cluster members in our analysis

Gaia DR3	KIC	Period [days]	G [mag]
2076489011128317824	5111916[X]	0.2954	19.854
2076488495732906496	5111771[X]	0.6336	20.106
2076487533659553024	5112097[X]	0.2629	19.411
2076299998215027968	–	0.7388	20.198
2076487224421838336	–	0.5368	19.785
2076299826420547200	5024510[X]	3.1140	14.827
2076299895135783168	–	0.4290	20.698
2076298447723494016	5024319[X]	0.3007	19.934
2076298791320709120	5024566[X]	0.7352	18.553
2076394517548400896	5112901[X]	0.6911	19.291
2076394384411456000	5113175[X]	0.1723	18.885
2076393314960052480	–	0.4764	20.839
2076393108798736384	5025311[X]	1.9564	15.472
2076392528993235968	5024986[X]	0.3169	16.960
2076581984282789632	5112326[X]	0.1085	17.258
2076487838597567104	5112332[X]	6.4325	18.557
2076393869023083776	–	2.9235	18.391
2076390123803775104	–	3.3921	18.469

See captions of Table 1 and 5 for explanation.

than 50%. In total, we found 128 cluster member variables, including 17 binaries, 24 pulsators, 82 rotationally and five unclassified. The locations of these cluster variable stars in the CMD diagram indicate their evolutionary status. In the CMD, a majority of our variable stars are located on the MS, while solar-like pulsators are mostly split into the RGB and RC, semi-regular variables are located on the AGB, and five in the BS region.

In the case of selected binary systems, we estimated mid-times of eclipses or minima of a continuous flux variation and derived ephemerides. We calculated the $O-C$ diagrams and checked for any orbital period variation. Four binary systems show significant period variation, however its nature is not confirmed. The solar-like as well as δ Scuti and γ Dor pulsators have been a subject of a detailed analysis of its pulsation content, and the results will be published by Themessl *et al.* (in preparation) and Guzik *et al.* (2023), respectively.

We used publicly available spectra of 42 variable stars. In addition, we analyzed spectra of eight stars collected with the 2.51 m NOT and spectra of five stars were taken with the 3.5 m APO telescopes. For the latter spectra, we quote a minimum uncertainty of 200 K due to the low S/N. Spectra of 21 stars were fitted with the XTGRID, while for the remainder of the sample, we adopted the fit values from the surveys. We derived $T_{\rm eff}$, $\log g$, [Fe/H] and RVs. Thanks to our spectral analysis we were able to recover consistent stellar parameters from very diverse spectroscopic data. This consistency is reflected by the similar distribution of stars in the CMD and HRD.

Table 9

List of equatorial coordinates that are associated with the superstamp pixels showing signal in their amplitude spectra

α_{2000} [hh mm ss.ss]	δ_{2000} [dd mm ss.s]	Period [days]	Type
19 41 20.77	***+40 17 18.77***	0.8824	eclipsing
19 40 57.78	***+40 10 11.87***	0.5085	active eclipsing
19 40 57.99	*+40 19 00.30*	0.2734	contact
19 41 0.81	***+40 18 20.35***	0.2342	contact
19 41 10.24	***+40 10 35.73***	0.2080	contact
19 41 23.73	***+40 18 54.4***	65.3493	outbursting
19 41 28.59	***+40 11 31.17***	29.6949	outbursting
19 41 29.61	***+40 11 19.35***	45.4381	outbursting
19 40 48.17	***+40 13 12.24***	0.4093	rotating
19 41 13.06	***+40 10 37.26***	0.6044	rotating
19 40 53.45	***+40 08 43.40***	0.3261	rotating
19 40 57.85	***+40 07 31.53***	0.7897	rotating
19 41 25.84	***+40 08 21.47***	2.6166	rotating
19 41 26.11	***+40 06 58.64***	1.7384	rotating
19 41 15.77	***+40 05 52.16***	8.1636	rotating
19 41 23.23	***+40 18 31.1***	2.2959	rotating
19 41 27.12	***+40 16 25.39***	3.7529	rotating
19 41 16.70	***+40 15 34.46***	2.0277	rotating
19 41 41.79	***+40 16 43.86***	15.2913	rotating
19 41 28.35	***+40 13 1.84***	41.1247	rotating
19 41 47.97	***+40 12 21.28***	0.2771	rotating
19 41 37.49	***+40 09 3.74***	52.5409	rotating
19 41 50.89	***+40 10 28.79***	0.9870	rotating
19 41 6.38	***+40 14 53.84***	0.3660	unclassified

The only coordinates not marked in bold were associated with a variable star NGC 6819 SHLP 25645 and reported by Street *et al.* (2002).

We used MIST isochrones to fit the positions of the cluster members in the CMD. Our variable star population was also included in the fit. The best solution was achieved for six isochrones giving [Fe/H] of $-0.01(2)$ and the age of 2.54(3) Gyr. The age estimate agrees with the value reported by Choi *et al.* (2018). The average distance estimate from the distance modulus is 2.3 kpc, which is in agreement with our independent estimate of 2.48(18) kpc derived from the Gaia astrometry of a selected sample of the cluster members.

Acknowledgements. Financial support from the National Science Centre under projects UMO-2017/26/E/ST9/00703 and UMO-2017/25/B/ST9/02218 is acknowledged. PN acknowledges support from the Grant Agency of the Czech Republic (GAČR 22-34467S). The Astronomical Institute in Ondřejov is supported by the project RVO:67985815. This paper includes data collected by the Kepler

mission and obtained from the MAST data archive at the Space Telescope Science Institute (STScI). Funding for the Kepler mission is provided by the NASA Science Mission Directorate. STScI is operated by the Association of Universities for Research in Astronomy, Inc., under NASA contract NAS 5-26555. This work has made use of data from the European Space Agency (ESA) mission. Gaia (*https://www.cosmos.esa.int/gaia*), processed by the Gaia Data Processing and Analysis Consortium (*https://www.cosmos.esa.int/web/gaia/dpac/consortium*). Funding for the DPAC has been provided by national institutions, in particular, the institutions participating in the Gaia Multilateral Agreement. This research has made use of the NASA/IPAC Extragalactic Database (NED), which is operated by the Jet Propulsion Laboratory, California Institute of Technology, under contract with the National Aeronautics and Space Administration. Based on observations obtained with the Apache Point Observatory 3.5-meter telescope, which is owned and operated by the Astrophysical Research Consortium (*https://www.apo.nmsu.edu*). This research has used the services of *www.Astroserver.org* under reference YIE7AQ and ZLNV9K.

REFERENCES

Ahn, C.P., Alexandroff, R., Allende, P.C., *et al.* 2014, *ApJ*, **211**, 17.
Ak, T., Bostanci, Z.F., Yontan T., *et al.* 2016, *Ap&SS*, **361**, 126.
Anthony-Twarog, B.J., Deliyannis, C.P., and Twarog, B.A. 2014, *AJ*, **148**, 51.
Auner, G. 1974, *A&AS*, **13**, 143.
Balona, L.A., Medupe, T., Abedigamba, O.P., *et al.* 2013, *MNRAS*, **430**, 3472.
Baran, A. 2013, *Acta Astron.*, **63**, 203.
Barkhatova, K.A., and Vasilevsky, A.E. 1967, *Peremennye Zvezdy*, **16**, 191.
Barnard, E.E. 1931, *Publications of the Yerkes Observatory*, **6**, 1.
Basu, S., Grundahl, F., Stello, D., *et al.* 2011, *ApJ*, **729**, L10.
Bohlin, R.C., Mészáros, S., Fleming, S.W., *et al.* 2017, *AJ*, **153**, 234.
Bragaglia, A., Carretta, E., Gratton, R.G., *et al.* 2001, *AJ*, **121**, 327.
Burkhead, M.S. 1971, *AJ*, **76**, 251.
Cantat-Gaudin, T., Jordi, C., Vallenari, A., *et al.* 2018, *A&A*, **618**, A93.
Chambers, K.C., Magnier, E. A., Metcalfe, N., *et al.* 2016, arXiv:1612.05560.
Choi, J., Dotter, A., Conroy, C., *et al.* 2016, *ApJ*, **823**, 102.
Choi, J., Conroy, Ch., Ting, Y.-S., *et al.* 2018, *ApJ*, **863**, 65.
Colman, I.L., Bedding, Timothy R., Huber, D., and Kjeldsen, H. 2022, *ApJS*, **258**, 39.
Dotter, A. 2016, *ApJS*, **222**, 8.
Fabricant, D., Fata, R., Roll, J., *et al.* 2005, *PASP*, **117**, 1411.
Ferguson, T.S. 1973, *The Annals of Statistics*, **1**, 209.
Flewelling, H.A., Magnier, E.A., Chambers, K.C., *et al.* 2020, *ApJS*, **251**, 7.
Friel, E.D., Liu, T., and Janes, K.A. 1989, *PASP*, **101**, 1105.
Gaia Collaboration, Vallenari, A., Brown, A.G.A., *et al.* 2022, arXiv:2208.00211.
Gao, X.-H., Xu, S.-K., and Chen, L. 2015, *Research in Astronomy and Astrophysics*, **15**, 2193.
Gosnell, N.M., Pooley, D., Geller, A.M., *et al.* 2012, *ApJ*, **745**, 57.
Guzik, J., Baran, A.S., Sanjayan, S., *et al.* 2023, *AJ*, **165**, 188.
Hole, K.T., Geller, A.M., Mathieu, R.D., *et al.* 2009, *AJ*, **138**, 159.
Hoskin, M. 2005, *Journal for the History of Astronomy*, **36**, 373.
Kalirai, J.S.,Richer, H.B., Fahlman, G.G., *et al.* 2001, *AJ*, **122**, 266.

Kaluzny, J., and Shara, M.M. 1988, *AJ*, **95**, 785.
Kamann, S., Bastian, N.J., Gieles, M., Balbinot, E., and Hénault-Brunet, V. 2019, *MNRAS*, **483**, 2197.
Kinemuchi, K., Barclay, T., Fanelli, M., *et al.* 2012, *PASP*, **124**, 963.
King, I.R. 1964, *Royal Greenwich Observatory Bulletins*, **82**, 106.
Kryachko, T.V. 2001, *IBVS*, 5058.
Kwee, K., and van Woerden, H. 1956, *Bulletin of the Astronomical Institutes of the Netherlands*, **12**, 327.
Lee-Brown, D.B., Anthony-Twarog, B.J., Deliyannis, C.P., Rich, E., and Twarog, B.A. 2015, *AJ*, **149**, 121.
Lindoff, U. 1971, *IBVS*, 601.
Lindoff, U. 1972, *A&AS*, **7**, 497.
Majewski, S.R., Schiavon, R.P., Frinchaboy, P.M., *et al.* 2017, *AJ*, **154**, 94.
Manteiga, M., Pickles, A.J., and Martinez-Roger, C. 1989, *AAP*, **210**, 66.
Németh, P., Kawka, A., and Vennes, S. 2012, *MNRAS*, **427**, 2180.
Pedregosa, F., Varoquaux, G., Gramfort, A., *et al.* 2011, *Journal of Machine Learning Research*, **12**, 2825.
Pigulski, A., Pojmański, G., Pilecki, B., and Szczygieł, D. 2009, *Acta Astron.*, **59**, 33.
Platais, I., Gosnell, N.M., Meibom, S., *et al.* 2013, *AJ*, **146**, 43.
Purgathofer, A. 1966, *Mitteilungen der Universitaets-Sternwarte Wien*, **13**, 7.
Rosvick, J.M., and Vandenberg, D.A. 1998, *AJ*, **115**, 1516.
Salaris, M., Weiss, A., and Percival, S.M. 2004, *A&A*, **414**, 163.
Sampedro, L., Dias, W.S., Alfaro, E.J., Monteiro, H., and Molino, A. 2017, *MNRAS*, **470**, 3937.
Samus, N.N., Kazarovets, E.V., Durlevich, O.V., Kireeva, N.N., and Pastukhova, E.N. 2017, *Astronomy Reports*, **61**, 80.
Sanders, W.L. 1972, *A&A*, **19**, 155.
Sanjayan, S., Baran, A.S., Németh, P., *et al.* 2022a, *Acta Astron.*, **72**, 77.
Sanjayan, S., Baran, A.S., Ostrowski, J., *et al.* 2022b, *MNRAS*, **509**, 763.
Stello, D., Basu, S., Bedding, T.R., *et al.* 2010, *Astron. Nachr.*, **331**, 985.
Stello, D., Meibom, S., Gilliland, R.L., *et al.* 2011, *ApJ*, **739**, 13.
Street, R.A., Horne, K., Lister, T.A., *et al.* 2002, *MNRAS*, **330**, 737.
Street, R.A., Horne, K., Lister, T.A., *et al.* 2003, *MNRAS*, **340**, 1287.
Street, R.A., Horne, K., Lister, T.A., *et al.* 2005, *MNRAS*, **358**, 795.
Talamantes, A., Sandquist, E.L., Clem, J.L., *et al.* 2010, *AJ*, **140**, 1268.
Tody, D. 1986, *SPIE Conference Series*, **627**, 733.
Tody, D. 1993, *ASP Conference Series*, **52**, 173.
Watson, C.L., Henden, A.A., and Price, A. 2006, *Society for Astronomical Sciences Annual Symposium*, **25**, 47.
Zhang, B., Chen, X.-Y., Liu, C., *et al.* 2015, *Research in Astronomy and Astrophysics*, **15**, 1197.
Zhao, G., Zhao, Y.-H., Chu, Y.-Q., *et al.* 2012, *A&A*, **12**, 723.